Electrochemistry and Production Optimization of Naturally Occuring Quinones for Flow Battery Technology

Kristensen, Sebastian Birkedal

DOI (link to publication from Publisher):
10.54337/aau456471612

Publication date:
2021

Document Version
Publisher's PDF, also known as Version of record

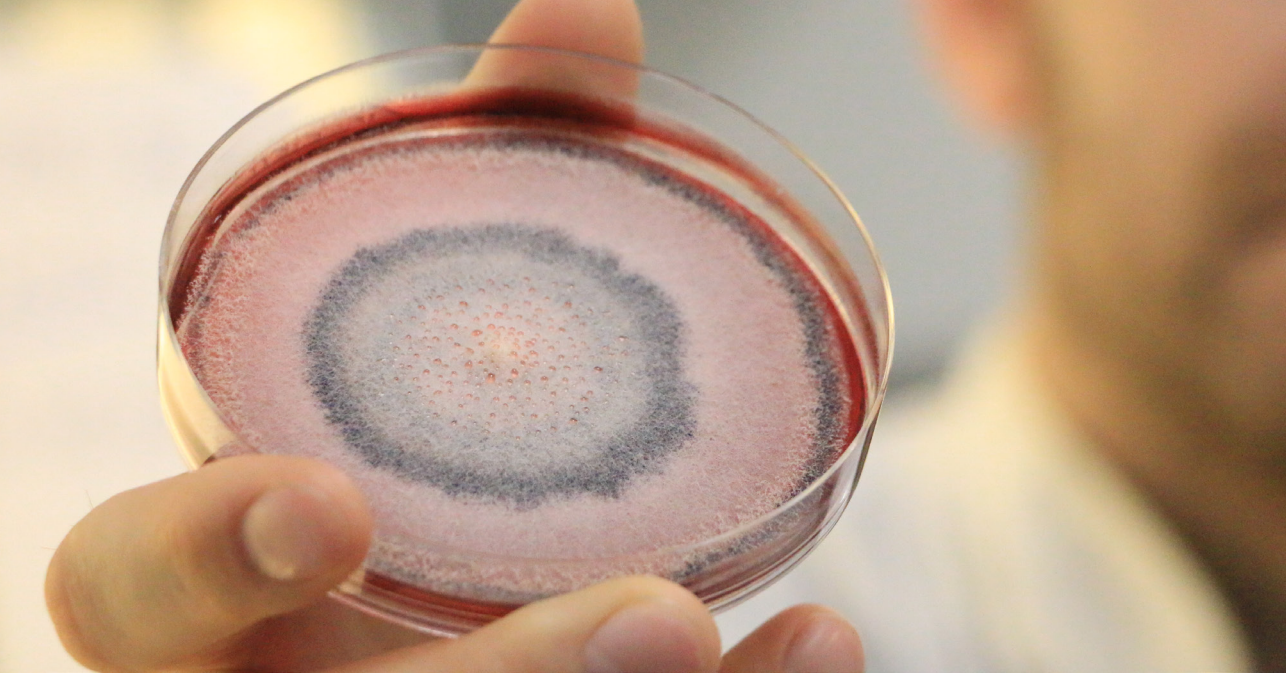

ELECTROCHEMISTRY AND PRODUCTION OPTIMIZATION OF NATURALLY OCCURING QUINONES FOR FLOW BATTERY TECHNOLOGY

BY

SEBASTIAN BIRKEDAL KRISTENSEN

DISSERTATION SUBMITTED 2021

AALBORG UNIVERSITY

DENMARK

ELECTROCHEMISTRY AND PRODUCTION OPTIMIZATION OF NATURALLY OCCURING QUINONES FOR FLOW BATTERY TECHNOLOGY

by

Sebastian Birkedal Kristensen

AALBORG UNIVERSITY
DENMARK

Dissertation submitted August 31st 2021

.

Dissertation submitted: 31-08-2021

PhD supervisor: Associate Professor. Jens Muff,
Aalborg University

PhD co-supervisor: Associate Professor. Jens Laurids Sørensen,
Aalborg University

PhD committee: Associate Professor Niels Thomas Eriksen (chair)
Aalborg University

PhD Alexandra Lex-Balducci
Friedrich Schiller University Jena

Professor Johan Hjelm
Technical University of Denmark

PhD Series: Faculty of Engineering and Science, Aalborg University

Department: Department of Chemistry and Bioscience

ISSN (online): 2446-1636
ISBN (online): 978-87-7210-987-9

Published by:
Aalborg University Press
Kroghstræde 3
DK – 9220 Aalborg Ø
Phone: +45 99407140
aauf@forlag.aau.dk
forlag.aau.dk

Printed in Denmark by Rosendahls, 2021

Preface

The thesis in the present form was submitted in accordance to the requirement for attaining the PhD degree at the faculty of Engineering and Science, Aalborg University. The project is structured as a 4+4 PhD project, and the work was carried out during the period of September 2017 to August 2021. The research project was fully funded and supported by the Danish Research Council, Technology and Production grant 7017-00167.

During my PhD project, I have been enrolled at the Department of Chemistry and Bioscience, Faculty of Engineering and Science. The research was conducted at Aalborg University, Esbjerg, Denmark. To expand my scientific horizon, I spend three months in the laboratory of Dr. Tanja van Mourik, University of St Andrews, St Andrews, Scotland. The PhD project has been a multidisciplinary research study, which includes elements of computational chemistry, electrochemistry, downstream process separation processes and biotechnology.

The photograph appearing on the cover is illustrating a *Fusarium solani* mutant, expressing some of the secondary metabolites of which I have worked within this study.

This thesis is based on the following papers:

1. **Kristensen, S.B.**; Mourik, T. Van; Pedersen, T.B.; Sørensen, J.L.; Muff, J. (2020) *Simulation of electrochemical properties of naturally occurring quinones*.
   Scientific Reports, doi:10.1038/s41598-020-70522-z.
2. **Kristensen, S.B.**; Pedersen, T.B.; Nielsen, M.R.; Wimmer, R.; Muff, J.; Sørensen, J.L. (2021) *Production and selectivity of key fusarubins from Fusarium solani due to media composition.*
   Toxins, doi:10.3390/toxins13060376.
3. **Kristensen, S.B**.; Fini, M.N.; Pedersen, T.B.; Sørensen, J.L.; Muff, J. (2021) *Membrane based separation and purification of fusarubins from Fusarium solani.*
   Separation and Purification Technology, doi:10.1016/j.seppur.2021.119576.

In addition to these papers, I have played a major role in the development and implementation of the experimental research facilities for redox flow battery studies in the laboratories of Section of Chemical Engineering, AAU Esbjerg. This work, in addition to introductory studies on phenicin and development of extraction procedures, laid the foundation of paper number 4, of which my contributions are included in the summary.

4. Wilhelmsen, C.O.; **Kristensen, S.B**.; Nolte, O.; Volodin, I.; Christiansen, J.V.; Petersen, T.I.; Larsen, T.O.; Frisvad, J.C.; Hager, M.; Schubert, S.U.; Muff, J; Sørensen, J.L. (2021) *The fungal battery: A redox flow battery containing the biosynthesised negolyte phoenicin.*
   Manuscript in draft.

Furthermore, I have contributed to the following publications as side-projects. The publications are related to the production of naturally occurring quinones, but are not directly within the core of the thesis. They are included to demonstrate the perspective of the multidisciplinary project I have been involved in.

5. Pedersen, T.B.; Nielsen, M.R.; **Kristensen, S.B**.; Spedtsberg, E.M.L.; Yasmine, W.; Matthiesen, R.; Kaniki, S.E.K.; Sørensen, T.; Petersen, C.; Muff, J.; et al. (2020) *Heterologous expression of the core genes in the complex fusarubin gene cluster of Fusarium Solani.*
   International Journal of Molecular Science, doi:10.3390/ijms21207601.
6. Pedersen, T.B.; Nielsen, M.R.; **Kristensen, S.B**.; Spedtsberg, E.M.L.; Sørensen, T.; Petersen, C.; Muff, J.; Søndergaard, T.S.; Nielsen, K.L.; Wimmer, R.; Gardiner, D.M.; Sørensen, J.L. (2021) *Speed dating for enzymes! Finding the perfect Phosphopantetheinyl Transferase partner for Your Polyketide Synthase.*
   Manuscript submitted to Microbial Cell Factories

Acknowledgements

First and foremost, I wish to say thank you to my project supervisor Associate Professor Jens Muff for the valuable support and good advice in the project. Secondly, I want to express my gratitude towards my co-supervisor Associate Professor Jens Laurids Sørensen for his guidance and support in the academic world and the area of biotechnology. To both of my supervisors, I wish to say thank you for allowing me to take the best of both worlds and for creating a well-balanced academic atmosphere with positive and inspiring outlook.

I want to say thank you to Dr. Tanja van Mourik for allowing me to work in her laboratory and welcoming me in a generous way at the University of St Andrews, and for helping me with the development of methods in the area of computational chemistry, which was a critical milestone of this project and the starting point for hopefully many other projects in the future. I wish to thank Professor Anders Bentien for welcoming me in his laboratory at Aarhus University and for showing me the tips and tricks with regards to flow cell testing which also proved essential in this project and others.

For patience in answering my countless questions, my thanks goes to Associate Professor Sergey Kucheryavskiy. To my colleagues in Esbjerg, Dorte and Linda, my deepest gratitude is given for all their help throughout my years at AAU Esbjerg. Without their hints, tips and tricks, good constructive questions, and help in the lab this PhD would have been even harder to finalize. I want to give a big thank you to Associate Professor Rudi P. Nielsen for helping me in the role as work employment representative, and leading the way with a positive foresight. My most sincere thank you goes out to my co-students Mikkel and Charlotte for all the talks, endless coffee breaks, and Friday beers. Thank you to the rest of my colleagues at the department for creating a friendly and positive working environment at AAU Esbjerg.

To my designated partner in crime, Tobias Bruun Pedersen, thank you for listening to all my complaints and for the endless advanced academic discussions about our projects in our office. And for being a good friend.

Last but very not least, I would like to show my deepest appreciation and gratitude to my family and friends for their support and encouragement during the last four years. You never doubted my capabilities even when I was doubting them myself. Thank you all. A special thank you goes to my girlfriend who has traveled up and down from the Netherlands to visit me over the last years, the support and consolation provided by you have been invaluable, thank you.

Sebastian Birkedal Kristensen
August 2021
Esbjerg, Denmark

English summary

The worldwide energy consumption is increasing each year, and has been throughout the history. The influence of fossil fuel-based energy sources on the climate changes has been wide reported and the green transition is ongoing with the renewable energy sources e.g. wind and solar power being the vastest investigated and promising solutions. To fulfill the potential of renewable energy sources to fit the demands of the energy grid, a steady and safe energy storage solution is evidentially needed to be found. However, it is not possible to have one specific solution in the current situation. An energy storage solution which marks itself as a potential candidate is the redox flow battery, which can be scaled according to the specific application needed, and possess relatively safe operating possibilities. An alternative to the commercially available, yet environmentally questionable, vanadium redox flow battery is the quinone based redox flow batteries. These have showed potential as a candidate to challenge the vanadium flow batteries. The potential of quinones as electrolyte is enormous when considering the redox behavioral properties and the amount of research which have been performed within this subject throughout the history. Until now, research in the use of quinones as electrolytes in flow batteries have been focused on synthetically produced quinones, derived from waste products from fossil fuel productions. Quinones are however produced naturally by various organisms, and herein lays an even greater potential for safe and environmental production of electrolytes, which can push the green transition one step closer to an even greener approach on energy storage. In this multidisciplinary project I have investigated the potential of using naturally occurring quinones as electrolytes and how to produce them in a sufficient and environmental considerate way.

Initially, I developed a local database containing 990 different naturally occurring quinones, originating from various natural sources. The quinones were all subjected to the computational chemistry simulations using density functional theory to calculate the redox potentials and solubility of the quinones with the purpose to screen for potential electrolyte candidates. The method was developed during my abroad stay at the University of St Andrews in Scotland. The investigations elucidated that the largest distribution of redox potential was to be found in the realm of fungi, as the quinones possessing the largest and lowest redox potentials was found here. It was also shown that the genus *Fusarium* and *Penicillium* were the largest contributors to the production of quinones. The solubility of the quinones was proved to be correlated to the presence of polar side chain groups rather than the size, molar weight, and the number of rings present in the molecule.

With the basis of a mutant strain of *Fusarium solani*, I investigated the influence of carbohydrate source and nitrogen source on the production of the secondary metabolites with specific purpose to enhance the yield of the fusarubins produced by the organism. The fusarubins are produced by the polyketide synthase PKS3 and depending on the availability of specific ions in the growth media specific compounds

could be extracted. Four different quinones were produced in high enough amounts to be relevant for future experiments and a quantifiable HPLC method was developed as well to determine the concentrations of the specific compounds. The learnings from this development sequence have been a significant outcome of this project as well as the findings in the study. The extraction procedure was developed specifically for these compounds, however prepared to yield maximum concentrations and not considering environmentally challenges with future upscaling projects. It was established that when using the carbohydrate maltose and the nitrogen source ammonium tartrate the production favored the quinone bostrycoidin as well as producing the compound with a high selectivity, yielding only small amounts of the other three compounds. The production could evidentially be enhanced further by prolonging the fermentation period from seven to nine days. The compounds fusarubin, javanicin and anhydrofusarubin were produced in the largest amount with relatively moderate selectivity in media composed of sucrose and sodium nitrate, where bostrycoidin was produced in very small amounts.

To utilize the extracted quinones in a future redox flow battery set up, significantly higher concentrations were needed for even lab scale testing of the quinones. Utilizing the findings with regards to the media composition which possessed high selectivity and high concentrations of bostrycoidin, an upscaling study was initiated. However, the extraction procedure posed as a significant challenge due to the extensive use of chloroform as the solvent. It was not desirable to use when handling larger volumes, as the ratio of solvent was 1:1. A potential way to lower the volumes needed extracted was to apply membrane filtration steps to separate and concentrate the quinones. Initially, a full separation train was investigated to elucidate if and how a potential filtration step could be utilized. This showed great potential in using microfiltration to separate bostrycoidin from the other three quinones. Additionally, the bostrycoidin yields could be greatly enhanced when using the optimized media composition. The concentrated retentates from the microfiltration step, which was exposed to the extraction procedure, showed a high concentration of bostrycoidin, making this a potential upscaling procedure for future productions of electrolytes.

The preliminary investigations of the naturally occurring quinone phenicin was conducted, which provided the foundation for the further study on this compound as a potential electrolyte. Lastly, to investigate if the compound bostrycoidin even possess the potential to be used as an electrolyte a preliminary electrochemical assessment was performed. The redox potential of the compound was found to be –0.58 V vs SHE, which is considered very compatible when other researched compounds is considered. The content of the thesis can therefore be seen as the first of many steps and the foundation towards finding the most optimal naturally occurring organic electrolyte for a greener energy storage of renewable energy.

Dansk resume

Det globale energiforbrug stiger hvert år og har været stigende gennem historien. Fossile brændstofbaserede energikilders indflydelse på klimaforandringerne er blevet bredt rapporteret, og den grønne omstilling er i fuld gang med vedvarende energikilder som eksempelvis vind og solenergi som de mest studerede og lovende løsninger. For at udnytte vedvarende energikilders potentiale til at imødekomme kravene i energinettet, er der et væsentligt behov for at finde en stabil og sikker energilagringsløsning. En enkelt specifik løsning er imidlertid ikke mulig, da situationen kræver større lagring end hvad der teknisk muligt på nuværende tidspunkt. En energilagringsløsning, der markerer sig som en potentiel kandidat, er redox flowbatteriet, som kan skaleres i forhold til den specifikke applikation, og har relativt sikre driftsmuligheder. Et alternativ til det kommercielt tilgængelige, men alligevel miljømæssigt tvivlsomme, vanadium redox flow batteri er de quinon baserede redox flow batterier. Disse har vist potentiale til at kunne udfordre vanadium flow batterierne. Quinonernes potentiale som elektrolytter er store, når man tager redox egenskaber og den store mængde forskning i disse gennem historien i betragtning. De quinoner, der er undersøgt til brug som elektrolytter i flowbatterier, har indtil nu været fokuseret på affaldsprodukter fra fossile brændstofproduktioner og heraf syntetisk producerede quinoner. Quinoner produceres imidlertid naturligt af forskellige organismer, og heri ligger et endnu større potentiale for sikker og miljømæssig produktion af elektrolytter som kan bruges til potentielt at skubbe den grønne omstilling et skridt tættere på en endnu grønnere tilgang til energilagring. I dette tværfaglige projekt har jeg undersøgt potentialet i at bruge naturligt forekommende quinoner som elektrolytter, og hvordan man producerer dem på en tilstrækkelig og miljømæssig hensynsfuld måde.

Som det første udviklede jeg en lokal database som indeholder 990 forskellige naturligt forekommende quinoner, som stammer fra forskellige kilder. Quinonerne blev alle udsat for simuleringer udført med beregningskemi hvori densitets funktionale teorien blev anvendt til at beregne redox potentiale og opløseligheder for quinonerne for at screene for potentielle elektrolyt kandidater. Metoden anvendt blev udviklet under mit udenlandsophold ved universitetet i St Andrews i Skotland. Undersøgelsen viste at den største fordeling af redox potentialer kunne findes i svampenes rige, hvor quinoneren med de højeste og laveste redox potentialer blev fundet. Ligeledes viste det sig at svampe typerne *Fusarium* og *Penicilium* producede flest quinones som var placeret i de ydre extremer. Opløseligheden af quinonerne blev vist at være afhængig af tilstedeværelsen af polære sidekædegrupper frem for størrelsen, molvægten og antallet af ringe, der er til stede i molekylet.

Med udgangspunkt i en mutant stamme af Fusarium solani undersøgte jeg kulhydratkildens og nitrogenkildens indflydelse på produktionen af de sekundære metabolitter med et specifikt formål at øge udbyttet af fusarubiner produceret af organismen. Fusarubinerne produceres af polyketidsyntasen PKS3, og afhængigt af

tilgængeligheden af specifikke ioner i vækstmediet kan specifikke forbindelser ekstraheres. Fire forskellige quinoner blev produceret i tilstrækkelige koncentrationer til at være relevante for fremtidige forsøg. Der blev endvidere udviklet en kvantificerbar HPLC -metode til bestemmelse af koncentrationerne af de specifikke forbindelser. Læringen fra denne udviklingssekvens har været et væsentligt resultat af dette projekt såvel som resultaterne i undersøgelsen. Ekstraktionsproceduren blev udviklet specifikt til disse forbindelser, dog med fokus på at give maksimale koncentrationer og ikke overveje miljømæssige udfordringer med fremtidige opskaleringsprojekter. Det blev fastslået, at ved anvendelse af maltose som kulhydratkilde og ammoniumtartrat som nitrogenkilde, favoriserede produktionen quinonen bostrycoidin og på samme tid med en høj selektivitet, hvilket kun gav små koncentrationer af de tre andre forbindelser. Produktionen kunne øges yderligere ved at forlænge gæringsperioden fra syv til ni dage. Forbindelserne fusarubin, javanicin og anhydrofusarubin blev produceret i højeste koncentrationer med relativt moderat selektivitet i medier sammensat af sucrose og natriumnitrat, hvor bostrycoidin kun blev produceret i ubetydelige mængder.

For at kunne udnytte de ekstraherede quinoner i et fremtidigt redox flow batteri, er der brug for betydelige højere koncentrationer for at kunne teste quinonerne i laboratoriet. Ved at tage udgangspunkt i resultaterne med hensyn til mediesammensætningen, der viste høj selektivitet og høje koncentrationer af bostrycoidin, blev et opskalerings forsøg startet. Ekstraktionsproceduren udgjorde imidlertid en betydelig udfordring, da anvendelsen af chloroform som opløsningsmiddel ved håndtering af større volumener ikke er hensigtsmæssig, og forholdet mellem anvendt opløsningsmiddel er 1: 1. En mulig måde at sænke de nødvendige volumener kan være at anvende membranfiltrering for at adskille og koncentrere quinonerne. Oprindeligt blev et separationstog undersøgt for at vise, hvorvidt og hvordan et potentielt filtreringstrin kunne udnyttes. Dette viste et stort potentiale ved anvendelse af mikrofiltrering til at adskille bostrycoidin fra de tre andre quinoner, og ved hjælp af den optimerede mediesammensætning for bostrycoidin kunne udbytterne forbedres betydeligt. De koncentrerede retentater fra mikrofiltreringstrinnet, som blev udsat for ekstraktionsproceduren, viste en høj koncentration af bostrycoidin, hvilket kan bruges som en potentiel opskaleringsprocedure for fremtidige produktioner af elektrolytter.

De indledende undersøgelser for hvorvidt den naturligt forekommende quinone phenicin kan anvendes som elektrolyt er udført, hvilket udgjorde grundlaget for de videre undersøgelser af dette stof. For at undersøge, om bostrycoidin overhovedet besidder potentialet for anvendelse som elektrolyt, blev der udfærdiget en foreløbig elektrokemisk vurdering. Forbindelsens redox potentiale viste sig at være - 0,58 V vs SHE, hvilket anses for meget kompatibelt og konkurrencedygtigt, når andre undersøgte forbindelser overvejes. Indhold af denne afhandling kan derfor ses som det første af mange trin og grundlaget for at finde optimale elektrolytte til en grønnere energilagring af grøn energi.

Table of contents

Aims and Research questions

The overall aim of this thesis was to investigate and develop the possibilities of using natural occurring quinones in redox flow battery technology. This can be divided into specific research questions:

- Which of the already known naturally occurring quinones is the best suited for use in a redox flow battery, and in addition to this, where in nature are they to be found? And which compound properties are governing the potential candidates?
- Is it possible to produce the found quinones in the native host in sufficient amounts for use in a redox flow battery? If not, what are the possibilities for optimization?
- Are the extraction procedures found in literature for similar compounds valid for extraction of quinones, and how can this be optimized for the specific compounds?
- When extracted, how can the electrochemical properties be verified and how to assess whether the quinone can be used as electrolyte in a redox flow battery?

The research questions led to the formulation of the extended objectives described hereunder:

- Develop a database concluding all known naturally occurring quinones and screen for possible candidates, based on reduction potential and solubility, using density functional theory, DFT, calculations.
- With basis in the screening find potential candidates and optimize production in native organisms and extraction methods. A secondary objective was to develop a quantitative method for concentration determination of the individual molecules. Additionally, molecular engineered organisms, like organisms with overexpressed genes for higher yield or have heterologous expression, can be used if available.
- Develop and perform practical assessment using electrochemical tools, such as cyclic voltammetry of the candidate, for the use in an RFB.
- In scope of future upscaling experiments, large scale production optimization should be investigated for the best suited candidate.

As indicated, the project grabs over several different disciplines whereas each of them over the project period have been worked with some in greater detail than others. The multidisciplinary project elements are visualized in the project wheel presented in **Figure 1**.

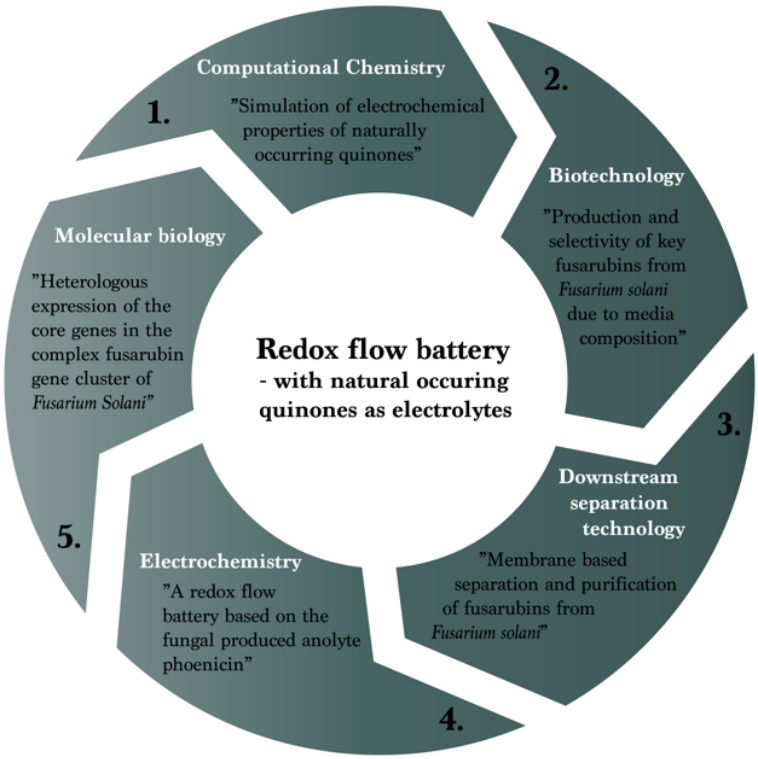

Figure 1 - Elements of the project, indicated by the subjects and papers with 1) Computational chemistry, 2) Biotechnology, 3) Downstream separation technology, 4) Electrochemistry, 5) Molecular biology. The 6th paper, is covered by the field of Molecular biology

In the following introductory chapter, the subject will be clarified in connection to the relevant theoretical aspects. The chapter initiates with describing why the solution of energy storage is needed, which provides the reasoning of the project. Hereafter, the different elements are explained with relevance to the research questions and objectives, which resulted in the research papers found in the end of this dissertation.

Chapter 1. Introduction

The world has an increasing use of energy, and has had this since the 1920's, where oil and gas production was introduced [1]. The Energy consumption reached a very high increase in 2018 of 2.8% where the average growth over a 10year period have been 1.6% increase. From 2018 to 2019, the increase was only 1.3% which was lower than the 10-year average. However, 41% of this was due to renewables and a decline in coal consumption was seen which reached the lowest level in the energy mix since 2003 [1,2]. So, overall a shift in energy matrix is seen going from coal and oil towards natural gas and renewables, leading to lowering the carbon emissions as well. Renewable energy sources grew the most of all energy types with an increase of 3.2 EJ and natural gas showed the second largest increase with 2.8 EJ. This picture was opposite in 2017 where natural gas showed the largest increase followed by renewables.[3] The renewables went from 4.5% to 5.0% of in the total energy mix, and the largest contributor to this was wind energy which increased with 1.4 EJ and hereafter the solar energy followed with 1.2 EJ increase. A very interesting point to note is that if electricity only is considered, the renewable part showed an increase from 9.3% to 10.4% in the total electricity consumption. This increase brings renewable energy in front of nuclear energy in the total energy mix for the first time in the history [1]. The overall energy consumption over the timeframe from 1965 to 2019 is visualized in **Figure 2.**

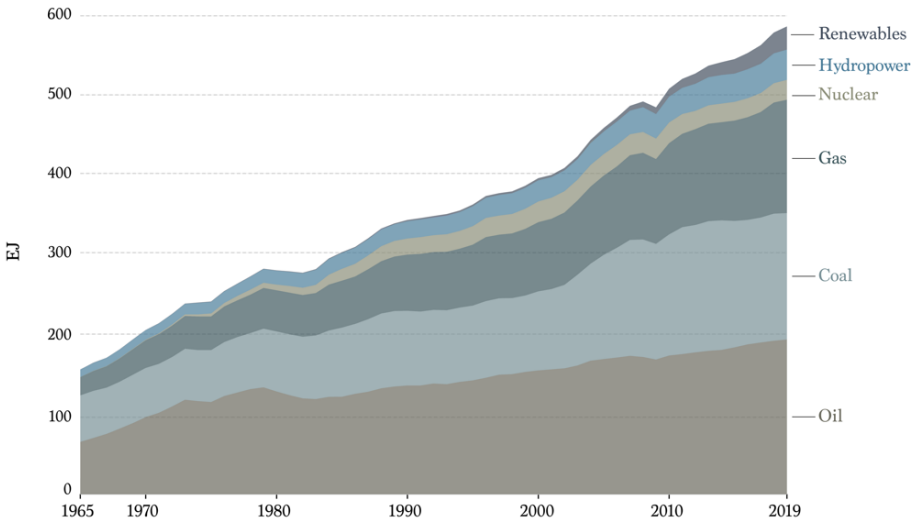

Figure 2 - The worlds energy consumption in Exajoules (EJ) in the period from 1965 to 2019 [1].

The shift from oil and coal-based energies to renewables has been over many different politicians' lips during the last ten years, with global warming being a real issue and dealt with accordingly. In 2015 at the international climate conference in Paris, 196 members of the UN signed an agreement which commits the countries to each lower the greenhouse emissions and work towards a greener approach. The agreement was named the Climate agreement of Paris.[4] Denmark has after the agreement in Paris improved these goals and chosen to work toward being independent of fossil fuels after 2050 [5]. The tendency of the green transition is however also seen in the energy production in Denmark. The usage of coal decreased with 44% from 2018 to 2019, and the renewable energy sources, such as wind, solar, biogas etc. showed an increase of 5.2%. Also, crude oil and natural gas exhibited a decrease in the production, with 11.4% and 25.4% respectively. When looking back to 2015, the percentage of electricity used that was produced by renewable sources was 56% of the total amount of electricity used in Denmark, where 41.8% of this was attributed to wind [6]. The year after in 2016 the number increased to a total renewable electricity use of 53.9%, and between 2016 and 2017 the production increased by 15.6% and was then composing 63.7% of the total electricity use, the amount attributed to wind turbines was then 43,2% as the highest of the contributors [7]. In 2018 a slight decrease was seen in the total amount of renewable electricity, where the percentage was 60.5%, but from 2018 to 2019 an increase of 16.2% was found and the percentage of renewable electricity was at the highest ever at 67.5%, where 46.8% was from wind energy. These tendencies can be attributed the increase use of biomass and wind turbines, where there have been large investments the last years. This can be seen if the overall increase in electricity produced by renewable sources from the year 1994 to 2019 is considered 1180% and if only wind turbine energy is considered the number is 1260%. When looking at the overall energy production the increase from 2016 to 2017 was 7.6% and the total produced energy in 2017 was shown to be 171 PJ. From 2018 to 2019 the increase was 5.2% to the highest level yet, of 176.4 PJ. The increase over the years from 1990 to 2019 was shown to be 288% of production of renewable energy in Denmark. The highest contributor to this in the wind energy, which composed of 58.1 PJ in 2019 which was an increase of 16.2% from 2018 [8], **Figure 3.** The group listed as "other" consist of solar energy, geothermal and hydropower energy. When looking at the total amount of energy produced in 2019 the percentage covered by renewables was 36.7%, and the CO_2 emissions was decreasing by 7.8%, and from 1990 to 2019 the decrease was at 43%.

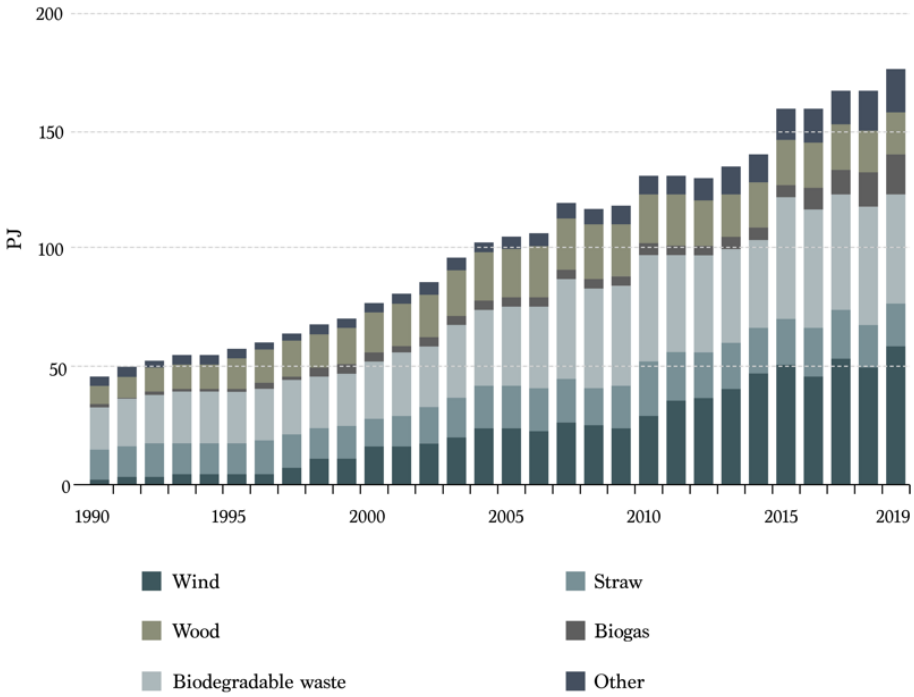

Figure 3 - Annual production of renewable energy in the period of 1990 to 2019, divided into the largest contributors measured in Petajoules, (PJ)[8].

The green shift towards renewable energy sources has over time brought knowledge and investments to the different technologies. This has led to 72% of all new additions to energy capacities worldwide is accounted for by renewables in 2019. The prices have, because of the maintained focus over time, also seen a significant drop, making the technologies widespread over the world. From 2010 to 2019 the levelized cost of electricity (LCOE) have decrease by 82% for the utility solar photovoltaic power sources, 47% decrease is seen for the concentrating solar power, 39% decrease for the onshore wind energy, and 29% for the offshore wind energy cost**, Figure 4.** This makes the renewable energy sources competitive with the fossil fuel industry, leading to more investments and more widespread technologies [9].

To make the green transition function in an optimal way a smarter grid scale energy storage solution will be required, because the renewable sources is based on e.g. sunlight and wind, where the fluctuation of production not necessary complies with the steady state demand on energy. This has been taken into account by the Danish government [10], that has agreed on investments in renewable energy storage solutions, going forward to 2030. The common storage possibilities as of today, e.g. solid state batteries, is not however viable when the economic and environmental properties is taken into consideration [11,12]. The issue is that the solution has to be scalable, inexpensive and efficient, and that different types of energy storage, such as

capacitators, flywheels, and enclosed secondary batteries can only be used for short duration of grid services. An example of this could be frequency regulation and grid power quality maintenance. The main solution for long term storage which is needed for wind and solar power is then pumped hydroelectric energy storage [12,13]. This type of storage is geographically limited to where it is possible to have to large reservoirs of water with significant large elevation [14].

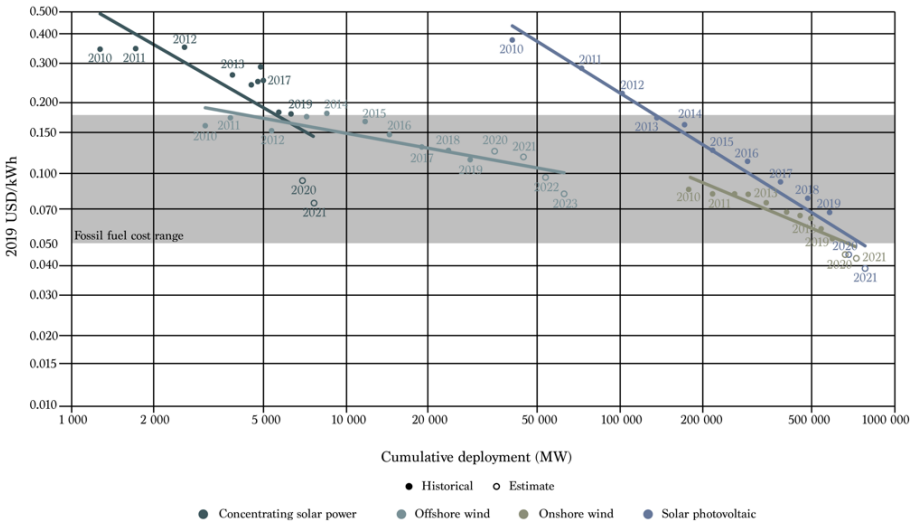

Figure 4 - Price development or the global weighted-average levelized cost of electricity (LCOE) over time, in USD/kWh for the four main contributors of renewable energy worldwide, [9].

Another type is compressed air energy storage in caverns where natural gas is combusted during discharge, which also then requires certain geographical properties. Secondary batteries are however not restrained by geographical demands, and could potentially enable the storage of fluctuating renewable energy at a large scale. The scalability and use of rechargeable batteries have until now been limited to few types, whereas lead-acid and lithium-ion batteries is the far most developed. The use of these batteries goes from automobile batteries, to the small lithium-ion batteries in cell phones and computers, due to the high energy density in the lithium-ion batteries. Despite these many well-defined properties of the lithium-ion battery and the extended funding to research the development of the battery into the utilization in cars, the integration into large grid scale application has been very limited. This because some challenges such as limitation and geopolitical issues around raw materials [15], and recently there has been issues with fire hazards due to the organic solvents which are contained in the batteries [16,17].

1.1. Redox flow batteries

A battery type that potentially can be used for large grid scale energy storage, peak shaving of production versus demand for intermittent renewable energy production is redox flow batteries, (RFB). The RFBs are scalable with regards to energy and power independently, whereas if a large power in/output is required a large number of cell stacks can be used, and if the requirement is large storage capacity, an increased volume of the electrolyte tanks can be utilized. When economy and safety are considered, the RFBs are also recognized as the realistic choice of energy storage for large scale applications in the ranges kW/kWh to MW/MWh [18,19]. Even though the energy density or the energy stored per unit volume of RFB is lower than for lithium-ion batteries, the scalability and economy of RFB still makes the battery type a valid candidate. Techno-economic studies estimates that an aqueous RFB with an open circuit voltage of 1.5V, with electrolyte costs of USD$ 5 per kg for the active

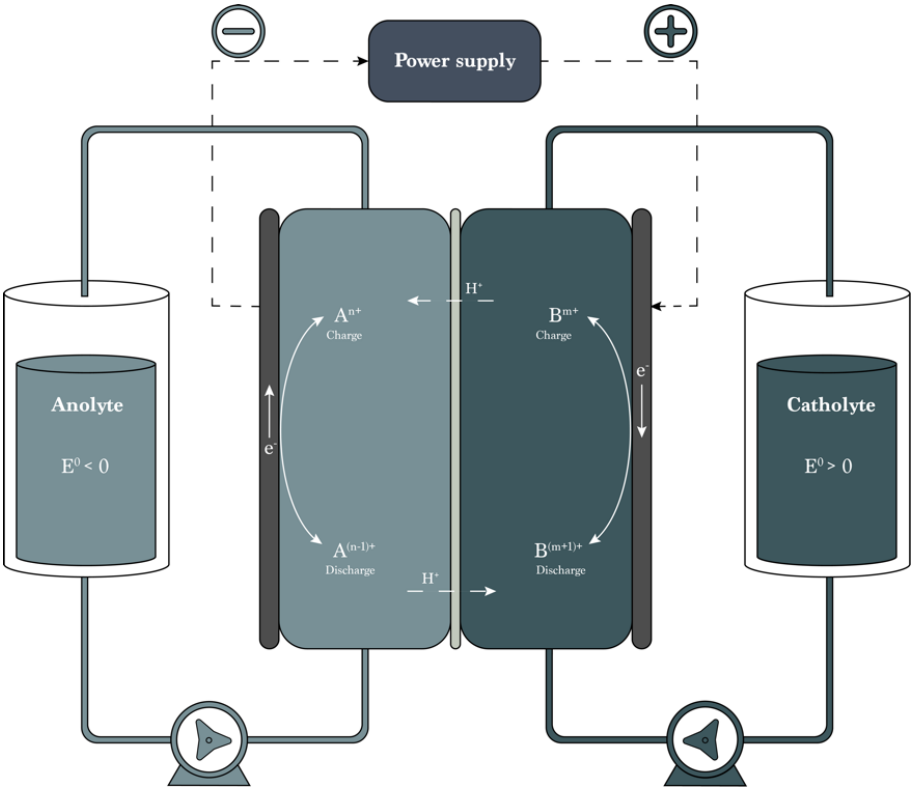

Figure 5 - Overview of the basic principle of a redox flow battery. Where A indicate the anolyte and B indicate the catholyte, in the two cell compartments. Separating them is the ion-selective membrane which is indicated by allowing H^+ to permeate through upholding the charge balance. The redox reactions of the two electrolytes is occurring at the two electrodes illustrating the electron flow through the flow cell.

material and up to 150 g per mole electrons transferable should be priced around USD$ 120/kWh, where there is still significant room for improvement of further production cost reductions. Where cheap electrolytes and large production volumes can be mentioned as examples [20].

In **Figure 5** the overall basic principle of an RFB is illustrated. When the battery is charged and discharged the following reaction will occur at the anode and cathode, [21];

$$A^{(n)+} + xe^- \underset{Discharge}{\overset{Charge}{\rightleftharpoons}} A^{(n-x)+} \quad \text{- in the anolyte } (E^0 < 0). \quad (1)$$

$$B^{(m)+} - xe^- \underset{Discharge}{\overset{Charge}{\rightleftharpoons}} B^{(m+x)+} \quad \text{- in the catholyte } (E^0 > 0) \quad (2)$$

In the RFB, electrical energy is converted into chemical energy which is stored in two reservoirs or tanks. The tanks are separated from each other, and contain the two electrolytes, often named anolyte and catholyte or negolyte and posolyte. The electrolyte is two different redox couples, which undergoes a reduction and oxidization when the battery is charged or discharged depending on their reduction potential. One of the tanks is containing a solution of electrolyte with a large (positive) standard reduction potential (E^0), which receives an electron spontaneously when the battery is being discharged. The second tank contains a solution that has a corresponding low (negative) E^0 which donates an electron spontaneously when the battery is discharging. In the charging phase of the battery, the two electrolytes undergo the non-spontaneous opposite reactions. The reactions occur in the battery cell at the surface of the two electrodes, the electrolytes are being recirculated through the cell by two separate pumps. The cell potential, (E_{cell}), is defined as the difference between the standard reduction potential of the anolyte and catholyte, whereas a larger cell potential can be obtained if an anolyte is used with a more negative E^0 and simultaneously a more positive catholyte is utilized. The battery flow cell is constituted by two half cells which is divided by an ion-selective membrane. For the optimal number of reactions to occur in the half cells, is a relatively large surface area provided by these. The purpose of the ion-selective membrane is, besides ensuring that the two electrolytes does not cross to the other half call and initiate unwanted side reaction which can potentially lower the capacity of the battery, to serve as an ionic charge balance facilitator. The membrane is allowing small ions, e.g. H^+ ions, to move between the two half cells ensuring the ionic charge balance to be maintained. Often Nafion membranes have been utilized as these have shown promising results when using organic electrolytes [22–24].

The most investigated and developed type of RFBs, is the vanadium redox flow battery, VRFB,[25–27]. The battery utilizes the metal vanadium as both anolyte and

catholyte, due to vanadium's ability to appear in solution in four different oxidization states. The half-cell reactions are described below.

$$V^{3+} + e^- \underset{Discharge}{\overset{Charge}{\rightleftharpoons}} V^{2+} \qquad (E^0 = -0.255\,V) \quad (3)$$

$$VO^{2+} + H_2O - e^- \underset{Discharge}{\overset{Charge}{\rightleftharpoons}} VO_2^+ + 2H^+ \qquad (E^0 = 1.004\,V) \quad (4)$$

The difference between the anolyte and catholyte is yielding 1.26V for a proton concentration of 1M, where only the second reaction is coupled to protons, and therefore the potential will increase at lower pH. Several companies in the industry all over the world have developed and evolved the VRFB, where the largest batteries in use is under construction by Rongke Power in Dalian, China, and it is rated at 200 MW/ 800 MWh. But even though the vanadium electrolytes are very stable and the crossover through the membrane is not of any significant meaning because it's the same electrolyte on both sides, the price of vanadium is fluctuation a lot and in average to high when considering worldwide large applications. As example the United states' department of Energy stated that a utility scale storage application should not cost more than USD$ 150/kWh [28] in 2023, of which the VRFB are expected to exceed [29], where systems can have costs between USD$ 3-800/kWh [30]. The vanadium itself is priced with fluctuation around USD$ 80/kWh, while the ion exchange membrane is the expensive part, taking up nearly 40% of the cost of the battery [31].

In addition to the expensive but reliable VRFB, several other types have over time been investigated and developed, among these chemistries are hydrogen-bromine [32], sulfur-oxygen [33], metal-hydride [34] and all-iron based which are in a slurry-form [35]. Others have developed hybrid system using zinc as a non-flowing electrolyte, in combinations such as zinc-bromine [36], zinc-iron [37] and zinc-cerium [38], however these batteries lose the separation capability of power and energy because the electroplating which occurs in these batteries is limited by the cell surface area instead of the volume of the electrolyte reservoirs.

In the recent years, a variety of organic compounds have been investigated for use in RFBs. These provide several benefits and advantages when comparing to the expensive inorganics. The organic materials provide a diverse molecular pallet with different properties and also being non corrosive, safe, and low cost [39–41]. There has been different variations of organic RFBs over the past, where metal-ligand complexes with organic ligands were used as electrolytes [42,43], also electrolyte couples which were composed of one organic and one inorganic electrolyte was researched [44], and where the couples were organic and halogens [45], and also types where both electrolytes were organic based, named all organic RFBs [46,47]. An early study from 2010 investigate a hybrid flow battery using lead and 4,5-dibenzoquinone-

1,3-benzenedisulfonate, or commonly named Tiron, as the electrolytes, being the first to investigate the class of organic compounds called quinones as electrolytes for use in RFBs [48]. In the recent years quinones have received some attention and showed to possess several qualities when considered in RFBs [18,22,45,49]. Quinones has been shown to be a cheap, reliable, and displaying fast energy transfers, which all are key parameters in flow battery technology [1].

1.2. Quinones and their electrochemical properties

Quinones are organic molecules which consists of at least one aromatic ring structure or hexacyclic saturated ring, combined with a di-one or di-ketone system. The molecules can occur as ortho or para-constituents, which is illustrated in **Figure 6.** Quinones can contain one or more ring structures, where the simplest form is the benzoquinones, containing one ring. The quinone containing two rings, which can be explained as a naphthalene backbone connected to two carbonyl groups, are called naphthoquinones, whereas the compounds containing three rings are named anthraquinones and are containing the backbone of anthracene, connected with two carbonyl groups[50,51].

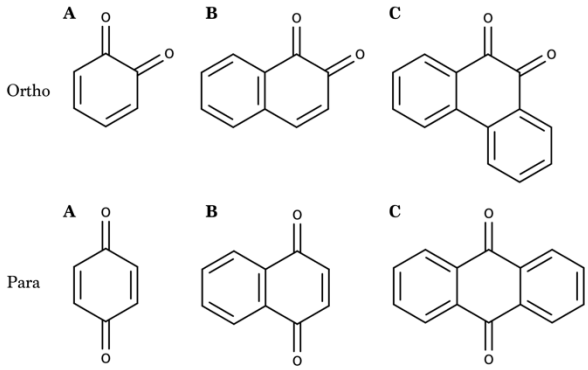

Figure 6 - Types of various quinones. Orthoquinones; A) 1,2-benzoquinone, B) 1,2-napthoquinone, C) 9,10-phenanthrenequinone. Paraquinones; A) 1,4-benzoquinone, B) 1,4-naphtoquinone, C) 9,10-anthraquinone.

Quinones have been researched thoroughly for many years based on the redox behavior and stability in aqueous solutions, where both para- and orthoquinones can be present in either fully reduced or oxidized forms, or in an intermediate state where the quinone occurs as a semiquinone radical. The redox behavior can be illustrated **Figure 7** [52].

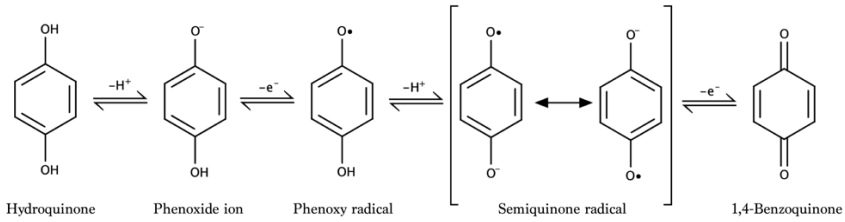

Figure 7 - Redox behavior of 1,4-benzoquinone, the process is however similar for all quinone compounds. Oxidation proceeds from left to right, reduction is opposite.

The hydroquinone is oxidized from left to right, and can be described through some steps. The first step is a loss of a proton, where after the compound is named a Phenoxide ion, a rapid loss of an electron yields the phenoxy radical. When this compound is oxidized and loosing another proton the semiquinone radical is formed, where two resonance forms is present. These forms are unstable so the loss of a second electron will take place and yield the fully oxidized 1,4-benzoquinone [52–54]. It is in general believed that the redox reaction of quinones is a rapid transfer of two electrons and two protons, [45,52,53,55]. However, depending on the pH of the solution, the amount of protons present in the reaction can differ, yielding slightly different compounds [56].

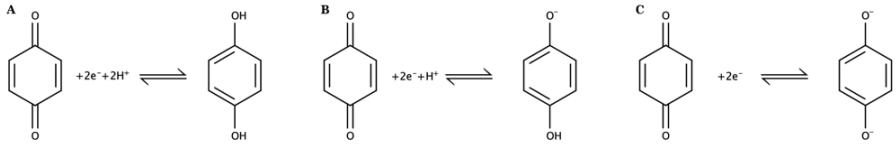

Figure 8 - Redox behavior of quinones in different pH. A) Acidic pH, B) Neutral pH, C) Alkaline pH [56].

In acidic solutions excess number of protons will lead to the reaction illustrated in **Figure 8A**. If the reaction occurs in a solution around neutral pH there will only be a limited number of protons available and the reaction could undergo the rapid two electron -two proton redox reaction, however, if not enough protons is available the reaction will proceed with only one proton as illustrated in **Figure 8B**. When the pH raises to alkaline, the number of protons will be very limited making the reaction undergo only a to electron transfer, illustrated in **Figure 8C**. The quinone is reduced, however not hydrolyzed, where the compound then is named a dianion.

These behavioral tendencies have been investigated as well with respect to the reduction potentials, where different quinones were analyzed at varying pH levels

between 0-13[49,57,58]. The relation between pH and reduction potential is explained to be a decreasing slope of 59mV/pH for reaction where two protons is involved, and 30mV/pH for reaction where only one proton is involved. The slope is 0 when no protons is involved in the reaction. The relation was described in detail using the Nernstian equation by Richard G. Compton et al. 2012 [59].

1.3. Quinone redox flow batteries

Quinones have been studied in some years for the use in RFBs, due to their reversible redox behaviors and versatile organic nature. The stability, solubility, and redox potential of the compounds can be adjusted to fit specific batteries based on side chain groups bonded to the backbone of the compounds, thereby designing the optimal quinone compound as electrolyte. Several different quinone combinations of electrolytes in full cell RFBs have been researched over the years, some examples hereof are presented in **Table 1**.

Table 1 - Overview of quinone based RFBs, the electrolyte combination, redox potential, molarity, capacity fade ratio when listed, pH of the electrolytes when published and author/date of the studies. Quinones and their E^0 and molarity have been highlighted by bold.

Electrolytes	Redox potential (V vs SHE)	Molarity (M)	Capacity fade % per cycle	pH	Author/year
2,6-DHAQ/$K_4Fe(CN)_6$	**-0.68**/0.50	**0.5**/0.4	0.1	14	Lin et al./2015 [49]
		0.1/0.05	0.1	14	Goulet et al./2019 [60]
DHBQ/$K_4Fe(CN)_6$	**-0.72**/0.50	**0.5**/0.4	0.24	14	Yang et al./2017 [58]
DMBQ/$K_4Fe(CN)_6$	**-0.75**/0.50	**0.1**/0.1	0.11	14	Sun et al./2019 [61]
DMOBQ/$K_4Fe(CN)_6$	**-0.70**/0.50	**0.1**/0.1	0.17	14	
Bislawsome/ $K_4Fe(CN)_6$	**-0.55**/0.50	**0.1**/0.2	3.8×10^{-2}	14	Tong et al./2019 [62]
2,6-DBEAQ/ $K_4Fe(CN)_6$	**-0.54**/0.50	**0.5**/0.3	1.0×10^{-3}	12	Kwabi et al./2018 [63]
2,3-HCNQ/ $K_4Fe(CN)_6$	**-0.53**/0.50	**0.5**/0.4	5.3×10^{-2}	14	Wang et al./2018 [64]
2,6-DPPEAQ/ $K_4Fe(CN)_6$	**-0.47**/0.50	**0.5**/0.4	4.0×10^{-4}	9-13	Ji et al./2019 [65]
PEGAQ/ $K_4Fe(CN)_6$	**-0.43**/0.50	**0.1**/0.1	4.0×10^{-2}	7	Jin et al./2019 [66]

AQS/HBr	**0.19**/1.06	**1.0**/3.0	1	0	Gerhardt et al./2017 [67]
AQDS/HBr	**0.21**/1.06	**1.0**/3.0	1.4×10^{-2}	0	Huskinson et al./2014 [45]
		1.0/3.5	0.1	0	Chen et al./2016 [68]
AQDS/$FeSO_4$	**0.15**/0.77	**0.33**/0.67	7.6×10^{-5}	0	Yang et al./2020 [69]
ARS/BQDS	**0.08/0.91**	**0.05/0.05**	2	0	Zhang et al./2015 [70]
AQDS/DHDMBS	**0.21/0.82**	**1.0/1.0**	1	0	Hoober-Burkhardt et al./2017 [71]
BQDS/AQS	**0.82/0.13**	**0.2/0.2**	-	0	Yang et al/2014 [46]
Quinoxaline/**BQDS**	-0.5/**0.82**	**0.1/0.1**	-	7-14	Brushett et al./2015 [72]
$PbSO_4$/**BQDS**	-0.35/**0.72**	solid/**0.25**	-	0-10	Xu et el/2010 [48]
$Zn(OH)_4^{2-}$/$\mathbf{FQH_2}$	-1.30/**0.70**	0.2/**0.1**	9.0×10^{-2}	-0.7	Park et al./2019 [73]
ZnCl/**1,4-BQ**	-0.76/**0.65**	1.5/**0.05**	-	7	
ZnCl /**1,2-BQ**	-0.76/**0.75**	1.5/**0.05**	-	7	Leung et al/2016 [74]
ZnCl /**BQDS**	-0.76/**0.85**	1.5/**0.05**	-	7	

There is great variation in the combinations of electrolytes, some use a quinone-iron complex at high pH, and HBr has been investigated as the second electrolyte combined with different quinones at low pHs. All-quinone RFBs have likewise been investigated and also several hybrid RFBs have been researched. It is noted that the majority of the published full cell studies have cell potentials around 1-1.5 V, and is therefore comparable and can be competitive with the cell potential of the VRFB. The variation of the capacity fading ratios reveals that there is still room for improvement even though some studies show low capacity fading ratios.

Several studies have researched the stability of the quinone by the structure of the compounds, e.g. Yunlong Ji et al. 2019, [65], which proposed a phosphonate-functionalized quinone, (((9,10-dioxo-9,10-dihydroanthracene-2,6-diyl)-bis(oxy))bis(propane-3,1-diyl))bis(phosphonic acid) or (2,6-DPPEAQ). This study

was a continued study based on an earlier published article by Kwabi et al. 2018, [63] in which they investigated four anthraquinones, with the base compound being hydroxyanthraquinone, and substituted two sidechain groups into 1.2-DBEAQ, 2,6-DBEAQ, and 1,8-DBEAQ, and they assessed the influence of these substituents on the electrochemical properties of the quinones. Yunlong Ji and co-workers, [65], showed that substitution of the functional groups could improve the electrolytes and thereby the RFB, with the capacity fading as low as 0.00036% per cycle. These improvements of electrolyte compounds are however very time consuming if all combinations, molecules, sidechain groups, and placements hereof should be considered. To investigate the optimal composition of the molecules several researchers have been using computational chemistry.

1.4. Computational evaluation of electrolytes for RFBs

Computational chemistry can be applied to investigate various combinations of molecules and different functional groups. The computational calculations can be used to gain important information about redox systems in an efficient way where unwanted side reactions and decomposition products can be studied in detail. Traditional density functional theory (DFT) has been applied to investigate the vanadium complexes reactions with water molecules, to the hydrated vanadyl ion $(VO(H_2O)_5)^{2+}$ [75–77]. Also hybrid RFBs have been investigated using DFT where the adsorption and diffusion of zinc ions to the carbon electrode was simulated [78]. Various studies have been conducted to study organic redox species. The use of computational chemistry elucidates a fast way of investigating many different molecules and their substituted functional side chain groups, thereby finding promising compounds before conducting experiments in the laboratory. The published research from Er et al. 2015, [79], presents a high throughput virtual screening of 1710 quinone molecules, where reduction potential and solubility are investigated based on functional sidechain groups and amount of rings in the quinone structure. The paper also presents valid information about the functionalization of the sidechain groups such as electron donating groups (EDGs), e.g. $-NH_2$ and -OH, which tend to lower the electron affinity and thereby results in a decrease in the reduction potential. When quinones are substituted with electron withdrawing groups (EWGs), such as $-NO_2$, $-SO_3H$, and $-PO_3H_2$, the opposite tendencies where higher reduction potentials are observed. It is also stated that the most promising compounds for the negative side is 9,10-AQ quinones, whereas on the positive side 1,2-BQ, 2,3-NQ, and 2,3-AQ derived quinones are the promising candidates. The solubility of the quinones could be improved by substituting the functional groups furthest away from the cyclic ketones [79]. The same tendencies of EDGs and EWGs was concluded by the study of Assary et al. 2014, [80], which investigated the reduction potentials of 40 nitrogen-containing molecules called quinoxalines. The quinoxalines has also been researched by Pasadakis-Kavounis et al. 2021, [81], where the electrochemical characterization of these types of compounds was investigated for use in flow batteries. The study of Cheng et al. 2015 [82], proposed a different workflow where a downstream selection

model was published to investigate potential candidates for a non-aqueous RFB. Simulations of 1417 derivatives of aromatic molecules were screened for their reduction potentials, and based on these 353 candidates were chosen to continue. The solvation energies were computed for the 353 potential candidates, and of these 262 were chosen to continue in the screening. The structural changes of the compounds were then assessed, by simulating the geometrical stability of the molecules, which led to the conclusive number of candidates of 231 for the non-aqueous RFB. Tabor et al. 2019, [83] , presented a study where the stability of quinones was investigated, which elucidated that depending on the backbone of the quinone, side chain group placement etc., the molecules reactiveness with water through the Michael addition was one of the important factors to consider and investigate when choosing electrolytes.

Table 2 provides an overview of some of the computational studies which have been conducted over the years. The tendency of which functional and basis set to use is relatively clear, as most of the studies share the B3LYP functional and then a variation of 6-31G basis set with or without polarization functions, noted either as (d,p) or by **. A general observation is that the majority of the studies use similar procedure in the structure of the work. To find the most stable form of the molecule of interest the potential energy surface is used to find the lowest amount of energy of the molecule. In a diatomic molecule, the potential energy increases if the bond length is stretched or compressed. A stationary point on the energy surface is often found to be the minimum potential energy, a saddle point or a transition state of the molecule. Conduction a geometric optimization is performed by submitting a structure of a molecule to a computational algorithm which systematically alters the structure until the minimum energy is found [84].

Table 2 - Overview of some computational studies of potential electrolytes for usage in RFB technology.

Compound	Computational methods	Study highlights	Author/year
35 different double redox-unit compounds	DFT B3LYP/6-311G(d,p)	Redox potentials and solubilities for use in symmetric aqueous organic redox flow batteries	Fornari/2020 [85]
DMB[1] and derivatives	DFT B3LYP/6-31G (2df, p)	Stability and redox behaviour, potentials in different solvents.	Assary/2016 [86]
1417, various aromatics	DFT (B3LYP/6-31+G(d)) and PCM[2]	High throughput screening of redox potentials, stability and solubility.	Cheng/2015 [82]
Quinoxaline derivatives	DFT B3LYP/6-31+G(d)	Functional sidechain groups influence on the redox potential.	Assary/2014 [80]

Various organic compounds	Multi descriptor – multiple kernel method	Solubility and pH dependency, logS.	Kim/2017 [87]
TDT[3]	DFT B3LYP/6-31+G(d)	Stability of active material for non-aqueous RFB, in combination with Li^+.	Carino/2016 [88]
Cyclic nitroxides	DFT B3LYP/6-31+G(d)	Solvation energies and redox potential.	Gryn'ova/2012 [89]
4178 organic molecules	DFT B3LYP/6-31+G(d) and IEF[4]-PCM	High throughput screening of molecules for non-aqueous RFBs.	Pelzer/2017 [90]
106 organic compounds	DFT B3LYP/6-31+G(d)	Screening of redox potential and solubility of various organic compounds for use in RFB technology.	Moon/2016 [91]
1710, various quinones	DFT PBE/6-31G**	High throughput screening of quinone compound, redox potential, solubility and stability, based on different functional groups.	Er/2015 [79]
5 basic quinones	DFT B3LYP/6-31+G(d)	Combined computational and experimental study of redox behaviour in RFBs.	Ding/2016 [92]
DHAQ and derivatives	Semi-empirical method PM7 – COSMO	Combined computational and experimental study decomposition of DHAQ in RFB.	Goulet/2019 [60]
134 various quinones	DFT B3LYP/6-31++G**	One and two e^- redox potential and pKa was computed. Various functional groups were also considered.	Huynh/2016 [93]
4 ρ-quinones	DFT BHandHLYP/M06-2x/PBE0 / 6-31+G(d,p)	Combined computational and experimental study of four quinone compounds and their redox behaviour.	Martinez-Cifuentez/2017 [94]
10611 quinones	DFT B3LYP/6-31+G(d,p)	Screening of thiophenoquinones and all possible combinations of functional group substituents, for redox potentials and solubility.	Pineda Flores/2015 [95]
25 quinones	Semi-empirical Molecular Orbital method	Relating redox potential to the free energy or atomization energy of the quinone compound.	Dewar/1969 [96]
6 basic quinones	DFT B3LYP/6-31+G(d,p)	Redox potentials for the quinones and semiquinone radicals.	Johnsson Wass/2006 [50]

AQDS and derivatives	DFT PBE/6-31G**	Combined theoretical and experimental study of ADQS and possible substituents in an RFB set up.	Huskinson/2014 [45]
DHBQ and derivatives	DFT PBE/6-31+G(d,p)	Combined theoretical and experimental study of DHBQ as electrolyte in an RFB.	Yang/2017 [58]

[1]1,4-demethoxybenzene, [2]Polarizable continuum model, [3]1,2,3,4-tetrahydro-6,7-dimethoxy-1,1,4,4-tetramethylnatphthalene, [4]integral equation formalism.

1.4.1. Density functional theory

The use of Density functional theory (DFT) is widespread in **Table 2**, and where as all *ab initio* methods take the starting point in the Hartree-Fock (HF) approximation the HF equations are solved for the spin-orbitals and these are utilized for the construction of the configuration state functions, and are widely used today. However, when working with large datasets these reveals some limitations with correct calculations, especially when handling basis sets containing large amounts of atoms and electrons [97].

DFT is used as an alternative to these computational heavy calculations when handling large molecules. Where HF methods uses configuration state functions, which is an eigenfunction of all the operators that commute with H, DFT uses the concept of electron probability density. This enables DFT calculations to consider electron correlation while being less computational costly. The principle of DFT is to consider the energy of an electronic system(molecule) as the electron density probability, ρ. Then for a molecule containing n electrons, ρ(r) notes the total number of electron density at a specific location, r in the space. The energy is then explained as a functional of the electron density and is noted E[ρ] [97].

1.4.2. Functionals and basis sets

The functionals used in DFT calculations are all taking the initial point from the formal proof written by P.Hohenberg and W.Kohn in 1964, which describes the ground state energy and all other ground state electronic properties could uniquely be described by the electron density. The Hohenberg-Kohn theory was only proving that a functional that had the potential did exist, not the functional itself. The electron density, however was derived from the theory and is described as following:

$$\rho(r) = \sum_{i=1}^{n} |\psi_i(r)|^2 \quad (5)$$

Several approximations (B3LYP, PBE, M06-2X, HTCH etc.) was composed to solve the functional, but this has not been completed so far. The generalized gradient (GGA) functionals consider gradients of local densities to the exchange-correlation energy of

the functional, which is considered to be the largest contributor of error in the functional. Taking this into account is seen as an essential correction of the estimation of bond energies [97,98].

The higher level of accuracy a functional possess, the higher up on the Jacobs ladder the functional is. The Jacobs ladder of functionals, **Figure 9**, is used for ranking the functionals with the lower levels being less accurate and less computational expensive and the higher the functionals is on the ladder, the more accurate and the more computational expensive they get.

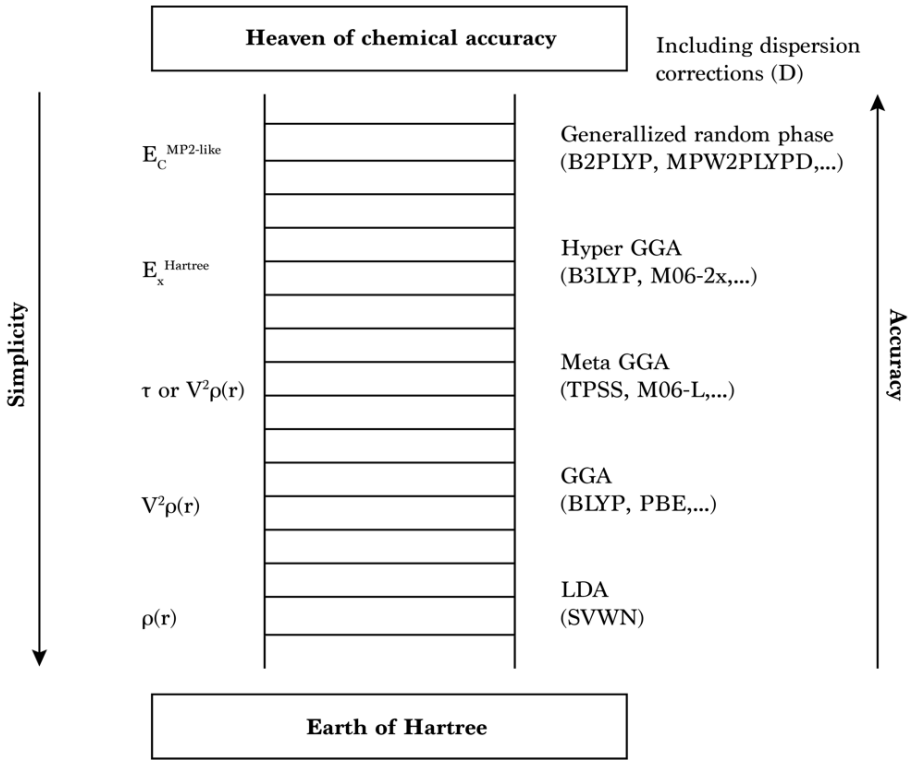

Figure 9 - The Jacobs ladder of functionals. The higher the functional is placed on the ladder, the more accurate and more computational costly the calculations will be, adapted from Perdew et al. 2005, [239] .

The Basis sets used in DFT is in general a set of atomic orbitals, which is representing all of the electrons in the molecule. A very simple form of a basis set contains the minimum number necessary for explaining the electrons in the molecule, e.g. the STO-3G basis set, which is a 3 Gaussian model for each orbital present, hence the 3 and G. A typically used type is the split valence basis set, e.g. 3-21G, which is more or less the double of all functions in the valence shell. Another example is the 6-31G** or 6-31G(d,p) basis set, which also is a split valence basis set. It uses one basis

function for each of the core orbitals, and two basis functions for each of the valence orbitals. Basis functions are in general a linear combination of gaussian functions, which are functions proportional to $\exp(-r^2)$ where r is the distance from the nucleus. The core orbital is modeled by a function that consists of 6 Gaussians, one of the two functions for the valence orbitals consists of 3 Gaussians, the other one Gaussian, this is indicated by 6-31. The polarization function for each atom, which is a function containing a higher momentum, is indicated by the ** or as a d for C, O atoms, etc. and a p for H atoms, indicating d and p-functions. The basis sets are thereby providing an expression for a wave function, and the more things that are present in the basis set, the more computational heavy the calculations will be, but it will also add more flexibility for the results and therefore a higher level of accuracy [97–99].

1.4.3. Solvation models and simulation of reduction potentials

Several of the studies presented in **Table 2**, were also considering solubility as a parameter for calculations. The computation of solvation or solubility is often considered as this is an important factor for RFB; the higher the concentration the more energy the electrolytes can uphold. Huskinson et al. 2014, [45] and Er et al. 2015, [79] present a method of computing the total energy difference between the molecules calculated in gaseous phase and aqueous phase, as described below:

$$\Delta G_{solv} = G_{gas} - G_{aq} \quad (6)$$

This was used as a descriptor of the solubility of the molecules, indicating that the more negative the solvation energy is the higher the solubility would be. To compute G_{aq}, a solvation model is however needed. There are two types of solvation models available;

Implicit solvation model: A simplistic model, where a molecule is simulated being in a solvent, where the dielectric constant of the solvent is used as simulation of the molecule being in solution. These models are often used when considering large numbers of molecules [84,98].

Explicit solvation model: A complex model where the molecule is placed in 3D and surrounding it numerous solvent molecules are placed. Various parameters have to be considered however, such as the number of solvent molecules surrounding the molecule of interest, and where and how many points of interactions should be examined. These model types are commonly used when specific molecules are investigated under specific conditions in a given solution. The models are often computation costly because of the high amount of molecules present in the simulations [84,98].

The study conducted by Dewar in 1969 [96], presented a model for correlation of experimental redox potentials of quinones versus calculated formation energies, ΔH_f. Forming following modified Nernst equation:

$$E^0 = -(nF)^{-1}\Delta H_f + b \quad (7)$$

This can be exploited to calculate the redox potentials for possible electrolyte candidates. Huskinson et al. 2014, [45] and Er et al. 2015, [79] used this as assimilation with the calibration curve correlation line presented in **Figure 10.** In the studies, they used six various basic quinones and experimental determined redox potentials. The entropy part of the energy is assumed to be equal for the quinone and corresponding hydroquinone, which is why ΔH_f, can be used instead of ΔG. The molecules were all simulated at 0K in gaseous phase with no solvation model.

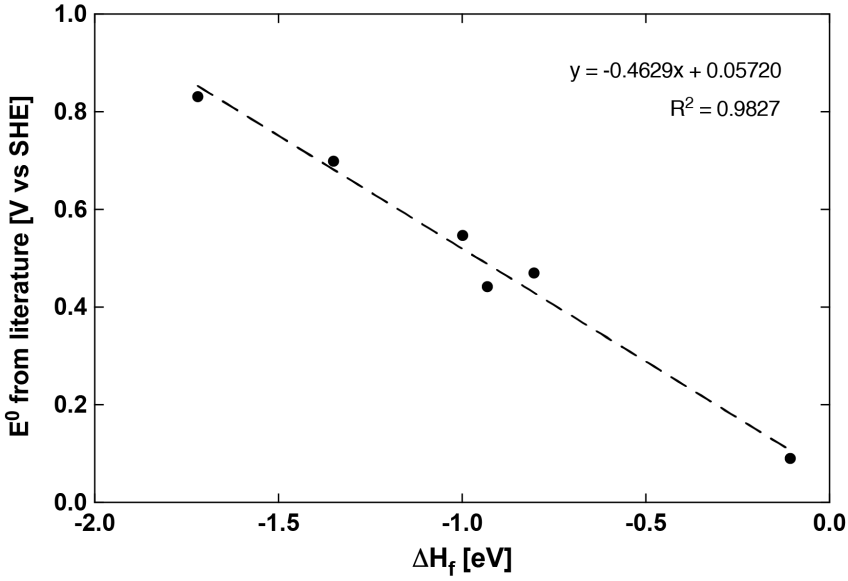

Figure 10 - Calibration curve presented in Paper 1, [236], of similar type used in the studies of Huskinson et al. 2014, [45] and Er et al. 2015, *[79]*. Literature provided the experimental redox potentials and the formation energies was computed.

1.5. Naturally occurring quinones

While the current focus of finding the optimal electrolyte-compounds until now has been limited to synthesized organic molecules, where different synthesize steps are needed to develop the best suited candidates, the quinone molecules are available and produced by natural sources. Quinones that occur in nature also include multiple

aromatic structures, similar to synthetically produced quinones, varying from the 1-ring BQs, to the NQs, AQs to the complex polyquinones [51,100–102].

In the majority of biological systems, the general quinones that are present can be limited to ubiquinones (2,3-dimetoxy-5-methyl-6-polyprenyl-1,4-benzoquinones), **Figure 11A**, which have a widespread presence in all mitochondria. Menaquinones (2-methyl-1,3-polyprenyl-1,4-napthoquinones), **Figure 11B**, are found in several types of bacteria. Plastoquinones (2,3-dimethyl-5-polyprenyl-1,4-benzoquinones), **Figure 11C**, which can be found present in the chloroplast, where the photosynthesis of plants occurs. All three types are mentioned as examples of the group of quinones, where functional side chain groups can differ depending on the specific organism. Some bacteria have proven to produce both the ubiquinones and menaquinones, whereas the majority of organisms are only producing one of the three types [103]. Interestingly, green plants have shown to possess ubiquinones in the mitochondria and plastoquinones in the chloroplast. The quinones acts as an electron transporter in cell membranes, where the addition of an electron creates the semiquinone or by two electrons forming dianion, that can occur in an equilibrium with the protonated form of the quinones [102–106].

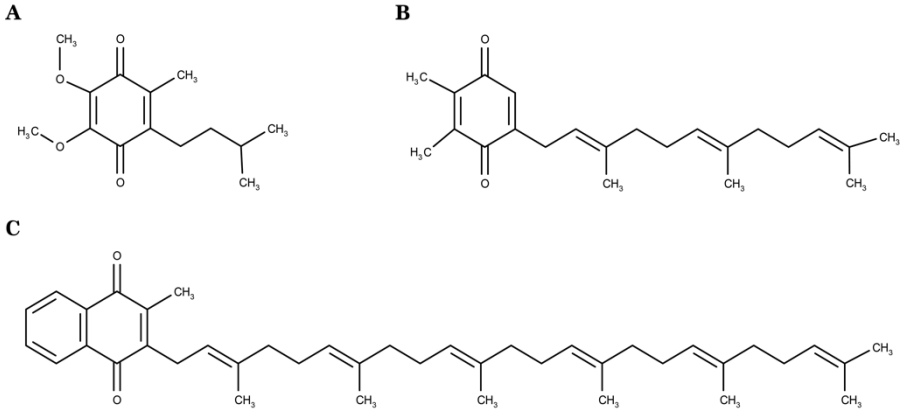

Figure 11 - Naturally occurring quinones, A) Ubiquinone, B) Menaquinone, C) Plastoquinone.

The occurrence of quinones in plants has been a point of interest for many years. In history, as far back as the Han dynasty, the use of rhubarb (*Rheum* spp.) as a medical plant was reported [107]. Anthraquinones observed in the rhubarb plant has since been investigated for treatment of cancer, inhibit bacterial growth and the inhibition of protein misfolding for use in the treatment of diabetes, where the quinones emodin, rhein, and physcion can be mentioned, **Figure 12**, [100,107,108]. In rhubarb, the anthraquinones have been determined to be a part of the defense mechanism against foreign microorganisms, where the plant produced the molecules in excess when exposed to elicitor-active chemicals [109]. The anthraquinones have also been utilized as pigments and components in dyes, where the antimicrobial properties of the quinones was discovered when thread was treated with the pigment and showed a

higher resistance tolerance towards bacteria. The studies relate the antimicrobial properties directly to the redox process occurring in the plant, where the quinones act an important part [110–112].

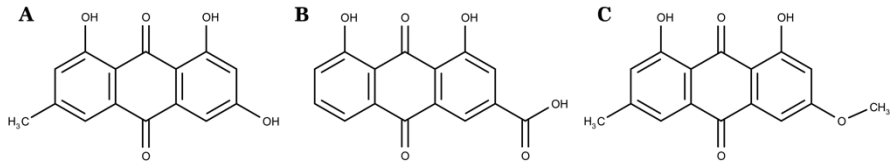

Figure 12 - Examples of anthraquinones observed in rhubarb; A) Emodin, B) Rhein, C) Physcion.

Ubiquinones and menaquinones have been found to act as important electron transfer agents in bacteria, being constituents of the plasma membranes. The mechanism has been studied in several projects and can be described as an important part of the electron supply chain in the mitochondria. The quinone is prone to electron and proton acceptance from the aqueous environment in the cell and because of this the quinone is able to diffuse through the mitochondria membrane and transport the electron to the next constituent of the respiratory chain. When this occurs, the protons are detached from the quinone yielding the oxidized form of the quinone, making the quinone ready for a second transport of electrons [102,105,106,113].
Similar to bacteria, ubiquinones and menaquinones are used for the electron transport in cell membranes in fungi. However, some organisms, just like the rhubarb plant mentioned, have other uses for quinone compounds. These quinones are produced as secondary metabolites, which is not a life-essential part of the organisms. Secondary metabolites have been researched in depth throughout the years, with one of the famous secondary metabolites produced by fungi being penicillin, produced by *Penicillium* and *Aspergillus* species [114].

1.6. Secondary metabolites

Secondary metabolites in general presents a structural diverse plethora of chemical compounds which can be attributed a wide array of biological activities [115,116]. Filamentous fungi represents a variety of molecules which include dangerous toxins and useful drug candidates [117,118]. The very specialized molecules are produced in the fungi for extending the ability of survival, where they can be used to fight of predators [119], combating other microorganisms, or act as protection against environmental changes in the surroundings of the microorganism [120]. The secondary metabolites are often produced with a high level of structural complexity, meaning that copying through chemical synthesis has been proven challenging if even possible [121,122]. Because of this, the molecules are often used as starting products or scaffolds in chemical synthesis which leads to an extended use for these products [123]. Fungal secondary metabolites have been utilized in the pharmaceutical industry

for several years and in 2009 β-lactam and cephalosporin antibiotics constituted the most comprehensive broad used antibiotics worldwide [124]. Several other secondary metabolites from fungal sources have found their way into the pharmaceutical industry, for use in cancer treatment an anti-tumor agent is found in aspergiolide [125], the compound cyclosporin, [126], is used for its immune suppressive properties, and lovastatin which is used as an cholesterol lowering treatment [127,128]. However, some secondary metabolites can cause severe loss of economics and affect humans harmfully, which is then monitored as mycotoxins in raw feed stock and food sources. These include the harmful potent carcinogenic aflatoxin [129], fumonisins [130], and ochratoxins [131].
The fungi genus of *Fusarium*, which is categorized as ascomycetes type, has been the subject of research due to the high impact on agricultures and health [132]. Many of the species are quite harmless, but types like *F. graminearum,* which is also called *Gibberalla zeae*, and *F. oxysporum* have been found to produce several mycotoxins and thereby damaging crops and harvest to an extend which lead to heavy economical losses [133]. The condition which is called *Fusarium* head blight has been considered one of the worst crop diseases and is caused by *F. graminearum* in Europe, Africa and Asia [134]. *Fusarium* genus concludes 100-500 species, [135], which like other eukaryote ascomycetes also have the ability of producing secondary metabolites [136]. The secondary metabolites produced by *Fusarium* represent a diverse collection of compounds which varies in structure and function. Usually, the molecules are formed by multi domain core syntheses after cooperation of different decorating enzymes in the compound specific pathway. The biosynthetic gene cluster is formed by the genes that encodes the enzymes and the core-synthase genes, which often are placed close together. Also genes coding for transport proteins and transcriptional regulators are found in these clusters [137,138].

1.6.1. Production of secondary metabolites

Secondary metabolites are biological synthesized by precursor monomer compounds similar to small chain carboxylic acids and amino acids yielding from the primary metabolism. The precursor molecules are then polymerized by enzymes called synthetases or synthase, and are often divided into three major groups; iterative polyketide synthases (PKS, type I and III), non-ribosomal peptide synthases (NRPS), and terpene cyclases (TC). The majority of secondary metabolites are produced via the PKS either reduced or non-reduced [139–141], where the quinones are produced as pigments, [142], via the PKS and is therefore the only part which is being investigated further in this thesis. The three predominant pigments found in the genus of *Fusarium* are bikaverin, **Figure 13A**, aurofusarin, **Figure 13B**, and fusarubin, **Figure 13C**, which also accounts for a group of molecules containing several quinone compounds such as bostrycoidin, javanicin, and 8-O-methylfusarubin as illustrated in **Figure 13C**. Different species of *Fusaria* produces the pigments as mycelial pigmentation in the perithecia [143,144], and some produce the pigments during the mycelial growth.

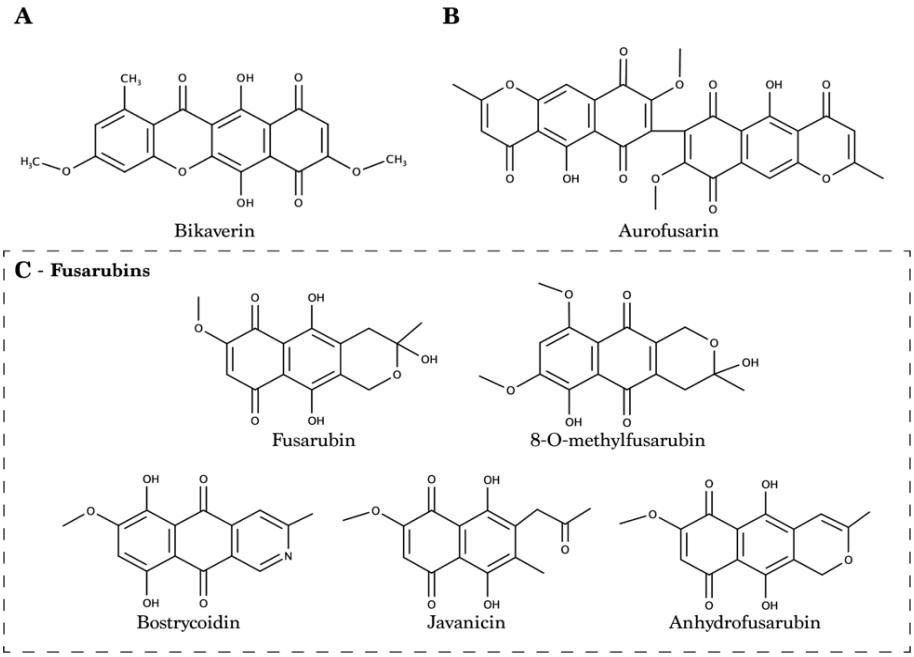

Figure 13 - Examples of some fungal pigments, A) Bikaverin, B) Aurofusarin, C) Fusarubins, which shows examples of key fusarubins.

The polyketide synthetic pathways are initiated by multidomain iterative PKSs, type I or III, which contain at least three core domains, β-ketoacyl synthase (KS), acyltransferase (AT), and acyl-carrier protein (ACP) which corresponds to the iterative cycle that elongate a polyketide chain with one ketide-group [145]. The synthesis will in general initiate with an acetyl coenzyme A (acetyl-CoA) molecule, which is elongated with a malonyl coenzyme A (malonyl-CoA) through the so called Claisen condensation, which is taking place in the KS domain [146].

Besides the three domains of KS-AT-ACP, there can also be various tailoring domains present such as reductase, methyltransferase, and dehydrogenase, that ensure chemical and structural diversity of the produced molecules [145,147,148]. The PKS type I, which accounted for the majority of PKSs in *Fusarium* [149], can be divided into two types. The reducing type, which results in fatty-acid like polyketides, and the non-reducing type, which is yielding in true polyketide structures. The polyketides produced as pigments of fungi are often synthesized by multidomain non-reducing PKS, which can be seen as the minimal fungal PKSs, only containing a KS domain, a malonyl-CoA, ACP transacylase (MAT) domain, and one or two ACP domains resulting in a carbon skeleton defined by several elongation steps[143,150,151].

1.6.2. Antimicrobial activity

A study performed by Søndergaard et al. 2016 [152], revealed that several of the pigmentation compounds and quinones produced by *Fusaria* possessed antibacterial properties against *lactobacillus* spp. and *Bifidobacterium* spp. They specifically showed that the *fsr* gene cluster or PKS3 in *F. solani* and also the PKS12 in *F. graminearum*, which produces the compound aurofusarin, was responsible for the antibacterial effects in the two organisms. The products of PKS3 are concluded to be the fusarubins and can be found is all genome sequenced species of *Fusarium* [143,144,149]. Several of the products, such as fusarubin and bostrycoidin, and the intermediates from PKS3 have shown other types of biological activities. This includes antimicrobial and antitubercular properties which was published by Shah et al. 2017 [153], where compounds such as fusarubin and javanicin were presented with these properties. Antifungal activity was demonstrated by Frandsen et al. 2014 [144], and cytotoxic activity towards cancer cells was shown to initiate from both naphthoquinones and the aza-anthraquinones published by Chowdhury et el. 2017 [154]. The study published by Khan et al 2018 [155], extracted several compounds including fusarubin, bostrycoidin, and anhydrofusarubin from *F. solani* and presented prominent cytotoxic activity towards several bacteria types and towards human leukemia cells.

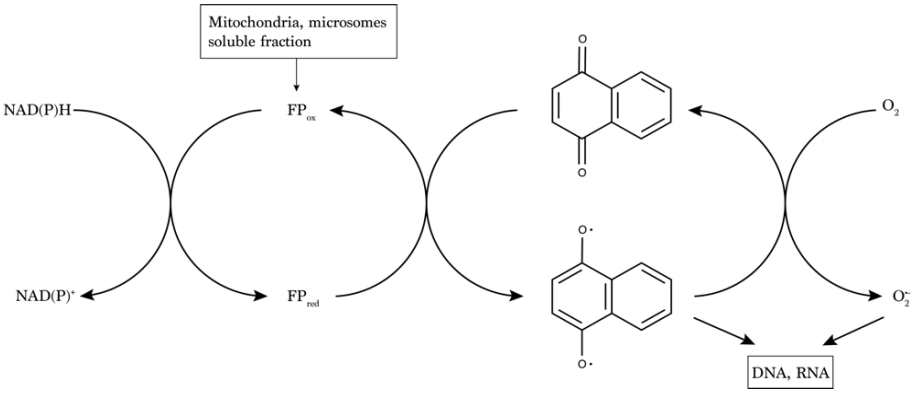

Figure 14 - Biomechanism of the cytotoxic activity of the fungal naphthoquinone compounds. The redox mechanism of the quinone, producing the semiquinone radical and the superoxides which can damage DNA and RNA of foreign organisms [157].

The antimicrobial and cytotoxic mechanism of the quinones have been researched and described by Medentsev et al. in 1996 and 1998, [156,157], and also by Futuro et al. 2018 [158]. The effects can be described as a stimulation of the cellular respiration and the oxidation of bacteria induce by the membrane NADH [155,159]. The biomechanism illustrated in **Figure 14** describes the involvement of the redox process from the naphthoquinones, which is induced by the mitochondrial NAD- and NADP dependent flavoprotein enzymes, resulting in the reduction of the naphthoquinone

which yields the semiquinone radical. These can react with oxygen and create superoxide molecules which together with the radicals can damage DNA, RNA, and other macromolecules [156]. This concludes the relation between the protective system of the organism and the redox process of the quinones, indicating that valuable information can be deducted from the redox potentials.

1.7. Regulation

As the secondary metabolites are not directly necessary for the organism to survive and not a part of the primary metabolism, the compounds are not produced continuously during the growth of the organism. The presence of the gene cluster does therefore not directly equal the production of the secondary metabolite. The secondary metabolism, is controlled by two main factors, pathway-specific transcription factors and global regulation factors [138,160].

The pathway-specific transcription factors covers protein structures which bind to a specific promotor sequence on the DNA stand of the cluster genes and hereby regulate the initiation of the transcription of the gene and, depending on the synthetic pathway, the production of a specific metabolite [160].

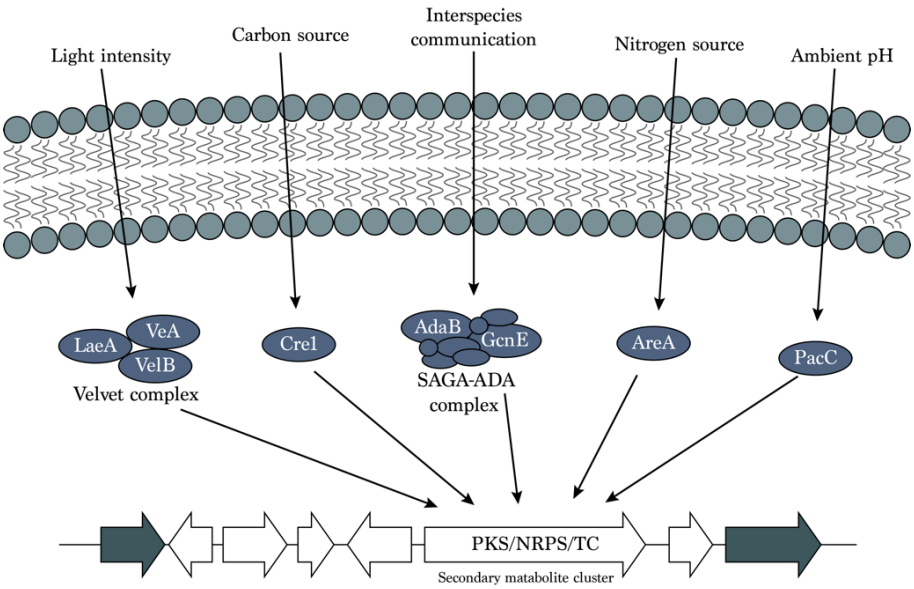

Figure 15 - Overview of global regulation factors, which can be defined as extracellular environmental factors and physiochemical conditions which activate the biosynthetic gene clusters, due to the regulatory protein activation [136].

The global regulation factors, **Figure 15**, include the biosynthetic response to the environmental influence on the production of secondary metabolites. More specific, the availability of growth conditional substrates such as carbon source and nitrogen

source, also the ambient temperature, pH, and light intensity exert influence on the secondary metabolism, as well as stimuli received from other organisms [136].

The availability and specific type of carbon source have been investigated for various organisms and proven to affect the production of the mycotoxins sterigmatocystin of aflatoxin in *Aspergillus* spp. Where simple carbon sources such as fructose, glucose, and sucrose as the only carbon source yielded high growth rates, sporulation and aflatoxin production ([161,162]), and more complex carbon sources such as galactose, xylose, and lactose did not yield production of aflatoxin [161–163]. This also corresponds with that fungal growth is favored in media types which consist of simple carbon sources such as glucose when compared to more complex types consisting of e.g. lactose, which are poorly metabolized by the fungi [164]. Also, the specific nitrogen source influences the production of the mycotoxins in *Aspergillus nidulans*. Nitrate as the nitrogen source has shown to repress the synthesis of aflatoxin intermediates in *A. parasiticus* [163], but enhance the production of sterigmatocystin in *A. nidulans* [165]. Different studies suggest that ammonium based media favors the production of the mycotoxins where nitrate based media shows a decrease in production [166,167]. In *F. fujikuroi* a repression of the gibberellin biosynthesis was shown due to the influence of nitrogen availability and type [168], as well as the production of fumonisin B1 in *F. vericillioides* [169]. Studt et al. 2012 showed that if the nitrogen source glutamine was substituted with sodium nitrate in a ICI medium, the pigmentation of *F. fujikuroi* would consist of fusarubins rather than bikaverin [170].

The pH regulator PacC activate different genes depending on the surrounding pH. This is interesting as the bacterial competition has been found to be more intense at alkaline pH. The fugal response is seen as the production of antimicrobial compounds, such as the regulation of the penicillin biosynthesis which is observed to be connected to the β-lactam antibiotics, exhibit higher toxicity to some bacteria at high pH [171]. The production of aflatoxin and sterigmatocystin has also been showed to be highly influenced by the pH of the media [172].

When fungi are cultivated close to another species, which lead to competition with regards to nutrition, the organism can be stimulated to enhance production of certain metabolites and mycotoxins, but also accelerate the rate of growth to outcompete the neighbor [173,174]. An example is *F. demicellulare* which, when grown together with competing organisms, enhances the production of furarutatin A which inflicts growth inhibition of the competitors and thereby enhances the growth conditions for the fungi itself [175].

The presence of precursor modules is also defined as a regulatory factor. It is implicit that if no precursor modules are present the PKS is unable to proceed and produce the desired molecules. The presence of acetyl-CoA is therefore assumed of importance to produce the polyketides. The prediction was investigated by Zhang et al. 2004 [176],

which showed that the various acetyl-CoA ratios could reduce and even terminate the production of polyketides in *Aspergillus nidulans* [138].

In order to find the optimal growth and secondary production conditions, many variations and combinations of media compositions were investigated, a common method to perform this is to use different cultivation parameters. The methodology is often referred to as the One Strain Many Compounds methodology or OSMAC [177,178]. The global regulation factors are important parameters to control when investigating the production of specific metabolites [179,180], and these highly influence the production depending on the specific components in the media which makes it possible to develop specialized media for production of specific metabolite [181,182].

1.8. Extraction and purification of naturally occurring quinones

Extraction or sample preparation of secondary metabolites is crucial for analysis of the specific desired molecules. Various methods have been investigated throughout the years, of which solvent extraction, liquid-liquid extraction, and solid phase extraction methods are the types most widely utilized [183,184]. Usually, solvent extraction is used for solid fermented fungi. Here, plugs are cut out from the fermentation agar media and an organic solvent or mixture of solvents is added. The submerged plugs are ultrasonicated or left to stand for some time, where the extraction then takes place from the solid to the solvent and can then be subsequently analyzed. In the study of Sørensen et al. 2014 [182], a mixture of solvents was used, acetonitrile/water/acetic acid in the ratio 79/20/1, and hereafter the samples were sonicated and the supernatant was spun down and analyzed using chromatography. The use of ethyl acetate has been widely used for solvent extraction of quinone compounds produced by *Fusarium* spp. In the studies of Khan et al. 2016 [185], Chowdhury et al. 2017 [154], and Khan et al 2018 [155], the plugs of the fermentation media are exposed to ethyl acetate in three stages where the three batches are then pooled and concentrated for optimal extraction yields.

In 1997 Smedsgaard published an article describing a Micro-scale extraction procedure for standardized screening of fungal metabolites [186], which uses a mixture of ethyl-acetate/dichloromethane/methanol in the ratios 3:2:1, including 1% v/v formic acid. This method has later been used by several other studies [152,182,187]. But as the name of the procedure indicates, the solvent extraction methology is used for small scale experiments where the quantity of the desired molecules is not important but rather the occurrence of the compounds.

When the amount of a desired molecule is important, and the optimization of production, yields of extraction etc. need to be accounted for, the usual method for cultivation of fungi, with respect to production of secondary metabolites, is the submerged fermentation or liquid fermentation. This fermentation type yields larger quantities of secondary metabolites in general, however the plethora of produced secondary metabolites can vary due to the environmental change going from solid state fermentation to liquid state. In general liquid-liquid extraction, LLE, can be explained by the transfer of desired compounds from one phase to another, when soluble and immiscible compounds are in contact with each other. The method is widely used and is seen as being simple and being of low cost compared to other extraction types. Conventionally a two-phase system is applied consisting of a water phase and an organic phase, **Figure 16A**, [184].

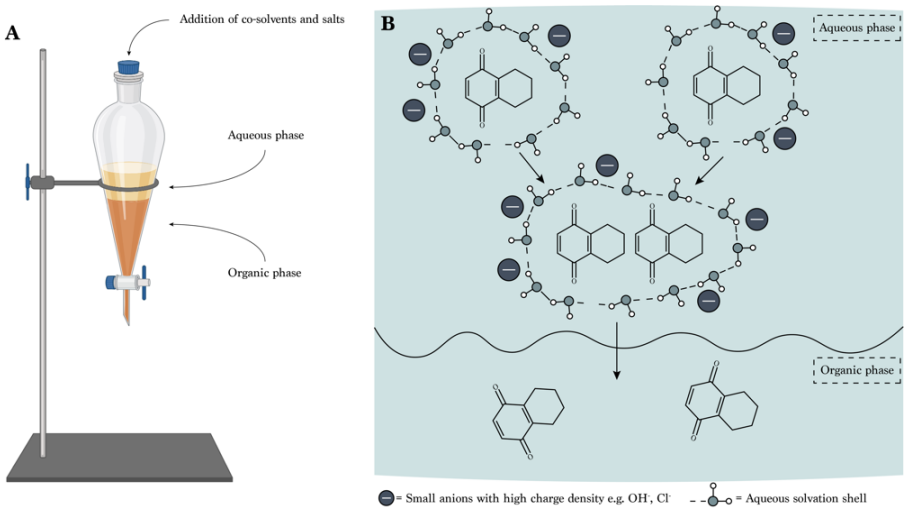

Figure 16 - Liquid-Liquid extraction. A) LLE laboratory setup, B) Salting out principle, [180].

The distribution of a desired compound between the two phases can be described by the partition coefficient, K_D.

$$K_D = \frac{[A_{org}]}{[A_{aq}]} \tag{8}$$

Where $[A_{org}]$ indicate the concentration of a compound A in the organic phase and $[A_{aq}]$ indicate the compound A concentration in the aqueous phase. The organic solvent used in LLE is of great importance to which compound that can be extracted and to what extent. There are several molecule interactions which should be considered when choosing the solvent. When only considering extraction properties and not e.g. safety when handling, hydrogen bonding donor/acceptor properties and dipole interaction properties of the solvents are seen as the primary parameters. A

common way to illustrate these parameters is to use the Kamlet and Taft solvatochromic parameters α, β, π*, as indicated in **Table 3,** [188].

Table 3 - Overview of some organic solvents and their Kamlet and Taft solvatochromic parameters, [188].

Solvent	α	β	π*
Nonpolar solvents			
Cyclohexane	0.00	0.00	0.00
Aromatic Solvents			
Toluene	0.00	0.11	0.54
Dipolar solvents			
Dichloromethane	0.13	0.10	0.82
Ethyl acetate	0.00	0.45	0.55
Hydrogen bonding donor solvents			
Chloroform	0.20	0.10	0.58
Hydrogen bonding acceptor solvents			
Diethyl ether	0.00	0.47	0.27

The α-value indicates the hydrogen bonding donor properties, where a high number illustrates that the solvent is prone to act as a hydrogen bonding donor. This means that solvents with a high α-parameter are desired when extracting basic compounds, and hereof is solvents like dichloromethane and chloroform often used. The β-value is the hydrogen bonding acceptor parameter, and therefore indicates the tendency of a solvent to act as a hydrogen bonding acceptor; the higher the number, the higher the tendency. Solvents showing a high β-value are desired when compounds containing acidic functional groups are extracted. The π*-parameter is the dipolarity-polarization of a solvent, and indicate the tendency of the solvent to interact through dipole and dispersion interactions. A high π*-value solvent is a desired solvent for polar compounds [188]. If solvents possess high values in several of the parameters they are usually considered strong solvents and is often used for LLE.
Ethyl acetate was used in LLE by Awakawa et al. 2012 [189], to extract fusarubin and bostrycoidin from the sexual form of *F. solani, Nectria haematococca.* Here, the fermentation broth was exposed to HCl prior to extraction to ensure fully hydrolyzed compounds to control the extraction. Similar approach was used by Shah et al. 2017 [153], but the LLE was conducted by addition of ethyl acetate over three times, and collecting the organic phases together and then evaporating to dryness.

In 2005 Mendentsev et al. published a study on the biosynthesis of several of the naphthoquinones produced by *Fusarium* spp. In this study an LLE method is presented where the solvent used is chloroform. The compound aurofusarin was

extracted from the mycelia using acetone and ethanol, combined with chloroform, where after the extracts was dried and separated using plates containing silica gel. Menezes et al. 2020 [190], showed that the addition of chloroform in ratios 1:1 v/v could be used to extract pigments from crude extracts of *F. solani.* The investigation of chloroform as the solvent for extraction was also utilized by Kurobane and Vining, where different metabolites of *F. solani* and the production hereof was published. The paper also contains a second extraction method where ethyl acetate was used for extraction of large volumes above 1L media [191]. This corresponds with the fact that chloroform is toxic and should be substituted if possible when handling large amounts of extracts. A mixture of chloroform and methanol in the ratio 1:1 was applied to the liquid fermentation broth which prior to exposure had been filtered through filter paper, in the study of VanderMolen et al 2013, [192], which had the purpose of evaluating different media composition for the production of secondary metabolites.

The addition of a third constituent in the LLE matrix, such as salts, can result in modification of the intramicellar and intermicellar interactions where water molecules form a boundary layer around the organic molecules and thereby enhances the solubility in the aqueous phase. By adding salts to the solution the salt ions will interact with the water molecules, which then leads to the organic molecules having higher affinity to the organic phase and will then be transferred to this phase, **Figure 16B**, [184,193,194]. The salting out principle has been utilized in the study of Westphal et al. 2018 [195], where aurofusarin was extracted by LLE using chloroform as the main solvent, and methanol and co-solvent, which enhances the crossover between the boundary layer between the two phases, and addition of NaCl for salting out the compounds to the organic phase. The salt was added after discarding of the majority of the aqueous phase. This method have also been used for extraction of fusarubins from liquid fermentation broths containing mutant stains of *F. solani* by Nielsen et al. 2019 [196], and also for extraction of fusarubins from liquid fermentation of heterologous expressions in yeast by Pedersen et al 2020 [197] (paper 5). The method was optimized and adapted in the paper by Kristensen et al 2021, (paper 2) [198], which resulted in methanol and NaCl was added twice to the solution to avoid unclear separation of the two phases. Also, to optimize the yield of the extraction by adding the NaCl before the aqueous phase was removed, allowing the leftover quinones in the aqueous phase to be drawn to the organic phase instead of simply discarding it. The substitution of chloroform for ethyl acetate was investigated, but the yields were somewhat lower and because ethyl acetate possesses higher solubility in the aqueous phase the separation of the phases was also not as sufficient as when using chloroform.

Lastly, some studies uses solid phase extraction, SPE, where liquid fermentation broths are being added to columns containing C-18 silica gel, and based on the affinity to the column contra mobile phase, specific compounds can be eluted through the column [143,199]. Using both solvent extraction of plugs with ethyl acetate, and LLE also containing ethyl acetate, and a purification step utilizing SPE, the study of

Frandsen et al 2016, [144], shows the versatility of extraction procedures which can be optimized to extract specific molecules and simultaneously yield samples containing high purity.

1.9. Large scale separation of fungal quinones

Because of the heavy use of harmful chemicals, like chloroform, in the extraction procedures, it can be hard to find a sustainable and safe extraction method to perform when the production of metabolite is scaled up to feed the industry or for electrolytes in RFBs. To solve this, pressure-driven membrane technologies have been introduced as a potential technology for pretreating, concentrating, and separation of metabolites originating from fermentation broths. Membrane filtration technology has been used to obtain concentrates which have been enriched by vitamins such as vitamin C [200], and also for extraction of pigments such as betaxanthines and betacyanines [201,202], and various sugar types such as sucrose, fructose and glucose [203]. Membranes have traditionally been used for size based separations for high-throughput operations and normally consist of microfiltration (MF), ultrafiltration (UF), nanofiltration (NF), and reversed osmosis filtration (RO) [204]. Membrane filtration have also been proposed for other types of selective separations, such as water treatment and remediation [205] and separation of gases [206]. The process of membrane filtration allows the separation of compounds and containing them in liquid solution e.g. fermentation broths. Examples of purification of compounds using membrane filtration could be molecules in and for the food industry which includes isolates from fruit and juices [207,208].

1.9.1. Membrane based separations

In general, the membrane is a semipermeable barrier which allows certain compounds the possibility to transfer across in a bulk solution. This splits the feed solution into two different streams, retentate, which is retained by the membrane, and the permeate, which is allowed to permeate through the membrane due to the molecular weight cut off (MWCO) [209]. The MWCO can be defined as molecular weight equivalent to the weight of the smallest molecule which would achieve 90% rejection of the membrane [204]. In classical membrane filtration the MWCO is directly linked to the pore size of the membrane, and typically the membranes are ranked as follows; MF (100-10,000 nm), UF (2-100 nm) and NF (0.5-2 nm) [210]. The general mode of operating membrane filtration can be divided into two types, crossflow filtration, **Figure 17A**, and dead-end filtration, **Figure 17B.** In crossflow filtration the feed solution is flowing in parallel to the membrane and permeates through due to pressure difference, this allows the fouling of the membrane to be kept at a minimum. In the dead-end filtration the feed is flowing directly towards the membrane, which can lead to membrane fouling [204]. The dead-end type is more commonly used in sterile filters, where an example is when 0.2 μm filters was applied to remove bacteria of the type *Brevundimondas diminuta* [211].

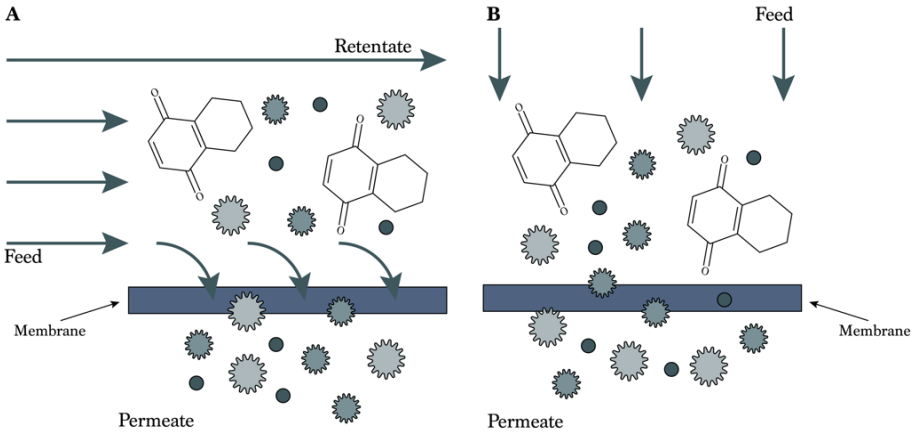

Figure 17 - Membrane filtration operation modes, A) cross-flow filtration, B) dead-end filtration

Because of the chance of the membrane fouling, the crossflow filtration mode is often used in the industry compared to the dead-end operation mode. However, the performance of all membranes are gradually affected by the fouling that is generated during filtration [212]. Fouling can be defined as the gradually deposition of inorganic and organic constituents in the pores and on the surface of the membrane. It depends entirely on the nature and composition of the feed solution whether fouling phenomenon occurs and to what extent it happens. Fouling can occur in four individual types which accounts for the complete blockage of the pores, filter cake formation, partial blockage of the pores and internal blockage of the pores, where some are more reversible than others [213]. The fouling condition of the membrane can be measured by the permeate flux of the membrane. The permeate flux can be defined as:

$$J = \frac{Permeate\ volume}{Membrane\ area * time} \tag{9}$$

And has the unit L m^{-2} h^{-1}, and indicate the flow through the membrane over time. Thereby will a decrease in the flux indicate the gradually forming of filter cake and fouling [214].

MF membranes was used to concentrate and purify exopolysaccharides from the red algae *Porphyridium cruentum* by Balti et al. 2018 [215], where several cross-flow velocities were investigated and the yielded permeate fluxes corresponded with ascending cross-flow velocities. In 1975, Knuckels et al. presented removal of a green pigment from Alfalfa juice, which was successfully carried out by membrane filtration. Also off-flavors and different small molecules was removed by the UF membrane applied in the study [216]. UF dead-end filtration was applied by Juang et al. 2012 [217], to fermentation broths containing the bacteria *Serratia marcescens* and

the recovery of the compound and pigment prodigiosin was studied. The flux in this study was measured to be high and therefore an additional filtration was proposed, so the first filtration was carried out with 80% recovery and thereafter a secondary filtration should be initiated. The recovery of surfactin from fermentation broths has also been investigated several times where UF membranes have been utilized to remove and recover the compound [218,219]. NF has been applied to separate amino acids from fermentation broths, such as the study of Li et al 2003 [220], where L-glutamin was separated even though the experiments showed that the separation was highly depended on the pH of the fermentation broth. Separation trains of UF and NF membranes are widely used for fermentation broth as well. In the study of Lee et al. 2017 [221], an UF membrane step is utilized to remove microbials where after a NF step is followed to remove glucose from the fermentation broth. After the filtration steps an ion exchange membrane and evaporation is used to purify the lactic acid to 99.5%. A membrane filtration combination has also been utilized in the study of Zagklis et al 2015 [222], where phenolic compounds found in grape marc, which is the solid waste bi-products produced in wine production, is being purified. The results showed that the combination of UF and NF membranes could be utilized for this purpose. Similar progression method was used in the study of Conidi et al. 2015 [223], where the media was wastewater from artichoke preparation, which was driven through UF membrane step and the permeate of this was submitted to a NF step producing a highly concentrated fraction which contained high amounts of the desired phenol compounds. Zhu et al. 2017 [224], presented a multi stage recovery process of pigments from seeweed. Where prior to the membrane filtration step, the plant was exposed to an ultrasonic extraction step. The following UF step resulted in the pigments being retained from the membrane which possessed of 5 kDA MWCO, whereas the 10 kDA MWCO UF membrane permeated the pigments. The versatile use of membrane filtration is therefore seen as a viable solution for largescale separation of quinones produced by fungi that can be scaled, combined, and specially designed for the individual specific compounds.

1.10. Electrochemical assessment of naturally occurring quinones

To investigate if the extracted quinones can be utilized in an actual RFB setup, several assessments need to be performed. These include, among others, electrochemical reduction potential assessment and electrochemical stability over time and cycles. The main method to study and visualize electron transfer processes such as redox reactions is voltammetry. Voltammetry is a broad group of different techniques used for studying current and voltage in electrochemistry. Cyclic voltammetry is widely used for reversible systems as redox couples because, as the name implies, it is performing voltammetry in cycles. Normally a linear sweep potential is applied to the electrodes and when the desired potential is reached the sweep is reversed and the potential is returned to the initial value [225]. The electrochemical cell is constituted as a three-electrode electrolysis cell, **Figure 18A**, which consist of a working electrode (WE), a counter electrode (CE), and a reference electrode (RE) which ensures that the currents

and potentials which are measured are constant and measurable. The linear sweep is then initiated by applying an excitation potential, often seen as a triangular wave form, to the WE which is referenced to the RE. This enables the current which flows between the WE and CE to be measured [225,226]. The result of a CV analysis is a voltammogram. In **Figure 18B** the resulting voltammogram of the CV analysis of a crude extract containing Phenicin is visualized. The analysis was performed in 1M KOH with a carbon rod electrode and Ag/AgCl RE and only one cycle is visualized. It is seen that the analysis has been cycled between -1.0 and 0.5 V and the resultant current have been plotted accordingly. At -0.4V the oxidization of Phenicin is occurring leading to the anodic peak, E_{pa}, of which the amount of molecules surrounding the electrode has been oxidized. Because of the only mass transport to the electrode occurs as diffusion when using a rod electrode, it is only the surrounding molecules which react. If additional mass transport is desired, a rotating disc electrode can be applied [225,227]. The fully oxidized Phenicin molecule is illustrated in the right side of **Figure 18B**, and when the potential reach 0.5V the sweep is reversed. Around -0.3V a decreasing peak is seen, indicating the reduction of Phenicin, leading to the cathodic peak, E_{pc}, where the surrounding Phenicin on the surface of the electrode is fully reduced. The potential is decreasing until the -1.0 V where the cycle is repeated several times to investigate potential irreversibilities, which would visualize as a decreasing peak in either the anodic or cathodic peak or an increased separation of the peaks. Often an irreversible reaction is mentioned as a slow occurring electron transfer, which will drag out the separation of the peaks in the voltammogram, and the peaks will also often seem less steep than for a fully reversible redox couple [228].

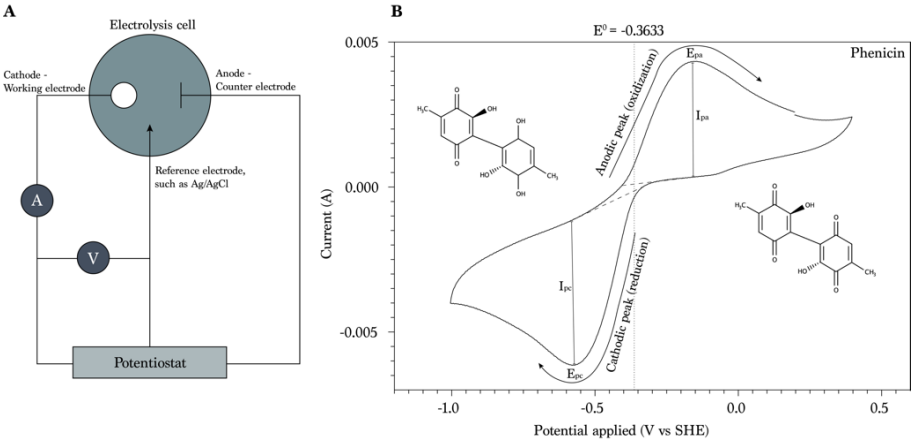

Figure 18 - Electrochemical characterization using cyclic voltammetry, A) voltammetry cell set up, [240], B) Voltammogram of the quinone Phenicin, indications of oxidization and reduction peaks and peak heights, as well as the reduction potential has been highlighted.

The potentials found in the analysis can be described using the Nernst equation;

$$E = E^0 + \frac{2.3RT}{nF} * \log(Q) \quad (10)$$

Or at 25°C or 298K;

$$E = E^0 + \frac{0.059}{n} * \log(Q) \quad (11)$$

Where E^0 is the standard reduction potential of the investigated redox active compounds, *n* is the number of electrons involved in the reaction, and *Q* describes the relationship between the concentrations of the redox couple. If the expression of Q equals 1 and the two species is equal in concentrations, a rapid increase can be seen in the voltammogram indicating either the oxidization or reduction of the species [225–227].

To illustrate the use of the formula, the following has been made to account for the redox reaction visualized in **Figure 18B**, where n is assumed to be two.

$$E = E^0_{Phenicin_{ox}/Phenicin_{red}} + \frac{0.059}{2} * \log\left(\frac{[Phenicin_{ox}]}{[Phenicin_{red}]}\right) \quad (12)$$

The two peaks for the anodic peak, E_{pa} and cathodic peak E_{pc}, is used for calculating the redox potential of the species, and is found as an average of the two peaks, and when the peaks are equal in height the reaction is determined to be reversible [227];

$$E^0 = \frac{E_{pa} + E_{pc}}{2} \quad (13)$$

When measuring the current, a RE is used and to unify reported data, a conversion is often needed. Often the RE used is Ag/AgCl as this is inert in most cases. The Ag/AgCl RE can be converted to SHE by adding 0.197V, which corresponds to the difference between the two.

Additional information can be determined from a voltammogram, which is the diffusion coefficient. For this, the current peaks I_{pa} and I_{pc} are utilized, and these are for a reversible reaction proportional with the concentration of the species and the square root of the scan rate, and can be derived as following at 25°C or 298K [228];

$$I_{pc} = (2.69 * 10^8) n^{3/2} A C D^{1/2} v^{1/2} \quad (14)$$

Where *n* is the number of electrons in the half-cell reaction, *A* is the surface area of the electrode in m^2, *C* describes the concentration in mol/L, *D* is the diffusion constant in m^2/s and *v* is the scan rate measured in V/s [227,228].

The CV analysis has bene widely utilized for determination of redox potentials of quinones. The study of Lin et al. 2015, [49], investigate the 2,6-

dihydroxyanthraquinone (2,6-DHAQ), together with the metal cyano complex redox couple $Fe^{III}(CN)_6^{3-}/Fe^{II}(CN)_6^{4-}$, and determines redox potential and thereby cell potential for the RFB electrolyte couples. Similar methologies are used in the studies of Huskinson et al. 2014 [45], and Kwabi et al. 2018 [63], to mention some examples, where synthetic quinones are investigated in both acidic and alkaline pH.

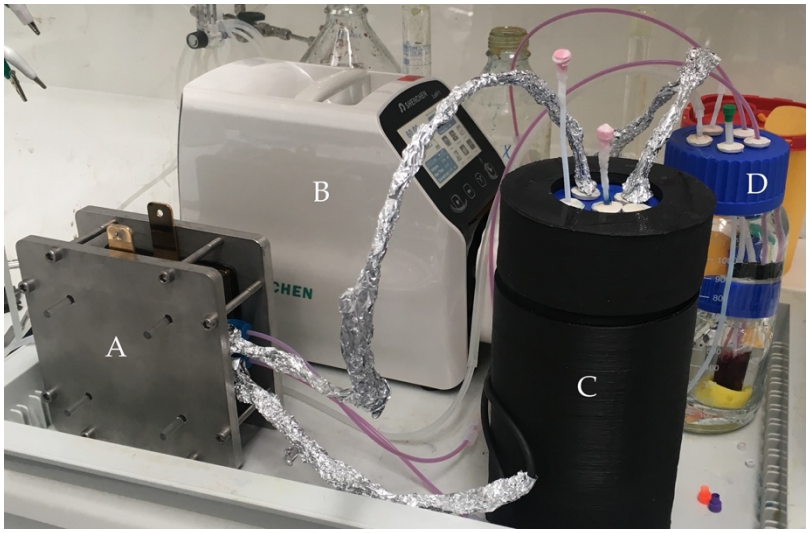

Figure 19 - Initial flow cell cycle test set up. A) Flow cell, B) Peristaltic pump, C) Catholyte tank, submerged in water, and covered for light protection. D) Anolyte tank, also submerged but not screened off in this picture.

The next step in the assessment of the quinone compounds potential in an RFB set up, **Figure 19**, is stability test in an actual RFB cell. The electrolyte tanks have been submerged in water in sealed compartments, which is then purged with nitrogen for 10 mins to ensure oxygen control during the experiment. Usually a cycle test is performed to evaluate the cell potential, capacity, the fading ratios, and efficiencies of the electrolytes. In **Figure 20** such a test is visualized for a preliminary experiment of the compound phenicin, where a crude extract was submitted to a cycle test of 20 cycles. The charge/discharge cycles are illustrated in **Figure 20A,** where the voltage is seen to be cycled between 0.6 V and 1.6 V as the cut off voltages, similar to the study of Lin et al. 2015, [49]. The results will be explained later in the thesis. However, it can be seen that the time for charge/discharge is decreasing which indicates a capacity drop. **Figure 20B**, indicates the capacity vs voltage plot which illustrates the decreasing capacity per cycle.

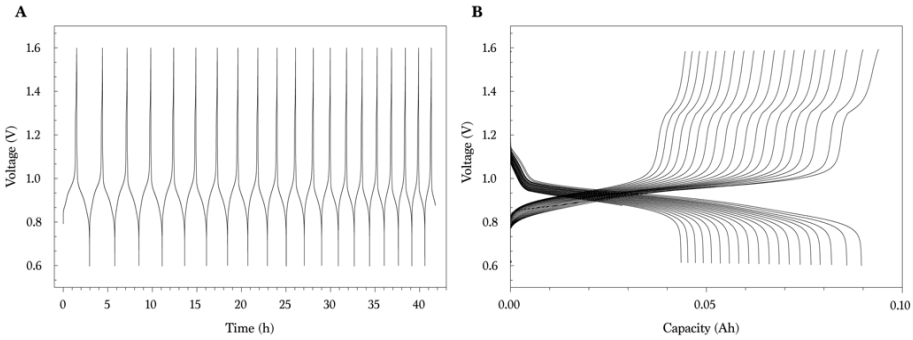

Figure 20 - Redox flow battery test of crude extract of Phenicin, preliminary results; A) cycle test including 20 cycles, B) voltage vs capacity plot of the 20 cycles.

Secondly, various other parameters indicating RFB performance are often presented, which includes current efficiency or columbic efficiency (CE) which is a measure of ratio between the discharging and charging charges retrieved during discharge/charge. The current efficiency can be described as;

$$CE = \frac{\int_0^{t_d} I_d dt}{\int_0^{t_c} I_c dt} \tag{15}$$

Where I_d is the discharge current and I_c is the charging current. Usually, a stable RFB will possess CE of 90-99% and when the CE is lower than 90% it could indicate crossover through the membrane between the two compartments and the CE increases corresponding to the current density used in the experiment [229,230]. The CE can also be written as following, which is more commonly used when performing experiments;

$$CE = \frac{Discharge\ capacity}{Charge\ capacity} * 100\% \tag{16}$$

The voltage efficiency (VE) are likewise used as a parameter to assess the performance of an RFB cell. The VE is associated with the current density, ionic conductivity of the membrane used, and the electrodes, as well as the electrolytes mass transport and the flowrate. The VE is described as;

$$VE = \frac{Avarage\ discharge\ voltage}{Avarage\ charge\ voltage} * 100\% \tag{17}$$

The energy efficiency (EE) is also a parameter commonly used, which indicates the product between the CE and VE and explains the capability of the RFB to store energy and is viewed as one of the most important parameters in battery testing. If the current is increased, the EE usually decreases [231,232].

$$EE = CE * VE \tag{18}$$

The energy density is a measure of how much energy a battery can store in a certain amount of electrolyte. The Energy density for RFBs is usually lower than the parameter for e.g. Lithium ion batteries [233]. The Energy density can be explained as;

$$ED = E_{cell} * Capacity \quad (19)$$

Cell testing is the predominant way of reporting new chemistries performance in an RFB setup, and thereby their potential as new electrolyte. Because of this, several studies are presenting data for cell cycling and performance of quinones in RFBs, such as Lin et al. 2015, [49] which presented the 2,6-DHAQ versus $K_4Fe(CN)_6$ alkaline flow battery possessing a cell potential of 1.18V vs SHE, showing a power density of 0.4 W cm^{-2}, and EE of 84% and CE of 99% over 100 cycles. Huskinson et al. 2014 [45] presented the AQDS vs HBr acidic flow battery with a cell potential of 0.85V vs SHE, and a capacity retention of 99% or 0.1-0.2% capacity fading per day. The power density was determined to be 0.6 W cm^{-2} which is higher than the one presented in the alkaline media, however the CE in this study was 95%. Kwabi et al. 2018 [63] presented a flow battery containing 2,6-DBEAQ and $K_4Fe(CN)_6$ in alkaline solution. The battery possessed a cell potential of 1.04 V vs SHE, a capacity fading ratio of 0.001% per cycle or less than 0.01% per day, the energy density was listed to be 12 Wh/L at pH 14, and the CE was found to be 99%. Khataee et al. 2018, [234] showed results from a flow battery containing ADQS and HBr as well, with a capacity loss of 0.026 per cycle and a power density of 0.4 W cm^{-2} as well, also in this study the CE was determined to be 99%. Wedege et al 2016, [235] presented a study on AQDS as well but coupled with $K_4Fe(CN)_6$ showing a cell potential of 0.74 vs SHE, and a capacity of 275 Ah, and possessing an EE of 75% and CE of 99%. In 2019 Sun and coworkers, [61], presented a flow battery which consisted of DMBQ and $K_4Fe(CN)_6$ which had a cell potential of 1.2 V vs SHE. The peak power density was shown to be 182.6 mW cm^{-2} for their setup, and EE was found to be between 73-80% and the capacity determined to be 86.7% of the theoretical capacity of 192.4 C, they present a CE of >98% for 200 cycles. In 2020 Yang and coworkers, [69], presented a mixed symmetric flow battery cell consisting of iron sulfate and AQDS in acidic solution. The cell potential was determined to be 0.62 V vs SHE. The capacity fading ratio was shown to be 7.6 $*10^{-5}$ % per cycle or $1.2*10^{-4}$% per hour. The CE was shown as 99.63% for their experiments. It is clear to see that flow batteries possessing lower CEs than 95% is barely relevant for further investigations, as the competitors are already beyond this. The capacity fading ratios are also good indicators for the electrolytes, if the capacity fading is high, it is not likely that the system of electrolytes is fitting for larger scale applications.

Chapter 2. Summary of results and discussions from papers

This section will consist of a summary of the results and discussions from the three primary research papers and the preliminary results of electrochemical characterization of the quinones phenicin and bostrycoidin;

- Simulation of electrochemical properties of natural occurring quinones (**Paper 1**, published in Scientific Reports)
- Production and Selectivity of Key Fusarubins from *Fusarium solani* due to Media Composition (**Paper 2**, published in Toxins)
- Membrane based separation and purification of fusarubins from *Fusarium solani* (**Paper 3**, published in Separation and Purification Technology)
- Initial findings that founded the manuscript; "The fungal battery: A redox flow battery containing the biosynthesised negolyte phoenicin" (**Paper 4**, in draft)
- Preliminary assessment results of the quinone Bostrycoidin (Unpublished results)

2.1. Simulation of electrochemical properties of natural occurring quinones

The redox potential of quinones can be directly linked to the microbial activity of the organisms of which produces the specific compound [152,156]. In addition to this, the field of quinones of synthetic and artificial origin has been investigated in great detail for the optimal structure to use in a RFB system, where computational methods have been used extensively to screen for potential candidates [45,58,79,83,235]. However, no study until now have been concerned about the quinones of which occur naturally and potentially can be produced in a cheaper and more sustainable way compared to synthetically manufactured quinones which origin comes from by products from the crude oil business. The main purpose of this paper is therefore to try and answer the research question "Which of the already known naturally occurring quinones is the best suited for use in a redox flow battery, and where are they to be found, and which parameters are used to determine this?" This study serves therefore as a broad screening of naturally occurring quinones, with respect to the microbial activity or redox potential and the solubility of the compounds, and can be utilized as guide in the biotechnology industry and in further research and development of electrolytes for RFB systems. The study methology was adapted from the studies of Huskinson et al. 2014 [45], and Er et al. 2015 [79], and further visualized in **Figure 21**. The 990 different quinones originate from various sources and we have divided them into three groups where 221 are produced by bacteria, 358 are produced by fungi, and 425 are contained in the group named other which includes organisms such as yeast, algae, and plants etc. It was found that the predominance of the quinones was located within the boundaries of redox potentials of -0.4 V and 0.7 V vs SHE, where the extreme boundaries was concluded to be -1.382 V and 1.485 V vs SHE. The distribution yielded a slight skew towards the left [236].

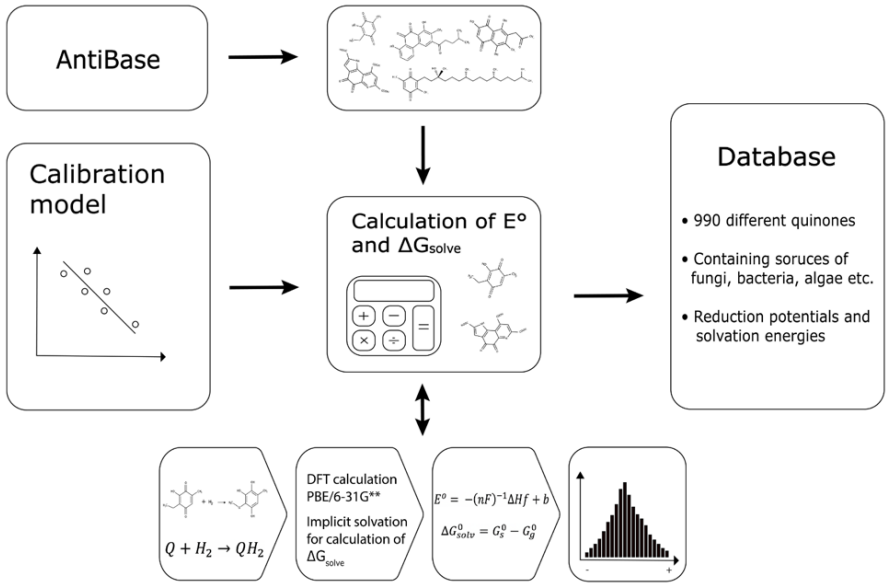

Figure 21 - Work flow of the simulation and screening study of naturally occurring quinones. The database was compiled by 990 different quinones found in Antibase, which all was exposed to the computational methodology of calculating E^0 and ΔG_{solve}, based on the calibration curve presented previously [236].

Secondly, the quinones were divided into BQs, which contained 276 different compounds, NQs, which consisted of 209 quinones, AQ which was composing the largest group of 411 compounds, and then a group which contained quinones with 4 or more rings that concluded the smallest group of 94 compounds. The distribution of E^0 based on the number of rings in the quinone revealed that the BQs was with a median of 0.4970 V vs SHE the most positive group, followed by the 4 or more rings structures, which possessed the largest distribution however a median of 0.3040 V vs SHE. The NQs yielded a mean value of 0.2340 V and a median of 0.2870 V vs SHE. The group showing the lowest distribution was the AQs, concluding a mean of 0.0024 V and a media of 0.0119 V vs SHE. Similar tendencies were seen when solubility descriptor ΔG_{solve} was plotted versus the E^0, which confirm the hypothesis of higher aromaticity thus lower reduction potential. Only marginal variations were found in the solubilities of the quinones based on aromatic rings and size of the compounds, and indications of dependency of occurrence of polar side chain groups was seen [236].

To investigate and illustrate the distribution of the quinones based on the three major groups **Figure 22** was composed. In **Figure 22A** the distribution of quinones with bacterial origin is visualized. The most positive E^0 is seen to be present in this group

however, the distribution of the E^0 is limited to the central boundaries, with only a few extreme values, which could be potential candidates as electrolytes in an RFB system. The distribution of quinones with origins from fungi is illustrated in **Figure 22B**, and it is seen that majority of the extreme values of E^0 is to be found in the realm of fungi. This groups exhibit therefore the largest potential of new candidates for use in an RFB system. the last group, other is illustrated in **Figure 22C**, and shows no sign of extreme E^0 values, and is therefore of limited interest for potential candidates of electrolytes for use in an RFB [236].

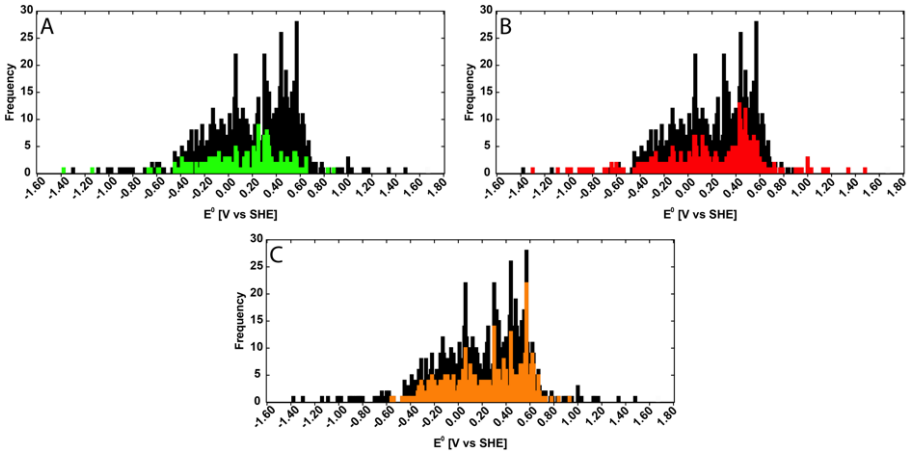

Figure 22 – Distribution of naturally occurring quinones divided into the three major groups of origin; A) Bacteria, B) Fungi, C) Other, which contains organisms as yeast, algae and plants etc. [236].

In the paper, [236], the seven quinones possessing the most positive redox potentials were presented and concluded that all of these quinones was produced by fungi, where *Fusarium* spp. and *Penicillium* spp. was dominant, **Table 4**. Tridentoquinone was found to possess the most positive redox potential of 1.485 V vs SHE, however the compound showed a relatively low solubility as the ΔG_{solve} value was high, which could be attributed to the long carbon chain of which the compound included with limited number of polar sidechain groups. The positive quinones, with respect to the redox potential, all included a low number of electron donating groups (EDGs), such as -OH, which in the literature have been the explained as a resulting low redox potential. Indicating that our findings correspond with the published results in literature [79]. When comparing the most positive quinones to the most negative, it was found that the positive compounds were smaller and showed less aromaticity, hence less aromaticity leading to higher redox potentials [236].

Table 4. Properties of the seven quinones with most positive potentials[1], [236].

Name	E^0 V vs SHE	ΔG_{solv}	Source	Structure
Tridentoquinone	1.485	-38.10	[F] *Suillus tridentinus*	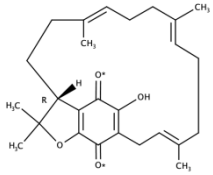
Stemphyperylenol	1.338	-75.20	[F] *Stemphylium botryosum*	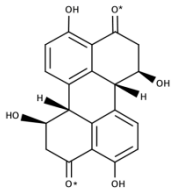
Citrinin hydrate	1.170	-60.82	[F] *Penicillium* spp. *Aspergillus* spp.	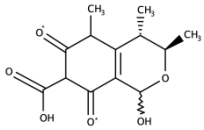
Fusarnaphthoquinone A	1.135	-32.95	[F] *Fusarium* spp.	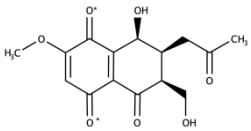
5-Hydroxydihydrofusarubin B	1.126	-52.50	[F] *Fusarium* spp.	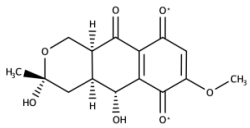
5-Hydroxy-3-methoxydihydrofusarubin D	1.028	-51.20	[F] *Fusarium* spp.	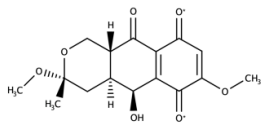
7-epi-Sclerotiorin	1.001	-55.08	[F] *Penicillium hirayamae*	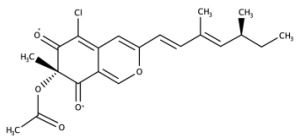

[1] [F]-fungi, * indicates the point of reduction of the reactant.

The quinones which yielded the most negative redox potentials are illustrated in **Table 5**. The list also contains quinones produced by bacteria, compared to the positive list which only consisted of fungal compounds, however fungal quinones are still predominant. The quinone Pradimicin M yielded the most negative redox potential of -1.382 V vs SHE, and showed a relatively high solubility due to a high number of EDGs, even though the compound possessed high aromaticity. The number of EDGs is higher in the seven most negative quinones when compared to the most positive compounds, which confirms the hypothesis that the number of EDGs influence the redox potential [236]. When considering both the most positive and most negative quinones it is seen that some of the reduction potentials lays outside the electrochemical stability window of water, which means that the formations of O_2 occurs if the potential exceeds 1.23 V and the formation of H_2 occurs if the potential is lower than -0.48 V [237]. The potentials shown for both the positive and negative in this study however, are performed in acidic solutions at pH 0, and the impact of pH has been shown to decrease the reduction potentials when increasing pH. The potentials have to be taken into account nevertheless when considering using the compounds as electrolytes as the quinones are highly reactive against oxygen, so if the formation of O_2 occurs, this could lead to loss of capacity of the battery.

Table 5 – Properties of the seven quinones with the most negative potentials[2], [236].

Name	E^0 V vs SHE	ΔG_{solv}	Source	Structure
Pradimicin M	-1.382	-74.94	[B] *Actinomadura hibisca*	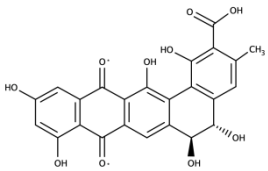
Stemphyltoxin I	-1.298	-40.15	[F] *Stemphylium botryosum*	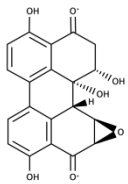
Granaticin B	-1.144	-72.42	[B] *Streptomyces spiroverticillatus*	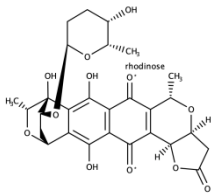

[2] [F]-fungi, [B]-bacteria, * indicates the point of reduction of the reactant.

Altertoxin I	-1.094	-37.34	[F] *Alternaria* spp.	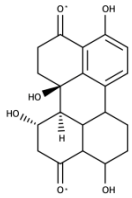
Altertoxin II	-1.008	-41.94	[F] *Stemphylium botryosum*. *Alternaria* spp.	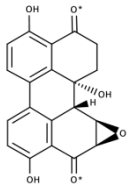
3-O-Methyldihydrofusarubin A	-1.001	-33.43	[F] *Fusarium martii*	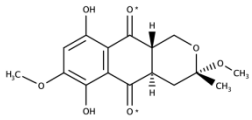
Stemphyltoxin IV	-0.976	-36.40	[F] *Stemphylium botryosum*	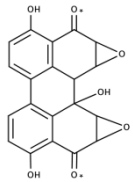

The results obtained in this study are meant as the foundation for exploring the future possibilities of finding and using potential electrolyte candidates for use in flow batteries. The majority of the organisms possessing the most positive and negative reduction potentials found in the study were the fungi *Fusarium* spp. and *Penicillium* spp. In the future works, it will be in these species we will focus our work in finding and optimizing production of the electrolytes.

2.2. Production and Selectivity of Key Fusarubins from *Fusarium solani* due to Media Composition

Fusarium species is notorious for producing several types of secondary metabolites and hereunder pigment and quinones [144,170]. Quinones produced by *Fusarium* spp. were also included in both the positive and negative lists presented in Paper 1, [236], hence it was relevant to investigate this further. A previous published paper from our group, [196], investigated the regulatory effects and produced a mutant of Fusarium solani, OE::*fsr6* of which have an overexpressed transcription factor that initiate the internal regulator *fsr6* gene, which regulates the PKS3 gene cluster, that is responsible for producing fusarubins in *Fusarium* spp. The PKS3 have been assigned to produce different compounds depending on the growth parameters and organism, which corresponds to the fact that fusarubins are produced as secondary metabolites. The aim of the study was then to investigate the optimal growth parameters with regards to media composition and more specific carbohydrate type, nitrogen source, and carbohydrate and nitrogen levels, to produce four desired compounds; fusarubin, javanicin, bostrycoidin, and anhydrofusarubin. The selectivity of the media composition was also considered as an important factor as the purification steps in the following production steps would become less demanding [198]. Initially, four different carbohydrates (maltose, glucose, sucrose and glycerol) and two different sources of nitrogen (ammonium tartrate and sodium nitrate) were investigated. Chromatograms of individual samples, **Figure 23**, showed a significant difference in production and selectivity of the four quinones. The standard concentrations in the figure were for comparison reasons 53 mg/L for fusarubin (red), 39 mg/L for both javanicin (orange) and bostrycoidin (purple) and 19 mg/L for anhydrofusarubin (red-brown). In **Figure 23A** samples containing ammonium tartrate are illustrated and it is seen that the ammonium tartrate favors production of bostrycoidin (purple) over the three other compounds in three of the media compositions containing maltose, glucose and sucrose. The glycerol media did not yield any significant amount of quinones. The media containing maltose did also show promising selectivity with the high production of bostrycoidin, with mean concentrations of 116 mg/L and corresponding low production levels of the other three compounds. The media composed with sucrose showed the highest mean concentration of bostrycoidin of 214 mg/L however indicating poor selectivity. **Figure 23B** illustrates the chromatogram of the media containing sodium nitrate. The glycerol media did not yield any quinones in this case either. The three resulting media showed no or minor levels of production of bostrycoidin, which indicates that the production is depended on free ammonia to initiate the production of the aza-anthraquinone. Sucrose showed production of all three compounds in high levels compared to the other media compositions, with

indications of favorizing fusarubin production of mean sample concentration of 132 mg/L [198].

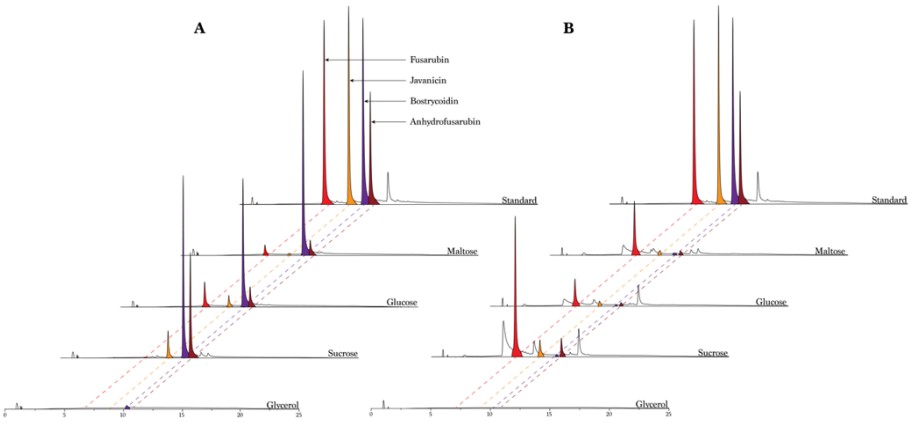

Figure 23 – The carbohydrate and nitrogen source effects on the production of the four fusarubins; (**A**) Chromatograms of samples with media containing ammonium tartrate, fusarubin (red), javanicin (orange), bostrycoidin (purple) and anhydrofusarubin (red-brown) are indicated on the standard and by the dotted lines. (**B**) Chromatograms of samples with media which was composed with sodium nitrate as nitrogen source. Fusarubin (red), Javanicin (orange), bostrycoidin (purple) and anhydrofusarubin (red-brown) is indicated by the dotted lines and color [198].

The investigation of sucrose media with the application of full factorial design is presented in **Figure 24**. The levels chosen for the sucrose were 50 g/L, 100 g/L and 150 g/L, and the levels for ammonium tartrate were 4.6 g/L, 6.9 g/L and 9.2 g/L, and for sodium nitrate the following levels were chosen; 3 g/L, 4.5 g/L and 6 g/L. Several variations were observed due to fermentation in liquid media. This was however expected, as the variations often are larger when using liquid fermentation compared to solid fermentation. In **Figure 24A** the full factorial design of media compositions containing sucrose and ammonium tartrate is illustrated. Fusarubin was produced in low concentrations in the low concentration combinations, yet yielding 47 mg/L with the combination of 50 g/L and 9.2 g/L. The highest production was however found with the combination of 100 g/L sucrose and the low level 4.6 g/L ammonium tartrate where the average concentration was found to be 287 mg/L. Indications of productions patterns of decreasing yields when increasing levels of ammonium tartrate was concluded. Javanicin was produced in highest average concentrations of 77 mg/L in the media composed of 100 g/L sucrose and 6.9 g/L ammonium tartrate. The production of bostrycoidin was overall high and stable, however patterns of decreasing production when increasing sucrose and ammonium tartrate levels was observed. Anhydrofusarubin was showing opposite tendencies as the lowest combination of 50 g/L and 4.6 g/L yielded the highest yields, which could indicate the conversion between compounds, as fusarubin showed opposite patterns. When

investigating the media containing sodium nitrate, **Figure 24B**, the production seemed to favor fusarubin when a low concentration of sucrose and a high level of sodium nitrate was chosen, yielding the highest average concentration of 130 mg/L. Javanicin was produced in smaller yields, where the highest was 33 mg/L when the combination of high sucrose and medium level sodium nitrate was used. Bostrycoidin was not found in the samples in higher concentrations than 2 mg/L. Anhydrofusarubin was favored when low level of sucrose and sodium nitrate was utilized [198].

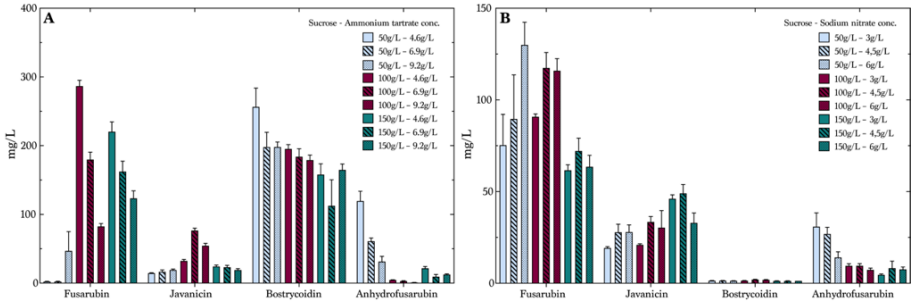

Figure 24 – Mean concentrations and standard error of mean, n = 4, of the combinations of different levels of sucrose and A) ammonium tartrate or B) Sodium nitrate [198].

The following response surface design, expanding the levels of the experiment by using the Box-Wilson central composite design, showed that as high as 400 mg/L fusarubin could be reached if the level of sucrose was increased to 180 g/L and a corresponding low level of ammonium tartar was utilized. Highest yields of bostrycoidin was found by lowering the sucrose level as well as the ammonium tartrate level. The linear trend of fusarubin production increase with the combinations of low sucrose and high level of sodium nitrate was also observed in these results, where the highest yield found was 150 mg/L.

The media most selectively producing bostrycoidin was found to be containing maltose as carbohydrate. By extending the growth period from seven to nine days, or from 168h to 216h, it was possible to let the fungi decompose the total amount of sucrose in the media yielding higher average concentrations of bostrycoidin of 305 mg/L, with no indication of stagnation and still performing more than acceptable selectivity. The fungal growth, indicated by the pellet weight, however did seem to stagnate in the end of the experiment which corresponds with the lack of newly added sucrose. Future experiments could extent the fermentation time further to determine whether an optimum in production can be found further out the timeline. Findings of this study enlightens the possibility of producing the desired electrolytes in the native host, however optimized and fermented in optimized media can enhance the production even further. The quantification method developed in this study will also be used in future studies as a guide for reaching the desired concentrations for the quinones. For future large-scale production, a safer and more environmentally friendly approach is needed when extraction is considered.

2.3. Membrane based separation and purification of fusarubins from *Fusarium solani*

To extend to possibility of using naturally produced quinones in a potential RFB setup, it is important to enhance the production of the pure compounds to a larger scale. However, in Paper 2 [198], an extraction procedure was utilized where the ratio of chloroform used was 1:1 with the volume of fermentation broth. This is not environmentally sustainable and if safety risks and economic perspectives are considered, an additional approach needs to be found. In this paper, we investigate the use of membrane filtration to separate the four fusarubins of interest, **Figure 25B**. The media composition which favors the production of bostrycoidin was chosen [238].

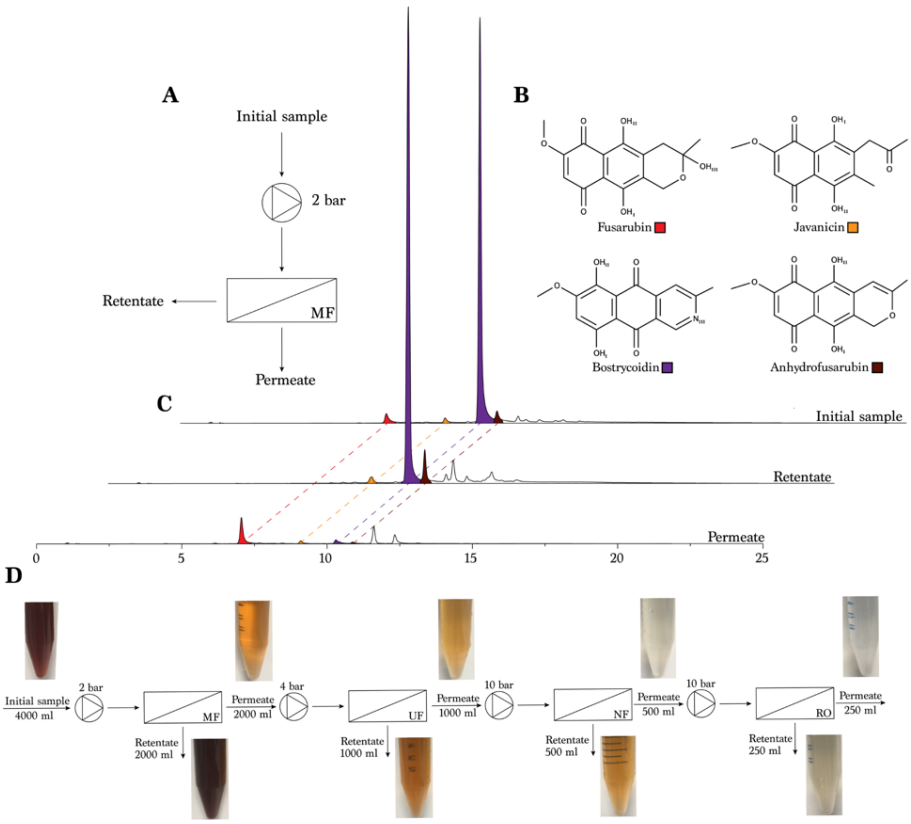

Figure 25 – A) flowchart of the initial MF experiment, B) structural formulas for the four, Fusarubin (red), Javanicin (orange), Bostrycoidin (purple) and Anhydrofusarubin (red-brown), C) Chromatogram of the samples of the initial MF experiment. D) Flowchart of the separation train, including the pigmentation along the separation steps [238].

The composition of the initial sample is illustrated in **Figure 25C**. It is seen that the primary constituent of the sample is bostrycoidin (purple), but also fusarubin (red), javanicin (orange) and anhydrofusarubin (red-brown). The MF filtration process is seen to retain almost all of the bostrycoidin, javanicin, and anhydrofusarubin, whereas fusarubin is permeated and seen primarily in the permeate. The full separation train and corresponding volumes and pressures is illustrated for each membrane step in **Figure 25D**. Additionally the colour difference of the samples is seen, indicating the separation of the pigments along the separation train. Starting with a dark red-brown colour in the initial sample, yielding an even darker retentate and significant lighter permeate of the MF step. This continues for the UF and NF, where most of the remaining pigments are filtered off to the retentate. The last remaining is retained by the RO membrane permeating no pigments at all. The same tendencies were shown when the concentrations were analyzed, where the initial sample contained the following absolute mass'; 576.3 mg of bostrycoidin, 31.3 mg fusarubin, 21.9 mg of anhydrofusarubin and 9.6 mg of javanicin, which was present in the 4 L fermentation broth initially. Resulting the MF step operated at 50% recovery, leaving 2 L in the retentate and 2 L in the permeate, the masses were found to be; 537.1 mg if bostrycoidin in the retentate and 10.8 mg in the permeate which corresponds to a rejection of 97.5%, this additionally corresponds to 95% of the relative mass separated by the MF membrane. Fusarubin was only present in the permeate and presenting a mass of 24.2 mg. Both javanicin and anhydrofusarubin were concentrated in the retentate to 10.1 mg and 27.6 mg respectively. The UF step, yielded little to no separation of the compounds, as all compounds were found in both permeate and retentate. The low concentrations of the remaining compounds are making the analysis challenging, however the NF step is retaining the majority of the remaining compounds so little to no compounds were found in the permeate. The RO step then concentrates the remaining compounds yielding no pigments in the permeate. The flux of the individual membranes was also investigated and showed a decreasing flux over time for all membranes. The MF membrane showed an initial flux of 25 L/(m^2h) which over the time of 200 mins decreased to 20 L/(m^2h). The UF step presented initially a flux of 13 L/(m^2h), but decreased rather rapidly to 10 L/(m^2h) and hereafter more slowly to 7.5 L/(m^2h). The NF membrane started at 11.5 L/(m^2h) and decreased to 5.0 L/(m^2h), whereas for the RO experiment the flux changed very little, due to the small amount of compounds present, only showing a decrease from 7.0 L/(m^2h) to 6.0 L/(m^2h) [238].

Three different MF membranes was additionally investigated as the MF step showed good separation of bostrycoidin compared to the other steps. Similar tendencies were shown for each of the three membranes, **Figure 26A-C**. Retaining the majority of bostrycoidin from 70.4 mg in the initial sample to 67.0 mg in the retentate shown in **Figure 26A**, VO.1 membrane. From 63.1 mg in the initial sample of the MF01 membrane to 65.4 mg in the retentate, **Figure 26B**, and from 63.0 mg in the initial sample to 65.8 mg in the retentate, concluding rejections of 98.0%, 97.8 and 98.2 % respectively. Simultaneously, all of fusarubin from the initial samples were permeated

and were found in the permeate, for all three membranes. Anhydrofusarubin and javanicin was also retained by the MF membranes. Some irregularities were seen in the mass balances, where some compounds were found in larger concentrations in e.g. the retentate or permeate. This could however be explained by changes in pH during the experiment, because both fusarubin and anhydrofusarubin have been described as conversion products of other compounds under alkaline and acidic concentrations respectively. When bostrycoidin is found in higher concentrations it can solely be explained by variation in the data, which lays in the standard deviation of the dataset. The permeate flux for all three membrane is visualized in **Figure 26D**, and is showing a decreasing flux for all three membranes. The steepest decrease is seen by the MF01 membranes followed by the MV020 membrane and the slowest decrease in flux is seen by the VO.1 membrane, also indicated by the longer experimental time which also corresponds to a lower initial flux of this membrane [238].

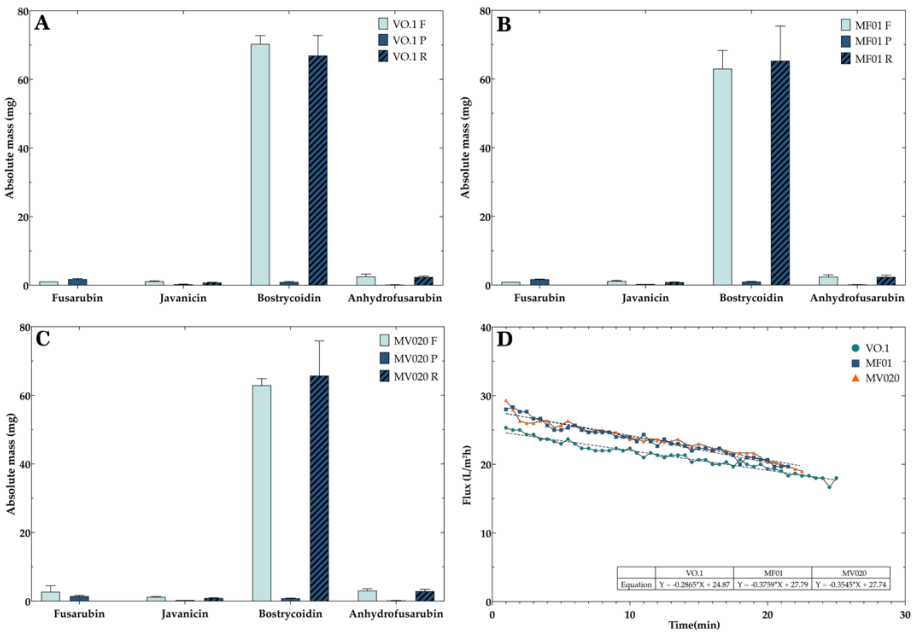

Figure 26 – Average absolute masses of the three investigated MF membranes; A) VO.1 membrane, B) MF01 membrane, C) MV020 membrane. D) Permeate flux for all three membranes [238].

A long term, large volume (8.1 L feed), and high concentration experiment was initiated using the VO.1 membrane. The 8.1 L was composed of the resulting retentate from prior experiments, yielding high concentrations of bostrycoidin and no trace of fusarubin. The results showed that only 28.9% of the relative mass was retained in the retentate and only 2.1% was found in the permeate. Similar tendencies were seen for the other two compounds, javanicin and anhydrofusarubin. The coloration of both the

permeate and retentate however appeared similar to prior experiment, even though the retentate seemed thicker and somehow showing higher concentration of cell material and other larger compounds, such as proteins. The extraction procedure of the samples also showed some challenges in recovery of the desired pigments. This was seen as not all of the pigmentation was transported from the aqueous retentate phase to the organic phase, and several back extractions would be needed for a complete extraction. The flux of this experiment showed an initial value of 24.8 L/(m^2h) similar to what was seen before, and a decrease over four hours to a relatively stable permeate flux of 12 L/(m^2h). The flux behavior was expected as the experiment was conducted using highly concentrated mixtures containing also larger particles which easily can conduct fouling of the membrane. The experiment concludes in that it is reasonable to expect that the separation and concentration of bostrycoidin is possible, but only one extraction is not enough to extract all of the containing bostrycoidin, concluding that several back extractions are necessary [238].

Based only on the molecular size and the polar sidechain groups of the four molecules it was to some extend surprising that bostrycoidin could be separated to such great extent, nonetheless very positive for the future upscaling of production of this compound. We did however find that the polarity of the compound could cause this separation due to the amine group in the molecule, which could interact with the membrane and create a greater repulsion of the compound compared to the other three compounds. Together with a fouling layer of biological matter such as cell components could also enhance the retainment of bostrycoidin. The findings in the study however shows a great potential in using membrane separation technology in the upscale production of naturally occurring quinones, where the initial extraction procedure is not meeting the criteria for safe and environmentally friendly handling for larger volumes. This together with learnings from the previous paper 2, concludes the second and third research question.

2.4. Initial findings that founded the manuscript; "The fungal battery: A redox flow battery containing the biosynthesised negolyte phoenicin"

The compound phenicin, or phoenicin which is also used as a synonym, is produced in vast amounts in the fungi *Penicilium manginii* and *Penicilium astrosanguineum* with only small to non-measurable concentrations of other secondary metabolites, making it a potential initial candidate to investigate. The computational screening yielded a redox potential of 0.216 V vs SHE, at pH 0. The fungal strain of *P. manginii* was acquired through the collaboration between AAU and the Institute of Biotechnology and Biomedicine, Department of Bioengineering at DTU. The fungi were grown first for five days on PDA plates in darkness at 25 degrees and plugs were taken from the plates into liquid PDB media, which were fermented for 14 days in complete darkness with no stirring, at 25 degrees Celsius. After this, I applied the extraction procedure which I developed to extract fusarubins, of which I expected an acceptable yield as the compounds share some common properties and functional groups. The purity of the crude extraction procedure was established to be around 75%, determined using HPLC-DAD at 495 nm, which could be optimized considerably in future experiments using e.g. preparative HPLC. A crude extract with no concentration determination was initially exposed to cyclic voltammetry to investigate the potential use of the quinone as electrolyte. The result of the experiment is visualized in **Figure 27**. The experimentally determined redox potential is seen to be -0.3633 V vs SHE at pH 14. This combined with the $K_4Fe(CN)_6$ with a redox potential of 0.5 V vs SHE could potentially compete with already published electrolyte couples. This leads to a cell potential of 0.86 V vs SHE, which corresponds with the findings in paper 4.

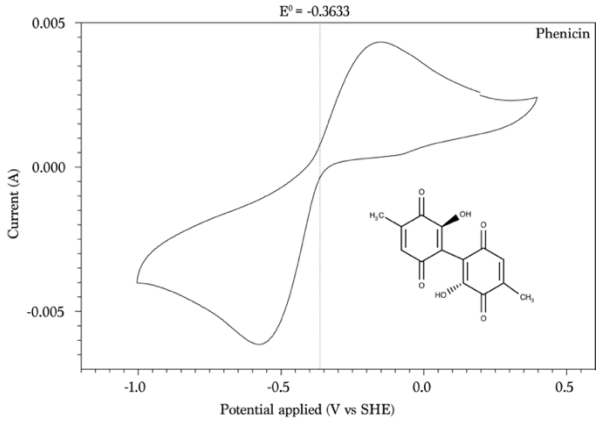

Figure 27 - Cyclic voltammetry analysis of phenicin, including the molecular structure.

The next step was to perform a simple cycle test to investigate the performance of the cell and electrolytes, to elucidate whether this combination of electrolyte should be pursued further. The experiment was set up in the testing facility established by myself

with the help of colleagues from Aarhus university. The result of the preliminary cycle test is illustrated in **Figure 28**. The experiment contained 20 cycles, ranging from cut off voltages 0.6 V to 1.6 V for the comparison possibilities, similar to the study of Lin et al. 2015, [49]. The cycles wideness is decreasing over the 20 cycles, indicating a more rapid time to charge and discharge, which could be explained as unwanted side effects due to the crude extract or exposure of oxygen to the electrolytes and cell. The capacity is furthermore decreasing, which is visualized in **Figure 28B** where voltage is presented against the capacity, and the line furthest to the right or possessing the highest capacity indicate the first cycle. At every cycle there, a decrease in capacity corresponding to the decrease in charge/discharge time is seen. The capacity can be explained as the stability of the system, and the decrease in capacity can also be because of destability of the compound. To conclude this, additional experiments are needed. In Paper 4 a capacity fading rate of 0.35% per cycle is showed, which is compatible when considering DHBQ that showed 0.32% per cycle when combined with the $K_4Fe(CN)_6$ [58]. This however is a higher rate than other systems.

The experiment was performed outside glovebox with no oxygen control of which seen in the perspective should most definitively have been conducted as this could explain the rapid decrease in the capacity along the fact that it was a crude product with purity of 75% only. However, the results showed potential for future investigation of the compound Phenicin as electrolyte. The further investigations were performed by a second PhD student, where I helped and supervised in the lab work and scope of the paper accordingly.

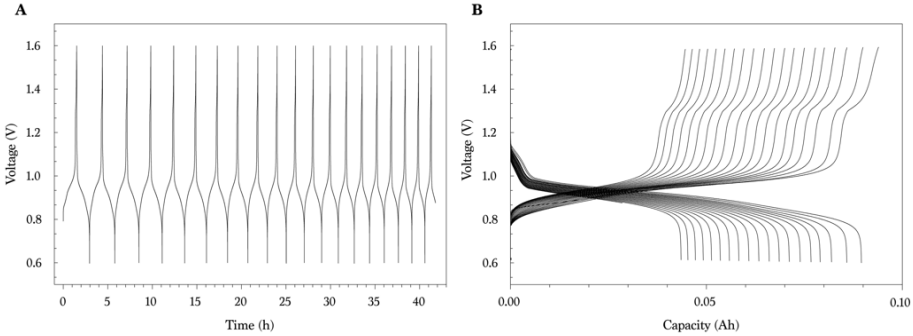

Figure 28 - Redox flow battery test of crude extract of Phenicin, preliminary results; A) cycle test including 20 cycles, B) voltage vs capacity plot of the 20 cycles.

As described, the scientific contributions described here made the basis for and formed the foundation for the paper "A redox flow battery based on the fungal produced anolyte phoenicin" which is in draft. And was together with supervision, training and knowledge sharing some of the contributions made to this paper. Whereas the paper is not a main component in this thesis, I have contributed more to it and of greater relevance than being a side project.

2.5. Preliminary assessment results of the fungal quinone Bostrycoidin

The assessment of bostrycoidin was based on extracted fermentation broth which has been filtered through a MF step, with recovery of 90%, as described in Paper 3 [238]. The resulting retentate was exposed to the extraction procedure explained in detail in Paper 2 [198], where chloroform was used as main solvent together with methanol as co-solvent. The extraction procedure was performed 4 times on the aqueous phase, as this appeared pigmented still after the first couple of extractions. This can be attributed to the high concentration of bostrycoidin and other larger particles such as proteins and cells. The quantification of the samples, **Figure 29**, showed a sample containing purity of 96% being bostrycoidin, based on the area found in the chromatogram at 495nm. The extracted bostrycoidin was dried to complete dryness and weighed, which yielded 10.95 g of ≈ 95% pure bostrycoidin. This can be concluded to be very acceptable of an initial volume of 8.1L, indicating the concentration in the fermentation broth exceeded 1.35 g/L if all bostrycoidin was extracted from the pooled retentates of the fermentation broths.

Figure 29 - HPLC-DAD analysis of the extracted bostrycoidin, yielding relatively high purity of 96% at 495nm.

Bostrycoidin was in paper 1 [236], simulated to possess a redox potential of -0.192 V vs SHE, so not the extreme end of the negative redox couples. However, it is a very interesting compound as it can be produced as shown relatively easy in larger quantities. Additionally, aza-aromatic compounds have been shown to increase the

stability and decrease the capacity fading ratios when assessed for use in RFB [13,80]. To investigate the redox potential 7.1 mg was dissolved in 25 ml 1 M KOH, to yield a concentration of 1mM of bostrycoidin in 1 M KOH. The resulting voltammogram is illustrated in **Figure 30A**. The reduction potential, E^0, was determined to be -0.58 V vs SHE. This number cannot however be directly compared to the simulated value as this was simulated in an acidic pH of 0, being a two electron and two proton redox reaction. When performing the experiment, the pH, as a result of the 1M KOH, is very alkaline of 14. To investigate the redox reaction, a conversion was prepared, **Figure 30B**. In the literature, the decrease has been described as -59mv equal to approximately $2H^+$. However, this differentiates for each molecule and can also be only one proton, equivalent to -30mv, a combination of the two or even zero protons yielding a flat progression. In **Figure 30B** three theoretical lines have been illustrated, and the best fit is seen with only one H^+ progression, ending at -0.61 V. This however, needs to be determined experimentally as well, because the progression might as well start with a two-proton reaction when the solution is acidic, changing to a one-proton reaction around neutral pH and ending in a zero-proton reaction after pH 8-9. These experiments have not been performed yet due to the time limitation of the PhD project.

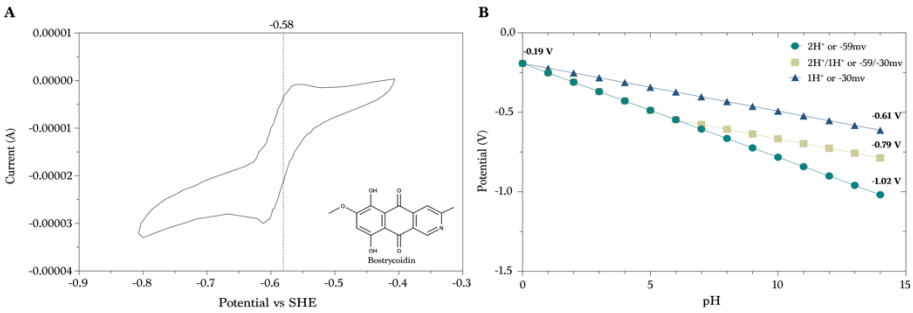

Figure 30 - Electrochemical assessment of bostrycoidin; A) Cyclic voltammetry analysis, voltammogram of 1mM bostrycoidin. B) Conversion of predicted redox potential of 0.19 V vs SHE at pH = 0, to pH = 14, using theoretical approach as described in [57,59], prior to future experimental findings.

The next steps of the assessment of bostrycoidin will include cell cycle testing and comparisons with other types of quinone RFB set ups. But so far, the reduction potential seems to be of good competition when comparing this to other already published RFB electrolytes, exceeding the reduction potential of Phenicin, presented in Paper 4. The cell cycling experiment have not been performed due to time restrictions in the PhD project, and challenges with some laboratory equipment. The initial findings presented here and for phenicin concludes the fourth research question.

Chapter 3. Conclusions and perspectives

The world energy production and usage are increasing, and where fossil fuels in the past were the main source of energy, renewable energy sources now showing an increase in attention. Present renewable energy sources are however in the need of a reliable source of energy storage to be effective for larger grid applications. The Redox flow battery systems are a valid option for this solution as the scalability and flexibility of the battery enables possibilities of designing individual batteries for specific purposes. The electrolytes used in RFBs have until now been focused primarily on metal ions such as vanadium and organic redox couples synthesized from waste product from the fossil fuel energy production. This does not however correspond to the sustainable aspect of storing energy produced by renewable energy sources. The main objective of this study was to investigate and elucidate the possibility of finding and using naturally produced quinones as electrolytes in an RFB system.

The initial point of investigation was to develop a database containing all known naturally occurring quinones. The database was formed from the commercially available database Antibase, and 990 different quinone compounds was found and compiled in the local database. The computational models used in this study were based on already published and validated studies from Huskinson et al. 2014 [45], and Er et al. 2016 [79], where the model presented in Paper 1 [236], out-performed the models of the two studies mentioned above in terms of better fit to the experimental values used in the calibration model. It was shown that the realm of fungi possesses the largest variety of the simulated redox potential, yielding the seven most negative redox potentials and five of the seven most positive redox potentials. The distribution of the simulated quinones varied from -1.4 V to 1.5 V vs SHE. This could create challenges with regards to the stability of the aqueous solvent, when exceeding the stability window hereof. The pH however could solve this to some extend as the most positive quinones reduction potentials will be more negative when more alkaline solutions are used for extended solubility. The correlation of EDGs and redox potential was shown as the higher amount of EDGs, the lower redox potential, and a high redox potential was observed when a low number of EDGs was present in the compounds. It was also showed that the presence of EDGs yield higher solubility descriptors, which indicate the increased polarity affects this more than e.g. molar mass or number of aromatic rings. The database created in this study containing the computationally simulated redox potentials and solubilities of the quinones, have been for the resulting part of this study and will be for future studies used as a guiding tool to look for potential new electrolytes for use in RFB technology.

Based on the computational screening it was found that the species of *Fusarium* yielded large varieties of quinones compounds with potential usage in RFB systems. A mutant strain of the fungi *Fusarium solani* was developed in an earlier published

study, [196], where the overexpression of the transcription factor of the gene *fsr6* showed an increase of the production of fusarubins. In paper 2, [198], the production of four of these fusarubin compounds was investigated with the purpose of developing a possible way of producing one of the compounds selectively in favor and in higher concentrations compared to the other compounds. Initially, a method of quantification was developed by extraction of purification of the pure substances using preparative HPLC-DAD with controlling the purity on NMR. The calibration curves were prepared on a HPLC-DAD afterwards. The investigation of the optimal media composition was initiated with four different carbohydrates (maltose, glucose, sucrose and glycerol), and two types of nitrogen source (ammonium tartrate and sodium nitrate). A full factorial design was applied with the concentration of 4.6, 6.9 and 9.2 g/L for the carbohydrates where ammonium tartrate was the nitrogen source and 3, 4.5 and 6 g/L carbohydrates where sodium nitrate was the nitrogen source. It was shown that sucrose produced the largest variety of the four compounds with largest potential of adjusting the selectivity. However, maltose was shown to yield the highest selectivity that favored the quinone bostrycoidin. In general, it was concluded that with the nitrogen source being ammonium tartrate the production of bostrycoidin was high, and little to none was produced by organisms grown in media where the nitrogen source was sodium nitrate, indicating the importance of free ammonium in the media for the biosynthesis of bostrycoidin to take place. The optimal media composition to favor fusarubin production was established to be 50 g/L of sucrose combined with 6 g/L sodium nitrate. For javanicin the media composition was 150 g/L sucrose and 6 g/L sodium nitrate. For anhydrofusarubin it was found that the media composed of 50 g/L sucrose and 3 g/L of sodium nitrate was producing highest yields. The theoretical response surface designs validated these conclusions. The production of bostrycoidin was investigated further by extending the fermentation time from seven to nine days, measuring the sugar concentration and pellet weight from the sample. This elucidated that by extending the fermentation time from seven to nine days, an increase in the production of bostrycoidin to above 300 mg/L was found. Yielding still high selectivity in the media composed with 50 g/L maltose and 4.6 g/L of ammonium tartrate.

Using the media composition which favored the production of bostrycoidin, an upscale study was initiated. Because of the liquid-liquid extraction method used in prior experiments and studies was using large amounts of chloroform as solvent, it was crucial for the future production upscale possibilities to investigate if separation and purification could be achieved in a sufficient scale using different techniques. Membrane filtration is seen as a potential solution for this, and a full separation train was investigated using MF, UF, NF and RO membranes. It was showed that Bostrycoidin was rejected by MF membranes, and could then be concentrated in the retentate from the MF step. The retentate was exposed of the same LLE extraction procedure and purity was found to be 94.1% of bostrycoidin, which is concluded to be acceptable. Three different MF membranes was investigated and did not show any difference in rejection of bostrycoidin, which make little to no difference in changing

the membranes with regards of the yield of pure bostrycoidin. The three other fusarubins were also present in the samples, however in very small concentrations compared to bostrycoidin. The method presented offers thereby a safer and more environmentally friendly approach for large scale purification of bostrycoidin, enhancing the future potential of using this compound as an electrolyte in a RFB system.

The preliminary results of the investigation of Phenicin showed a relevant potential to continue the further investigation of this compound. Along with the relatively simple production method, extraction procedure, and how the compound behaved electrochemically, it can be concluded that the further investigations carried out by another PhD student and presented in Paper 4, is viable when compared to other similar studies. Paper 4 shows a capacity fading rate of 0.35% per cycle, which is somewhat higher than other similar systems, but yet compatible when considering DHBQ that showed 0.32% per cycle when combined with the $K_4Fe(CN)_6$ [58]. However, there are still elements where the compound shows limitations. The contributions from my side have helped in a significant way to develop the test setup, protocols, and test the compound. Which can be implemented and used by future researchers as well as students.

To investigate if bostrycoidin possessed any potential as a candidate of usage as electrolyte, the resulting retentates was pooled together and concentrated even further by MF, resulting in a recovery of 90%, or a reduction of volume of 90% going from 8.1 L to 0.81 L. The 0.81L was exposed of the LLE protocol, extended with several back extractions to extract as much as possible. This yielded 10.95 g bostrycoidin with a purity of 96% analyzed at 495 nm. The electrochemical test of the compound was resulted in a redox potential of -0.58 V vs SHE, which is considered valid for use in an RFB system, when compared to other quinone compounds and electrolytes. Simple regression analysis of the simulated redox potential of 0.19 V vs SHE at pH 0 to the measured value indicated a one proton two electron reaction, however this is something future experiments will enlighten. Furthermore, additional cyclic voltammetry is needed to establish the stability over time and electron transfer coefficients. Secondly, full cell cycling test is needed to conclude in more detail if the compound bostrycoidin will be a relevant candidate as electrolyte in an RFB system. Even though the preliminary results indicate possible potential.

I am confident that the future will hold a solution to the storage of energy from renewables, so that the use of these energy sources can be extended even further. I do believe that not only one solution is viable for this to work, but I do see redox flow batteries as a potential candidate to store energy for larger scale applications. If the future flow batteries are containing naturally occurring quinones is hard to answer. I do believe that the potential of these quinones are of just as great potential as synthetically produced quinones. Why shouldn't nature already have optimized the solubility and stability of the compound? It's just up to us to find that compound and

utilize it. The learnings provided to me during this PhD have enabled me to gain experience in many different fields and this project illustrates the wideness of technical knowledge are needed to develop and explore a new type of energy storage. The results obtained during this project will be used in future research projects and I am confident that within a time frame of 5-10 years the first large scale RFB containing fungal quinones will be published. This project has barely scratched the surface to an area of research where much more is found every day and new compounds are still to be investigated to find the optimal combination, for even eventually creating a quinone- quinone RFB. Based on the literature, I find the naturally occurring quinones just as valid a candidate for future RFB electrolytes than other published combinations of aqueous soluble electrolytes. The one thing that is often discussed is the stability of the quinones and I think that this will be the main challenges for the natural quinones as well. When no oxygen control was performed in the initial experiments of phenicin, the capacity fade was rather large compared to the optimized experiments where the results were compatible with other published electrolytes as presented in paper 4. In this study, I have been limited to only consider quinones as electrolytes, for good reason as otherwise everything would have been even broader. However, additional redox active could be considered. TEMPO and derivatives have been showing promising results in regards to stability, and would also be interesting to investigate further if similar compounds could be produced naturally. As for vanadium flow batteries, I think that this is still going to be there for the futures years to come, as these possess good stability and if the prices can be held at a relatively low and steady level this will also help. The fact that crossover does not impact the stability is something which is very valuable because this is causing a lot of challenges around the battery labs of the world where quinones are investigated. The possibility of using a natural quinone which holds multiple redox states could also be a potential way to focus future research projects. The production optimization goes however hand in hand with the individual desired compound. The findings and protocols from this project can be used as starting points and guides to investigate and optimize the parameters for future projects. As mentioned, I feel confident in that the research performed during this PhD have been laying the foundation for hopefully many new researchers and their projects.

Literature list

[1] BP, Statistical Review of World Energy 2020, (2020) 66. https://www.bp.com/content/dam/bp/business-sites/en/global/corporate/pdfs/energy-economics/statistical-review/bp-stats-review-2020-full-report.pdf.

[2] IEA, World Energy Outlook 2019, World Energy Outlook 2019. (2019) 1. https://www.iea.org/reports/world-energy-outlook-2019%0Ahttps://www.iea.org/reports/world-energy-outlook-2019%0Ahttps://webstore.iea.org/download/summary/2467?fileName=Japanese-Summary-WEO2019.pdf.

[3] BP, Statistical Review of World Energy, Stat. Rev. World Energy. (2018) 1–56.

[4] UNFCCC, Convention on Climate Change: Climate Agreement of Paris., (2015) 1–25. https://unfccc.int/process-and-meetings/the-paris-agreement/the-paris-agreement.

[5] the Danish Government, Energy Agreement, June 29th 2018, (2018) 1–19. https://efkm.dk/media/12222/energiaftale2018.pdf.

[6] Energistyrelsen, Energistatistik 2015, Energistyrelsen, 2015. http://www.ens.dk.

[7] Energistyrelsen, Energistatistik 2017, Energistyrelsen, 2017. http://www.ens.dk.

[8] Energistyrelsen, Energistatistik 2019, Energistyrelsen, 2019. http://www.ens.dk.

[9] I.R.E. Agency, Renewable Power Generation Costs in 2019, 2020. https://www.irena.org/-/media/Files/IRENA/Agency/Publication/2018/Jan/IRENA_2017_Power_Costs_2018.pdf.

[10] Danish Energy Agency, Aftale mellem regeringen (Socialdemokraterne, Det Radikale Venstre, Socialistisk Folkeparti) og Venstre, Dansk Folkeparti, Enhedslisten og Det Konservative Folkeparti om den danske energipolitik 2012-2020, (2012) 1–16. http://www.ens.dk/sites/ens.dk/files/politik/dansk-klima-energipolitik/politiske-aftaler-paa-energiomraadet/energiaftalen-22-marts-2012/Aftale_22-03-2012_FINAL_ren.doc.pdf.

[11] J. Rugolo, M.J. Aziz, Electricity storage for intermittent renewable sources, Energy Environ. Sci. 5 (2012) 7151. https://doi.org/10.1039/c2ee02542f.

[12] B. Dunn, H. Kamath, J.-M. Tarascon, Electrical Energy Storage for the Grid: A Battery of Choices, Science (80-.). 334 (2011) 928–935. https://doi.org/10.1126/science.1212741.

[13] D.G. Kwabi, Y. Ji, M.J. Aziz, Electrolyte Lifetime in Aqueous Organic Redox Flow Batteries: A Critical Review, Chem. Rev. (2020). https://doi.org/10.1021/acs.chemrev.9b00599.

[14] S. Rehman, L.M. Al-Hadhrami, M.M. Alam, Pumped hydro energy storage system: A technological review, Renew. Sustain. Energy Rev. 44 (2015) 586–598. https://doi.org/10.1016/j.rser.2014.12.040.

[15] E.A. Olivetti, G. Ceder, G.G. Gaustad, X. Fu, Lithium-Ion Battery Supply Chain Considerations: Analysis of Potential Bottlenecks in Critical Metals, Joule. 1 (2017) 229–243. https://doi.org/10.1016/j.joule.2017.08.019.

[16] D. Lisbona, T. Snee, A review of hazards associated with primary lithium and lithium-ion batteries, Process Saf. Environ. Prot. 89 (2011) 434–442. https://doi.org/10.1016/j.psep.2011.06.022.

[17] Q. Wang, P. Ping, X. Zhao, G. Chu, J. Sun, C. Chen, Thermal runaway caused fire and explosion of lithium ion battery, J. Power Sources. 208 (2012) 210–224. https://doi.org/10.1016/j.jpowsour.2012.02.038.

[18] C. Ponce de León, A. Frías-Ferrer, J. González-García, D.A. Szánto, F.C. Walsh, Redox flow cells for energy conversion, J. Power Sources. 160 (2006) 716–732. https://doi.org/10.1016/j.jpowsour.2006.02.095.

[19] P. Leung, X. Li, C. Ponce De León, L. Berlouis, C.T.J. Low, F.C. Walsh, Progress in redox flow batteries, remaining challenges and their applications in energy storage, RSC Adv. 2 (2012) 10125–10156. https://doi.org/10.1039/c2ra21342g.

[20] R.M. Darling, K.G. Gallagher, J.A. Kowalski, S. Ha, F.R. Brushett, Pathways to low-cost electrochemical energy storage: A comparison of aqueous and nonaqueous flow batteries, Energy Environ. Sci. 7 (2014) 3459–3477. https://doi.org/10.1039/c4ee02158d.

[21] A.Z. Weber, M.M. Mench, J.P. Meyers, P.N. Ross, J.T. Gostick, Q. Liu, Redox flow batteries: A review, J. Appl. Electrochem. 41 (2011) 1137–1164. https://doi.org/10.1007/s10800-011-0348-2.

[22] W. Wang, Q. Luo, B. Li, X. Wei, L. Li, Z. Yang, Recent progress in redox flow battery research and development, Adv. Funct. Mater. 23 (2013) 970–986. https://doi.org/10.1002/adfm.201200694.

[23] J. Winsberg, T. Hagemann, T. Janoschka, M.D. Hager, U.S. Schubert, Redox-Flow Batteries: From Metals to Organic Redox-Active Materials, Angew. Chemie - Int. Ed. 56 (2017) 686–711. https://doi.org/10.1002/anie.201604925.

[24] V. Singh, S. Kim, J. Kang, H.R. Byon, Aqueous organic redox flow batteries, Nano Res. 12 (2019) 1988–2001. https://doi.org/10.1007/s12274-019-2355-2.

[25] M. Skyllas-Kazacos, G. Kazaco, G. Poon, H. Verseema, Recent advances with UNSW vanadium-based redox flow batteries, Int. J. Energy Res. 34 (2010) 182–189. https://doi.org/10.1002/er.1658.

[26] M. Skyllas-Kazacos, M.H. Chakrabarti, S.A. Hajimolana, F.S. Mjalli, M. Saleem, Progress in Flow Battery Research and Development, J. Electrochem. Soc. 158 (2011) R55. https://doi.org/10.1149/1.3599565.

[27] M. Skyllas-Kazacos, D. Kasherman, D.R. Hong, M. Kazacos, Characteristics and performance of 1 kW UNSW vanadium redox battery, J. Power Sources. 35 (1991) 399–404. https://doi.org/10.1016/0378-7753(91)80058-6.

[28] U.S. Department of Energy, Grid Energy Storage Report, (2013) 67. http://energy.gov/sites/prod/files/2014/09/f18/Grid Energy Storage December 2013.pdf.

[29] G.L. Soloveichik, Flow Batteries: Current Status and Trends, Chem. Rev. 115 (2015) 11533–11558. https://doi.org/10.1021/cr500720t.

[30] G. Kear, A.A. Shar, F.C. Walsh, Development of the all-vanadium redox flow battery for energy storage: a review of technological, financial and policy aspects, Int. J. Energy Res. 36 (2012) 1105–1120. https://doi.org/10.1002/er.1863.

[31] L. Joerissen, J. Garche, C. Fabjan, G. Tomazic, Possible use of vanadium redox-flow batteries for energy storage in small grids and stand-alone photovoltaic systems, J. Power Sources. 127 (2004) 98–104. https://doi.org/10.1016/j.jpowsour.2003.09.066.

[32] H. Kreutzer, V. Yarlagadda, T. Van Nguyen, Performance Evaluation of a Regenerative Hydrogen-Bromine Fuel Cell, J. Electrochem. Soc. 159 (2012)

F331–F337. https://doi.org/10.1149/2.086207jes.

[33] Z. Li, M.S. Pan, L. Su, P.C. Tsai, A.F. Badel, J.M. Valle, S.L. Eiler, K. Xiang, F.R. Brushett, Y.M. Chiang, Air-Breathing Aqueous Sulfur Flow Battery for Ultralow-Cost Long-Duration Electrical Storage, Joule. 1 (2017) 306–327. https://doi.org/10.1016/j.joule.2017.08.007.

[34] J. Andrews, S. Seif Mohammadi, Towards a "proton flow battery": Investigation of a reversible PEM fuel cell with integrated metal-hydride hydrogen storage, Int. J. Hydrogen Energy. 39 (2014) 1740–1751. https://doi.org/10.1016/j.ijhydene.2013.11.010.

[35] M.C. Tucker, A. Phillips, A.Z. Weber, All-Iron Redox Flow Battery Tailored for Off-Grid Portable Applications, ChemSusChem. 8 (2015) 3996–4004. https://doi.org/10.1002/cssc.201500845.

[36] M.C. Wu, T.S. Zhao, H.R. Jiang, Y.K. Zeng, Y.X. Ren, High-performance zinc bromine flow battery via improved design of electrolyte and electrode, J. Power Sources. 355 (2017) 62–68. https://doi.org/10.1016/j.jpowsour.2017.04.058.

[37] K. Gong, X. Ma, K.M. Conforti, K.J. Kuttler, J.B. Grunewald, K.L. Yeager, M.Z. Bazant, S. Gu, Y. Yan, A zinc-iron redox-flow battery under $100 per kW h of system capital cost, Energy Environ. Sci. 8 (2015) 2941–2945. https://doi.org/10.1039/c5ee02315g.

[38] P.K. Leung, C. Ponce-De-León, C.T.J. Low, A.A. Shah, F.C. Walsh, Characterization of a zinc-cerium flow battery, J. Power Sources. 196 (2011) 5174–5185. https://doi.org/10.1016/j.jpowsour.2011.01.095.

[39] T. Janoschka, N. Martin, U. Martin, C. Friebe, S. Morgenstern, H. Hiller, M.D. Hager, U.S. Schubert, An aqueous, polymer-based redox-flow battery using non-corrosive, safe, and low-cost materials, (2015). https://doi.org/10.1038/nature15746.

[40] M. Armand, J.-M. Tarascon, Building better batteries, Nature. 451 (2008) 652–657. https://doi.org/10.1038/451652a.

[41] C.J. Barnhart, S.M. Benson, On the importance of reducing the energetic and material demands of electrical energy storage, Energy Environ. Sci. 6 (2013) 1083–1092. https://doi.org/10.1039/c3ee24040a.

[42] J.H. Kim, K.J. Kim, M.S. Park, N.J. Lee, U. Hwang, H. Kim, Y.J. Kim, Development of metal-based electrodes for non-aqueous redox flow batteries,

Electrochem. Commun. 13 (2011) 997–1000. https://doi.org/10.1016/j.elecom.2011.06.022.

[43] M.H. Chakrabarti, R.A.W. Dryfe, E.P.L. Roberts, Evaluation of electrolytes for redox flow battery applications, Electrochim. Acta. 52 (2007) 2189–2195. https://doi.org/10.1016/j.electacta.2006.08.052.

[44] J. Winsberg, T. Janoschka, S. Morgenstern, T. Hagemann, S. Muench, G. Hauffman, J.F. Gohy, M.D. Hager, U.S. Schubert, Poly(TEMPO)/Zinc Hybrid-Flow Battery: A Novel, "green," High Voltage, and Safe Energy Storage System, Adv. Mater. 28 (2016) 2238–2243. https://doi.org/10.1002/adma.201505000.

[45] B. Huskinson, M.P. Marshak, C. Suh, S. Er, M.R. Gerhardt, C.J. Galvin, X. Chen, A. Aspuru-Guzik, R.G. Gordon, M.J. Aziz, A metal-free organic–inorganic aqueous flow battery, Nature. 505 (2014) 195–198. https://doi.org/10.1038/nature12909.

[46] B. Yang, L. Hoober-Burkhardt, F. Wang, G.K. Surya Prakash, S.R. Narayanan, An Inexpensive Aqueous Flow Battery for Large-Scale Electrical Energy Storage Based on Water-Soluble Organic Redox Couples, J. Electrochem. Soc. 161 (2014) A1371–A1380. https://doi.org/10.1149/2.1001409jes.

[47] Z. Li, S. Li, S. Liu, K. Huang, D. Fang, F. Wang, S. Peng, Electrochemical properties of an all-organic redox flow battery using 2,2,6,6-tetramethyl-1-piperidinyloxy and N-Methylphthalimide, Electrochem. Solid-State Lett. 14 (2011) 171–174. https://doi.org/10.1149/2.012112esl.

[48] Y. Xu, Y.H. Wen, J. Cheng, G.P. Cao, Y.S. Yang, A study of tiron in aqueous solutions for redox flow battery application, Electrochim. Acta. 55 (2010) 715–720. https://doi.org/10.1016/j.electacta.2009.09.031.

[49] K. Lin, Q. Chen, M.R. Gerhardt, L. Tong, S.B. Kim, L. Eisenach, A.W. Valle, D. Hardee, R.G. Gordon, M.J. Aziz, M.P. Marshak, Alkaline quinone flow battery, Science (80-.). 349 (2015) 1529–1532. https://doi.org/10.1126/science.aab3033.

[50] J.R. Tobias Johnsson Wass, E. Ahlberg, I. Panas, D.J. Schiffrin, Quantum chemical modeling of the reduction of quinones, J. Phys. Chem. A. 110 (2006) 2005–2020. https://doi.org/10.1021/jp055414z.

[51] K.O. Eyong, V. Kuete, T. Efferth, Quinones and Benzophenones from the Medicinal Plants of Africa, 2013. https://doi.org/10.1016/B978-0-12-405927-

6.00010-2.

[52] M. Uchimiya, A.T. Stone, Reversible redox chemistry of quinones: Impact on biogeochemical cycles, Chemosphere. 77 (2009) 451–458. https://doi.org/10.1016/j.chemosphere.2009.07.025.

[53] J.T. Nurmi, P.G. Tratnyek, Electrochemical properties of natural organic matter (NOM), fractions of NOM, and model biogeochemical electron shuttles, Environ. Sci. Technol. 36 (2002) 617–624. https://doi.org/10.1021/es0110731.

[54] J.B. Conant, H.M. Kahn, L.F. Fieser, S.S. Kurtz, An electrochemical study of the reversible reduction of organic compounds, J. Am. Chem. Soc. 44 (1922) 1382–1396. https://doi.org/10.1021/ja01427a020.

[55] F. Pan, Q. Wang, Redox species of redox flow batteries: A review, Molecules. 20 (2015) 20499–20517. https://doi.org/10.3390/molecules201119711.

[56] P.S. Guin, S. Das, P.C. Mandal, Electrochemical Reduction of Quinones in Different Media: A Review, Int. J. Electrochem. 2011 (2011) 1–22. https://doi.org/10.4061/2011/816202.

[57] K. Wedege, E. Dražević, D. Konya, A. Bentien, Organic Redox Species in Aqueous Flow Batteries: Redox Potentials, Chemical Stability and Solubility, Sci. Rep. 6 (2016) 1–13. https://doi.org/10.1038/srep39101.

[58] Z. Yang, L. Tong, D.P. Tabor, E.S. Beh, M.A. Goulet, D. De Porcellinis, A. Aspuru-Guzik, R.G. Gordon, M.J. Aziz, Alkaline Benzoquinone Aqueous Flow Battery for Large-Scale Storage of Electrical Energy, Adv. Energy Mater. 8 (2017) 1702056. https://doi.org/10.1002/aenm.201702056.

[59] R.G. Compton, Richard G ; Bathelor-mcauley, Christopher ; Dickinson F J, Edmund ;, Understanding Voltammetry - problems and solutions, Imperial College Press, Oxford, 2012.

[60] M.A. Goulet, L. Tong, D.A. Pollack, D.P. Tabor, S.A. Odom, A. Aspuru-Guzik, E.E. Kwan, R.G. Gordon, M.J. Aziz, Extending the lifetime of organic flow batteries via redox state management, J. Am. Chem. Soc. 141 (2019) 8014–8019. https://doi.org/10.1021/jacs.8b13295.

[61] P. Sun, Y. Liu, Y. Li, M.A. Shehzad, Y. Liu, P. Zuo, Q. Chen, Z. Yang, T. Xu, 110th Anniversary: Unleashing the Full Potential of Quinones for High Performance Aqueous Organic Flow Battery, Ind. Eng. Chem. Res. 58 (2019) 3994–3999. https://doi.org/10.1021/acs.iecr.8b06391.

[62] L. Tong, M.A. Goulet, D.P. Tabor, E.F. Kerr, D. De Porcellinis, E.M. Fell, A. Aspuru-Guzik, R.G. Gordon, M.J. Aziz, Molecular Engineering of an Alkaline Naphthoquinone Flow Battery, ACS Energy Lett. 4 (2019) 1880–1887. https://doi.org/10.1021/acsenergylett.9b01321.

[63] D.G. Kwabi, K. Lin, Y. Ji, E.F. Kerr, M.A. Goulet, D. De Porcellinis, D.P. Tabor, D.A. Pollack, A. Aspuru-Guzik, R.G. Gordon, M.J. Aziz, Alkaline Quinone Flow Battery with Long Lifetime at pH 12, Joule. 2 (2018) 1894–1906. https://doi.org/10.1016/j.joule.2018.07.005.

[64] C. Wang, Z. Yang, Y. Wang, P. Zhao, W. Yan, G. Zhu, L. Ma, B. Yu, L. Wang, G. Li, J. Liu, Z. Jin, High-Performance Alkaline Organic Redox Flow Batteries Based on 2-Hydroxy-3-carboxy-1,4-naphthoquinone, ACS Energy Lett. 3 (2018) 2404–2409. https://doi.org/10.1021/acsenergylett.8b01296.

[65] Y. Ji, M.A. Goulet, D.A. Pollack, D.G. Kwabi, S. Jin, D. De Porcellinis, E.F. Kerr, R.G. Gordon, M.J. Aziz, A Phosphonate-Functionalized Quinone Redox Flow Battery at Near-Neutral pH with Record Capacity Retention Rate, Adv. Energy Mater. 9 (2019) 1–7. https://doi.org/10.1002/aenm.201900039.

[66] S. Jin, Y. Jing, D.G. Kwabi, Y. Ji, L. Tong, D. De Porcellinis, M.A. Goulet, D.A. Pollack, R.G. Gordon, M.J. Aziz, A Water-Miscible Quinone Flow Battery with High Volumetric Capacity and Energy Density, ACS Energy Lett. 4 (2019) 1342–1348. https://doi.org/10.1021/acsenergylett.9b00739.

[67] M.R. Gerhardt, L. Tong, R. Gómez-Bombarelli, Q. Chen, M.P. Marshak, C.J. Galvin, A. Aspuru-Guzik, R.G. Gordon, M.J. Aziz, Anthraquinone Derivatives in Aqueous Flow Batteries, Adv. Energy Mater. 7 (2017). https://doi.org/10.1002/aenm.201601488.

[68] Q. Chen, L. Eisenach, M.J. Aziz, Cycling Analysis of a Quinone-Bromide Redox Flow Battery, J. Electrochem. Soc. 163 (2016) A5057–A5063. https://doi.org/10.1149/2.0081601jes.

[69] B. Yang, A. Murali, A. Nirmalchandar, B. Jayathilake, G.K.S. Prakash, S.R. Narayanan, A Durable, Inexpensive and Scalable Redox Flow Battery Based on Iron Sulfate and Anthraquinone Disulfonic Acid, J. Electrochem. Soc. 167 (2020) 060520. https://doi.org/10.1149/1945-7111/ab84f8.

[70] D.C. Shu Zhang, Xin Li*, Beijing, An Organic Electroactive Material for Flow Batteries, Electrochim. Acta. 190 (2016) 737–743. https://doi.org/10.1016/j.electacta.2015.12.139.

[71] L. Hoober-burkhardt, S. Krishnamoorthy, B. Yang, A. Murali, A. Nirmalchandar, G.K.S. Prakash, S.R. Narayanan, A New Michael-Reaction-Resistant Benzoquinone for Aqueous Organic Redox Flow Batteries, 164 (2017) 600–607. https://doi.org/10.1149/2.0351704jes.

[72] F.R. Brushett, A.N. Jansen, J.T. Vaughey, L. Su, J.D. Millshtein, Materials for use with aqueous redox flow batteries and related methods and systems, US 2015 / 0236543 A1, 2015.

[73] M. Park, E.S. Beh, E.M. Fell, Y. Jing, E.F. Kerr, D. De Porcellinis, M.A. Goulet, J. Ryu, A.A. Wong, R.G. Gordon, J. Cho, M.J. Aziz, A High Voltage Aqueous Zinc–Organic Hybrid Flow Battery, Adv. Energy Mater. 9 (2019) 1–8. https://doi.org/10.1002/aenm.201900694.

[74] P.K. Leung, T. Martin, A.A. Shah, M.A. Anderson, J. Palma, Membrane-less organic-inorganic aqueous flow batteries with improved cell potential, Chem. Commun. 52 (2016) 14270–14273. https://doi.org/10.1039/C6CC07692K.

[75] M. Vijayakumar, L. Li, Z. Nie, Z. Yang, J. Hu, Structure and stability of hexa-aqua V(III) cations in vanadium redox flow battery electrolytes, Phys. Chem. Chem. Phys. 14 (2012) 10233–10242. https://doi.org/10.1039/c2cp40707h.

[76] M. Vijayakumar, L. Li, G. Graff, J. Liu, H. Zhang, Z. Yang, J.Z. Hu, Towards understanding the poor thermal stability of V5+ electrolyte solution in Vanadium Redox Flow Batteries, J. Power Sources. 196 (2011) 3669–3672. https://doi.org/10.1016/j.jpowsour.2010.11.126.

[77] M. Vijayakumar, S.D. Burton, C. Huang, L. Li, Z. Yang, G.L. Graff, J. Liu, J. Hu, S.K. Maria, Nuclear magnetic resonance studies on vanadium(IV) electrolyte solutions for vanadium redox flow battery, J. Power Sources. 195 (2010) 7709–7717. https://doi.org/10.1016/j.jpowsour.2010.05.008.

[78] H.R. Jiang, M.C. Wu, Y.X. Ren, W. Shyy, T.S. Zhao, Towards a uniform distribution of zinc in the negative electrode for zinc bromine flow batteries, Appl. Energy. 213 (2018) 366–374. https://doi.org/10.1016/j.apenergy.2018.01.061.

[79] S. Er, C. Suh, M.P. Marshak, A. Aspuru-Guzik, Computational design of molecules for an all-quinone redox flow battery, Chem. Sci. 6 (2015) 885–893. https://doi.org/10.1039/c4sc03030c.

[80] R.S. Assary, F.R. Brushett, L.A. Curtiss, Reduction potential predictions of some aromatic nitrogen-containing molecules, RSC Adv. 4 (2014) 57442–57451. https://doi.org/10.1039/c4ra08563a.

[81] A. Pasadakis-Kavounis, V. Baj, J. Hjelm, Electrochemical characterization of aromatic molecules with 1,4-diaza groups for flow battery applications, Molecules. 26 (2021) 1–13. https://doi.org/10.3390/molecules26082227.

[82] L. Cheng, R.S. Assary, X. Qu, A. Jain, S.P. Ong, N.N. Rajput, K. Persson, L.A. Curtiss, Accelerating Electrolyte Discovery for Energy Storage with High-Throughput Screening, J. Phys. Chem. Lett. 6 (2015) 283–291. https://doi.org/10.1021/jz502319n.

[83] D.P. Tabor, R. Gómez-Bombarelli, L. Tong, R.G. Gordon, M.J. Aziz, A. Aspuru-Guzik, Mapping the frontiers of quinone stability in aqueous media: Implications for organic aqueous redox flow batteries, J. Mater. Chem. A. 7 (2019) 12833–12841. https://doi.org/10.1039/c9ta03219c.

[84] E. Lewars, G, Computational chemistry, third, Springer Nature, 2016.

[85] R.P. Fornari, M. Mesta, J. Hjelm, T. Vegge, P. De Silva, Molecular Engineering Strategies for Symmetric Aqueous Organic Redox Flow Batteries, ACS Mater. Lett. 2 (2020) 239–246. https://doi.org/10.1021/acsmaterialslett.0c00028.

[86] R.S. Assary, L. Zhang, J. Huang, L.A. Curtiss, Molecular level understanding of the factors affecting the stability of dimethoxy benzene catholyte candidates from first-principles investigations, J. Phys. Chem. C. 120 (2016) 14531–14538. https://doi.org/10.1021/acs.jpcc.6b04263.

[87] S. Kim, A. Jinich, A. Aspuru-Guzik, MultiDK: A Multiple Descriptor Multiple Kernel Approach for Molecular Discovery and Its Application to Organic Flow Battery Electrolytes, J. Chem. Inf. Model. 57 (2017) 657–668. https://doi.org/10.1021/acs.jcim.6b00332.

[88] E. V. Carino, J. Staszak-Jirkovsky, R.S. Assary, L.A. Curtiss, N.M. Markovic, F.R. Brushett, Tuning the Stability of Organic Active Materials for Nonaqueous Redox Flow Batteries via Reversible, Electrochemically Mediated Li+ Coordination, Chem. Mater. 28 (2016) 2529–2539. https://doi.org/10.1021/acs.chemmater.5b04053.

[89] G. Gryn'ova, J.M. Barakat, J.P. Blinco, S.E. Bottle, M.L. Coote, Computational design of cyclic nitroxides as efficient redox mediators for dye-sensitized solar cells, Chem. - A Eur. J. 18 (2012) 7582–7593. https://doi.org/10.1002/chem.201103598.

[90] K.M. Pelzer, L. Cheng, L.A. Curtiss, Effects of functional groups in redox-active organic molecules: A high-throughput screening approach, J. Phys.

Chem. C. 121 (2017) 237–245. https://doi.org/10.1021/acs.jpcc.6b11473.

[91] Y. Moon, Y. Han, Computational screening of organic molecules as redox active species in redox fl ow batteries, Curr. Appl. Phys. 16 (2016) 939–943. https://doi.org/10.1016/j.cap.2016.05.012.

[92] Y. Ding, Y. Li, G. Yu, Exploring Bio-inspired Quinone-Based Organic Redox Flow Batteries: A Combined Experimental and Computational Study, Chem. 1 (2016) 790–801. https://doi.org/10.1016/j.chempr.2016.09.004.

[93] M.T. Huynh, C.W. Anson, A.C. Cavell, S.S. Stahl, S. Hammes-Schiffer, Quinone 1 e- and 2 e-/2 H+ Reduction Potentials: Identification and Analysis of Deviations from Systematic Scaling Relationships, J. Am. Chem. Soc. 138 (2016) 15903–15910. https://doi.org/10.1021/jacs.6b05797.

[94] M. Martínez-Cifuentes, R. Salazar, O. Ramírez-Rodríguez, B. Weiss-López, R. Araya-Maturana, Experimental and theoretical reduction potentials of some biologically active ortho-carbonyl para-quinones, Molecules. 22 (2017). https://doi.org/10.3390/molecules22040577.

[95] S.D. Pineda Flores, G.C. Martin-Noble, R.L. Phillips, J. Schrier, Bio-Inspired Electroactive Organic Molecules for Aqueous Redox Flow Batteries. 1. Thiophenoquinones, J. Phys. Chem. C. 119 (2015) 21800–21809. https://doi.org/10.1021/acs.jpcc.5b05346.

[96] M.J.S. Dewar, N. Trinajstic, Ground states of conjugated molecules-XIV. Redox potentials of quinones, Tetrahedron. 25 (1969) 4529–4534. https://doi.org/10.1016/S0040-4020(01)82995-1.

[97] R. Atkins, Peter; Friedman, Molecular quantum mechanics, 4th ed., oxford university press, 2008.

[98] J. Leszczynski, A. Kaczmarek-kedziera, T. Puzyn, M. G. Papadopoulos, H. Reis, M. K. Shukla, Handbook of Computational Chemistry, second edi, Springer Nature, 2012.

[99] C.D. Sherrill, Basis Sets in Quantum Chemistry C. David Sherrill School of Chemistry and Biochemistry Georgia Institute of Technology, 56 (2002) 276–278. http://www.ncbi.nlm.nih.gov/pubmed/12649950.

[100] H. Gong, Z. He, A. Peng, X. Zhang, B. Cheng, Y. Sun, L. Zheng, K. Huang, Effects of several quinones on insulin aggregation, Sci. Rep. 4 (2014) 1–8. https://doi.org/10.1038/srep05648.

[101] R.H. Thomson, Distribution of naturally occorruing quinones, Pharm. Weekbl. Sci. Ed. 13 (1991) 70–73.

[102] R.H. Thomson., Naturally Occurring Quinones IV - Recent advances, 1997. https://doi.org/10.1016/0031-9422(72)85070-2.

[103] R.C. Prince, P. Leslie Dutton, J. Malcolm Bruce, Electrochemistry of ubiquinones. Menaquinones and plastoquinones in aprotic solvents, FEBS Lett. 160 (1983) 273–276. https://doi.org/10.1016/0014-5793(83)80981-8.

[104] M. Liu, S. Lu, Plastoquinone and Ubiquinone in Plants: Biosynthesis, Physiological Function and Metabolic Engineering, Front. Plant Sci. 7 (2016) 1–18. https://doi.org/10.3389/fpls.2016.01898.

[105] M.D. Collins, H.N.M. Ross, B.J. Tindall, W.D. Grant, Distribution of Isoprenoid Quinones in Halophilic Bacteria, J. Appl. Bacteriol. 50 (1981) 559–565. https://doi.org/10.1111/j.1365-2672.1981.tb04258.x.

[106] J.F. Imhoff, Quinones of phototrophic purple bacteria, FEMS Microbiol. Lett. 25 (1984) 85–89. https://doi.org/10.1111/j.1574-6968.1984.tb01381.x.

[107] Q. Huang, G. Lu, H.M. Shen, M.C.M. Chung, N.O. Choon, Anti-cancer properties of anthraquinones from rhubarb, Med. Res. Rev. 27 (2007) 609–630. https://doi.org/10.1002/med.20094.

[108] F. Fang, J.B. Wang, Y.L. Zhao, C. Jin, W.J. Kong, H.P. Zhao, H.J. Wang, X.H. Xiao, A comparative study on the tissue distributions of rhubarb anthraquinones in normal and CCl 4-injured rats orally administered rhubarb extract, J. Ethnopharmacol. 137 (2011) 1492–1497. https://doi.org/10.1016/j.jep.2011.08.028.

[109] F. Kurosaki, H. Nagase, A. Nishi, Stimulation of anthraquinone production in rhubarb tissue culture by an ethylene-generating reagent, Phytochemistry. 31 (1992) 2735–2738. https://doi.org/10.1016/0031-9422(92)83621-5.

[110] S.A. Khan, A. Ahmad, M.I. Khan, M. Yusuf, M. Shahid, N. Manzoor, F. Mohammad, Antimicrobial activity of wool yarn dyed with Rheum emodi L. (Indian Rhubarb), Dye. Pigment. 95 (2012) 206–214. https://doi.org/10.1016/j.dyepig.2012.04.010.

[111] V. Page, J.P. Schwitzguébel, Metabolism of sulphonated anthraquinones in rhubarb, maize and celery: the role of cytochromes P450 and peroxidases., Plant Cell Rep. 28 (2009) 1725–1735. https://doi.org/10.1007/s00299-009-0772-5.

[112] N. El-Najjar, H. Gali-Muhtasib, R.A. Ketola, P. Vuorela, A. Urtti, H. Vuorela, The chemical and biological activities of quinones: Overview and implications in analytical detection, Phytochem. Rev. 10 (2011) 353–370. https://doi.org/10.1007/s11101-011-9209-1.

[113] Bruce Alberts, Essential Cell Biology, 4th ed., WW Norton & Co, 2013.

[114] A. Fleming, On the antibacterial action of cultures of a penicillium, with special reference to their use in the isolation of B.influenzae, Brit. J. Exp. Pethol. 10 (1929) 226–236.

[115] N.P. Keller, Translating biosynthetic gene clusters into fungal armor and weaponry, Nat. Chem. Biol. 11 (2015) 671–677. https://doi.org/10.1038/nchembio.1897.

[116] N.P. Keller, G. Turner, J.W. Bennett, Fungal secondary metabolism - From biochemistry to genomics, Nat. Rev. Microbiol. 3 (2005) 937–947. https://doi.org/10.1038/nrmicro1286.

[117] J. Berdi, Bioactive Microbial Metabolites, J. Antibiot. (Tokyo). 58 (2005) 1–26. https://doi.org/https://doi.org/10.1038/ja.2005.1.

[118] A.L. Demain, Importance of microbial natural products and the need to revitalize their discovery, J. Ind. Microbiol. Biotechnol. 41 (2014) 185–201. https://doi.org/10.1007/s10295-013-1325-z.

[119] M. Künzler, How fungi defend themselves against microbial competitors and animal predators, PLoS Pathog. 14 (2018) 1–10. https://doi.org/10.1371/journal.ppat.1007184.

[120] H.C. Eisenman, A. Casadevall, Synthesis and assembly of fungal melanin, Appl. Microbiol. Biotechnol. 93 (2012) 931–940. https://doi.org/10.1007/s00253-011-3777-2.

[121] M. Carlile, S. Watkinson, G.G. Gooday, The Fungi, 2nd ed., Acedemic Press, 2001.

[122] C. Hertweck, The biosynthetic logic of polyketide diversity, Angew. Chemie - Int. Ed. 48 (2009) 4688–4716. https://doi.org/10.1002/anie.200806121.

[123] J. Chun, V. Brinkman, A Mechanistically Novel, First Oral Therapy for Multiple Sclerosis: The Development of Fingolimod (FTY720, Gilenya), Discov. Med. 12 (2011) 213–228. https://www.ncbi.nlm.nih.gov/pmc/articles/PMC3624763/pdf/nihms412728.

pdf.

[124] B. Hamad, The antibiotics market, Nat. Rev. Drug Discov. 9 (2010) 675–676. https://doi.org/10.1038/nrd3267.

[125] K. Tao, L. Du, X. Sun, M. Cai, T. Zhu, X. Zhou, Q. Gu, Y. Zhang, Biosynthesis of aspergiolide A, a novel antitumor compound by a marine-derived fungus Aspergillus glaucus via the polyketide pathway, Tetrahedron Lett. 50 (2009) 1082–1085. https://doi.org/10.1016/j.tetlet.2008.12.094.

[126] R.L. Wong, C.M. Winslow, C. Kevin D., The mechanisms of action of cyclosporin A in the treatment of psoriasis, Immunol. Today. 14 (1993) 69–74. https://doi.org/10.1016/0167-5699(93)90061-O.

[127] M. Faseleh Jahromi, J.B. Liang, Y.W. Ho, R. Mohamad, Y.M. Goh, P. Shokryazdan, Lovastatin production by Aspergillus terreus using agro-biomass as substrate in solid state fermentation, J. Biomed. Biotechnol. 2012 (2012). https://doi.org/10.1155/2012/196264.

[128] J.A. Tobert, Lovastatin and beyond: The history of the HMG-CoA reductase inhibitors, Nat. Rev. Drug Discov. 2 (2003) 517–526. https://doi.org/10.1038/nrd1112.

[129] M. Peraica, B. Radić, A. Lucić, M. Pavlović, Toxic effects of mycotoxins in humans, Bull. World Health Organ. 77 (1999) 754–766.

[130] E. Streit, K. Naehrer, I. Rodrigues, G. Schatzmayr, Mycotoxin occurrence in feed and feed raw materials worldwide: Long-term analysis with special focus on Europe and Asia, J. Sci. Food Agric. 93 (2013) 2892–2899. https://doi.org/10.1002/jsfa.6225.

[131] T. Kuiper-Goodman, P.M. Scott, Risk assessment of the mycotoxin ochratoxin A, Biomed. Environ. Sci. 2 (1989) 179—248. http://europepmc.org/abstract/MED/2692617.

[132] R. Dean, J.A.L. Van Kan, Z.A. Pretorius, K.E. Hammond-Kosack, A. Di Pietro, P.D. Spanu, J.J. Rudd, M. Dickman, R. Kahmann, J. Ellis, G.D. Foster, The Top 10 fungal pathogens in molecular plant pathology, Mol. Plant Pathol. 13 (2012) 414–430. https://doi.org/10.1111/j.1364-3703.2011.00783.x.

[133] C.E. Windels, Economic and social impacts of Fusarium head blight: Changing farms and rural communities in the Northern Great Plains, Phytopathology. 90 (2000) 17–21. https://doi.org/10.1094/PHYTO.2000.90.1.17.

[134] J. Gilbert, S. Haber, Overview of some recent research developments in fusarium head blight of wheat, Can. J. Plant Pathol. 35 (2013) 149–174. https://doi.org/10.1080/07060661.2013.772921.

[135] J.F. Leslie, B.A. Summerell, The Fusarium Laboratory Manual, Blackwell Publishing, 2006.

[136] A.A. Brakhage, Regulation of fungal secondary metabolism, Nat. Rev. Microbiol. 11 (2013) 21–32. https://doi.org/10.1038/nrmicro2916.

[137] N.P. Keller, T.M. Hohnt, Metabolic Pathway Gene Clusters in Filamentous Fungi, Fungal Genet. Biol. 21 (1997) 17–29. https://doi.org/10.1006/fgbi.1997.0970.

[138] J.H. Yu, N. Keller, Regulation of secondary metabolism in filamentous fungi, Annu. Rev. Phytopathol. 43 (2005) 437–458. https://doi.org/10.1146/annurev.phyto.43.040204.140214.

[139] C.M.K. Sieber, W. Lee, P. Wong, M. Münsterkötter, H.W. Mewes, C. Schmeitzl, E. Varga, F. Berthiller, G. Adam, U. Güldener, The Fusarium graminearumgenome reveals more secondary metabolite gene clusters and hints of horizontal gene transfer, PLoS One. 9 (2014). https://doi.org/10.1371/journal.pone.0110311.

[140] K. Hoogendoorn, L. Barra, C. Waalwijk, J.S. Dickschat, T.A.J. van der Lee, M.H. Medema, Evolution and diversity of biosynthetic gene clusters in Fusarium, Front. Microbiol. 9 (2018) 1–12. https://doi.org/10.3389/fmicb.2018.01158.

[141] M.R. Nielsen, T.E. Sondergaard, H. Giese, J.L. Sørensen, Advances in linking polyketides and non-ribosomal peptides to their biosynthetic gene clusters in Fusarium, Curr. Genet. 65 (2019) 1263–1280. https://doi.org/10.1007/s00294-019-00998-4.

[142] R. Kalra, X.A. Conlan, M. Goel, Fungi as a Potential Source of Pigments: Harnessing Filamentous Fungi, Front. Chem. 8 (2020) 1–23. https://doi.org/10.3389/fchem.2020.00369.

[143] L. Studt, P. Wiemann, K. Kleigrewe, H.U. Humpf, B. Tudzynski, Biosynthesis of fusarubins accounts for pigmentation of fusarium Fujikuroi perithecia, Appl. Environ. Microbiol. 78 (2012) 4468–4480. https://doi.org/10.1128/AEM.00823-12.

[144] R.J.N. Frandsen, S.A. Rasmussen, P.B. Knudsen, S. Uhlig, D. Petersen, E.

Lysøe, C.H. Gotfredsen, H. Giese, T.O. Larsen, Black perithecial pigmentation in Fusarium species is due to the accumulation of 5-deoxybostrycoidin-based melanin, Sci. Rep. 6 (2016) 1–13. https://doi.org/10.1038/srep26206.

[145] R. McDaniel, S. Ebert-Khosla, C. Khosla, D.A. Hopwood, Engineered Biosynthesis of Novel Polyketides: ActVII and actIV Genes Encode Aromatase and Cyclase Enzymes, Respectively, J. Am. Chem. Soc. 116 (1994) 10855–10859. https://doi.org/10.1021/ja00103a001.

[146] R.J. Heath, C.O. Rock, The Claisen condensation in biology, Nat. Prod. Rep. 19 (2002) 581–596. https://doi.org/10.1039/b110221b.

[147] J.L. Meier, M.D. Burkart, The chemical biology of modular biosynthetic enzymes, Chem. Soc. Rev. 38 (2009) 2012–2045. https://doi.org/10.1039/b805115c.

[148] F.T. Hansen, D.M. Gardiner, E. Lysøe, P.R. Fuertes, B. Tudzynski, P. Wiemann, T.E. Sondergaard, H. Giese, D.E. Brodersen, J.L. Sørensen, An update to polyketide synthase and non-ribosomal synthetase genes and nomenclature in Fusarium, Fungal Genet. Biol. 75 (2015) 20–29. https://doi.org/10.1016/j.fgb.2014.12.004.

[149] D.W. Brown, R.H. Proctor, Insights into natural products biosynthesis from analysis of 490 polyketide synthases from Fusarium, Fungal Genet. Biol. 89 (2016) 37–51. https://doi.org/10.1016/j.fgb.2016.01.008.

[150] Y.M. Chiang, B.R. Oakley, N.P. Keller, C.C.C. Wang, Unraveling polyketide synthesis in members of the genus Aspergillus, Appl. Microbiol. Biotechnol. 86 (2010) 1719–1736. https://doi.org/10.1007/s00253-010-2525-3.

[151] F.T. Hansen, J.L. Sørensen, H. Giese, T.E. Sondergaard, R.J.N. Frandsen, Quick guide to polyketide synthase and nonribosomal synthetase genes in Fusarium, Int. J. Food Microbiol. 155 (2012) 128–136. https://doi.org/10.1016/j.ijfoodmicro.2012.01.018.

[152] T.E. Sondergaard, M. Fredborg, A.M. Oppenhagen Christensen, S.K. Damsgaard, N.F. Kramer, H. Giese, J.L. Sørensen, Fast Screening of Antibacterial Compounds from Fusaria, Toxins (Basel). 8 (2016) 1–9. https://doi.org/10.3390/toxins8120355.

[153] A. Shah, M.A. Rather, Q.P. Hassan, M.A. Aga, S. Mushtaq, A.M. Shah, A. Hussain, S.A. Baba, Z. Ahmad, Discovery of anti-microbial and anti-tubercular molecules from Fusarium solani: an endophyte of Glycyrrhiza

glabra, J. Appl. Microbiol. 122 (2017) 1168–1176. https://doi.org/10.1111/jam.13410.

[154] N.S. Chowdhury, M.H. Sohrab, M.S. Rana, C.M. Hasan, S. Jamshidi, K.M. Rahman, Cytotoxic Naphthoquinone and Azaanthraquinone Derivatives from an Endophytic Fusarium solani, J. Nat. Prod. 80 (2017) 1173–1177. https://doi.org/10.1021/acs.jnatprod.6b00610.

[155] N. Khan, F. Afroz, M.N. Begum, S. Roy Rony, S. Sharmin, F. Moni, C. Mahmood Hasan, K. Shaha, M.H. Sohrab, Endophytic Fusarium solani: A rich source of cytotoxic and antimicrobial napthaquinone and aza-anthraquinone derivatives, Toxicol. Reports. 5 (2018) 970–976. https://doi.org/10.1016/j.toxrep.2018.08.016.

[156] A. Medentsev, Fungal Naphthoquinone metabolites (review), Appl. Microbiol. Biotechnol. 32 (1996) 7–29.

[157] A.G. Medentsev, V.K. Akimenko, Naphthoquinone metabolites of the fungi, Phytochemistry. 47 (1998) 935–959. https://doi.org/10.1016/S0031-9422(98)80053-8.

[158] D.O. Futuro, P.G. Ferreira, C.D. Nicoletti, L.P. Borba-Santos, F.C. Da Silva, S. Rozental, V.F. Ferreira, The antifungal activity of naphthoquinones: An integrative review, An. Acad. Bras. Cienc. 90 (2018) 1187–1214. https://doi.org/10.1590/0001-3765201820170815.

[159] H. Haraguchi, K. Yokoyama, S. Oike, M. Ito, H. Nozaki, Respiratory stimulation and generation of superoxide radicals in Pseudomonas aeruginosa by fungal naphthoquinones, Arch. Microbiol. 167 (1997) 6–10. https://doi.org/10.1007/s002030050409.

[160] A.M. Calvo, R.A. Wilson, J.W. Bok, N.P. Keller, Relationship between Secondary Metabolism and Fungal Development, Microbiol. Mol. Biol. Rev. 66 (2002) 447–459. https://doi.org/10.1128/MMBR.66.3.447-459.2002.

[161] R.L. Buchanan, H.G. Stahl, Ability of various carbon sourced to induce and support Aflatoxin synthesis by Apergillus parasiticus, J. Food Saf. 6 (1984) 271–279. https://doi.org/https://doi.org/10.1111/j.1745-4565.1984.tb00488.x.

[162] A. Abdollahi, R.L. Buchanan, Regulation of Aflatoxin Biosynthesis: Characterization of Glucose as an Apparent Inducer of Aflatoxin Production, J. Food Sci. 46 (1981) 143–146. https://doi.org/https://doi.org/10.1111/j.1365-2621.1981.tb14549.x.

[163] T. Kachholz, A.L. Demain, Nitrate repression of averufin and aflatoxin biosynthesis, J. Nat. Prod. 46 (1983) 499–506. https://doi.org/10.1021/np50028a013.

[164] A.A. Brakhage, Molecular Regulation of β-Lactam Biosynthesis in Filamentous Fungi, Microbiol. Mol. Biol. Rev. 62 (1998) 547–585. https://doi.org/10.1128/mmbr.62.3.547-585.1998.

[165] G.H. Feng, T.J. Leonard, Culture conditions control expression of the genes for aflatoxin and sterigmatocystin biosynthesis in Aspergillus parasiticus and A. nidulans, Appl. Environ. Microbiol. 64 (1998) 2275–2277. https://doi.org/10.1128/aem.64.6.2275-2277.1998.

[166] N.P. Keller, C. Nesbitt, B. Sarr, T.D. Phillips, G.B. Burow, pH regulation of sterigmatocystin and aflatoxin biosynthesis in Aspergillus spp., Phytopathology. 87 (1997) 643–648. https://doi.org/10.1094/PHYTO.1997.87.6.643.

[167] J. Morrice, D.A. MacKenzie, A.J. Parr, D.B. Archer, Isolation and characterisation of the acetyl-CoA carboxylase gene from Aspergillus nidulans, Curr. Genet. 34 (1998) 379–385. https://doi.org/10.1007/s002940050410.

[168] B. Tudzynski, V. Homann, B. Feng, G.A. Marzluf, Isolation, characterization and disruption of the areA nitrogen regulatory gene of Gibberella fujikuroi, Mol. Gen. Genet. 261 (1999) 106–114. https://doi.org/10.1007/s004380050947.

[169] H. Kim, C.P. Woloshuk, Role of AREA, a regulator of nitrogen metabolism, during colonization of maize kernels and fumonisin biosynthesis in Fusarium verticillioides, Fungal Genet. Biol. 45 (2008) 947–953. https://doi.org/10.1016/j.fgb.2008.03.007.

[170] L. Studt, P. Wiemann, K. Kleigrewe, H.U. Humpf, B. Tudzynski, Biosynthesis of fusarubins accounts for pigmentation of fusarium Fujikuroi perithecia, Appl. Environ. Microbiol. 78 (2012) 4468–4480. https://doi.org/10.1128/AEM.00823-12.

[171] R. Bramble, G.A. Marzluf, The Mycota, Springer Berlin Heidelberg, 1996. https://doi.org/10.1007/978-3-662-06064-3.

[172] P.J. Cotty, Aflatoxin and sclerotial production by Aspergillus flavus; Influence of pH, Physiol. Biochem. 78 (1988) 1250–1253.

[173] M.E.H. Müller, I. Steier, R. Köppen, D. Siegel, M. Proske, U. Korn, M. Koch, Cocultivation of phytopathogenic Fusarium and Alternaria strains affects fungal growth and mycotoxin production, J. Appl. Microbiol. 113 (2012) 874–887. https://doi.org/10.1111/j.1365-2672.2012.05388.x.

[174] T. Netzker, J. Fischer, J. Weber, D.J. Mattern, C.C. König, V. Valiante, V. Schroeckh, A.A. Brakhage, Microbial communication leading to the activation of silent fungal secondary metabolite gene clusters, Front. Microbiol. 6 (2015) 1–13. https://doi.org/10.3389/fmicb.2015.00299.

[175] G. Li, S. Kusari, C. Golz, C. Strohmann, M. Spiteller, Three cyclic pentapeptides and a cyclic lipopeptide produced by endophytic: Fusarium decemcellulare LG53, RSC Adv. 6 (2016) 54092–54098. https://doi.org/10.1039/c6ra10905e.

[176] Y.Q. Zhang, M. Brock, N.P. Keller, Connection of propionyl-CoA metabolism to polyketide biosynthesis in Aspergillus nidulans, Genetics. 168 (2004) 785–794. https://doi.org/10.1534/genetics.104.027540.

[177] H.B. Bode, B. Bethe, R. Höfs, A. Zeeck, Big effects from small changes: Possible ways to explore nature's chemical diversity, ChemBioChem. 3 (2002) 619–627. https://doi.org/10.1002/1439-7633(20020703)3:7<619::AID-CBIC619>3.0.CO;2-9.

[178] C.F.P. Hemphill, P. Sureechatchaiyan, M.U. Kassack, R.S. Orfali, W. Lin, G. Daletos, P. Proksch, OSMAC approach leads to new fusarielin metabolites from Fusarium tricinctum, J. Antibiot. (Tokyo). 70 (2017) 726–732. https://doi.org/10.1038/ja.2017.21.

[179] P. Linnemannstöns, J. Schulte, M. Del Mar Prado, R.H. Proctor, J. Avalos, B. Tudzynski, The polyketide synthase gene pks4 from Gibberella fujikuroi encodes a key enzyme in the biosynthesis of the red pigment bikaverin, Fungal Genet. Biol. 37 (2002) 134–148. https://doi.org/10.1016/S1087-1845(02)00501-7.

[180] Y.T. Kim, Y.R. Lee, J. Jin, K.H. Han, H. Kim, J.C. Kim, T. Lee, S.H. Yun, Y.W. Lee, Two different polyketide synthase genes are required for synthesis of zearalenone in Gibberella zeae, Mol. Microbiol. 58 (2005) 1102–1113. https://doi.org/10.1111/j.1365-2958.2005.04884.x.

[181] K.R. Westphal, S. Heidelbach, E.J. Zeuner, M. Riisgaard-Jensen, M.E. Nielsen, S.Z. Vestergaard, N.S. Bekker, J. Skovmark, C.K. Olesen, K.H. Thomsen, S.K. Niebling, J.L. Sørensen, T.E. Sondergaard, The effects of different potato dextrose agar media on secondary metabolite production in

Fusarium, Int. J. Food Microbiol. 347 (2021) 109171. https://doi.org/10.1016/j.ijfoodmicro.2021.109171.

[182] J.L. Sørensen, T.E. Sondergaard, The effects of different yeast extracts on secondary metabolite production in Fusarium, Int. J. Food Microbiol. 170 (2014) 55–60. https://doi.org/10.1016/j.ijfoodmicro.2013.10.024.

[183] Q.W. Zhang, L.G. Lin, W.C. Ye, Techniques for extraction and isolation of natural products: A comprehensive review, Chinese Med. (United Kingdom). 13 (2018) 1–26. https://doi.org/10.1186/s13020-018-0177-x.

[184] P.G. Mazzola, A.M. Lopes, F.A. Hasmann, A.F. Jozala, T.C. Penna, P.O. Magalhaes, C.O.R.-Y. Rangel-Yagui, A.P. Pessoa Jr, Review Liquid–liquid extraction of biomolecules: an overview and update of the main techniques, J. Chem. Technol. Biotechnol. 83 (2008) 143–157. https://doi.org/10.1002/jctb.1794.

[185] M.I.H. Khan, M.H. Sohrab, S.R. Rony, F.S. Tareq, C.M. Hasan, M.A. Mazid, Cytotoxic and antibacterial naphthoquinones from an endophytic fungus, Cladosporium sp., Toxicol. Reports. 3 (2016) 861–865. https://doi.org/10.1016/j.toxrep.2016.10.005.

[186] J. Smedsgaard, Micro-scale extraction procedure for standardization screening of fungal metabolite production in cultures, J. Chromatogr. A. 760 (1997) 264–270. https://doi.org/10.1016/S0021-9673(96)00803-5.

[187] J.L. Sørensen, K.F. Nielsen, T.E. Sondergaard, Redirection of pigment biosynthesis to isocoumarins in Fusarium, Fungal Genet. Biol. 49 (2012) 613–618. https://doi.org/10.1016/j.fgb.2012.06.004.

[188] S.H. Hansen, S. Pedersen-Bjergaard, Bioanalysis of Pharmaceuticals, John Wiley and sons ltd, 2015. https://doi.org/10.1002/9781118716830.

[189] T. Awakawa, T. Kaji, T. Wakimoto, I. Abe, A heptaketide naphthaldehyde produced by a polyketide synthase from Nectria haematococca, Bioorganic Med. Chem. Lett. 22 (2012) 4338–4340. https://doi.org/10.1016/j.bmcl.2012.05.005.

[190] B.S. Menezes, L.S. Solidade, A.A. Conceição, M.N. Santos Junior, P.L. Leal, E.S. de Brito, K.M. Canuto, S. Mendonça, F.G. de Siqueira, L.M. Marques, Pigment production by Fusarium solani BRM054066 and determination of antioxidant and anti-inflammatory properties, AMB Express. 10 (2020). https://doi.org/10.1186/s13568-020-01054-y.

[191] I. Kurobane, L.C. Vining, Metabolites of Fusarium Solani related to Dihydrofusarubin, J. Antibiot. (Tokyo). XXXIII (1980) 1376–1379.

[192] K. M VanderMolen, H. A Raja, T. El-Elimat, N. H Oberlies, Evaluation of culture media for the production of secondary metabolites in a natural products screening program, AMB Express. 3 (2013) 71. https://doi.org/10.1186/2191-0855-3-71.

[193] A.M. Hyde, S.L. Zultanski, J.H. Waldman, Y.L. Zhong, M. Shevlin, F. Peng, General Principles and Strategies for Salting-Out Informed by the Hofmeister Series, Org. Process Res. Dev. 21 (2017) 1355–1370. https://doi.org/10.1021/acs.oprd.7b00197.

[194] H.I. Okur, J. Hladílková, K.B. Rembert, Y. Cho, J. Heyda, J. Dzubiella, P.S. Cremer, P. Jungwirth, Beyond the Hofmeister Series: Ion-Specific Effects on Proteins and Their Biological Functions, J. Phys. Chem. B. 121 (2017) 1997–2014. https://doi.org/10.1021/acs.jpcb.6b10797.

[195] K.R. Westphal, R.D. Wollenberg, F.A. Herbst, J.L. Sørensen, T.E. Sondergaard, R. Wimmer, Enhancing the production of the fungal pigment aurofusarin in Fusarium graminearum, Toxins (Basel). 10 (2018) 1–11. https://doi.org/10.3390/toxins10110485.

[196] M.R. Nielsen, A. Karolina, R. Holzwarth, E. Brew, N. Chrapkova, S. Evelyne, K. Kaniki, K. Kastaniegaard, T. Sørensen, K.R. Westphal, R. Wimmer, T.E. Sondergaard, J.L. Sørensen, A new vector system for targeted integration and overexpression of genes in the crop pathogen Fusarium solani, Fungal Biol. Biotechnol. (2019) 1–10. https://doi.org/10.1186/s40694-019-0089-2.

[197] T.B. Pedersen, M.R. Nielsen, S.B. Kristensen, E.M.L. Spedtsberg, W. Yasmine, R. Matthiesen, S.E.K. Kaniki, T. Sørensen, C. Petersen, J. Muff, T.E. Sondergaard, K.L. Nielsen, R. Wimmer, J.L. Sørensen, Heterologous expression of the core genes in the complex fusarubin gene cluster of Fusarium Solani, Int. J. Mol. Sci. 21 (2020) 1–10. https://doi.org/10.3390/ijms21207601.

[198] S.B. Kristensen, T.B. Pedersen, M.R. Nielsen, R. Wimmer, J. Muff, J.L. Sørensen, Production and selectivity of key fusarubins from Fusarium solani due to media composition ., Toxins (Basel). 13 (2021) 1–12. https://doi.org/https://doi.org/10.3390/toxins13060376.

[199] R.A. Baker, J.H. Tatum, S. Nemec, Antimicrobial activity of naphthoquinones from Fusaria, Mycopathologia. 111 (1990) 9–15. https://doi.org/10.1007/BF02277294.

[200] M. Cisse, F. Vaillant, D. Soro, M. Reynes, M. Dornier, Crossflow microfiltration for the cold stabilization of roselle (Hibiscus sabdariffa L.) extract, J. Food Eng. 106 (2011) 20–27. https://doi.org/10.1016/j.jfoodeng.2011.04.001.

[201] A. Cassano, F. Tasselli, C. Conidi, E. Drioli, Ultrafiltration of Clementine mandarin juice by hollow fibre membranes, Desalination. 241 (2009) 302–308. https://doi.org/10.1016/j.desal.2007.10.102.

[202] A. Cassano, C. Conidi, E. Drioli, Physico-chemical parameters of cactus pear (Opuntia ficus-indica) juice clarified by microfiltration and ultrafiltration processes, Desalination. 250 (2010) 1101–1104. https://doi.org/10.1016/j.desal.2009.09.117.

[203] L.M.J. de Carvalho, I.M. de Castro, C.A.B. da Silva, A study of retention of sugars in the process of clarification of pineapple juice (Ananas comosus, L. Merril) by micro- and ultra-filtration, J. Food Eng. 87 (2008) 447–454. https://doi.org/10.1016/j.jfoodeng.2007.12.015.

[204] A. Saxena, B.P. Tripathi, M. Kumar, V.K. Shahi, Membrane-based techniques for the separation and purification of proteins: An overview, Adv. Colloid Interface Sci. 145 (2009) 1–22. https://doi.org/10.1016/j.cis.2008.07.004.

[205] C. Ursino, R. Castro-Muñoz, E. Drioli, L. Gzara, M.H. Albeirutty, A. Figoli, Progress of nanocomposite membranes for water treatment, Membranes (Basel). 8 (2018) 1–40. https://doi.org/10.3390/membranes8020018.

[206] R. Castro-Muñoz, C. Conidi, A. Cassano, Membrane-based technologies for meeting the recovery of biologically active compounds from foods and their by-products, Crit. Rev. Food Sci. Nutr. 59 (2019) 2927–2948. https://doi.org/10.1080/10408398.2018.1478796.

[207] G.T. Vladisavljević, P. Vukosavljević, B. Bukvić, Permeate flux and fouling resistance in ultrafiltration of depectinized apple juice using ceramic membranes, J. Food Eng. 60 (2003) 241–247. https://doi.org/10.1016/S0260-8774(03)00044-X.

[208] J. Li, H.A. Chase, Applications of membrane techniques for purification of natural products, Biotechnol. Lett. 32 (2010) 601–608. https://doi.org/10.1007/s10529-009-0199-7.

[209] E. Díaz-Montes, R. Castro-Muñoz, Metabolites recovery from fermentation broths via pressure-driven membrane processes, Asia-Pacific J. Chem. Eng.

14 (2019). https://doi.org/10.1002/apj.2332.

[210] C.M. Galanakis, R. Castro-Muñoz, A. Cassano, C. Conidi, Recovery of high-added-value compounds from food waste by membrane technology, Membr. Technol. Biorefining. (2016) 189–215. https://doi.org/10.1016/B978-0-08-100451-7.00008-6.

[211] R. Kuriyel, A.L. Zydney, Sterile Filtration and Virus Filtration, Humana Press. 9 (2000) 185–194. https://doi.org/10.1007/978-1-59259-027-8_14.

[212] C.L. Astudillo-Castro, Limiting flux and critical transmembrane pressure determination using an exponential model: The effect of concentration factor, temperature, and cross-flow velocity during casein micelle concentration by microfiltration, Ind. Eng. Chem. Res. 54 (2015) 414–425. https://doi.org/10.1021/ie5033292.

[213] R. Castro-Muñoz, V. Fíla, Membrane-based technologies as an emerging tool for separating high-added-value compounds from natural products, Trends Food Sci. Technol. 82 (2018) 8–20. https://doi.org/10.1016/j.tifs.2018.09.017.

[214] Y. Li, A. Shahbazi, C.T. Kadzere, Separation of cells and proteins from fermentation broth using ultrafiltration, J. Food Eng. 75 (2006) 574–580. https://doi.org/10.1016/j.jfoodeng.2005.04.045.

[215] R. Balti, R. Le Balc'h, N. Brodu, M. Gilbert, B. Le Gouic, S. Le Gall, C. Sinquin, A. Massé, Concentration and purification of Porphyridium cruentum exopolysaccharides by membrane filtration at various cross-flow velocities, Process Biochem. 74 (2018) 175–184. https://doi.org/10.1016/j.procbio.2018.06.021.

[216] B.E. Knuckles, D. De Fremery, E.M. Bickoff, G.O. Kohler, Soluble Protein from Alfalfa Juice by Membrane Filtration, J. Agric. Food Chem. 23 (1975) 209–212. https://doi.org/10.1021/jf60198a030.

[217] R.S. Juang, H.L. Chen, Y.C. Lin, Ultrafiltration of Coagulation-Pretreated Serratia marcescens Fermentation Broth: Flux Characteristics and Prodigiosin Recovery, Sep. Sci. Technol. 47 (2012) 1849–1856. https://doi.org/10.1080/01496395.2012.665117.

[218] M.H.M. Isa, R.A. Frazier, P. Jauregi, A further study of the recovery and purification of surfactin from fermentation broth by membrane filtration, Sep. Purif. Technol. 64 (2008) 176–182. https://doi.org/10.1016/j.seppur.2008.09.008.

[219] K. Prochaska, J. Antczak, M. Regel-Rosocka, M. Szczygiełda, Removal of succinic acid from fermentation broth by multistage process (membrane separation and reactive extraction), Sep. Purif. Technol. 192 (2018) 360–368. https://doi.org/10.1016/j.seppur.2017.10.043.

[220] S.L. Li, C. Li, Y.S. Liu, X.L. Wang, Z.A. Cao, Separation of L-glutamine from fermentation broth by nanofiltration, J. Memb. Sci. 222 (2003) 191–201. https://doi.org/10.1016/S0376-7388(03)00290-4.

[221] H.D. Lee, M.Y. Lee, Y.S. Hwang, Y.H. Cho, H.W. Kim, H.B. Park, Separation and Purification of Lactic Acid from Fermentation Broth Using Membrane-Integrated Separation Processes, Ind. Eng. Chem. Res. 56 (2017) 8301–8310. https://doi.org/10.1021/acs.iecr.7b02011.

[222] D.P. Zagklis, C.A. Paraskeva, Purification of grape marc phenolic compounds through solvent extraction, membrane filtration and resin adsorption/desorption, Sep. Purif. Technol. 156 (2015) 328–335. https://doi.org/10.1016/j.seppur.2015.10.019.

[223] C. Conidi, A.D. Rodriguez-Lopez, E.M. Garcia-Castello, A. Cassano, Purification of artichoke polyphenols by using membrane filtration and polymeric resins, Sep. Purif. Technol. 144 (2015) 153–161. https://doi.org/10.1016/j.seppur.2015.02.025.

[224] Z. Zhu, Q. Wu, X. Di, S. Li, F.J. Barba, M. Koubaa, S. Roohinejad, X. Xiong, J. He, Multistage recovery process of seaweed pigments: Investigation of ultrasound assisted extraction and ultra-filtration performances, Food Bioprod. Process. 104 (2017) 40–47. https://doi.org/10.1016/j.fbp.2017.04.008.

[225] J. Heinze, Cyclic Voltammetry—"Electrochemical Spectroscopy". New Analytical Methods (25), Angew. Chemie Int. Ed. English. 23 (1984) 831–847. https://doi.org/10.1002/anie.198408313.

[226] N. Elgrishi, K.J. Rountree, B.D. McCarthy, E.S. Rountree, T.T. Eisenhart, J.L. Dempsey, A Practical Beginner's Guide to Cyclic Voltammetry, J. Chem. Educ. 95 (2018) 197–206. https://doi.org/10.1021/acs.jchemed.7b00361.

[227] P.T. Kissinger, W.R. Heineman, Cyclic voltammetry, J. Chem. Educ. 60 (1983) 702. https://doi.org/10.1021/ed060p702.

[228] D. Pletcher, A first course in electrode processes, 2nd ed., RSC publishing, 2009.

[229] K. Likit-Anurak, K. Uthaichana, K. Punyawudho, Y. Khunatorn, The Performance and Efficiency of Organic Electrolyte Redox Flow Battery Prototype, Energy Procedia. 118 (2017) 54–62. https://doi.org/10.1016/j.egypro.2017.07.012.

[230] A. Benjamin, E. Agar, C.R. Dennison, E.C. Kumbur, On the quantification of coulombic efficiency for vanadium redox flow batteries: Cutoff voltages vs. state-of-charge limits, Electrochem. Commun. 35 (2013) 42–44. https://doi.org/10.1016/j.elecom.2013.07.041.

[231] A. Eftekhari, Energy efficiency: A critically important but neglected factor in battery research, Sustain. Energy Fuels. 1 (2017) 2053–2060. https://doi.org/10.1039/c7se00350a.

[232] R. Chen, S. Kim, Z. Chang, Redox Flow Batteries: Fundamentals and Applications, Redox - Princ. Adv. Appl. (2017). https://doi.org/10.5772/intechopen.68752.

[233] E. Sánchez-Díez, E. Ventosa, M. Guarnieri, A. Trovò, C. Flox, R. Marcilla, F. Soavi, P. Mazur, E. Aranzabe, R. Ferret, Redox flow batteries: Status and perspective towards sustainable stationary energy storage, J. Power Sources. 481 (2021). https://doi.org/10.1016/j.jpowsour.2020.228804.

[234] A. Khataee, E. Dražević, J. Catalano, A. Bentien, Performance Optimization of Differential pH Quinone-Bromide Redox Flow Battery, J. Electrochem. Soc. 165 (2018) A3918–A3924. https://doi.org/10.1149/2.0681816jes.

[235] K. Wedege, J. Azevedo, A. Khataee, A. Bentien, A. Mendes, Direct Solar Charging of an Organic–Inorganic, Stable, and Aqueous Alkaline Redox Flow Battery with a Hematite Photoanode, Angew. Chemie - Int. Ed. 55 (2016) 7142–7147. https://doi.org/10.1002/anie.201602451.

[236] S.B. Kristensen, T. Van Mourik, T.B. Pedersen, J.L. Sørensen, J. Muff, Simulation of electrochemical properties of naturally occurring quinones, Sci. Rep. (2020) 1–10. https://doi.org/10.1038/s41598-020-70522-z.

[237] B.R. Chalamala, T. Soundappan, G.R. Fisher, M.R. Anstey, V. V. Viswanathan, M.L. Perry, Redox flow batteries: An engineering perspective, Proc. IEEE. 102 (2014) 976–999. https://doi.org/10.1109/JPROC.2014.2320317.

[238] S.B. Kristensen, M.N. Fini, T.B. Pedersen, J.L. Sørensen, J. Muff, Membrane based separation and purification of fusarubins from Fusarium solani, Sep. Purif. Technol. 278 (2021) 1–9.

https://doi.org/10.1016/j.seppur.2021.119576.

[239] J.P. Perdew, A. Ruzsinszky, J. Tao, V.N. Staroverov, G.E. Scuseria, G.I. Csonka, Prescription for the design and selection of density functional approximations: More constraint satisfaction with fewer fits, J. Chem. Phys. 123 (2005). https://doi.org/10.1063/1.1904565.

[240] D.C. Haris, Quantitative chemical analysis, 8th ed., W.H. Freeman and company, 2010.

Papers

List of papers

1. **Kristensen, S.B.**; Mourik, T. Van; Pedersen, T.B.; Sørensen, J.L.; Muff, J. (2020) *Simulation of electrochemical properties of naturally occurring quinones*.
Scientific Reports, doi:10.1038/s41598-020-70522-z.

2. **Kristensen, S.B.**; Pedersen, T.B.; Nielsen, M.R.; Wimmer, R.; Muff, J.; Sørensen, J.L. (2021) *Production and selectivity of key fusarubins from Fusarium solani due to media composition*.
Toxins, doi:10.3390/toxins13060376.

3. **Kristensen, S.B**.; Fini, M.N.; Pedersen, T.B.; Sørensen, J.L.; Muff, J. *Membrane based separation and purification of fusarubins from Fusarium solani.*
Separation and Purification Technology, doi:10.1016/j.seppur.2021.119576.

4. Wilhelmsen, C.O.; **Kristensen, S.B**.; Nolte, O.; Volodin, I.; Christiansen, J.V.; Petersen, T.I.; Larsen, T.O.; Frisvad, J.C.; Hager, M.; Schubert, S.U.; Muff, J; Sørensen, J.L. (2021) *The fungal battery: A redox flow battery containing the biosynthesised negolyte phoenicin.*
Manuscript in draft

Side projects:

5. Pedersen, T.B.; Nielsen, M.R.; **Kristensen, S.B**.; Spedtsberg, E.M.L.; Yasmine, W.; Matthiesen, R.; Kaniki, S.E.K.; Sørensen, T.; Petersen, C.; Muff, J.; et al. (2020) *Heterologous expression of the core genes in the complex fusarubin gene cluster of Fusarium Solani.*
International Journal of Molecular Science, doi:10.3390/ijms21207601.

6. Pedersen, T.B.; Nielsen, M.R.; **Kristensen, S.B**.; Spedtsberg, E.M.L.; Sørensen, T.; Petersen, C.; Muff, J.; Søndergaard, T.S.; Nielsen, K.L.; Wimmer, R.; Gardiner, D.M.; Sørensen, J.L. (2021) *Speed dating for enzymes! Finding the perfect Phosphopantetheinyl Transferase partner for Your Polyketide Synthase.*
Manuscript submitted to Microbial Cell Factories

Paper 1

Kristensen, S.B.; Mourik, T. Van; Pedersen, T.B.; Sørensen, J.L.; Muff, J. (2020) *Simulation of electrochemical properties of naturally occurring quinones*.

www.nature.com/scientificreports

SCIENTIFIC REPORTS
nature research

OPEN

Simulation of electrochemical properties of naturally occurring quinones

Sebastian Birkedal Kristensen[1], Tanja van Mourik[2], Tobias Bruun Pedersen[1], Jens Laurids Sørensen[1]✉ & Jens Muff[1]

Quinones are produced in organisms and are utilized as electron transfer agents, pigments and in defence mechanisms. Furthermore, naturally occurring quinones can also be cytotoxins with antibacterial properties. These properties can be linked to their redox properties. Recent studies have also shown that quinones can be utilized in flow battery technology, though naturally occurring quinones have not yet been investigated. Here, we have analyzed the properties of 990 different quinones of various biological sources through a computation approach to determine their standard reduction potentials and aqueous solubility. The screening was performed using the PBE functional and the 6-31G basis set, providing a distribution of reduction potentials of the naturally occurring quinones varying from − 1.4 V to 1.5 V vs. the standard hydrogen electrode. The solvation energy for each quinone, which indicates the solubility in aqueous solution, was calculated at the same level. A large distribution of solubilities was obtained, containing both molecules that show tendencies of good solubilities and molecules that do not. The solubilities are dependent on the nature of the side groups and the size of the molecules. Our study shows that the group containing the quinones of fungal origin, which is also the largest of the groups considered, has the largest antimicrobial and electrochemical potential, when considering the distribution of reduction potentials for the compounds.**

Quinones are organic molecules found in nature in a variety of different types with different properties based on chemical and aromatic ring structure, side-chain groups, etc. Quinones in nature fall into the category of secondary metabolites, and are found in flowering plants, fungi, bacteria, algae and in some amounts in animals[1,2]. Common to all of them is the aromatic di-one or di-ketone system, which can be placed both in para or ortho positions. Quinones are often described as derivatives from oxidization of hydroquinones or polyphenols[3,4]. Naturally occurring quinones include aromatic ring structures ranging from the common 1-ring structures named benzoquinones (BQ), 2-ring structures named naphtoquinones (NQ) and 3-ring structures named anthraquinones (AQ) as well as more complex polyquinones[1–4]. In most eukaryote cells plastoquinone and ubiquinone conduct electron transport in the oxygenic photosynthesis and the aerobic respiratory chain, respectively [2,5–7]. The function of quinones in living organisms is primarily due to their ability to undergo reversible $2e^-$ redox reactions that through complex reaction mechanisms protect the cells against free radicals and other potential harmful oxidants.

Quinones have during the past two decades been investigated in detail in plants, due to their medicinal properties in e.g. rhubarb (*Rheum* spp.[3,8–12]). The plant itself has been used in Chinese medicine since the Han dynasty[9]. It has also been shown that the AQs of rhubarb can inhibit bacterial growth, treat cancer, and inhibit protein misfolding and aggregation, which can be useful in the treatment of diabetes[3,9,10]. When challenged by microorganisms, rhubarb uses the secondary metabolites as a defence mechanism and it has been shown that the production of quinones increases when the plant is exposed to elicitor-active chemicals[13]. The compounds found in rhubarb can also be utilized as dyes and pigments as numerous quinones naturally absorb light in the visible range of the electromagnetic spectrum due to the presence of conjugated double bonds in the structure. The pigments and dyes can furthermore act as antibacterial agents when used as treatment of woolen thread[14].

[1]Department of Chemistry and Bioscience, Section of Chemical Engineering, Aalborg University, Niels Bohrs Vej 8, 6700 Esbjerg, Denmark. [2]School of Chemistry, University of St. Andrews, North Haugh, St. Andrews, Fife KY16 9ST, Scotland, UK. ✉email: jls@bio.aau.dk

These antimicrobial properties have been linked to the plant's redox biochemistry, and consequently to the quinones, as they often acts as electron transfer agents[11,15].

The occurrence of quinones in bacteria is also well known and widely described. In phototrophic bacteria the quinones perform different functions as electron transfer agents in respiratory and photosynthetic processes. Menaquinones and ubiquinones are constituents of bacterial plasma membranes and represent an important role in electron transfer and possibly also in phosphorylation[2,6,7]. It is well known that fungi produce a plethora of secondary metabolites with a variety of functions, used in survival and communication in natural habitats. Among the most famous antibacterial agents found in fungi is penicillin, found in the *Penicillium* and *Aspergillus* species[16]. Some of the secondary metabolites from fungi contain quinone structures in different variations[2,17–20]. The complex mechanism of cytotoxic properties of the quinone metabolites can be attributed to the interaction with the mitochondrial nicotinamide adenine dinucleotide (NAD) and NAD phosphate (NADP) dependent flavin enzymes, where the quinone undergoes a reduction, and hereby produces semiquinone radicals. These can react with oxygen and hereby create superoxides which, together with the semiquinone radicals, can damage DNA, RNA and other macromolecules[20–22]. Furthermore, the oxidative stress can induce apoptosis, which has been observed in several organisms and cancer cells[23,24]. Similarly to plants, the defence mechanism in fungi can therefore also be attributed to the redox behavior of these compounds. However, due to versatile structure and characteristics of biologically produced quinones, the cytotoxic mechanism for each quinone is far from fully determined. An example of determined cytotoxic properties can be seen in the *Fusarium* species, that produces, among others, the quinone aurofusarin. This compound has shown inhibitory effects towards different types of bacteria including *Lactobacillus* and *Bifidobacterium*[25]. Understanding the redox behavior of quinones is a key component in understanding how these compounds work antimicrobially, for example in dyes of various sorts, thereby expanding our knowledge of the biochemistry of organisms, especially with respect to the medical use of quinones. The reduction potential can be directly linked to the microbial properties of the quinone structure[20,25]. The solubility of the compounds is also an important property to take into account, as a quinone with a higher solubility can travel easier around cells, through cell walls etc., and can be utilized to a larger extent than a compound with a lower solubility. Due to the redox properties of quinones, the use of quinones as electrolytes in flow batteries has in recent years become an area of interest, where quinones have shown potential as substitutes for metals such as vanadium[26–33]. In this field of research the focus has so far been on synthetically prepared quinones, and changing sidechain groups for improvement of reduction potentials and solubility has been the main emphasis[26–33]. The naturally occuring quinones however present the same kind of redox activity. This paper is thereby also a screening for the extent of reduction potentials found in natural occurring quinones and their solubility in aqueous solutions for potential uses in flow battery technology. Previous reports have determined the electrochemical potential of artificial or chemically synthesized quinones through various computational methods[26,27,34–37]. In this paper, we have used a similar approach on 990 natural occurring quinones, primarily derived from bacteria and fungi.

Results and discussion

Distribution of E^0 of naturally occurring quinones. In order to predict the redox potentials (E^0) of known quinones of biological origin, we followed the pipeline outlined in Fig. 1. The dataset consisted of quinones from various sources, including 221 quinones from bacteria, 358 derived from fungi and 425 from "other" sources such as yeast, algae and plants. All was analyzed using density functional theory (DFT). Some of the quinones (e.g. herbarin, which is produced both in yeast[38], and in fungi[39]) are produced in several different sources and are included twice, thereby making the sum of the above listed numbers exceed 990 (Supplementary Table 1). The distribution of the predicted E^0 of the naturally occurring quinones is visualized in Fig. 2A. The histogram shows that the majority of the predicted E^0 falls between − 0.4 V versus SHE and 0.7 V versus SHE, with slight indication towards a normal distribution of the potentials. The predicted values stretch from the most negative value at − 1.382 V versus SHE to the most positive value at 1.485 V versus SHE. The skewness of the distribution, − 0.6179, indicates that the distribution is slightly skewed towards the left (Supplemental Fig. 1). Dividing the quinones in groups according to the number of rings, shows that single-ring compounds (BQs) are located primarily around a median value of 0.4970 V versus SHE, although two compounds are placed at the positive extreme (Fig. 2B). The NQs (209 structures) display a wider distribution at both ends compared to the BQs, with a median value of 0.2870 V versus SHE and a mean value of 0.2340 V versus SHE. The largest group of quinone structures contains 411 different AQ structures. The mean and median of the AQs are 0.0024 V versus SHE and 0.0119 V versus SHE, respectively, the lowest of the four groups. The BQs, 276 structures, have the most positive mean value of 0.4788 V versus SHE. The structures with four or more rings form the smallest group, with 94 members. These have the largest diversity in potentials, with both positive and negative values. The mean is at the positive side of the diagram, 0.1803 V versus SHE, and the median is 0.3040 V versus SHE.

Closer examination of the analysed quinones shows that the seven quinones with the most positive potentials are all produced from various species of fungi, mostly from the species *Penicillium* and *Fusarium* (Table 1). With a value of 1.485 V versus SHE, the compound with the most positive redox potential is tridentoquinone, a molecule produced by *Suillus tridentinus*[40]. Tridentoquinone is a benzoquinone, and the solubility descriptor indicates that it has a rather low relative solubility in water, which could be due to the large carbon chain in the compound, including several methyl groups, and double bonds. In general the seven most positive quinones show low numbers of electron donating groups (EDGs), such as –OH. These groups have been described as lowering the reduction potential when present[34], and they show a similar tendency in this study. The positive list also includes compounds that are smaller than the negative compounds, displaying less aromacity leading to higher reduction potentials.

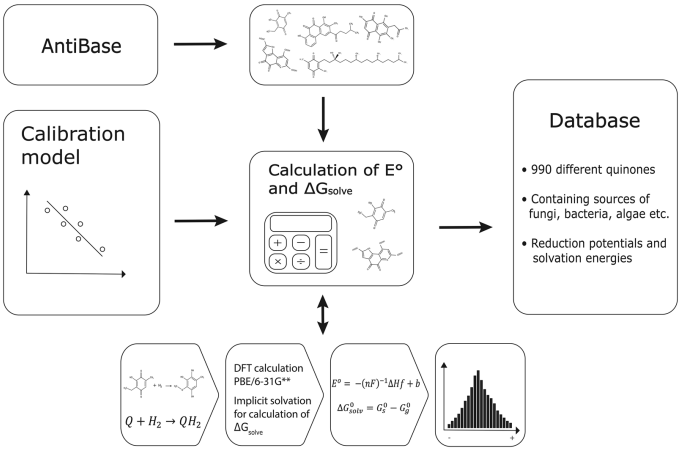

Figure 1. Flow diagram of the computational procedure employed in the study.

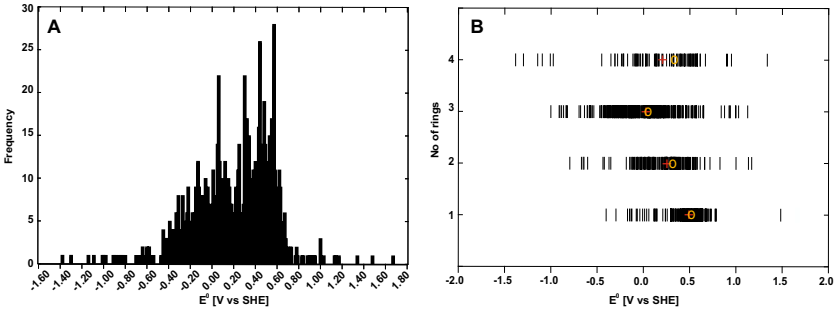

Figure 2. (**A**) histogram of distribution of predicted redox potentials. (**B**) distribution of redox potentials based on the number of aromatic rings within the compounds.

Whereas the quinones with the most positive potentials predominately originated from fungi and are relatively small and simple compounds, the quinones with the most negative potentials are larger and more complex quinone structures (Table 2). The compound with the most negative redox potential (− 1.382 V vs. SHE) is pradimicin M, which is produced in a mutant of the bacterium *Actinomadura hibisca*. The compound contains five rings and is therefore within the group of ≥ 4 ring structures. The results shows that, even though the compounds are larger than the quinones with predicted positive potentials, they have higher solubility descriptors, which can be linked to the presence of seven EDGs leading to an enhancement of the polarity of the compound. The number of EDGs present in the seven most negative compounds is significantly higher than in the compounds presenting positive reduction potentials, in agreement with findings in similar studies[34]. It is furthermore interesting that the structures of stemphyltoxin, altertoxin I, altertoxin II and stemphyltoxin IV are so similar; they only differ in the placement of the side chain groups. The structure of stemphyperylenol (Table 1), which has a positive potential, is also similar to the negative-potential compounds discussed above; however, the aromatic rings in this compound are placed opposite each other, and the compound contains a larger number of polar side chain groups. This may explain the large difference in reduction potential. The compound 7-epi-sclerotiorin (Table 1) , which has a simulated reduction potential of 1.001 V versus SHE, contains no EDGs,

Name	E^0 V versus SHE	ΔG_{solv}	Source	Structure
Tridentoquinone	1.485	− 38.10	[F] *Suillus tridentinus*	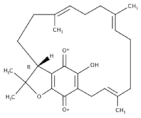
Stemphyperylenol	1.338	− 75.20	[F] *Stemphylium botryosum*	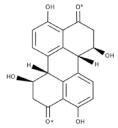
Citrinin hydrate	1.170	− 60.82	[F] *Penicillium* spp. *Aspergillus* spp.	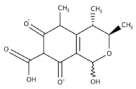
Fusarnaphthoquinone A	1.135	− 32.95	[F] *Fusarium* spp.	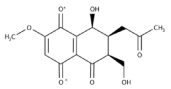
5-Hydroxydihydrofusarubin B	1.126	− 52.50	[F] *Fusarium* sp.	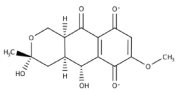
5-Hydroxy-3-methoxydihydrofusarubin D	1.028	− 51.20	[F] *Fusarium* sp.	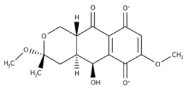
7-epi-Sclerotiorin	1.001	− 55.08	[F] *Penicillium hirayamae*	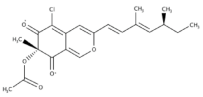

Table 1. Properties of the seven quinones with the most negative potentials. [F]-fungi, [B]-bacteria, * indicates the point of reduction of the reactant.

but a –Cl group which tends to make the reduction potential positive according to the study of Er et al.[34], in agreement with findings in this manuscript. The full list of quinones and their predicted potentials is provided in the supporting information.

Distribution of E^0 according to biological origin. To get an overview of the electrochemical properties of the quinones according to their biological origin we divided the dataset into three groups: bacteria, fungi and others (plants, algea, animals etc.; Fig. 3 and Supplementary Fig. 2). The majority of the reduction potentials of the bacterial quinones is located in the middle of the histogram (Fig. 3A and Supplemental Fig. 3). The reduction potentials of the fungal quinones are more widely distributed compared to those in the other two groups (Fig. 3B and Supplemental Fig. 4). Thus, the fungi-produced compounds constitute the most varied group. The reduction potentials of the collective group of "other" quinones is centered around the middle values of the histogram with no extreme values (Fig. 3C and Supplemental Fig. 5).

Name	E^0 V versus SHE	ΔG_{solv}	Source	Structure
Pradimicin M	− 1.382	− 74.94	[B] *Actinomadura hibisca*	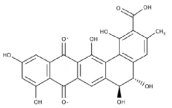
Stemphyltoxin I	− 1.298	− 40.15	[F] *Stemphylium botryosum*	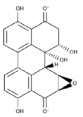
Granaticin B	− 1.144	− 72.42	[B] *Streptomyces spiroverticillatus*	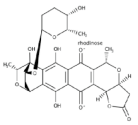
Altertoxin I	− 1.094	− 37.34	[F] *Alternaria* spp.	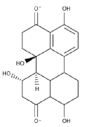
Altertoxin II	− 1.008	− 41.94	[F] *Stemphylium botryosum* *Alternaria* spp.	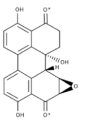
3-*O*-methyldihydrofusarubin A	− 1.001	− 33.43	[F] *Fusarium martii*	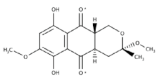
Stemphyltoxin IV	− 0.976	− 36.40	[F] *Stemphylium botryosum*	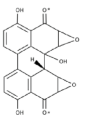

Table 2. Properties of the seven quinones with the most negative potentials [F]-fungi, [B]-bacteria, * indicates the point of reduction of the reactant.

Correlation of solubility and electrochemical potential. The calculated solubility of the quinones ranges between 0–100 kJ/mol, with only a few compounds outside this range (Fig. 4A). A breakdown of the ΔG_{solv} descriptors according to the number of rings in the quinones shows only marginal differences (Fig. 4B). The ≥ 4 group has the largest mean value of − 54.1543 kJ/mol and median of − 53.2041 kJ/mol, whereas the three other groups do not show any significant differences in solubility. This disagrees with the expectation that larger organic molecules have a lower solubility due to their larger non-polar surface. Apparently, the solubility of the quinones studied here is more dependent on the polar side chain groups than on their number of rings.

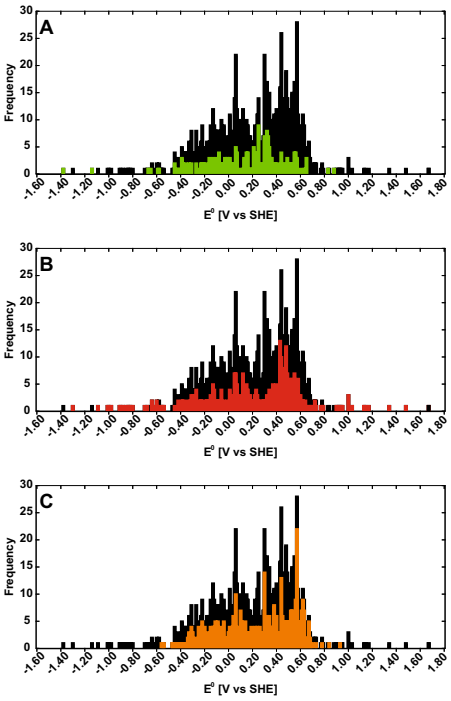

Figure 3. (**A**) distribution of reduction potentials for quinones produced in bacteria, (**B**) distribution of reduction potential for quinones produced in fungi, (**C**) distribution of reduction potentials for quinones produced in "other"(plants, algea , animals etc.). The distribution of the reduction potentials for all quinones is shown in black.

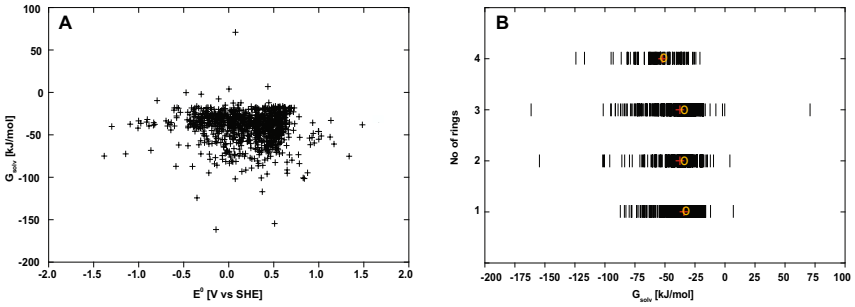

Figure 4. (**A**) Redox-solubility maps of all predicted quinone structures. (**B**) breakdown of solubility according to the number of rings.

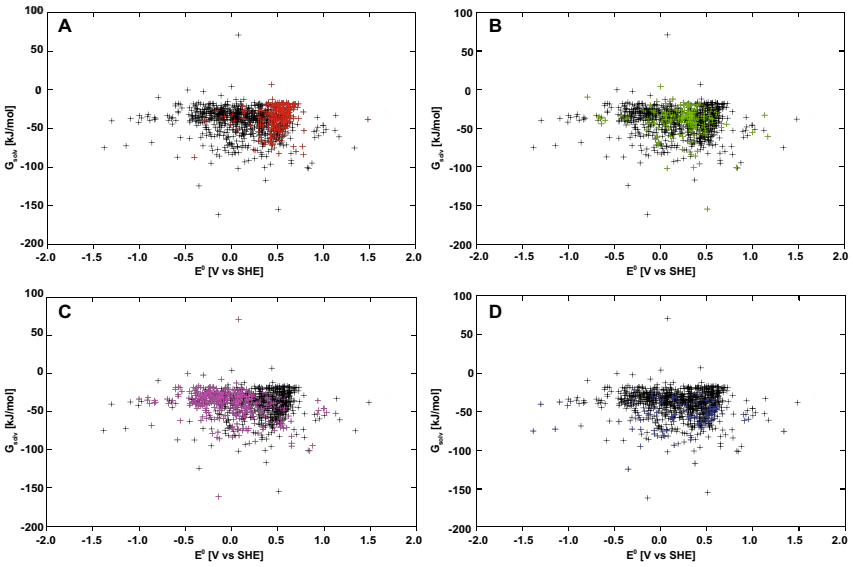

Figure 5. Distribution of quinones based on predicted reduction potential and solubility. (**A**) BQs highlighted with red, (**B**) NQs highlighted with green, (**C**) AQs illustrated with purple, (**D**) ≥ 4 rings is visualized with blue. The black marked points correspond to the values for the other quinone groups.

A breakdown into the BQs, NQs, AQs and ≥ 4 ring groups categories of the distribution of the solubility as a function of the redox potentials is shown in Fig. 5. The solubilities of the BQs tend to be at the positive side of the distribution, whereas the solubilities of the NQs are more centrally located (Fig. 5A,B). The solubilities of the AQs are more distributed towards the negative side compared to the BQs and NQs, which indicates a higher solubility of these compounds (Fig. 5C). The distribution of the BQs, NQs and AQs appears to indicate that the more rings the compound contains the lower is the redox potential, which corresponds to the correlation between higher aromacity and lower reduction potential, discussed above. However, the E^0 values of the ≥ 4 ring structure group are much more varied than those of the BQs, NQs and AQs, which is likely due to the larger variety in overall chemical structure within this group. These compounds have on average a slightly more negative descriptor of solubility, indicating that they have a slightly higher solubility compared to the other groups of quinones (Fig. 5D).

The size of the compounds is usually a significant indicator for the solubility, as larger compounds tend to be less soluble than smaller compounds. In Fig. 6, molecular weight (MW) is presented versus reduction potential and solubility descriptor ΔG_{solv} respectively. The largest compound found in the database, ubiquinone Q12, has a MW of 999.58 g/mol, , and shows a reduction potential of 0.59 V and a ΔG_{solv} of − 40.36 kJ/mol. The ΔG_{solv} and E^0 of this compound are not placed at the extreme ends of the dataset, but placed more positive in both of the parameters. There is not a clear correlation between MW and reduction potential (Fig. 6A); however, the largest distribution of reduction potentials is observed to occur for compounds with smaller MW. Furthermore, a weak tendency towards larger compounds having a more negative ΔG_{solv} can be observed, which corresponds to the general hypothesis; however, the plot shows two slightly correlating tendencies, one which is going vertical, meaning no cooralation (Fig. 6B). The second correlation indicates that the higher MW, the lower the ΔG_{solv} is. The correlation is not significant, and thus, it cannot be concluded that the molecular weight directly influences the E^0 or ΔG_{solv}, the occurrence of polar groups appears to have a larger impact on the E^0 or ΔG_{solv} than the MW of the compounds.

Experimental

A flow diagram of the workflow used in the project is presented in Fig. 1. The reaction of the naturally occurring quinones to hydroquinones was treated as a single step: a rapid, two-electron and two-proton transfer as previously described[26,27,34–37]. The naturally occurring quinones that have been isolated as hydroquinones were initially prepared into oxidized versions, and only two of the hydroxyl or ketone groups were used for the simulation. If a compound presented several redox sites, only one of these was taken into account. The redox site used for the

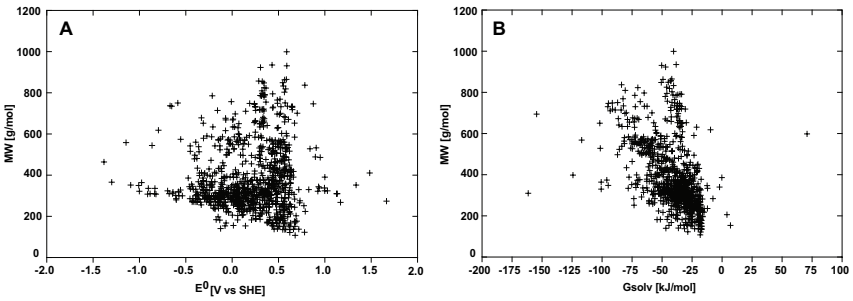

Figure 6. (**A**) Molecular weight versus predicted reduction potential distribution. (**B**) Molecular weight versus G_{solv} distribution.

simulation has been marked with a * in Tables 1 and 2. The quinones that have been changed from the isolated form are marked with either a (1) or (2), according to the number of sites that have been changed prior to simulation, in the complete list of simulated naturally occurring quinones (Supplemental Table 1). The reaction scheme applied in the screening used the thermodynamic cycle shown in Supplemental Fig. 6.

Database creation. A local database was compiled from AntiBase 2012[41]. The quinones were obtained through multiple searches in AntiBase which contains 41,000 recorded compounds. An initial search identified compounds containing "quinone" as structure name tag, which yielded 767 hits. A search of specific quinones was also conducted; this yielded approximately 40 hits. Lastly, a search for "quinones" in the "properties" search field was conducted; this search yielded 425 quinone structures. A proportion of the compounds appeared in more than one of the searches; these compounds were noted and removed so they only appear once in the database. This resulted in a database containing 990 different quinone structures originating from various sources i.e. fungi, bacteria, plants and animals.

Development of the calibration model. To calculate the electrochemical properties of the 990 identified quinones we developed a method based on earlier published research on the screening of quinones[26,30,34,42], which also employed DFT. All DFT calculations in the current project were carried out using the Gaussian 09 software[43]. First, results obtained by the Perdew-Burke-Ernzerhof (PBE[44]) Results obtained with the GGA (generalized gradient approximation) functional PBE and the more computationally demanding meta-hybrid M06-2X functional[45], both coupled with the split-valence 6-31G** basis set, were compared. To calibrate the model, six basic quinones were chosen as representatives of BQs, NQs and AQs. The calibration model employed experimental redox potentials (E^0_{exp}) of these compounds and the change of enthalpies of formation (ΔH_f) of the quinone redox reaction calculated using the two different functionals[46,47]. A line was fitted though the data points using least-squares fitting (Supplemental Fig. 7). The calibration model is based on the modified Nernst equation:

$$E^0 = -(nF)^{-1}\Delta H_f + b \tag{1}$$

where n is the number of electrons transferred (2), F is the Faraday constant and b is the y-axis intercept obtained from the calibration model.

The PBE functional yielded slightly better correlation, $R^2 = 0.9827$ (Supplemental Fig. 7A), compared to the more computationally expensive M06-2X functional with R^2 of 0.9767 (Supplemental Fig. 7B). Therefore, the PBE/6-31G** data is applied to Eq. 1 to obtain the calibration model used in this work (Eq. 2).

$$E^0 = -0.4629\Delta H_f + 0.0572 \tag{2}$$

This equation enabled us to correlate the calculated change in gas-phase enthalpy of formation (ΔH_f) at 0 K to the experimental redox potential for the reaction Q/QH_2.

Computational workflow. The structures in our database were converted from 2D structures into 3D structures using the Avogadro software[48], visualized with GaussView[49], and Gaussian input files were then created for both the reduced and oxidized form of the quinone. The calibration model (Eq. 2) was used to calculate the reduction potentials based on the computed energies, using the PBE/6-31G** functional/basis set combination. For solubility prediction in aqueous media, we used ΔG_{solv} as a descriptor calculated using PBE/6-31G**, for the oxidized forms of the quinones, as these are assumed to have a lower solubility compared to their reduced forms. The ΔG_{solv} was calculated as the difference between the total Gibbs energy of the oxidized quinone in aqueous solution (ΔG_{aq}), calculated using the Polarizable Continuum Model (PCM) implicit solvation model,

using the integral equation formalism variant (IEFPCM), with water as the solvent, using the dielectric constant of water (ε = 78.3553)[50,51], and the total Gibbs energy of the oxidized quinone in gaseous phase (ΔG_{gas}). This infers that the more negative the value of ΔG_{solv}, the higher the solubility of the quinone.

Received: 5 June 2020; Accepted: 30 July 2020
Published online: 11 August 2020

References

1. Thomson, R. H. Distribution of naturally occurring quinones. *Pharm Weekblad.* **13**, 70–73 (1991).
2. Thomson., R. H. Naturally occurring quinones IV—Recent advances (Springer Science+Business Media, 1997).
3. Gong, H. *et al.* Effects of several quinones on insulin aggregation. *Sci. Rep.* **4**, 1–8 (2014).
4. Eyong, K. O., Kuete, V. & Efferth, T. Quinones and benzophenones from the medicinal plants of Africa. *Med. Plant Res. Afr. Pharmacol. Chem.* https://doi.org/10.1016/B978-0-12-405927-6.00010-2 (2013).
5. Liu, M. & Lu, S. Plastoquinone and ubiquinone in plants: Biosynthesis, physiological function and metabolic engineering. *Front. Plant Sci.* **7**, 1–18 (2016).
6. Collins, M. D., Ross, H. N. M., Tindall, B. J. & Grant, W. D. Distribution of isoprenoid quinones in halophilic bacteria. *J. Appl. Bacteriol.* **50**, 559–565 (1981).
7. Imhoff, J. F. Quinones of phototrophic purple bacteria. *FEMS Microbiol. Lett.* **25**, 85–89 (1984).
8. Chen, J. Y., Pan, F., Zhang, T., Xia, J. & Li, Y. J. Experimental study on the molecular mechanism of anthraquinone cathartics in inducing melanosis coli. *Chin. J. Integr. Med.* **17**, 525–530 (2011).
9. Huang, Q., Lu, G., Shen, H. M., Chung, M. C. M. & Choon, N. O. Anti-cancer properties of anthraquinones from rhubarb. *Med. Res. Rev.* **27**, 609–630 (2007).
10. Fang, F. *et al.* A comparative study on the tissue distributions of rhubarb anthraquinones in normal and CCl 4-injured rats orally administered rhubarb extract. *J. Ethnopharmacol.* **137**, 1492–1497 (2011).
11. Page, V. & Schwitzguébel, J. P. Metabolism of sulphonated anthraquinones in rhubarb, maize and celery: the role of cytochromes P450 and peroxidases. *Plant Cell Rep.* **28**, 1725–1735 (2009).
12. Ding, J., Ning, B., Fu, G., Lu, Y. & Dong, S. Separation of rhubarb anthraquinones by capillary electrochromatography. *Chromatographia* **52**, 285–288 (2000).
13. Kurosaki, F., Nagase, H. & Nishi, A. Stimulation of anthraquinone production in rhubarb tissue culture by an ethylene-generating reagent. *Phytochemistry* **31**, 2735–2738 (1992).
14. Khan, S. A. *et al.* Antimicrobial activity of wool yarn dyed with *Rheum emodi* L. (Indian Rhubarb). *Dye. Pigment.* **95**, 206–214 (2012).
15. El-Najjar, N. *et al.* The chemical and biological activities of quinones: Overview and implications in analytical detection. *Phytochem. Rev.* **10**, 353–370 (2011).
16. Fleming, A. On the antibacterial action of cultures of a penicillium, with special reference to their use in the isolation of *B. influenzae*. *Br. J. Exp. Pethol.* **10**, 226–236 (1929).
17. Hansen, F. T. *et al.* An update to polyketide synthase and non-ribosomal synthetase genes and nomenclature in Fusarium. *Fungal Genet. Biol.* **75**, 20–29 (2015).
18. Frandsen, R. J. N. *et al.* Methylenetetrahydrofolate reductase activity is involved in the plasma membrane redox system required for pigment biosynthesis in filamentous fungi. *Eukaryot. Cell* **9**, 1225–1235 (2010).
19. Mapari, S. A. S. *et al.* Exploring fungal biodiversity for the production of water-soluble pigments as potential natural food colorants. *Curr. Opin. Biotechnol.* **16**, 231–238 (2005).
20. Medentsev, A. Fungal naphthoquinone metabolites (review). *Appl. Microbiol. Biotechnol.* **32**, 7–29 (1996).
21. Bolton, J. L., Trush, M. A., Penning, T. M., Dryhurst, G. & Monks, T. J. Role of quinones in toxicology. *Chem. Res. Toxicol.* **13**, 135–160 (2000).
22. O'Brien, P. Molecular mechanisms of quinone cytotoxicity. *Chem. Biol. Interact.* **80**, 1–41 (1991).
23. Di, X., Shiu, R. P., Newsham, I. F. & Gewirtz, D. A. Apoptosis, autophagy, accelerated senescence and reactive oxygen in the response of human breast tumor cells to adriamycin. *Biochem. Pharmacol.* **77**, 1139–1150 (2009).
24. Xu, C. *et al.* The anthracenedione compound bostrycin induces mitochondria-mediated apoptosis in the yeast *Saccharomyces cerevisiae*. *FEMS Yeast Res.* **10**, 297–308 (2010).
25. Sondergaard, T. E. *et al.* Fast screening of antibacterial compounds from fusaria. *Toxins (Basel)* **8**, 1–9 (2016).
26. Huskinson, B. *et al.* A metal-free organic–inorganic aqueous flow battery. *Nature* **505**, 195–198 (2014).
27. Tabor, D. P. *et al.* Mapping the frontiers of quinone stability in aqueous media: Implications for organic aqueous redox flow batteries. *J. Mater. Chem. A* **7**, 12833–12841 (2019).
28. Khataee, A., Dražević, E., Catalano, J. & Bentien, A. Performance optimization of differential pH quinone-bromide redox flow battery. *J. Electrochem. Soc.* **165**, A3918–A3924 (2018).
29. Kwabi, D. G. *et al.* Alkaline quinone flow battery with long lifetime at pH 12. *Joule* **2**, 1894–1906 (2018).
30. Pineda Flores, S. D., Martin-Noble, G. C., Phillips, R. L. & Schrier, J. Bio-inspired electroactive organic molecules for aqueous redox flow batteries. 1. Thiophenoquinones. *J. Phys. Chem. C* **119**, 21800–21809 (2015).
31. Yang, B. *et al.* High-performance aqueous organic flow battery with quinone-based redox couples at both electrodes. *J. Electrochem. Soc.* **163**, A1442–A1449 (2016).
32. Lin, K. *et al.* Alkaline quinone flow battery. *Science (80-)* **349**, 1529–1532 (2015).
33. Hofmann, J. D. *et al.* Quest for organic active materials for redox flow batteries: 2,3-diaza-anthraquinones and their electrochemical properties. *Chem. Mater.* **30**, 762–774 (2018).
34. Er, S., Suh, C., Marshak, M. P. & Aspuru-Guzik, A. Computational design of molecules for an all-quinone redox flow battery. *Chem. Sci.* **6**, 885–893 (2015).
35. Wedege, K., Azevedo, J., Khataee, A., Bentien, A. & Mendes, A. Direct solar charging of an organic–inorganic, stable, and aqueous alkaline redox flow battery with a hematite photoanode. *Angew. Chem. Int. Ed.* **55**, 7142–7147 (2016).
36. Yang, Z. *et al.* Alkaline benzoquinone aqueous flow battery for large-scale storage of electrical energy. *Adv. Energy Mater.* **8**, 1702056 (2017).
37. Huynh, M. T., Anson, C. W., Cavell, A. C., Stahl, S. S. & Hammes-Schiffer, S. Quinone 1 e− and 2 e−/2 H+ reduction potentials: Identification and analysis of deviations from systematic scaling relationships. *J. Am. Chem. Soc.* **138**, 15903–15910 (2016).
38. Kadkol, M. V., Gopalkrishnan, K. S. & Narasimhachari, N. Isolation and charaterization of naphtaquinone pigments from Torula Herbarum (Pers). Herbarin and Dehydroherbarin. *J. Antibiot.* **XXIV**, 245–248 (1971).
39. Heimberger, J., Cade, H. C., Padgett, J., Sittaramane, V. & Shaikh, A. Total synthesis of herbarin A and B, determination of their antioxidant properties and toxicity in zebrafish embryo model. *Bioorgan. Med. Chem. Lett.* **25**, 1192–1195 (2015).

40. Thomson, R. H. *Naturally Occurring Quinones III: Recent Advances* (Chapman and Hall, London, 1987).
41. Wiley-VCH, Weinheim, G. *Antibase*. (Wiley-VCH, Weinheim, Germany, 2012).
42. Pelzer, K. M., Cheng, L. & Curtiss, L. A. Effects of functional groups in redox-active organic molecules: A high-throughput screening approach. *J. Phys. Chem. C* **121**, 237–245 (2017).
43. Frisch, M. J., Trucks, G. W., Schlegel, H. B., Scuseria, G. E., Robb, M. A., Cheeseman, J. R., Scalmani, G., Barone, V., Mennucci, B., Petersson, G. A., Nakatsuji, H., Caricato, M., Li, X., Hratchian, H. P., Izmaylov, A. F., Bloino, J., Zheng, G., Sonnenberg, J. L., Had, M., Fox, D. J. *Gaussian 09* (2016).
44. Perdew, J. P., Burke, K. & Ernzerhof, M. Generalized gradient approximation made simple. *Phys. Rev. Lett.* **77**, 3865–3868 (1996).
45. Zhao, Y. & Truhlar, D. G. The M06 suite of density functionals for main group thermochemistry, thermochemical kinetics, noncovalent interactions, excited states, and transition elements: Two new functionals and systematic testing of four M06-class functionals and 12 other function. *Theor. Chem. Acc.* **120**, 215–241 (2008).
46. Dewar, M. J. S. & Trinajstic, N. Ground states of conjugated molecules-XIV. Redox potentials of quinones. *Tetrahedron* **25**, 4529–4534 (1969).
47. Tobias Johnsson Wass, J. R., Ahlberg, E., Panas, I. & Schiffrin, D. J. Quantum chemical modeling of the reduction of quinones. *J. Phys. Chem. A* **110**, 2005–2020 (2006).
48. Hanwell, M. D. *et al*. Avogadro: an advanced semantic chemical editor, visualization, and analysis platform. *J. Cheminform.* **4**, 1–17 (2012).
49. Dennington, R., Keith, T. A. & Millam, J. M. *GaussView, Version 6* (2016).
50. Miertuš, S. & Tomasi, J. Approximate evaluations of the electrostatic free energy and internal energy changes in solution processes. *Chem. Phys.* **65**, 239–245 (1982).
51. Miertuš, S., Scrocco, E. & Tomasi, J. Electrostatic interaction of a solute with a continuum. A direct utilizaion of AB initio molecular potentials for the prevision of solvent effects. *Chem. Phys.* **55**, 117 (1981).

Acknowledgements

This study was supported by grants from The Danish Research Council, Technology and Production (Grant No. 7017-00167) and the Novo Nordisk Foundation (NNF18OC0034952). We thank EaStCHEM for support via the EaStCHEM Research Computing Facility.

Author contributions

Conceived and designed the experiments: S.B.K., T.V.M., J.L.S. and J.M. Performed the experiments: S.B.K. and T.B.P. Analyzed the data: S.B.K., T.V.M., T.B.P, J.L.S. and J.M. Contributed to the writing of the manuscript: S.B.K., T.V.M., J.L.S. and J.M.

Additional information

Supplementary information is available for this paper at https://doi.org/10.1038/s41598-020-70522-z.

Correspondence and requests for materials should be addressed to J.L.S.

Reprints and permissions information is available at www.nature.com/reprints.

Publisher's note Springer Nature remains neutral with regard to jurisdictional claims in published maps and institutional affiliations.

Paper 2

Kristensen, S.B.; Pedersen, T.B.; Nielsen, M.R.; Wimmer, R.; Muff, J.; Sørensen, J.L. (2021) *Production and selectivity of key fusarubins from Fusarium solani due to media composition*.

toxins

MDPI

Communication

Production and Selectivity of Key Fusarubins from *Fusarium solani* due to Media Composition

Sebastian Birkedal Kristensen [1], Tobias Bruun Pedersen [1], Mikkel Rank Nielsen [1], Reinhard Wimmer [2], Jens Muff [1] and Jens Laurids Sørensen [1,*]

[1] Department of Chemistry and Bioscience, Aalborg University, 6700 Esbjerg, Denmark; sbk@bio.aau.dk (S.B.K.); tbp@bio.aau.dk (T.B.P.); mrn@bio.aau.dk (M.R.N.); jm@bio.aau.dk (J.M.)
[2] Department of Chemistry and Bioscience, Aalborg University, 9220 Aalborg, Denmark; rw@bio.aau.dk
* Correspondence: jls@bio.aau.dk; Tel.: +45-99-407-659

Abstract: Natural products display a large structural variation and different uses within a broad spectrum of industries. In this study, we investigate the influence of carbohydrates and nitrogen sources on the production and selectivity of production of four different polyketides produced by *Fusarium solani*, fusarubin, javanicin, bostrycoidin and anhydrofusarubin. We introduce four different carbohydrates and two types of nitrogen sources. Hereafter, a full factorial design was applied using combinations of three levels of sucrose and three levels of the two types of nitrogen. Each combination displayed different selectivity and production yields for all the compounds of interest. Response surface design was utilized to investigate possible maximum yields for the surrounding combinations of media. It was also shown that the maximum yields were not always the ones illustrating high selectivity, which is an important factor for making purification steps easier. We visualized the production over time for one of the media types, illustrating high yields and selectivity.

Keywords: *Fusarium*; secondary metabolites; polyketides; mycotoxins; pigments; quinones; fusarubins; *PKS3*; natural products

Key Contribution: High production yields and selectivity for interesting pigments, which possess several different useful properties.

check for updates

Citation: Kristensen, S.B.; Pedersen, T.B.; Nielsen, M.R.; Wimmer, R.; Muff, J.; Sørensen, J.L. Production and Selectivity of Key Fusarubins from *Fusarium solani* due to Media Composition. *Toxins* **2021**, *13*, 376. https://doi.org/10.3390/toxins13060376

Received: 15 April 2021
Accepted: 22 May 2021
Published: 25 May 2021

1. Introduction

Fungi produce a plethora of different polyketides, some of which have beneficial pharmaceutical properties, including anti-tumor (e.g., aspergiolide A [1]), immunosuppressants (cyclosporin [2]), cholesterol lowering (e.g., lovastatin [3,4]) and antibacterial (e.g., penicillin [5]). Other compounds have mycotoxin effects on raw feed for livestock, crops and also humans [6–8] and are potent carcinogens (e.g., aflatoxin [6] and fumonisins [9]) or estrogenic (e.g., zearalenone [10], fusarin C [11] and fusarielins [12]).

In fungi, pigmentation could also primarily be attributed to polyketides [13]. The genus *Fusarium* is collectively able to produce the three polyketide pigments aurofusarin, bikaverin and fusarubins (incl. bostrycoidin, javanicin, Figure 1). Most *Fusarium* species use aurofusarin and bikaverin as mycelial pigmentation and fusarubins in perithecia [14,15]. However, in *F. solani* and closely related species, fusarubins are produced during mycelial growth, while a yet unidentified pigment is produced during sexual development in perithecia. The fusarubin gene cluster, *PKS3* (also described as *fsr* and *pgl*), is found in all genome sequenced Fusaria, and is a non-reducing iterative type I PKS [16], which has been assigned earlier to produce 8-O-methylfusarubin in *F. fujikuroi* [14] and also the azaanthraquinone bostrycoidin in *F. graminearum*. Bostrycoidin and fusarubin are believed to be synthesized from the same precursor, by the formation of a C14 heptaketide-aldehyde as the common intermediate [17,18]. Both fusarubin, bostrycoidin and many of the other

intermediates in the biosynthetic pathway have proved to possess biological activity, including antimicrobial and antitubercular properties [19], antifungal activity [15], anticancer properties [20] as well as prominent activity toward *Staphylococcus aureus*, *Escherichia coli*, *Pseudomonas aeruginosa* and *Bacillus megaterium*. They also display potential cytotoxic properties toward human leukemia cells [21,22].

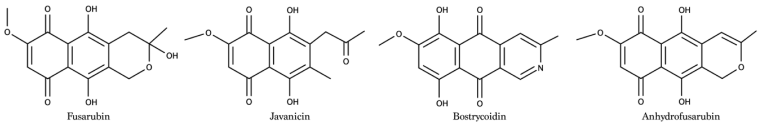

Figure 1. Structures of the four selected polyketide pigments produced by PKS3 in *Fusarium solani*.

The cytotoxic and antimicrobial effect can be explained by the stimulation of cellular respiration and membrane NADH oxidation of bacteria [23,24]. The cytotoxic mechanism of naphthoquinones has also been described by Medentsev et al. [25,26] and Futuro et al. [27], where the flavoprotein-catalyzed redox cycle of the naphthoquinone creates a cascade of free radicals and superoxide molecules and other biochemical processes, which can damage DNA or RNA. The redox activity of natural occurring quinones was recently determined in silico, and several members of the fusarubin class were among the most reactive [28].

The fungal polyketides and secondary metabolites are often produced together with many different compounds. Therefore, it can prove challenging to produce pure compounds for use in the industry. The heterologous expression of genes in, e.g., yeast or bacteria is often used to produce fungal compounds in a different organism [29,30]. Pedersen et al. showed a heterologous expression of core genes in *F. solani* for a high-concentration production of pigments in *Saccharomyces cerevisiae* [31]. The yield of the compound bostrycoidin was not higher than 2.2 mg/L, which is low when compared to the metabolite extracted from the fungi, e.g., 21 mg/L by Kurobane et al. [32]. They have also shown production levels of 189 mg/L of fusarubin and 45 mg/L of the metabolite javanicin. Because the quinones and polyketides in general are produced as secondary metabolites depending on regulation factors, such as pH, carbohydrates, etc., it will be possible to alter the production portfolio of the fungi depending on the growth conditions and media composition. This has previously been demonstrated in a study by Sørensen et al., where the influence of both a different yeast extract [33] and carbohydrates [34] has been shown to influence the production of secondary metabolites. Medentsev and Akimenko discovered the influence of pH on the production of pigments in fungi, where both high and low pH provided inhibitory effects on the growth rate of the fungi. It was also shown that the nature of the pigments produced was different [25].

The aim of this study is to investigate the influence of medium composition on the production of the polyketides, fusarubin, javanicin, anhydrofusarubin and bostrycoidin by the fungus *F. solani*.

2. Results and Discussion

As the *Fusarium solani* species complex is responsible for producing several compounds from the fusarubin biosynthetic pathway, it is interesting to investigate whether it is possible to enhance the production of these valuable compounds and if to produce compounds more selectively by varying their main substances and their concentrations in the growth medium. We started by investigating the effect of four different types of carbohydrates (maltose, glucose, sucrose and glycerol) and two different types of nitrogen sources (ammonium tartrate and sodium nitrate) on pigment production. The resulting chromatograms revealed a significant difference in the peak heights and number of peaks, depending on the carbohydrate type and nitrogen source (Figure 2). Fusarubin was only produced in small amounts in the samples including ammonium tartrate, except when using glucose as the carbohydrate source. The opposite behavior was observed for bostrycoidin,

which was abundant when the fungus was grown in media containing ammonium tartrate, and when cultivated in media containing glycerol, where no compounds were produced in any significance. In a similar way, bostrycoidin was almost absent when the fungus grew in media containing sodium nitrate. Javanicin was produced in all different media, besides the glycerol media, with the highest peaks originating from the media with a combination of sucrose and ammonium tartrate. The media type containing glycerol showed no indication of producing fusarubins besides small quantities of bostrycoidin, when combined with ammonium tartrate. The media did not seem to favor the growth of the fungi, with no visible mycelium formation.

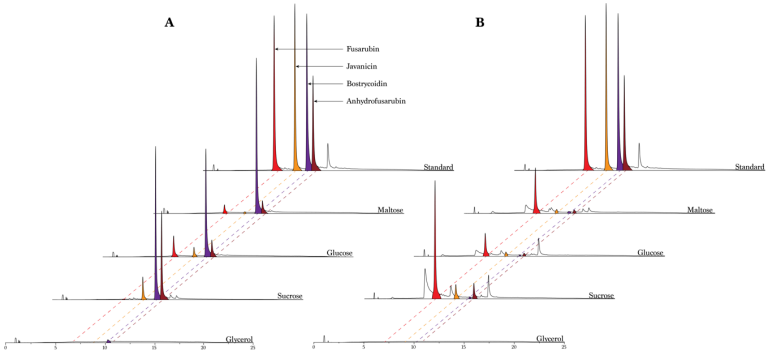

Figure 2. The effect of carbon and nitrogen sources on the production of PKS3-derived polyketides. All media contained 50 g/L carbohydrate and have been cultivated for seven days. (**A**) Chromatograms from samples where the media contained ammonium tartrate, fusarubin (red), javanicin (orange), bostrycoidin (purple) and anhydrofusarubin (red-brown) are indicated on the standard and by the dotted lines. (**B**) Chromatograms from samples where the media contained sodium nitrate. Fusarubin (red), Javanicin (orange), bostrycoidin (purple) and anhydrofusarubin (red-brown) is indicated by the dotted lines and color. Standard concentrations for both (**A**,**B**) are 53 mg/L for fusarubin, 39 mg/L for javanicin and bostrycoidin, and 19 mg/L for anhydrofusarubin.

We decided to use the same mass of carbohydrates, neglecting the fact that the carbohydrates used in this study do not have the same molar mass, and hence the molarity will be higher for carbohydrates with a lower molar mass. However, this did not influence our study, as the two selected disaccharides, sucrose and maltose, stimulated a higher production of the pigments on both sodium nitrate and ammonium tartrate (Figure 3 and Tables S1–S3). The optimal medium for bostrycoidin production was maltose combined with ammonium tartrate, yielding a mean concentration of 116 mg/L (Figure 3A), but the media types containing sucrose and glycose produced a mean concentration of 214 mg/L and 127 mg/L, respectively, though showing less selectivity, whereas the maltose media was chosen to be optimal for the production of bostrycoidin. Glycerol resulted in the lowest bostrycoidin concentrations of all media containing ammonium tartrate, no higher than 0.89 mg/L. The sucrose and ammonium tartrate combination was most favorable for anhydrofusarubin production, yielding 113 mg/L in average. This medium, however, did not produce much fusarubin. In the glycerol medium, fusarubin was produced with a mean concentration of 77 mg/L, and javanicin and anhydrofusarubin yielded 20 mg/L and 25 mg/L, respectively. In the medium containing sodium nitrate (Figure 3B), the production clearly favored fusarubin, with a yield of 56 mg/L in maltose medium, 37 mg/L in glucose medium and a mean concentration of 132 mg/L in the sucrose medium. Sucrose also yielded the highest production of javanicin (19 mg/L) and anhydrofusarubin (36 mg/L) in media with nitrate as the source of nitrogen. Bostrycoidin was produced only

in minor quantities on glucose (1.2 mg/L) and on maltose (1.7 mg/L). No compounds were detectable in the glycerol medium. Except for fusarubin, the mean concentrations in the medium containing sodium nitrate were lower than the mean concentrations seen in the medium composed with ammonium tartrate.

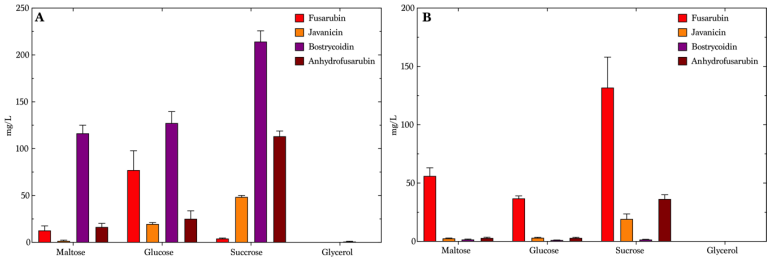

Figure 3. Mean concentrations (n = 4) of the four compounds of interest. Error bars indicate the standard error of mean in the media containing different carbohydrates and a nitrogen source. Cultivation period was seven days. (**A**) Ammonium tartrate, (**B**) Sodium nitrate.

The media containing sucrose was selected for further investigation, due to the variety of the difference in produced compounds and the high overall concentrations. We omitted maltose media despite the high production of bostrycoidin, because they already showed selectivity and high production yields.

To optimize production on sucrose, we used a full factorial design of the experiments including three factors: carbohydrate concentration, nitrogen concentration and nitrogen source. The carbohydrate concentrations were 50 g/L, 100 g/L and 150 g/L and the concentration of nitrogen varied from 4.6 g/to 6.9 g/L and 9.2 g/L for the media containing ammonium tartrate. The second nitrogen source, sodium nitrate, had the following concentration levels: 3 g/L, 4.5 g/L and 6 g/L. As expected, the variation of concentration of the four target compounds was quite significant, indicating the possibility of tailoring a medium for the production of specific compounds. Due to fermentation in liquid media, we expected to see variations in the yields from experiment to experiment, larger than those of the experiments performed with fermentation in solid phases [35–38]. The variations and deviations between experiments when comparing the first experiment, illustrated in Figure 3A,B, and the second experiment, visualized in Figure 4A,B, are seen as natural variations in growth patterns due to, e.g., global regulation factors. The average values including the SD and SEM of the two experiments overlap and, therefore, cannot be determined as significant. Fusarubin was produced in low concentrations (Figure 4A) in the media composed of 50 g/L sucrose and ammonium tartrate, with an increase from 2.5 mg/L at an ammonium tartrate concentration of 4.6 g/L to 47 mg/L with an ammonium tartrate concentration of 9.2 g/L. However, the data showed that increasing sucrose and decreasing ammonium tartrate improved fusarubin production. Here, the 100 g/L sucrose and 4.6 g/L ammonium tartrate combination resulted in the highest production, of 287 mg/L, which was substantially higher than the previously described productions of fusarubin [32]. Furthermore, the effect plots showed that sucrose was the most important factor combined with the nitrogen concentration (Figures S1–S6). The remaining combinations of sucrose and ammonium tartrate decreased fusarubin production when ammonium tartrate levels were increased. Different tendencies were seen in the production of javanicin, even though the concentration levels were lower than for fusarubin. It was seen that a sucrose concentration of 100 g/L and an ammonium tartrate concentration of 6.9 g/L yielded the highest average concentration, of 77 mg/L. The production of bostrycoidin was overall stable, and high yields were observed in all of the samples. However, a slight

decrease was seen with increasing sucrose and ammonium tartrate levels, as the lowest levels yielded the highest production. Anhydrofusarubin showed opposite tendencies of fusarubin, as it was seen that the 50 g/L and 4.6 g/L combination yielded the highest concentrations. This could indicate a correlation between the compounds, as a conversion might happen from one compound to the other. This has, however, not been investigated further. Figure 4B shows the average concentrations of the compounds in the sucrose media containing sodium nitrate. Here, fusarubin production displayed a different pattern than ammonium tartrate. There were indications that the production was slightly favored by a lower concentration of sucrose and a high nitrate concentration, with the production reaching 130 mg/L.

Javanicin production was optimal at the highest level of sucrose and the medium level of sodium nitrate, yielding 33 mg/L. It was noticeable that bostrycoidin was produced in significantly low levels compared to the first media containing ammonium tartrate, with a maximum average value of 2 mg/L. This was due to the need of a free ammonium to undergo the nonenzymatic oxidization producing bostrycoidin, as described by Kurobane et al. in 1980 [32]. Anhydrofusarubin was also produced in the highest quantities in the medium with the lowest level of sucrose and sodium nitrate. The data for individual compounds are presented in Figure S7 in the Supplementary Material.

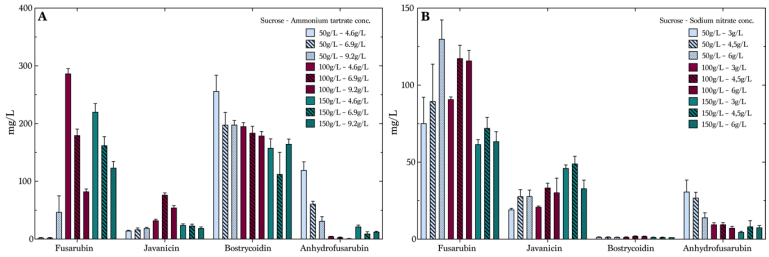

Figure 4. The effect of sucrose and nitrogen source concentrations on polyketide production. Average polyketide/product concentrations and standard error of mean (n = 4); cultivation period was seven days. (**A**) Media containing ammonium tartrate and (**B**) Media composed with sodium nitrate.

To further investigate the observed tendencies, a response surface design was prepared using the Box–Wilson central composite design, and can be seen in Figures 5 and 6. Once again, fusarubin (Figure 5A) showed the highest production in a combination of high sucrose (180 g/L) and low ammonium tartrate, yielding up to 400 mg/L. Interestingly, the plot indicated that the optimum had not been found within these values. Javanicin (Figure 5B) displayed a hilltop shape, which indicated the presence of an optimum at 100 g/L of sucrose and 7–8 g/L of ammonium tartrate. For bostrycoidin (Figure 5C) and anhydrofusarubin (Figure 5D), the highest yields were achieved by lowering the sucrose and ammonium tartrate levels.

As observed in the previous experiments, fusarubin followed a linear trend of increasing yields under low sucrose and high nitrate (Figure 6A). However, the response surface plot also indicated that the optimal combination was not found within the tested values, even though a yield of 150 mg/L was achieved. The response surface of javanicin production (Figure 6B) suggested the existence of two distinct combinations of conditions for optimal production: for the first, a combination of high sucrose concentration and low sodium nitrate concentration; for the second, a low level of sucrose combined with a high concentration of sodium nitrate. This supports the hypothesis of javanicin being a co-metabolite and not a conversion compound like fusarubin or anhydrofusarubin.

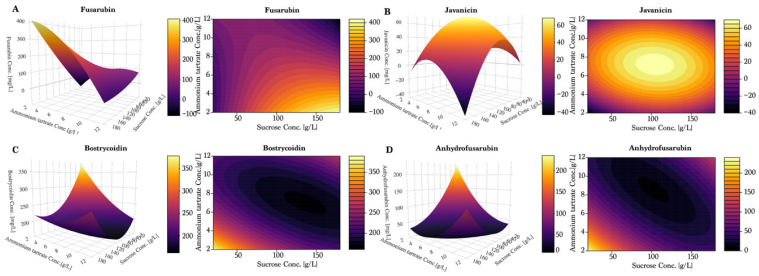

Figure 5. Response surface models and contour plots for predicted and measured concentrations of media composed of ammonium tartrate and sucrose. Cultivation time was seven days for the fungi used for measurements. (**A**) Fusarubin, (**B**) Javanicin, (**C**) Bostrycoidin and (**D**) Anhydrofusarubin.

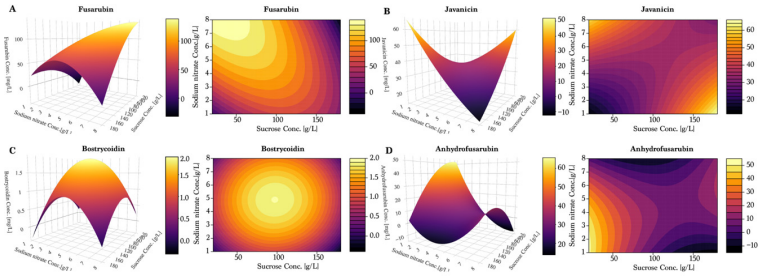

Figure 6. Response surface models and contour plots for predicted and measured concentrations of media composed of sucrose and sodium nitrate. Cultivation time was seven days for the fungi used for measurements. (**A**) Fusarubin, (**B**) Javanicin, (**C**) Bostrycoidin and (**D**) Anhydrofusarubin.

In the response surface model, as measured previously, bostrycoidin (Figure 6C) production was low when nitrate was used as nitrogen source. The plot indicated that the maximum production was achieved with a combination of 100 g/L sucrose and 5 g/L sodium nitrate. Anhydrofusarubin tended to be produced in the highest quantities when composing the medium of low sucrose and sodium nitrate levels (Figure 6D). Furthermore, we observed an indication of a second optimum if sucrose and sodium nitrate were increased beyond the levels applied in our study.

To investigate the isolated production of bostrycoidin, we chose to analyze the production levels at different time points during growth. For that, we used maltose medium with 50 g/L maltose and 4.6 g/L ammonium tartrate, as this illustrated high yields and good selectivity for bostrycoidin compared to the seven other combinations of the media found in the first part of the study in presence of ammonium tartrate. We decided to investigate bostrycoidin production, as this compound was produced in the overall highest concentrations throughout the whole study. The cultivation time was extended to 9 days (216 h) instead of the initial 7 days (168 h) which were used in previous experiments, based on earlier studies by Kurobane et al. [32], in order to investigate whether the production had reached a maximum or additional production could be achieved. The production of bostrycoidin was detected after 60 h with an average concentration of 3.2 mg/L (Figure 7A). The production slowly increased until 120 h, where the average yield was 33 mg/L. The average measured yields hereafter increased rapidly to the

end of the experiments, reaching 305 mg/L, with no indication of declining production. The experiment was terminated at 216 h (9 days), when all maltose had been consumed in the medium (Figure 7B). The pellet weight also indicated that the fungi did not grow significantly between 192 h and 216 h, as the curve flattened out. The other three quinones were not present in high levels, as the highest average values measured were 28 mg/L of fusarubin at 96 h, 6.7 mg/L javanicin at 216 h and 43 mg/L of anhydrofusarubin at 216 h. The pigmentation of the media at every sampling time is illustrated in Figure S8 in the Supplementary Materials.

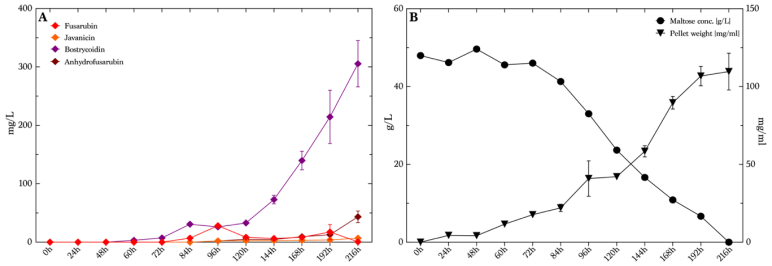

Figure 7. Production of pigments over time in bostrycoidin-favoring media conditions. (**A**) Average concentrations and standard deviation (n = 4) of the four quinones/polyketides produced over time, ranging from 0–216 h. (**B**) Carbohydrate consumption over time illustrated as circles referring to the left y-axis, and the mean dry weight of the cells (n = 4) in the samples referring to the right y-axis.

3. Conclusions

In this study, we present, how the production of fusarubin, javanicin, bostrycoidin and anhydrofusarubin in *F. solani* constitutively expressing the responsible gene cluster varies when grown on four different carbohydrates and two different nitrogen sources. It was shown that the media composed of maltose and ammonium tartrate yielded large amounts of bostrycoidin, with little to none of the other compounds. The sucrose medium was investigated further, as this medium produced all of the four compounds in different concentrations. A full factorial experimental design was initialized to investigate the effect of the different factors on the production of the compounds. It was concluded that the highest production of fusarubin was seen using the media containing ammonium tartrate, but the selectivity was not optimal, as bostrycoidin was also produced in large quantities. The optimal medium for producing fusarubin was established to be 50 g/L sucrose combined with 6 g/L sodium nitrate. For javanicin, the optimal medium was 150 g/L sucrose and 6 g/L of sodium nitrate. For anhydrofusarubin, the medium composed of 50 g/L of sucrose and 3 g/L of sodium nitrate indicated the highest yields when combining yields. These tendencies were validated by the response surface design models where indications of even higher theoretical yields could be seen. However, those media combinations remain to be tested. Because we used a constitutive promotor, we have assumed that the transcripts would be on similar levels in all cells, and then the difference in the production between the media could be assigned to the growth pattern of the fungi or the availability of substrates, such as acetyl-CoA and malonyl-CoA. Future experiments targeting this availability would enlighten this. The project also investigated maltose media and the production of bostrycoidin over a timeframe of 9 days. This led us to conclude that it was possible to exceed 300 mg/L of bostrycoidin for this medium type as well, with a high level of selectivity yielding little to no production of the three other compounds.

4. Materials and Methods

4.1. Fungal Strain and Macroconidia Isolation

Fusarium solani 77-13-4 OE::*fsr6* G418^R (Nielsen et al., 2019 [39]) was maintained on a PDA containing 100 µg/mL geneticin G418 at 28 °C. For inducing sporulation, a 100 mL CMC medium (15 g/L carboxymethylcellulose sodium salt, 1g/L NH_4NO_3, 1 g/L KH_2PO_4, 0.5 g/L $MgSO_4{\cdot}7H_2O$, 1 g/L bacto yeast extract) was inoculated with 5–10 agar squares from a week-old plate and incubated at 20 °C and 100 rpm for five days. The spores were harvested by pouring the culture through a sterile plastic syringe packed with glass wool removing agar and mycelium. The medium was removed by centrifugation at 10,000× *g* 4 °C for 15 min, discarding the supernatant. The spores were washed twice in 50 mL ice-cold sterile ultrapure water, followed by a final resuspension in 1 mL 10% glycerol, and stored at −80 °C.

4.2. Effect of Varying Carbon and Nitrogen Sources on Pigment Production

All media were initially based on Kurobane et al. [32] and modified following the base recipe according to our experiments. In the study investigating different carbohydrates, the OE::*fsr6 F. solani* strain was inoculated in media composed of: 50 g/L carbohydrate (maltose monohydrate (Merk KGaA, Darmstadt, Germany), glucose (Sigma-Aldrich, St. Louis, MO, USA), glycerol (Honeywell, Germany) or sucrose (MP biomedicals, Eschwege, Germany)), 4.6 g/L of ammonium tartrate (Acros organics, New Jersey, USA) or 3 g/L sodium nitrate (VWR, Herlev, Denmark), 1 g/L potassium dihydrogen phosphate (KH_2PO_4) (Merk KGaA, Darmstadt, Germany), 0.5 g/L magnesium sulfate heptahydrate ($MgSO_4{\cdot}7H_2O$) (VWR, Herlev, Denmark), 0.01 g/L ferrous sulfate heptahydrate ($FeSO_4{\cdot}7H_2O$) (Fluka, Sigma-Aldrich, St. Louis, MO, USA), 0.01 g/L sodium chloride (NaCl) (VWR, Herlev, Denmark) and 0.01 g/L calcium chloride ($CaCl_2$) (Merk KGaA, Darmstadt, Germany), and 1 mL of the trace metal solution which contains 1.0 g $ZnSO_4{\cdot}7H_2O$ (Merk KGaA, Darmstadt, Germany) and 0.5 g $CuSO_4{\cdot}5H_2O$ (Acros organics, New Jersey, USA) in 100 mL MQ H_2O. MQ H_2O was produced by Synergy system UV (Millipore SAS, Molsheim, France). The pH was adjusted to 5.6 ± 0.2 for all media. OE::*fsr6* was inoculated containing 10,000 spores per 50 mL medium and incubated at 25 °C at 100 rpm for seven days, composing quadruplicates of all samples. The conditions correspond to a combination of the methods from Kurobane et al. [32] and Westphal et al. [40].

4.3. Production of Pigments in Response to Varying Concentrations of Sucrose

In the study, investigating different levels of carbohydrate and nitrogen source, the liquid media contained 50 g/L,100 g/L and 150 g/L of sucrose (MP biomedicals, Eschwege, Germany), and 4.6 g/L, 6.9 g/L and 9.2 g/L of ammonium tartrate (Acros organics, NJ, USA) or 3 g/L, 4.5 g/L and 6 g/l of sodium nitrate (VWR, Herlev, Denmark), and the rest of the media were composed as the base recipe. In all media, 250 mL were prepared using MQ H_2O and autoclaved for 15 min at 121 °C after mixing. A capacity of 50 mL was then decanted into four Erlenmeyer flasks inoculated with 10,000 spores of OE::fsr6 and incubated at 25 °C at 100 rpm for seven days, constituting the quadruplicates of all experiments. The pH was adjusted to 5.6 ± 0.2 for all media.

4.4. Production of Bostrycoidin over Time

The media chosen to monitor bostrycoidin production over time contained 50 g/L maltose monohydrate (Merk KGaA, Darmstadt, Germany) and 4.6 g/L ammonium tartrate (Acros organics, New Jersey, USA). The rest of the medium was composed as the base recipe. The experiment was conducted with quadruplicates, where the 50,000 spores of the OE::*fsr6* strain were inoculated in 1000 mL Erlenmeyer flasks containing a 250 mL medium. The strain was cultivated at 25 °C at 100 rpm for 9 days.

Samples of 5 mL for pigment concentration determination, including 1 mL for carbohydrate concentration determination, were taken out after inoculation at 0 h, 24 h, 48 h and thereafter with 12 h intervals until 96 h. Later, the intervals were again of 24 h until

216 h or 9 days. The 12 h intervals were chosen because prior experiments had found the pigmentation starting phase to be around 48 h-96 h. The 5 mL samples were centrifuged at 5000× *g* for 5 min. The supernatant was extracted using LLE as described below. The pellet was weighed in wet weight and dried in an oven for 12 h at 105 °C, and then weighed again to determine the dry weight of the filaments in the sample. The 1 mL sample was filtered through 0.45 µm syringe filters (Frisenette, Knebel, Denmark), directly into 2 mL HPLC vials, and analyzed using HPLC-RID (Perkin Elmer Series 200, Perkin Elmer, MA, USA), coupled with a Perkin Elmer series 200 pump, Perkin Elmer series 200 autosampler, Perkin Elmer series 200a Refractive index detector, and a column oven. Injected volumes of 10 µL were analyzed at 85 °C, using an isocratic flow of 0.6 mL/min, of MQ H_2O, through a Bio-Rad Aminex HPX-87P column (300 × 7.8 mm, Bio-Rad laboratories, USA).

4.5. Liquid-Liquid Extraction and HPLC-DAD Analysis of Secondary Metabolites from Liquid Media

The extraction procedure used in this study was initially based on Westphal et al.'s (2018) study on the production of aurofusarin [40], but the method was modified for the compounds and fungi extracted in this study. The growth media were filtrated through Miracloth (Millipore EMD, Billerica MA, USA). A sample size of a 10 mL medium was taken out for extraction and acidified by adding 0.7 mL 5 M HCl and shaken in 50 mL centrifuge tubes. Ten milliliters of chloroform (Sharlau, Sharlab S.L, Spain) were added to the media and shaken, and thereafter two phases were observed in the liquid and the color would primarily be in the water phase. We then added 6.7 mL methanol (VWR, Herlev, Denmark) and 6.7 mL 10 *w/v* % NaCl in MQ H_2O solution to the mixture, which was shaken energetically. After the phases were separated, the majority of the color was observed in the organic phase. Most of the water was carefully decanted. Additionally, 6.7 mL methanol (VWR, Herlev, Denmark) and 6.7 mL 10 *w/v* % NaCl in MQ H_2O solution were added to drive the last impurities to the water phase and all the pigment to the organic phase. The mixture was swirled and shaken calmly, and the phases were allowed to settle. The organic phase was collected by removing the water phase by pipetting. The organic phase was transferred to glass test tubes, and the chloroform was evaporated at 40 °C under N_2 gas until complete dryness. The dried metabolites were resuspended in 2 mL methanol (VWR, Herlev, Denmark) and set for 10 min in an ultrasonic bath to ensure that all possible metabolites were dissolved. The dissolved metabolites were filtered through 0.22 µm syringe filters (Frisenette, Knebel, Denmark), directly into 2 mL HPLC vials.

Extracts were analyzed using HPLC-DAD on an Agilent 1260 infinity II HPLC system (Agilent, Santa Clara, USA), equipped with a 1260 vial sampler, a 1260 Quat. pump inclusive column oven set to 40 °C with a C6-phenyl column (Kinetex®2.6 µm, 100 Å, 150 × 3 mm, Phenomenex, Torrance, CA, USA) and together with a guard column (UHPLC phenyl, 2.1mm ID column, Phenomenex, Torrance, CA, USA), 1260 DAD-HS measuring wavelengths at 280 nm, 310 nm and 495 nm, chosen—based on UV spectra yielded by pure compounds of fusarubin, javanicin and bostrycoidin, obtained by preparative HPLC and verified by NMR as described by Nielsen et al., 2019 [40]—and a 1260 RID unit.

The 0.5 mL/min gradient initiated at 80% solvent A (MQ H_2O) and 20% solvent B (Acetonitrile, Hypersolve, VWR, Herlev, Denmark) added 50µL/L Trifluoroacetic acid (TFA Chromsolv, Sigma-Aldrich, St. Louis, MO, USA). The gradient increased linearly to 100% solvent B over 20 min, held for 5 min and then went back to the initial start composition, at 80% solvent A and 20% solvent B over a 5-min period, followed by 4 min post run.

4.6. Calibration and Standards for the Pigments

In order to be able to quantify the four target pigments, they were initially isolated from the extracts derived from OE::*fsr6*. This was performed by preparative HPLC (Thermo Scientific Ultimate 3000; Dionex Ultimate 3000 pump; Dionex Ultimate 3000 autosampler) coupled to a diode array detector (Dionex Ultimate 3000 DAD) and fraction collector (Dionex Ultimate 3000 fraction collector). The samples were fractionated using a C-18 column (Thermo Scientific, Hypersil Gold, 250 × 21.2 mm, 5 µm), injecting 0.5 mL per

run, and applying a linear flow gradient of 10 mL/min. The gradient initiated at 80% solvent A (MQ H_2O) and 20% solvent B (Acetonitrile, Hypersolve, VWR, Herlev, Denmark), both supplemented with 50 µL/L Trifluoroacetic acid (TFA Chromsolv, Sigma-Aldrich, St. Louis, MO, USA). The gradient increased linearly to 100% solvent B over 10 min, held for 5 min and then went back to the initial start composition, at 80% solvent A and 20% solvent B over a 3 min period. This gradient was continued for 5 min. The DAD was set to collect chromatograms at wavelengths 230 nm, 280 nm, 310 nm and 495 nm. The fraction collector (Dionex Ultimate 3000 fraction collector) was set to collect peaks in the chromatogram at 310 nm, with a peak start/end threshold of 10.00 mAu and peak slopes at ±0.500 mAu/s. The collected samples were analyzed using HPLC-DAD (Agilent 1260 infinity II HPLC system, Agilent, Santa Clara, USA), with the method and system described earlier, verifying the compounds fusarubin, javanicin, bostrycoidin and anhydrofusarubin. The fractions were dried at 40 °C under N_2 gas until complete dryness and dry weight were noted. Stock solutions were made by resuspending samples in methanol (VWR, Herlev, Denmark), of which all concentrations were 5 g/L pigments, and then using previously determined compositions of the fractions to compose standard calibration solutions for fusarubin, javanicin, bostrycoidin and anhydrofusarubin. All calibration curves can be seen in Figure S9.

4.7. Statistical Analysis

All statistical analyses were performed using R studio (version 1.2.5033, Rstudio Inc.) and GraphPad prism 9 version 9.0.0 for macOS (GraphPad Software, San Diego, CA, USA).

Supplementary Materials: The following are available online at https://www.mdpi.com/article/10.3390/toxins13060376/s1, Figure S1: Tukey HSD tests for the effects of different carbohydrates and nitrogen sources, without interactions. Figure S2: Tukey HSD tests for the effects of different carbohydrates and nitrogen sources, with interactions. Figure S3: Tukey HSD test for the effect from sucrose levels and ammonium tartrate levels, without interactions. Figure S4: Tukey HSD test for the effect from sucrose levels and ammonium tartrate levels, including interactions. Figure S5: Tukey HSD test for the effect from sucrose levels and sodium nitrate levels, without interactions. Figure S6: Tukey HSD test for the effect from sucrose levels and sodium nitrate levels, with interactions. Figure S7: individual data for the four compounds, for the full factorial design experiment. Figure S8: Pigmentation of the media. Figure S9: Calibration curves. Table S1: Average yields of the media with different carbohydrates and the two types of nitrogen source. Table S2: Average yields of the media composed of three different levels of sucrose and three levels of ammonium tartrate. Table S3: Average yields of the media composed of three different levels of sucrose and three levels of sodium nitrate.

Author Contributions: Conceptualization, S.B.K. and J.L.S.; methodology, S.B.K.; software, S.B.K.; validation, S.B.K.; Performing experiments, S.B.K., T.B.P., M.R.N., R.W.; writing—original draft preparation, S.B.K.; writing—review and editing, S.B.K., J.L.S., J.M.; Visualization and analysis of data, S.B.K.; supervision, J.L.S., J.M.; project administration, J.L.S.; funding acquisition, J.L.S. All authors have read and agreed to the published version of the manuscript.

Funding: This study was supported by grants from The Danish Research Council, Technology and Production (grant no. 7017-00167) and the Novo Nordisk Foundation (NNF18OC0034952).

Conflicts of Interest: The authors declare no conflict of interest.

References

1. Tao, K.; Du, L.; Sun, X.; Cai, M.; Zhu, T.; Zhou, X.; Gu, Q.; Zhang, Y. Biosynthesis of aspergiolide A, a novel antitumor compound by a marine-derived fungus Aspergillus glaucus via the polyketide pathway. *Tetrahedron Lett.* **2009**, *50*, 1082–1085. [CrossRef]
2. Wong, R.L.; Winslow, C.M.; Kevin, D.C. The mechanisms of action of cyclosporin A in the treatment of psoriasis. *Immunol. Today* **1993**, *14*, 69–74. [CrossRef]
3. Tobert, J.A. Lovastatin and beyond: The history of the HMG-CoA reductase inhibitors. *Nat. Rev. Drug Discov.* **2003**, *2*, 517–526. [CrossRef] [PubMed]
4. Faseleh Jahromi, M.; Liang, J.B.; Ho, Y.W.; Mohamad, R.; Goh, Y.M.; Shokryazdan, P. Lovastatin production by Aspergillus terreus using agro-biomass as substrate in solid state fermentation. *J. Biomed. Biotechnol.* **2012**, *2012*. [CrossRef] [PubMed]

5. Fleming, A. On the antibacterial action of cultures of a penicillium, with special reference to their use in the isolation of B.influenzae. *Br. J. Exp. Pethol.* **1929**, *10*, 226–236.
6. Peraica, M.; Radić, B.; Lucić, A.; Pavlović, M. Toxic effects of mycotoxins in humans. *Bull. World Health Organ.* **1999**, *77*, 754–766.
7. Streit, E.; Naehrer, K.; Rodrigues, I.; Schatzmayr, G. Mycotoxin occurrence in feed and feed raw materials worldwide: Long-term analysis with special focus on Europe and Asia. *J. Sci. Food Agric.* **2013**, *93*, 2892–2899. [CrossRef]
8. Hafizi, R.; Salleh, B.; Latiffah, Z. Morphological and molecular characterization of Fusarium. solani and F. oxysporum associated with crown disease of oil palm. *Braz. J. Microbiol.* **2013**, *44*, 959–968. [CrossRef] [PubMed]
9. Gelderblom, W.C.A.; Kriek, N.P.J.; Marasas, W.F.O.; Thiel, P.G. Toxicity and carcinogenicity of the fusanum monilzforine metabolite, fumonisin b1, in rats. *Carcinogenesis* **1991**, *12*, 1247–1251. [CrossRef] [PubMed]
10. Shier, W.T.; Shier, A.C.; Xie, W.; Mirocha, C.J. Structure-activity relationships for human estrogenic activity in zearalenone mycotoxins. *Toxicon* **2001**, *39*, 1435–1438. [CrossRef]
11. Sondergaard, T.E.; Hansen, F.T.; Purup, S.; Nielsen, A.K.; Bonefeld-Jørgensen, E.C.; Giese, H.; Sørensen, J.L. Fusarin C acts like an estrogenic agonist and stimulates breast cancer cells in vitro. *Toxicol. Lett.* **2011**, *205*, 116–121. [CrossRef]
12. Sondergaard, T.E.; Klitgaard, L.G.; Purup, S.; Kobayashi, H.; Giese, H.; Sørensen, J.L. Estrogenic effects of fusarielins in human breast cancer cell lines. *Toxicol. Lett.* **2012**, *214*, 259–262. [CrossRef] [PubMed]
13. Kalra, R.; Conlan, X.A.; Goel, M. Fungi as a Potential Source of Pigments: Harnessing Filamentous Fungi. *Front. Chem.* **2020**, *8*, 1–23. [CrossRef]
14. Studt, L.; Wiemann, P.; Kleigrewe, K.; Humpf, H.U.; Tudzynski, B. Biosynthesis of fusarubins accounts for pigmentation of fusarium Fujikuroi perithecia. *Appl. Environ. Microbiol.* **2012**, *78*, 4468–4480. [CrossRef]
15. Frandsen, R.J.N.; Rasmussen, S.A.; Knudsen, P.B.; Uhlig, S.; Petersen, D.; Lysøe, E.; Gotfredsen, C.H.; Giese, H.; Larsen, T.O. Black perithecial pigmentation in Fusarium species is due to the accumulation of 5-deoxybostrycoidin-based melanin. *Sci. Rep.* **2016**, *6*, 1–13. [CrossRef] [PubMed]
16. Brown, D.W.; Proctor, R.H. Insights into natural products biosynthesis from analysis of 490 polyketide synthases from Fusarium. *Fungal Genet. Biol.* **2016**, *89*, 37–51. [CrossRef]
17. Menezes, B.S.; Solidade, L.S.; Conceição, A.A.; Santos Junior, M.N.; Leal, P.L.; de Brito, E.S.; Canuto, K.M.; Mendonça, S.; de Siqueira, F.G.; Marques, L.M. Pigment production by Fusarium solani BRM054066 and determination of antioxidant and anti-inflammatory properties. *AMB Express* **2020**, *10*. [CrossRef] [PubMed]
18. Awakawa, T.; Kaji, T.; Wakimoto, T.; Abe, I. A heptaketide naphthaldehyde produced by a polyketide synthase from Nectria haematococca. *Bioorg. Med. Chem. Lett.* **2012**, *22*, 4338–4340. [CrossRef]
19. Shah, A.; Rather, M.A.; Hassan, Q.P.; Aga, M.A.; Mushtaq, S.; Shah, A.M.; Hussain, A.; Baba, S.A.; Ahmad, Z. Discovery of anti-microbial and anti-tubercular molecules from Fusarium solani: An endophyte of Glycyrrhiza glabra. *J. Appl. Microbiol.* **2017**, *122*, 1168–1176. [CrossRef]
20. Chowdhury, N.S.; Sohrab, M.H.; Rana, M.S.; Hasan, C.M.; Jamshidi, S.; Rahman, K.M. Cytotoxic Naphthoquinone and Azaanthraquinone Derivatives from an Endophytic Fusarium solani. *J. Nat. Prod.* **2017**, *80*, 1173–1177. [CrossRef]
21. Khan, M.I.H.; Sohrab, M.H.; Rony, S.R.; Tareq, F.S.; Hasan, C.M.; Mazid, M.A. Cytotoxic and antibacterial naphthoquinones from an endophytic fungus, *Cladosporium* sp. *Toxicol. Rep.* **2016**, *3*, 861–865. [CrossRef]
22. Sondergaard, T.E.; Fredborg, M.; Oppenhagen Christensen, A.M.; Damsgaard, S.K.; Kramer, N.F.; Giese, H.; Sørensen, J.L. Fast Screening of Antibacterial Compounds from Fusaria. *Toxins* **2016**, *8*, 355. [CrossRef] [PubMed]
23. Khan, N.; Afroz, F.; Begum, M.N.; Roy Rony, S.; Sharmin, S.; Moni, F.; Mahmood Hasan, C.; Shaha, K.; Sohrab, M.H. Endophytic Fusarium solani: A rich source of cytotoxic and antimicrobial napthaquinone and aza-anthraquinone derivatives. *Toxicol. Rep.* **2018**, *5*, 970–976. [CrossRef]
24. Haraguchi, H.; Yokoyama, K.; Oike, S.; Ito, M.; Nozaki, H. Respiratory stimulation and generation of superoxide radicals in Pseudomonas aeruginosa by fungal naphthoquinones. *Arch. Microbiol.* **1997**, *167*, 6–10. [CrossRef] [PubMed]
25. Medentsev, A.G.; Akimenko, V.K. Naphthoquinone metabolites of the fungi. *Phytochemistry* **1998**, *47*, 935–959. [CrossRef]
26. Medentsev, A. Fungal Naphthoquinone metabolites (review). *Appl. Microbiol. Biotechnol.* **1996**, *32*, 7–29.
27. Futuro, D.O.; Ferreira, P.G.; Nicoletti, C.D.; Borba-Santos, L.P.; Da Silva, F.C.; Rozental, S.; Ferreira, V.F. The antifungal activity of naphthoquinones: An integrative review. *An. Acad. Bras. Cienc.* **2018**, *90*, 1187–1214. [CrossRef]
28. Kristensen, S.B.; Van Mourik, T.; Pedersen, T.B.; Sørensen, J.L.; Muff, J. Simulation of electrochemical properties of naturally occurring quinones. *Sci. Rep.* **2020**, 1–10. [CrossRef]
29. Alberti, F.; Foster, G.D.; Bailey, A.M. Natural products from filamentous fungi and production by heterologous expression. *Appl. Microbiol. Biotechnol.* **2017**, *101*, 493–500. [CrossRef]
30. Rugbjerg, P.; Naesby, M.; Mortensen, U.H.; Frandsen, R.J.N. Reconstruction of the biosynthetic pathway for the core fungal polyketide scaffold rubrofusarin in Saccharomyces cerevisiae. *Microb. Cell Fact.* **2013**, *12*, 1–9. [CrossRef]
31. Pedersen, T.B.; Nielsen, M.R.; Kristensen, S.B.; Spedtsberg, E.M.L.; Yasmine, W.; Matthiesen, R.; Kaniki, S.E.K.; Sørensen, T.; Petersen, C.; Muff, J.; et al. Heterologous expression of the core genes in the complex fusarubin gene cluster of Fusarium Solani. *Int. J. Mol. Sci.* **2020**, *21*, 7601. [CrossRef]
32. Kurobane, I.; Vining, L.C. Metabolites of Fusarium Solani related to Dihydrofusarubin. *J. Antibiot.* **1980**, *XXXIII*, 1376–1379. [CrossRef] [PubMed]

33. Sørensen, J.L.; Sondergaard, T.E. The effects of different yeast extracts on secondary metabolite production in Fusarium. *Int. J. Food Microbiol.* **2014**, *170*, 55–60. [CrossRef] [PubMed]
34. Sørensen, J.L.; Giese, H. Influence of carbohydrates on secondary metabolism in Fusarium avenaceum. *Toxins* **2013**, *5*, 1655–1663. [CrossRef] [PubMed]
35. VanderMolen, K.M.; Raja, H.A.; El-Elimat, T.; Oberlies, N.H. Evaluation of culture media for the production of secondary metabolites in a natural products screening program. *AMB Express* **2013**, *3*, 71. [CrossRef]
36. Burkholder, P.R.; Sinnott, E.W. Morphogenesis of Fungus Colonies in Submerged Shaken Cultures Author. *Am. J. Bot.* **1945**, *32*, 424–431. [CrossRef]
37. Raimbault, M.; Alazard, D. Culture Method to Study Fungal Growth in Solid Fermentation. *Eur. J. Appl. Micrbiol. Biotechnol.* **1980**, *209*, 199–209. [CrossRef]
38. Manan, M.A.; Webb, C.; Manan, M.A. Estimating fungal growth in submerged fermentation in the presence of solid particles based on colour development. *Biotechnol. Biotechnol. Equip.* **2018**, *2818*. [CrossRef]
39. Nielsen, M.R.; Karolina, A.; Holzwarth, R.; Brew, E.; Chrapkova, N.; Evelyne, S.; Kaniki, K.; Kastaniegaard, K.; Sørensen, T.; Westphal, K.R.; et al. A new vector system for targeted integration and overexpression of genes in the crop pathogen Fusarium solani. *Fungal Biol. Biotechnol.* **2019**, 1–10. [CrossRef]
40. Westphal, K.R.; Wollenberg, R.D.; Herbst, F.A.; Sørensen, J.L.; Sondergaard, T.E.; Wimmer, R. Enhancing the production of the fungal pigment aurofusarin in Fusarium graminearum. *Toxins* **2018**, *10*, 485. [CrossRef]

Paper 3

Kristensen, S.B.; Fini, M.N.; Pedersen, T.B.; Sørensen, J.L.; Muff, J. (2021) *Membranebased separation and purification of fusarubins from Fusarium solani.*

Separation and Purification Technology 278 (2022) 119576

Contents lists available at ScienceDirect

Separation and Purification Technology

journal homepage: www.elsevier.com/locate/seppur

Membrane based separation and purification of fusarubins from *Fusarium solani*

Sebastian Birkedal Kristensen, Mahdi Nikbakht Fini, Tobias Bruun Pedersen, Jens Laurids Sørensen, Jens Muff *

Department of Chemistry and Bioscience, Aalborg University, Esbjerg 6700, Denmark

ARTICLE INFO

Keywords:
Fusarium
Secondary metabolites
Polyketides
Purification
Mycotoxins
Pigments

ABSTRACT

The use of fugal secondary metabolites is extensive throughout several industries, and the compounds are often extracted using loads of harmful organic solvents. The issues with several different and also similar products produced by the same biosyntethic pathways are challenging the downstream separation and purification, especially when scaling up production for the industry. The main objective of this study was to investigate the separation, concentration and purification possibilities of four different valuable fungal pigments produced by *Fusarium solani*. We present a full membrane based filtration train to elucidate which membrane type can be useful in the separation and concentration of the compounds. This visualized the possibility if using microfiltration to concentrate bostrycoidin and also to separate fusarubin from the rest of the pigments. Also, a comparison study between three types of microfiltration membranes is presented, showing little to none difference in the investigated membranes. Lastly, a high concentration- high recovery filtration study is presented, concentrating bostrycoidin in an even higher concentration. It is shown in this paper, that it is possible to use membrane filtration to separate, concentrate and purify the fusarubins investigated.

1. Introduction

Natural products, such as secondary metabolites, represent a large variated collection of chemical compounds, that can be attributed to a wide display of biological activities [1,2]. A subdivision of natural products is called polyketides, which accommodate large structural diversity and have been investigated extensively for many years, due to their bioactivity and industrial applicability in the pharmaceutical industry, agriculture and food industry [3–5]. In recent years, other fields have shown interest in polyketides such as electrolyte production for energy storage [6–8]. Filamentous fungi have been attributed to the production of many different polyketides with several specific uses such as antibacterial properties like penicillium [9], carcinogenic toxicity like aflatoxin [10], fusarielins [11] and lovastatin which is used for lowering cholesterol [12,13]. Some of these polyketides are also produced as pigments, which has shown great potential for additional value in production in biorefineries [14–16], but also as a natural alternative for syntactically produced pigments which show limitations [17]. *Fusarium* species have long been studied for the vast amount of secondary metabolite production [18–20], which also includes several quinone-like pigments depending on subspecies [21–23]. The PKS3; *fsr1* gene cluster is present in all genome sequenced *Fusaria* and has been assigned to the production of the pigments 8-methylfusarubin in *F.fujikoroi* [24], and bostrycoidin in *F.graminearum* [25]. Both compounds, however, share the same precursor in their biosynthetic pathway, and the common intermediate is believed to be a C14 heptaketide-aldehyde [23,26]. A common pigment also found is fusarubin, which can be produced from dihydrofusarubin by a spontaneous nonenzymatic oxidization step occuring under alkaline conditions [18,27]. The compound anhydrofusarubin has been shown to be produced by a nonenzymatic dehydroxylation under acidic conditions [28].

Fungal secondary metabolites, polyketides and pigments are produced by the fungi as supplementary products to a variety of different compounds, which from a production perspective makes the purification difficult. Conventionally, large amounts of organic solvents as chloroform, acetone, methanol and hexane are being used for the extraction of secondary metabolites and pigments [29–32]. For industrial-scale applications, the use of large amounts of low selectivity organics extraction

* Corresponding author.
E-mail addresses: sbk@bio.aau.dk (S. Birkedal Kristensen), mnf@bio.aau.dk (M. Nikbakht Fini), tbp@bio.aau.dk (T. Bruun Pedersen), jls@bio.aau.dk (J. Laurids Sørensen), jm@bio.aau.dk (J. Muff).

https://doi.org/10.1016/j.seppur.2021.119576
Received 3 June 2021; Received in revised form 23 August 2021; Accepted 23 August 2021
Available online 25 August 2021

solvents is often used which both present economic, safety and environmental challenges. Membrane filtration offers competitive, economical [33], less time and energy consuming down steam processing steps for upscale production in biotechnological industries [34]. Pressure-driven membranes have been used for separation and extraction of natural products such as vitamin C [35,36], and pigments (betaxanthines [37] and betacyanines [38]). Benzylpenicillin or penicillin G is also produced using membrane filtration of the fermentation broth a part of the downstream process [39,40] as is the production of lactic acid [41–43]. Pressure-driven membrane filtration has also been used for concentration of compounds at large-scale productions, which is presenting a mature technology possessing multiple uses [44]. Membranes are often characterized by the molecular weight cut-off, MWCO, which is determined by the molecule weight where the compound is rejected by 90% [45].

Conventionally, microfiltration (MF) is used to remove organic matter and large impurities, recover larger macromolecules such as carbohydrates and proteins, and is often used as a pretreatment step [45]. Ultrafiltration (UF) has been used to recover specific compounds, such as insulin and other valuable compounds [34,39], whereas nanofiltration (NF), has been used for recovery of specific low molecular weight molecules e.g. polyphenols [34,46], NF is also widely used in water softening, desalination and wastewater treatment, but also for separation of amino acids from fermentation broths, e.g. L-glutamine [47]. NF has shown high separation of small charged molecules due to selectivity in the membranes, which has made NF an important advance in the industry [48]. The reverse osmosis membranes (RO), are used to remove ionic compounds. The two standard operation modes for membrane filtration are used widely, dead-end filtration and cross-flow filtration. At cross-flow mode, the fluid flows in parallel with the membrane surface, and permeates through due to pressure difference, this way reducing the filter cake formation significantly when compared with the dead-end mode where the fluid flows directly through the membrane, hence the flux can be increased for a longer period of time [45,49]. Membranes are often used as a downstream process in connection with other types of extraction, such as solvent extraction and the use of polymeric resins [50,51], thereby making it possible to combine membrane filtration with earlier published production methods for fungal pigments [32].

The aim of the study was to evaluate the potential of integrating cross-flow membrane filtration systems as a part of the extraction and purification of pigments produced by *Fusarium solani*. Stepwise filtration in the sequence MF-UF-NF-RO were used to study the fractionation of the compounds and different polymeric membrane materials were used in order to study the influence of the membrane material properties on the performance of the process with respect to specific compound rejection and permeation flux.

2. Materials and methods

2.1. Secondary metabolite production and properties

For the production of the compounds in this paper, we used the *Fusarium solani* mutant 77–13-4 OE::*fsr6* G418^R (Nielsen et al 2019 [52]).

The production of secondary metabolites or pigments was based on earlier published studies [32], which elucidated the optimized media composition to selectively produce chosen quinone pigments. In this study, we applied the media composition that favored the production of bostrycoidin. Three other pigments were produced in parallel and still present in the media, however in low concentrations levels when compared to bostrycoidin. The amount of media was scaled up to produce 4.0 L and 4.5 L fermentation broth, for the first and second experimental run, respectively, the pH was adjusted to 5.5 ± 2 and the fungi incubated for 7 days. For the third experiment, we used the combined retentates of experiments 1 and 2, to lower the waste of valuable products and media components, and to achieve as a high concentration of the desired products as possible. Data for the four different pigments are listed in Table 1.

The water solubility of the molecules is not listed in the literature, however, earlier published data [6], give an indication of the relative aqueous solubility by the solubility descriptor, ΔG_{solv}, where the more negative the value, the higher the solubility. Estimated pK_a values have been computed by the program Marvin sketch [53], and the numbers refer to the specific functional group on the molecule as indicated in Fig. 2B. The hydrophobicity/hydrophilicity of the pigments is also presented in Table 1 based on the octanol/water partition coefficient, Log K_{ow}.

2.2. Membrane properties

In the first part of this study, we investigated four commercially available flat sheet membranes, Table 2; the MF membrane, Synder V0.1 (Sterlitech), the UF membrane, Synder MQ (Sterlitech), the NF membrane, Alfa Laval NF99HF (Alfa Laval) and the RO membrane, Dow Filmtech XLE (Sterlitech). The pure water flux was measured prior to every experiment, however, it was not possible to measure the pure water flux for the MF membranes. The rest of the data was reported by the manufacturers.

The pure water flux was determined using the cross-flow filtration set up, measured over a time of 5 mins where Milli-Q water was filtered through the membrane and monitoring the mass of permeate. For the second experiment, two additional MF membranes, as presented in Table 3, were compared together with the MF membrane used in experiment one. The second MF membrane was a Trisep MF01 (Sterlitech) and the third was Microdyn Nadir MV020 (Sterlitech). The main difference between V0.1 and MF01 is the polymer used in the membrane, where V0.1 is polyvinylidene fluoride (PVDF) and MF01 is polyethersulfone (PES). MV020 is also made from PVDF, but a larger declared pore size, and a slightly different pH stability window.

For the third part of the study, The V0.1 membrane was chosen to investigate long term filtration.

2.3. Membrane filtration

The cross-flow filtration set-up, FT17-50 unit, Armfield (UK), illustrated in Fig. 1, was used in all experiments. The system is controlled by a computer and all data is logged. For each experiment, a membrane disc of 90 mm in diameter (effective surface area 63.6 cm^2) was used. Prior to each experiment, all membranes were flushed for two minutes in Milli-Q water to ensure the protection film was removed. At each experiment, Milli-Q water was used to establish pure water flux. The system temperature was controlled by a cooler element and was stabilized at 22 °C. The system was thoroughly flushed with Milli-Q water and 70% ethanol after each experiment.

The first experiment was conducted as a filtration train (MF-UF-NF-

Table 1
. Data for the pigments investigated in this study. The pk_a values I-III refers to Fig. 2B, where the related functional group is indicated. Pka values are estimated using Marvin sketch [53], at 25C°.

	MW [g/mol]	ΔG_{solv} [kJ/mol] [6]	pK_a I	pK_a II	pK_a III	Log K_{ow}
Fusarubin	306.27	−51,82	8.14	9.94	12.20	1.4 [54]
Javanicin	290.27	−35,60	8.42	10.35	–	2 [55]
Bostrycoidin	285.26	−29,26	8.61	10.56	2.63	2.6 [56]
Anhydrofusarubin	288.26	−45,48	7.94	9.69	–	2.4 [57]

Table 2
. Data for the membranes used in the first part of the study as obtained from the material data sheets.

Flat sheet membrane	MF	UF	NF	RO
	Synder V0.1	Synder MQ	Alfa Laval NF99HF	Dow Filmtech, XLE
Typical feed	Industrial/Dairy	Industrial	Dairy, pharma/ biotech, beverage	Brackish Water
Type	"Intermediate", Fat/microbial removal, protein fractionation	Protein, Beverage clarification	Concentration and purification	Extra-low energy
pH range	1–11	1–10	3–10	2–11
Pure water Flux [$Lm^{-2}h^{-1}$]/ bar	–	21 ± 2	17 ± 1	8 ± 1
MWCO/ Pore size	0.1 µm	50.000 Da	300 Da	≈ 100 Da
Polymer	PVDF*	PES**	PET***	PA-TFC****

* PVDF: Polyvinylidene fluoride ; ** PES: Polyethersulfone ; *** PET: Polyethylene terephthalate ; **** PA-TFC: Polyamide thin film composite

Table 3
. Data for the additional two MF membranes, for the second part of the study as obtained from the material datasheets.

Flat sheet membrane	Trisep, MF01	Microdyn Nadir, MV020
Typical feed	Dairy/Process	Environment, paint, paper, metal, chemical, pharma/ biotech
Type	Food & Dairy, Concentration of macromolecules and large organic solutes	High stability against oxidizing agent
pH range	1–12	2–11
Pore size	0.1 µm	0.2 µm
Polymer	PES	PVDF

RO), where all individual cross-flow batch filtrations was conducted with 50% recovery, which indicates that 50% feed volume goes to both the permeate and the retentate respectively. The minimum volume of feed in the vessel for the pumps to operate was approximately 250 mL. The initial feed volume was 4.0 L, where 2.0 L passed through the MF at 2 bar transmembrane pressure (TMP), leaving 2.0 L as the retentate. The 2.0 L permeate was used for the next batch filtration with the UF membrane at 4 bar TMP, yielding 1.0 L retentate and 1.0 L permeate. The 1.0 L permeate was used for the NF batch filtration, which was run at 10 bar TMP resulting in 500 mL retentate and 500 mL permeate. This permeate was used for the RO membrane filtration, which was conducted at 10 bar TMP. 10 mL samples was taken from the feed vessel for further extraction and analysis at each step, starting from the initial feed sample. The experiment was performed three times (triplicate). A flow chart of the experiment is seen in Fig. 2D.

The second part of experiments with the three different MF membranes was conducted in a similar fashion to the first experiment, and all batch filtrations were performed at 2 bar TMP. However, the initial feed volume was adjusted to the minimum needed 500 mL to save fermentation broth. 50% recovery was used in this experiment as well. Samples of 10 mL were taken at each step. The experiment was performed in triplicate, using a fresh membrane coupon every time. A scheme of the experiment is found in supplementary information Figure S1.

The purpose of the third experiment was to investigate how the process behaved during a high concentration high recovery experiment. All the retentates from the completed MF batch filtrations were collected and mixed into a highly concentrated feed solution. Triplicate samples of 10 mL were taken from the feed, the retentate and the permeate. The experiment was conducted with a permeate recovery of 90%. The feed volume was 8.1 L, 7.3 L was filtered through the MF1 membrane as permeate, and 800 mL was maintained as retentate. The experiment was performed at 2 bar TMP. A scheme of the experiment is found in supplementary information Figure S2.

The permeate flux was logged by a computer and was calculated using Eq. (1).

$$J = \frac{V_P}{A \times t} \tag{1}$$

where, V_P is the volume of permeated water, A is active membrane surface area and t is the time of filtration.

The apparent rejection of the fusarubins was caluculated using Eq. (2).

$$\text{Rejection}\% = \left(1 - \frac{C_P}{\frac{1}{2}(C_F + C_R)}\right) x100 \tag{2}$$

Where, C_P is the concentration of permeated compound, C_F is the feed concentration and C_R is the concentration in the retentate.

The relative mass percentage is described using Eq.3

$$\text{Relativemass}\% = \frac{m_S}{m_F} x100 \tag{3}$$

where m_s is the mass in the sample, either permeate or retentate, and m_F is the mass in the feed solution.

2.4. Extraction and analysis

All samples taken out during experiments were extracted using liquid–liquid extraction procedure and analyzed, for concentration levels of fusaruibin, javanicin, anhydrofusarubin and Bostrycoidin, using HPLC-DAD system as described in our previously published paper [32].

3. Results and discussion

In Fig. 2A the initial MF scheme of filtration is illustrated. In order to investigate whether it was possible to concentrate and separate the four quinone pigments produced by *F.solani*, Fig. 2B, we used the optimized media found in our previously published work, [32]. We used the media optimized to favor the production of bostrycoidin. Fig. 2C shows the chromatograms of the MF feed, retentate and permeate samples illustrating the change in composition of the four different quinones indicated by colour. It is seen that there is a clear visual separation of the compounds, where fusarubin passed through the MF membrane to a much greater extent than the other compounds. Bostrycoidin remained primarily in the retentate and got concentrated. A number of unidentified peaks is also seen in the chromatograms, these peaks can be attributed to different other compounds, which is produced by the same biosynthetic pathway. The peaks have not been included in the calibrations and are therefore not quantified. In Fig. 2D the full separation train is illustrated as a scheme. The significant colour change throughout the separation is visualized, from the initial sample to the dark concentrated retentate and light orange permeate from the MF membrane. The NF membrane almost removes all of the pigments from the solution, leaving only little to be retained in the RO retentate, permeating no pigments at all.

Analysis of the initial fermentation broth sample show indeed that as intended, bostrycoidin was present in the highest concentration (144.1 mg/L), fusarubin and anhydrofusarubin followed with 5.2 and 5.5 mg/L respectively, and javanicin was present in the lowest concentration (2.4 mg/L on average). All specific concentrations for all experiments can be seen in the supplementary information Table S1-3 and visualized in

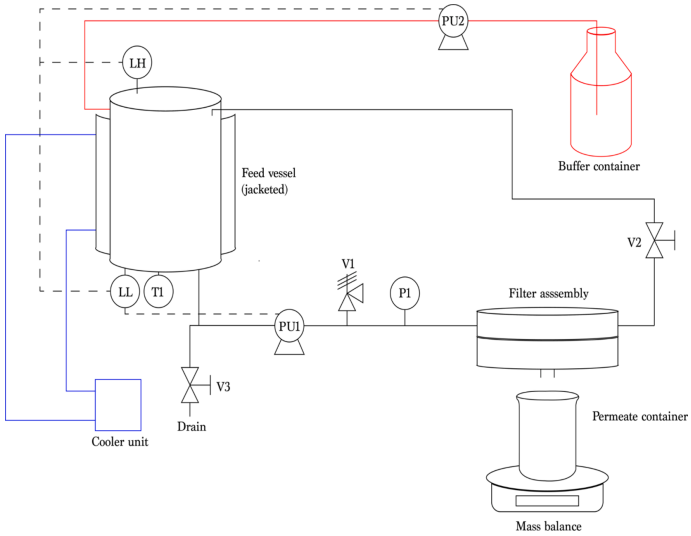

Fig. 1. Overview of the cross-flow membrane set up used in this study. Fluid runs from the buffer container, via the pump, PU2, to the feed vessel. This is adjusted by the LH and LL floater indicators, when the feed level is low PU1 will stop and PU2 will go until the LH indicates that the level is high, this ensure the feed vessel to be filled up continuously. Feed runs through the filter assembly via the pump, PU1, and down to the permeate container, which is placed on a mass balance. The feed vessel is jacked and connected to a cooler for ensuring a constant temperature, which is measured at T1.

supplementary information Figure S3-S4. The absolute masses in the 4 L of feed, Fig. 3A, corresponds to 576.3 mg of bostrycoidin, 31,3 mg of fusarubin, 21.9 mg of anhydrofusarubin and 9.6 mg og javanicin. After MF, operated at 50% recovery, bostrycoidin gets concentrated to 537.1 mg in the retentate, and only 10.8 mg in the permeate, which corresponds to an average rejection of 97.5%. Fusarubin is not present in the retentate and shows an absolute mass of 24.2 mg in the permeate. Anhydrofusarubin and javanicin were both concentrated in the retentate to 27.6 and 10.1 mg respectively, showing average rejection percentages of 91.4% and 52.4%.

The MF membrane with a pore size of 0.1 μm was capable of removal of the targeted pigment, bostrycoidin, with a molecular weight of 285.26 Da significantly higher than expected based on size exclusion mechanism where the species are rejected by a membrane with respect to molecular size and membrane pore size. This is because the solution contains other suspended cells as well as proteins and organic cell matter which might cause fouling on the membrane surface and resulting in the pore blocking effect [58–60]. Using a visual inspection, the formation of a foulant layer could also be observed after the filtration on the surface of V0.1 membrane as presented in Figure S10. Moreover, the permeate flux data of the V0.1 membrane in Fig. 3B demonstrates a flux decline within 200 min of the filtration test. The average permeate flux declined 20% from the initial value of 25 L/(m2h) to 20 L/(m2h). The initial permeate flux value of the MF test per se also suggests that fouling has occurred since the permeate flux for MF membranes is known to be notably higher than 25 L/(m2h). On the other hand, Adsorption also plays a minor role in the high rejection value of bostrycoidin. As presented in Table 1 by Log Kow, bostrycoidin is a hydrophobic molecule (Log Kow > 2) and it is well known in the literature that hydrophobic species tend to adsorb more on the membrane surface resulting in an enhanced rejection performance [61–63]. Using a mass balance for bostrycoidin over the MF step, nearly 3% of bostrycoidin was adsorbed onto the V0.1 membrane (See supplementary information Table S4).

The UF step seemed to have little separation effect on the remaining compounds, as all compounds were found in both retentate and permeate. The data from the NF filtration clearly showed that the NF membrane retained the majority of the remaining compounds, concentrating fusarubin to 13.6 mg, javanicin to 1.1 mg, bostrycoidin to 2.9 mg and anhydrofusarubin to 0.5 mg, where little to none, were to be found in the permeate. The XLE RO membrane filtered out the last small amounts and left no pigment in the permeate.

These tendencies become clearer when investigating the relative mass in percentage**.** The initial feed mass is set as being 100%. For fusarubin 100.2% is to be found in the permeate from MF, and at the UF step, 56.5% is found in the permeate and 63.1% is to be found in the retentate. The NF membrane retains afterwards 45.9% and permeates 4.3%. Similar tendencies are seen for javanicin. For bostrycoidin it is seen that 95.1% is retained by the MF membrane, leaving 1.9% to permeate, which corresponds to the rejection of 97.5%. This tendency is also seen for anhydrofusarubin. For some of the molecules, it is seen that over 100% can be achieved in the relative mass %, this can be explained by the change in pH throughout the experiment, starting out acidic, making bostrycoidin ionic at the -N, making the permeate more alkaline, oxidizing additional compounds to fusarubin when exposed to air, as explained by Kurobane and Vining [18,27], which also corresponds to anhydrofusarubin is to be found in the acidic retentate. These compounds are however in very low concentration and the variation can also be explained by this. Statistical anlysis verified the explained tendincies, however no significance in means was found in the filtration steps for javanicin due to very low concentrations. For fusarubin the statistical analysis showed a significant difference in the NF step where fusarubin was retained. The anaylsis yielded a significance in difference of

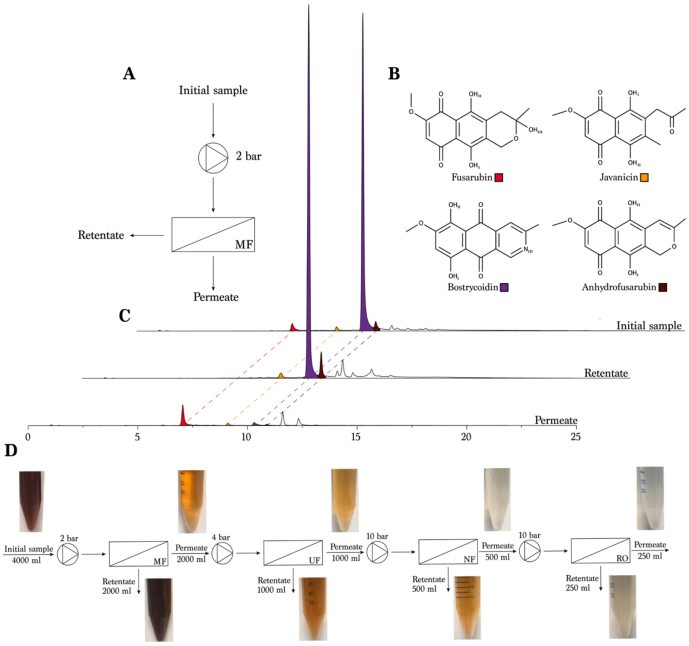

Fig. 2. A) Scheme for the initial MF experiment. B) structural formulas for the four quinones of interest, colours represent the peaks in the chromatogram, numbers on the molecules, refer to the Pka values listed in Table 1. C) chromatogram of the filtration steps, showing clear separation and the magnitude of the different molecules in the media. D) scheme for the full separation train, which also shows the colour difference between the filtration steps.

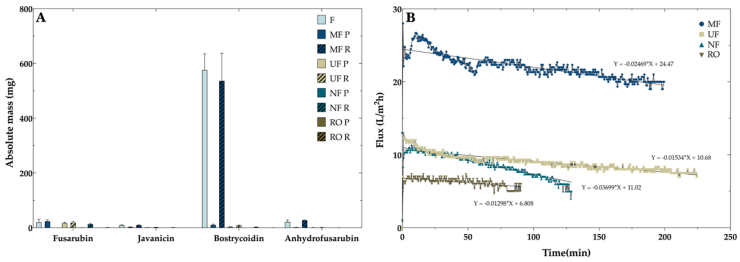

Fig. 3. Experimental data for the separation train, A) Absolute mass, indicate the amount of each pigment is filtrated at which filtration step. B) permeate flux data.

bostrycoidin at the MF step, correspoinding with previously explained tendencies. Due to large variation of the data, some of the tendencies is not found as significant when analyzed, as for anhydrofusarubin, however the statictical analysis can be challenging when conversion products is present and concentrations a low in the sample matrix. Statistical results can be seen in Figure S5. Fig. 3B illustrates the average permeate flux for the individual filtration steps. The MF step starts at 25 L/(m^2h) and increases to 26.5, whereafter it decreases over 200 min to 20 L/(m^2h) as a result of fouling as described earlier. The experiment using UF membrane have an initial value of 13, which fast decreases to 10 and after this it slowly decays to 7.5 L/(m^2h). The NF membrane shows starting values of 11.5, decreasing to 5.0 L/(m^2h) over the experiment. The RO membrane also shows a decrease from 7.0 to 6.0 L/(m^2h) over the experiment. These tendencies were expected, as there might be fouling occurring on the membrane surface. The decrease was not something we consider crucial as the feed volumes filtered were

relatively large, going from starting volume at 4.0 L, to 250 mL. Specific data for the relative mass% can be found in the supplementary information for all experiments in Table S4-S6 and Figure S6-S8.

Because it was possible to retain bostrycoidin in the MF retentate, it was interesting to investigate different types of MF Membranes. We saw similar patterns with the three investigated MF membranes, where fusarubin was permeated through the membrane completely yielding nothing in the retentate and small concentrations in the permeate. Javanicin was found in both permeate and retentate of all membranes, yielding rejection percentages of 55.9%, 52.9% and 57.7% for the three membranes respectively. Bostrycoidin was concentrated from 70.4, 63.1 and 63.0 mg in the three feed solutions, Fig. 4A, V0.1 membrane, Fig. 4B, MF01 and Fig. 4C, MV020, respectively to 67.0, 65.4 and 65.8 mg in the retentate, concluding in 98.0% , 97.8% and 98.2% rejection for the three membrane types respectively. The same tendencies were observed for anhydrofusarubin, which initially had an absolute mass of 2.6, 2.5 and 3.1 mg, whereas in the retentate 2.5, 2.4 and 2.9 mg was found, which adds up to 91.6%, 90.6% and 92.5% of rejection for the three membrane types respectively. When investigating the relative masses it is seen that fusarubin is being oxidized in all cases, exceeding 100% in the permeate, leaving nothing in the retentate, this again indicate that aeration throughtout the filtration experiments leads to formation of fusarubin from oxidation and conversion of "not identified compounds" from the solution. Javanicin, showing 26.5%, 28.7%, and 26.4% in the permeates for the three membranes respectively, and 69.9%, 71.6% and 74.8% were found in the retentates for each membrane. Bostrycoidin was found as 1.4%, 1.7% and 1.4% in the permeate and 95.1%, 105.0%, and 104.1% for V0.1, MF01 and MV020 respectively for the retentate. The reason for the slightly higher amount of bostrycoidin in the MF01 and MV020 experiments, can be explained by the higher deviation in the datasets due to irregularities in samples. The tendencies was varified by the statistical analysis, where no significance besides what has been stated earlier was found in the multible comparisons carried out in the study. The results of the statistical anlysis can be seen in Figure S9. Visually, the permeate was significant more transparent than the retentate, which can be seen in Figure S10. In Fig. 4D the average permeate flux for the three membranes is visualized, all showing a significantly decreasing curve. The initial flux of the V0.1 membrane was 25.3 which decreased to 18 corresponding to the MF flux in Fig. 3B. The initial flux of the MF01 membrane was slightly higher at 28, and decreased to 19.6 over the 21 mins, being the fastest of the three membranes. The MV020 membrane showed the highest initial flux measured at 29.3 L/(m^2h) which corresponded to the higher pore size but also showed the fastest decline to 19 L/(m^2h) over the time of 22 min. This rapid flux decline for all three MF membranes over nearly 20 min of filtration is attributed to the fouling as a result of the presence of other species in the solution e.g. proteins and cellular parts, as discussed previously. It was not possible to determine any significant difference in the filtration behavior of the three analyzed membranes when comparing them to each other.

To investigate long term, high concentration, high permeate recovery, the retentates from previous experiments were combined to a starting feed volume of 8.1L and used for MF filtration with the V0.1 membrane and operated with a permeate recovery of 90%. In the initial samples, there was no trace of fusarubin, as this was filtered off by previous experiments. Therefore, data on fusarubin is not present in Fig. 5A. We found javanicin in the initial sample to be 90.4 mg and after filtration 17.9 mg was in the permeate or 19.8% of the relative mass. In the retentate, the absolute mass was 34.3 mg or 38.0% of the relative mass. Bostrycoidin was found in the initial sample with an average absolute mass of 2744.7 mg and only 55.4 mg was found in the permeate, leaving 744.6 mg in the retentate. This however only corresponded to 28.9% of the relative mass. A possible explanation is related to the subsequent liquid–liquid extraction used for the chemical analysis. Due to the high amount of cell tissue and fatty acids present in the highly concentrated retentate as well as the pigments it was harder to perform the extraction as utilized before, leaving some of the pigments still in the media after extraction. Furthermore, the pattern was the same for all the

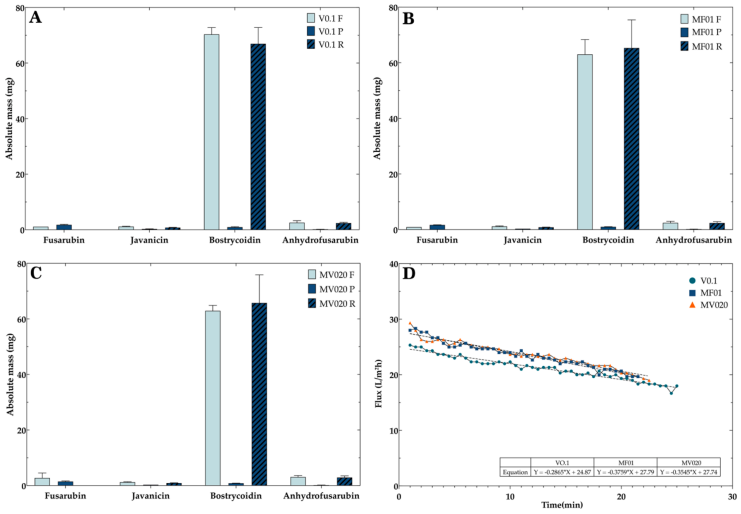

Fig. 4. experimental data for the three investigated MF membranes. A) V0.1 membrane, B) MF01 membrane, C) MV020 membrane. D) Permeate flux for all three membranes.

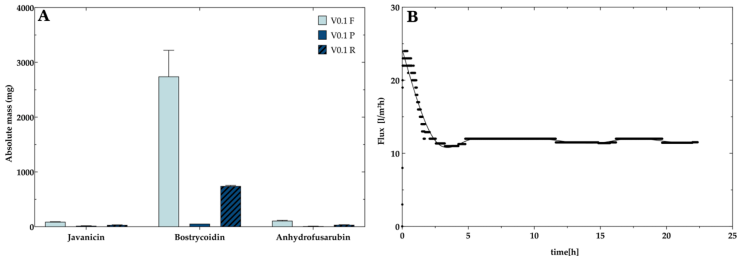

Fig. 5. Large volume separation experiment, A) absolute mass, B) permeate flux data, which has been smoothened.

quinones, in the study, and thereby it is thought to be plausible. Another hypothesis was tested, as the samples could have overloaded the column of the HPLC system, but even when samples were diluted a thousand times, similar results were obtained. So even though the relative mass percentage did not add up to 100% it is still plausible that near to 100% of the desired pigments, was concentrated in the retentate. With the exception of javanicin, as this compound was present in both permeate and retentate.

When comparing with results from experiments 1 and 2, the amount of bostrycoidin in relative percentage matched, it can therefore be assumed that almost all the bostrycoidin should be present in the retentate. For this to be concluded, a new extraction method should be investigated or additional filtration steps could be relevant. The average permeate flux of the experiment, Fig. 5B, is illustrating an initial value of 24.8 L/(m2h) similar to values obtained before. After four hours of steady decrease, the average permeate flux stabilize around 12 L/(m2h), where the flux is maintained until the end of the experiment after 22.5 h. This behavior was expected, as dealing with heavily concentrated feed the membrane will over time be fouled with particles, whereas the pattern of the flux will stabilize and a steady-state of the filtration will occur.

It is reasonable to assume that it is possible to concentrate bostrycoidin at a recovery of 90%, as the results shows an increase of average concentrations from 338.8 mg/L to 930.8 mg/L in the retentate and only 2.1% of the relative mass was found in the permeate. The same could be assumed for the compounds javanicin and anhydrofusarubin. The 800 mL retentate was extracted and analysis yielded sample purity of 94.1% when analyzed at 495 nm. The amount of bostrycoidin extracted was concluded to be 10.4 g, which is higher than the 930.8 mg/L which also concludes the assumption of the challenges with the extraction of highly concentrated liquids. Chromatogram measured at 495 nm can be found in Figure S11.

4. Conclusion

In this study, we highly focused on the compound bostrycoidin and performed experiments based on a media optimized to favor the production of bostrycoidin. However, we also found three other quinone compounds, in significantly lower concentrations though. It has been shown that it is possible to use membrane filtration to separate the compound fusarubin completely from bostrycoidin, by microfiltration, yielding rejection of bostrycoidin of 98% and 0% for fusarubin. In the study we investigated three different MF membranes, which showed rejection of bostrycoidin of 98%, 97.8% and 98.2% respectively, fusarubin was only found in the permeate. Leaving bostrycoidin in the retentate, and being concentrated with a purity of 94.1%, and permeating fusarubin. We, therefore, conclude that it is plausible to concentrate and purify the compounds investigated in this study. This can be achieved in a less harmful, more environmentally friendly way for larger-scale applications when compared to previously used methods.

Declaration of Competing Interest

The authors declare that they have no known competing financial interests or personal relationships that could have appeared to influence the work reported in this paper.

Acknowledgements

This study was supported by grants from The Danish Research Council, Technology and Production(grant no. 7017-00167) and the Novo Nordisk Foundation (NNF18OC0034952).

Appendix A. Supplementary material

Supplementary data to this article can be found online at https://doi.org/10.1016/j.seppur.2021.119576.

References

[1] N.P. Keller, Translating biosynthetic gene clusters into fungal armor and weaponry, Nat. Chem. Biol. 11 (2015) 671–677, https://doi.org/10.1038/nchembio.1897.
[2] N.P. Keller, G. Turner, J.W. Bennett, Fungal secondary metabolism - From biochemistry to genomics, Nat. Rev. Microbiol. 3 (2005) 937–947, https://doi.org/10.1038/nrmicro1286.
[3] J.J. Coleman, The Fusarium solani species complex: Ubiquitous pathogens of agricultural importance, Mol. Plant Pathol. 17 (2016) 146–158, https://doi.org/10.1111/mpp.12289.
[4] L. Katz, R.H. Baltz, Natural product discovery: past, present, and future, J. Ind. Microbiol. Biotechnol. 43 (2016) 155–176, https://doi.org/10.1007/s10295-015-1723-5.
[5] A.H. Aly, A. Debbab, P. Proksch, Fifty years of drug discovery from fungi, Fungal Divers. 50 (2011) 3–19, https://doi.org/10.1007/s13225-011-0116-y.
[6] S.B. Kristensen, T. Van Mourik, T.B. Pedersen, J.L. Sørensen, J. Muff, Simulation of electrochemical properties of naturally occurring quinones, Sci. Rep. (2020) 1–10, https://doi.org/10.1038/s41598-020-70522-z.
[7] D.G. Kwabi, K. Lin, Y. Ji, E.F. Kerr, M.A. Goulet, D. De Porcellinis, D.P. Tabor, D. A. Pollack, A. Aspuru-Guzik, R.G. Gordon, M.J. Aziz, Alkaline Quinone Flow Battery with Long Lifetime at pH 12, Joule. 2 (2018) 1894–1906, https://doi.org/10.1016/j.joule.2018.07.005.
[8] K. Lin, Q. Chen, M.R. Gerhardt, L. Tong, S.B. Kim, L. Eisenach, A.W. Valle, D. Hardee, R.G. Gordon, M.J. Aziz, M.P. Marshak, Alkaline quinone flow battery, Science (80-.). 349 (2015) 1529–1532. https://doi.org/10.1126/science.aab3033.
[9] A. Fleming, On the antibacterial action of cultures of a penicillium, with special reference to their use in the isolation of B.influenzae, Brit. J. Exp. Pethol. 10 (1929) 226–236.
[10] M. Peraica, B. Radić, A. Lucić, M. Pavlović, Toxic effects of mycotoxins in humans, Bull. World Health Organ. 77 (1999) 754–766.
[11] T.E. Sondergaard, L.G. Klitgaard, S. Purup, H. Kobayashi, H. Giese, J.L. Sørensen, Estrogenic effects of fusarielins in human breast cancer cell lines, Toxicol. Lett. 214 (2012) 259–262, https://doi.org/10.1016/j.toxlet.2012.09.004.
[12] J.A. Tobert, Lovastatin and beyond: The history of the HMG-CoA reductase inhibitors, Nat. Rev. Drug Discov. 2 (2003) 517–526, https://doi.org/10.1038/nrd1112.

[13] M. Faseleh Jahromi, J.B. Liang, Y.W. Ho, R. Mohamad, Y.M. Goh, P. Shokryazdan, Lovastatin production by Aspergillus terreus using agro-biomass as substrate in solid state fermentation, J. Biomed. Biotechnol. (2012 (2012).), https://doi.org/10.1155/2012/196264.

[14] L. Dufossé, M. Fouillaud, Y. Caro, S.A.S. Mapari, N. Sutthiwong, Filamentous fungi are large-scale producers of pigments and colorants for the food industry, Curr. Opin. Biotechnol. 26 (2014) 56–61, https://doi.org/10.1016/j.copbio.2013.09.007.

[15] Y. Caro, L. Anamale, M. Fouillaud, P. Laurent, T. Petit, L. Dufosse, Natural hydroxyanthraquinoid pigments as potent food grade colorants: an overview, Nat. Products Bioprospect. 2 (2012) 174–193, https://doi.org/10.1007/s13659-012-0086-0.

[16] S.A.S. Mapari, U. Thrane, A.S. Meyer, Fungal polyketide azaphilone pigments as future natural food colorants? Trends Biotechnol. 28 (2010) 300–307, https://doi.org/10.1016/j.tibtech.2010.03.004.

[17] R. Gmoser, J.A. Ferreira, P.R. Lennartsson, M.J. Taherzadeh, Filamentous ascomycetes fungi as a source of natural pigments, Fungal Biol. Biotechnol. 4 (2017) 1–25, https://doi.org/10.1186/s40694-017-0033-2.

[18] I. Kurobane, L.C. Vining, Metabolites of Fusarium Solani related to Dihydrofusarubin, J. Antibiot. (Tokyo). XXXII I (1980) 1376–1379.

[19] I. Kurobane, N. Zaita, A. Fukuda, New Metabolites of Fusarium Martii related to Dihydrofusarubin, J. Antibiot. (Tokyo) 39 (1985) 205–214, https://doi.org/10.7164/antibiotics.39.205.

[20] J.L. Sørensen, K.F. Nielsen, T.E. Sondergaard, Redirection of pigment biosynthesis to isocoumarins in Fusarium, Fungal Genet. Biol. 49 (2012) 613–618, https://doi.org/10.1016/j.fgb.2012.06.004.

[21] F.A.E. Torres, B.R. Zaccarim, L.C. de Lencastre Novaes, A.F. Jozala, C.A. dos Santos, M.F.S. Teixeira, V.C. Santos-Ebinuma, Natural colorants from filamentous fungi, Appl. Microbiol. Biotechnol. 100 (2016) 2511–2521, https://doi.org/10.1007/s00253-015-7274-x.

[22] P. Wiemann, A. Willmann, M. Straeten, K. Kleigrewe, M. Beyer, H.U. Humpf, B. Tudzynski, Biosynthesis of the red pigment bikaverin in Fusarium fujikuroi: Genes, their function and regulation, Mol. Microbiol. 72 (2009) 931–946, https://doi.org/10.1111/j.1365-2958.2009.06695.x.

[23] B.S. Menezes, L.S. Solidade, A.A. Conceição, M.N. Santos Junior, P.L. Leal, E.S. de Brito, K.M. Canuto, S. Mendonça, F.G. de Siqueira, L.M. Marques, Pigment production by Fusarium solani BRM054066 and determination of antioxidant and anti-inflammatory properties, AMB Express. 10 (2020), https://doi.org/10.1186/s13568-020-01054-y.

[24] L. Studt, P. Wiemann, K. Kleigrewe, H.U. Humpf, B. Tudzynski, Biosynthesis of fusarubins accounts for pigmentation of fusarium Fujikuroi perithecia, Appl. Environ. Microbiol. 78 (2012) 4468–4480, https://doi.org/10.1128/AEM.00823-12.

[25] R.J.N. Frandsen, S.A. Rasmussen, P.B. Knudsen, S. Uhlig, D. Petersen, E. Lysøe, C. H. Gotfredsen, H. Giese, T.O. Larsen, Black perithecial pigmentation in Fusarium species is due to the accumulation of 5-deoxybostrycoidin-based melanin, Sci. Rep. 6 (2016) 1–13, https://doi.org/10.1038/srep26206.

[26] T. Awakawa, T. Kaji, T. Wakimoto, I. Abe, A heptaketide naphthaldehyde produced by a polyketide synthase from Nectria haematococca, Bioorganic Med. Chem. Lett. 22 (2012) 4338–4340, https://doi.org/10.1016/j.bmcl.2012.05.005.

[27] A.W. McCulloch, A.G. McInnes, D.G. Smith, I. Kurobane, L.C. Vining, Alkaline oxidation of diastereoisomeric 4a,10a-dihydrofusarubins to norjavanicin, fusarubin, and a new antibiotic isofusarubin: Nonenzymic formation of products in Fusarium solani cultures, Can. J. Chem. 60 (1982) 2943–2949, https://doi.org/10.1139/v82-422.

[28] I. Kurobane, L.C. Vining, A.G. McInnes, J.A. Walter, Use of 13 C in biosynthetic studies. The labeling pattern in dihydrofusarubin enriched from [13 C]- and [13 C, 2 H]acetate in cultures of Fusarium solani, Can. J. Chem. 58 (1980) 1380–1385, https://doi.org/10.1139/v80-217.

[29] Z. Zhu, Q. Wu, X. Di, S. Li, F.J. Barba, M. Koubaa, S. Roohinejad, X. Xiong, J. He, Multistage recovery process of seaweed pigments: Investigation of ultrasound assisted extraction and ultra-filtration performances, Food Bioprod. Process. 104 (2017) 40–47, https://doi.org/10.1016/j.fbp.2017.04.008.

[30] E. Roselló-Soto, C.M. Galanakis, M. Brnčić, V. Orlien, F.J. Trujillo, R. Mawson, K. Knoerzer, B.K. Tiwari, F.J. Barba, Clean recovery of antioxidant compounds from plant foods, by-products and algae assisted by ultrasounds processing. Modeling approaches to optimize processing conditions, Trends Food Sci. Technol. 42 (2015) 134–149, https://doi.org/10.1016/j.tifs.2015.01.002.

[31] K.R. Westphal, R.D. Wollenberg, F.A. Herbst, J.L. Sørensen, T.E. Sondergaard, R. Wimmer, Enhancing the production of the fungal pigment aurofusarin in Fusarium graminearum, Toxins (Basel). 10 (2018) 1–11, https://doi.org/10.3390/toxins10110485.

[32] S.B. Kristensen, T.B. Pedersen, M.R. Nielsen, R. Wimmer, J. Muff, J.L. Sørensen, Production and selectivity of key fusarubins from Fusarium solani due to media composition, Toxins (Basel). 13 (2021) 1–12, https://doi.org/10.3390/toxins13060376.

[33] P. Pal, J. Sikder, S. Roy, L. Giorno, Process intensification in lactic acid production: A review of membrane based processes, Chem. Eng. Process. Process Intensif. 48 (2009) 1549–1559, https://doi.org/10.1016/j.cep.2009.09.003.

[34] E. Díaz-Montes, R. Castro-Muñoz, Metabolites recovery from fermentation broths via pressure-driven membrane processes, Asia-Pacific J. Chem. Eng. 14 (2019), https://doi.org/10.1002/apj.2332.

[35] M. Cisse, F. Vaillant, D. Soro, M. Reynes, M. Dornier, Crossflow microfiltration for the cold stabilization of roselle (Hibiscus sabdariffa L.) extract, J. Food Eng. 106 (2011) 20–27, https://doi.org/10.1016/j.jfoodeng.2011.04.001.

[36] R.C. De Oliveira, R.C. Docé, S.T.D. De Barros, Clarification of passion fruit juice by microfiltration: Analyses of operating parameters, study of membrane fouling and juice quality, J. Food Eng. 111 (2012) 432–439, https://doi.org/10.1016/j.jfoodeng.2012.01.021.

[37] A. Cassano, F. Tasselli, C. Conidi, E. Drioli, Ultrafiltration of Clementine mandarin juice by hollow fibre membranes, Desalination 241 (2009) 302–308, https://doi.org/10.1016/j.desal.2007.10.102.

[38] A. Cassano, C. Conidi, E. Drioli, Physico-chemical parameters of cactus pear (Opuntia ficus-indica) juice clarified by microfiltration and ultrafiltration processes, Desalination 250 (2010) 1101–1104, https://doi.org/10.1016/j.desal.2009.09.117.

[39] L. Tessier, P. Bouchard, M. Rahni, Separation and purification of benzylpenicillin produced by fermentation using coupled ultrafiltration and nanofiltration technologies, J. Biotechnol. 116 (2005) 79–89, https://doi.org/10.1016/j.jbiotec.2004.09.002.

[40] H.V. Adikane, R.K. Singh, S.N. Nene, Recovery of penicillin G from fermentation broth by microfiltration, J. Memb. Sci. 162 (1999) 119–123, https://doi.org/10.1016/S0376-7388(99)00129-5.

[41] Y. Li, A. Shahbazi, C.T. Kadzere, Separation of cells and proteins from fermentation broth using ultrafiltration, J. Food Eng. 75 (2006) 574–580, https://doi.org/10.1016/j.jfoodeng.2005.04.045.

[42] H.D. Lee, M.Y. Lee, Y.S. Hwang, Y.H. Cho, H.W. Kim, H.B. Park, Separation and Purification of Lactic Acid from Fermentation Broth Using Membrane-Integrated Separation Processes, Ind. Eng. Chem. Res. 56 (2017) 8301–8310, https://doi.org/10.1021/acs.iecr.7b02011.

[43] P. Dey, L. Linnanen, P. Pal, Separation of lactic acid from fermentation broth by cross flow nanofiltration: Membrane characterization and transport modelling, Desalination 288 (2012) 47–57, https://doi.org/10.1016/j.desal.2011.12.009.

[44] R. Balti, R. Le Balc'h, N. Brodu, M. Gilbert, B. Le Gouic, S. Le Gall, C. Sinquin, A. Massé, Concentration and purification of Porphyridium cruentum exopolysaccharides by membrane filtration at various cross-flow velocities, Process Biochem. 74 (2018) 175–184. https://doi.org/10.1016/j.procbio.2018.06.021.

[45] A. Saxena, B.P. Tripathi, M. Kumar, V.K. Shahi, Membrane-based techniques for the separation and purification of proteins: An overview, Adv. Colloid Interface Sci. 145 (2009) 1–22, https://doi.org/10.1016/j.cis.2008.07.004.

[46] A. Cassano, C. Conidi, R. Ruby-Figueroa, R. Castro-Muñoz, Nanofiltration and tight ultrafiltration membranes for the recovery of polyphenols from agro-food by-products, Int. J. Mol. Sci. 19 (2018), https://doi.org/10.3390/ijms19020351.

[47] S.L. Li, C. Li, Y.S. Liu, X.L. Wang, Z.A. Cao, Separation of L-glutamine from fermentation broth by nanofiltration, J. Memb. Sci. 222 (2003) 191–201, https://doi.org/10.1016/S0376-7388(03)00290-4.

[48] C. Martín-Orue, S. Bouhallab, A. Garem, Nanofiltration of amino acid and peptide solutions: Mechanisms of separation, J. Memb. Sci. 142 (1998) 225–233, https://doi.org/10.1016/S0376-7388(97)00325-6.

[49] M.H.M. Isa, R.A. Frazier, P. Jauregi, A further study of the recovery and purification of surfactin from fermentation broth by membrane filtration, Sep. Purif. Technol. 64 (2008) 176–182, https://doi.org/10.1016/j.seppur.2008.09.008.

[50] C. Conidi, A.D. Rodriguez-Lopez, E.M. Garcia-Castello, A. Cassano, Purification of artichoke polyphenols by using membrane filtration and polymeric resins, Sep. Purif. Technol. 144 (2015) 153–161, https://doi.org/10.1016/j.seppur.2015.02.025.

[51] D.P. Zagklis, C.A. Paraskeva, Purification of grape marc phenolic compounds through solvent extraction, membrane filtration and resin adsorption/desorption, Sep. Purif. Technol. 156 (2015) 328–335, https://doi.org/10.1016/j.seppur.2015.10.019.

[52] M.R. Nielsen, A. Karolina, R. Holzwarth, E. Brew, N. Chrapkova, S. Evelyne, K. Kaniki, K. Kastaniegaard, T. Sørensen, K.R. Westphal, R. Wimmer, T. E. Sondergaard, J.L. Sørensen, A new vector system for targeted integration and overexpression of genes in the crop pathogen Fusarium solani, Fungal Biol, Biotechnol. (2019) 1–10, https://doi.org/10.1186/s40694-019-0089-2.

[53] ChemAxon, Marvin 17.27, (2017). http://www.chemaxon.com.

[54] PubChem Compound Summary for CID 73421, Fusarubin, Natl. Cent. Biotechnol. Inf. (2021). https://pubchem.ncbi.nlm.nih.gov/compound/73421.

[55] PubChem Compound Summary for CID 10149, Javanicin., Natl. Cent. Biotechnol. Inf. (2021). https://pubchem.ncbi.nlm.nih.gov/compound/Javanicin (accessed August 16, 2021).

[56] PubChem Compound Summary for CID 72631, Bostrycoidin., Natl. Cent. Biotechnol. Inf. (2021). https://pubchem.ncbi.nlm.nih.gov/compound/Bostrycoidin#section=Other-Identifiers.

[57] PubChem Compound Summary for CID 157509, Anhydrofusarubin., Natl. Cent. Biotechnol. Inf. (2021).

[58] M. Nikbakht Fini, H.T. Madsen, J. Muff, The effect of water matrix, feed concentration and recovery on the rejection of pesticides using NF/RO membranes in water treatment, Sep. Purif. Technol. 215 (2019) 521–527, https://doi.org/10.1016/j.seppur.2019.01.047.

[59] K.V. Plakas, A.J. Karabelas, Membrane retention of herbicides from single and multi-solute media: The effect of ionic environment, J. Memb. Sci. 320 (2008) 325–334, https://doi.org/10.1016/j.memsci.2008.04.016.

[60] O. Hylling, M. Nikbakht Fini, L. Ellegaard-Jensen, J. Muff, H.T. Madsen, J. Aamand, L.H. Hansen, A novel hybrid concept for implementation in drinking water treatment targets micropollutant removal by combining membrane filtration with biodegradation, Sci. Total Environ. 694 (2019), 133710, https://doi.org/10.1016/j.scitotenv.2019.133710.

[61] L.D. Nghiem, A.I. Schäfer, Trace contaminant removal with nanofiltration, Nanofiltration - Princ. Appl. Chapter 8 (2004) 479–520.
[62] A. Karabelas, K. Plakas, Membrane Treatment of Potable Water for Pesticides Removal, Herbic. Theory Appl. (2011), https://doi.org/10.5772/13240.
[63] Y. Kiso, Y. Sugiura, T. Kitao, K. Nishimura, Effects of hydrophobicity and molecular size on rejection of aromatic pesticides with nanofiltration membranes, J. Memb. Sci. 192 (2001) 1–10, https://doi.org/10.1016/S0376-7388(01)00411-2.

Paper 4

Wilhelmsen, C.O.; **Kristensen, S.B**.; Nolte, O.; Volodin, I.; Christiansen, J.V.; Petersen, T.I.; Larsen, T.O.; Frisvad, J.C.; Hager, M.; Schubert, S.U.; Muff, J; Sørensen, J.L. (2021) *The fungal battery: A redox flow battery containing the biosynthesised negolyte phenicin.*

Due to rights and permissions is this paper not present for publishing.

Paper 5

Pedersen, T.B.; Nielsen, M.R.; **Kristensen, S.B**.; Spedtsberg, E.M.L.; Yasmine, W.; Matthiesen, R.; Kaniki, S.E.K.; Sørensen, T.; Petersen, C.; Muff, J.; et al. (2020) *Heterologous expression of the core genes in the complex fusarubin gene cluster of Fusarium Solani.*

International Journal of
Molecular Sciences

MDPI

Communication

Heterologous Expression of the Core Genes in the Complex Fusarubin Gene Cluster of *Fusarium Solani*

Tobias Bruun Pedersen [1], Mikkel Rank Nielsen [1], Sebastian Birkedal Kristensen [1], Eva Mie Lang Spedtsberg [1], Wafaa Yasmine [1], Rikke Matthiesen [1], Samba Evelyne Kabemba Kaniki [1], Trine Sørensen [2], Celine Petersen [2], Jens Muff [1], Teis Esben Sondergaard [2], Kåre Lehmann Nielsen [2], Reinhard Wimmer [2] and Jens Laurids Sørensen [1,*]

[1] Aalborg University Esbjerg, Department of Chemistry and Bioscience, Niels Bohrs Vej 8, 6700 Esbjerg, Denmark; tbp@bio.aau.dk (T.B.P.); mrn@bio.aau.dk (M.R.N.); sbk@bio.aau.dk (S.B.K.); espedt16@student.aau.dk (E.M.L.S.); wyasmi14@student.aau.dk (W.Y.); rmatth14@student.aau.dk (R.M.); skabem15@student.aau.dk (S.E.K.K.); jm@bio.aau.dk (J.M.)

[2] Aalborg University Aalborg, Department of Chemistry and Bioscience, Fredrik Bajers Vej 7H, 9220 Aalborg, Denmark; trso@bio.aau.dk (T.S.); cepe@bio.aau.dk (C.P.); tes@bio.aau.dk (T.E.S.); kln@bio.aau.dk (K.L.N.); rw@bio.aau.dk (R.W.)

* Correspondence: jls@bio.aau.dk; Tel.: +45-9440-7659; Fax: +45-9940-7710

Received: 28 August 2020; Accepted: 12 October 2020; Published: 14 October 2020

check for updates

Abstract: Through stepwise recreation of the biosynthetic gene cluster containing *PKS3* from *Fusarium solani*, it was possible to produce the core scaffold compound of bostrycoidin, a red aza-anthraquinone pigment in *Saccharomyces cerevisiae*. This was achieved through sequential transformation associated recombination (TAR) cloning of *FvPPT*, *fsr1*, *fsr2*, and *fsr3* into the pESC-vector system, utilizing the inducible bidirectional galactose promoter for heterologous expression in *S. cerevisiae*. The production of the core metabolite bostrycoidin was investigated through triplicate growth cultures for 1–4 days, where the maximum titer of bostrycoidin was achieved after 2 days of induction, yielding 2.2 mg/L.

Keywords: polyketides; yeast; heterologous expression; Fusarium; pigments; fungi; bostrycoidin

1. Introduction

Within the realm of natural product chemistry, a specific group of compounds known as polyketides has been vigorously studied for many years because of their structural diversity, bioactivity, and industrial applicability. A few examples such as the cholesterol lowering compound lovastatin, anti-cancer compound cytochalasin E, and the antibiotic tetracyclines display only a fraction of the diverse beneficial properties of polyketides [1–3]. Other properties often associated with polyketides are anti-bacterial and anti-fungal activity, pigmentation, and possibly even electrolytic capacity in batteries [4]. In nature, these compounds are a result of the complex secondary metabolism of plants, fungi, and bacteria, expressing not only polyketides, but a plethora of other bioactive molecules. This renders purification of a single compound from natural sources laborious and difficult because crude extracts comprise a cocktail of metabolites.

In order to obtain high-titers of purified polyketides, a popular strategy is to engineer heterologous expression hosts that display a minimalistic secondary metabolite profile, while being well suited for large-scale fermentation [5]. An example of such a host is *Saccharomyces cerevisiae*, with a highly developed molecular toolbox [6], a simplistic metabolism [7], and a generally regarded as safe (GRAS) status organism suited for fermentation [8]. Model polyketides 6-methylsalisylic acid (6-MSA) and triacetic acid lactone (TAL) have been heterologously expressed in *S. cerevisiae* with titers of 1.6–1.7 g/L,

which further emphasizes the potential for production of polyketides in this host [9,10]. In order to obtain these levels of production, the primary metabolism of *S. cerevisiae* was optimized for higher flux towards the acetyl- and malonyl-Coenzyme A (CoA) pathways, rendering a higher concentration of precursor molecules for polyketide assembly. More complex polyketides of multiple ring-structures such as the pigment compounds bikaverin and rubrofusarin from the *Fusarium* species complex have also been expressed in *S. cerevisiae*, although lower titers of production were obtained, 3.65 mg/L and 1.1 mg/L, respectively, owing to the structural complexity of these polyketides [11,12].

In this study, we target the core genes of the fusarubin biosynthetic gene cluster in *F. solani*. The gene cluster is found in all genome sequenced Fusaria [13] and has previously been assigned to the production of 8-*O*-methylfusarubin in *F. fujikuroi* [14] and the aza-anthraquinone bostrycoidin in *F. graminearum* [15]. Besides the polyketide synthase (PKS) FSR1 (PKS3, PGL1), two enzymes were needed to yield the end products in these species—the *O-methyltransferase* FSR2 and the FAD-binding monooxygenase FSR3. For effective heterologous expression of polyketides in *S. cerevisiae*, it is necessary to co-express a 4'-phosphopantetheinyl transferase (PPTase) along with the tailoring enzymes as the acyl carrier protein (ACP)-domain of the polyketide synthase requires additional phosphopantetheinylation to drive the iterative enzymatic process of elongating the ketide-backbone. Therefore, a PPTase native to *F. verticillioides* was also introduced into the expression strains.

PKS3 has previously been heterologously expressed in *Escherichia coli*, which resulted in production of 6-*O*-demethylfusarubinaldehyde [16]. This compound is also predicted to be the entry molecule in the biosynthetic pathways in *F. fujikuroi* and *F. graminearum.* The production of fusarubins appears to be more enigmatic in the *F. solani* species complex, where more than 50 related compounds have been isolated, with fusarubin, javanicin, and bostrycoidin as the most prominent [17] (Figure 1).

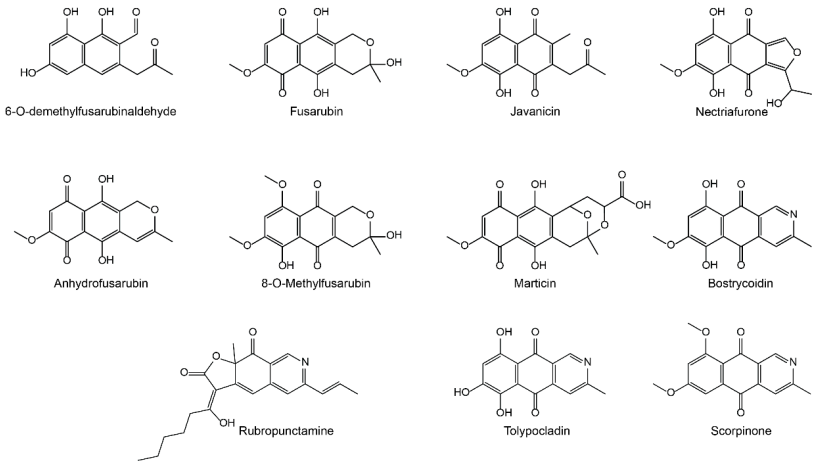

Figure 1. Structures of prominent fusarubins isolated from members of the *Fusarium solani* species complex as well as the structurally similar rubropunctamine from Monascus spp. [18], tolypocladin from *Tolypocladium inflatum* [19], and scorpinone from *Amorosia littoralis* [20].

Furthermore, the PKS3 gene cluster of *Fusarium solani* sp. exhibits a significant diversity from other members of the *Fusarium* genus [21], as it comprises the seven core genes (*fsr1–7*) with 17 additional genes, including some genes with potential tailoring capacity, which could explain the higher diversity of fusarubins produced by *Fusarium solani* (Figure 2a). In this study, transcription of the genes was controlled by the inducible *Gal1/10* promotor, leveling the transcription rate dissimilar to natural flux in wild-type transcription.

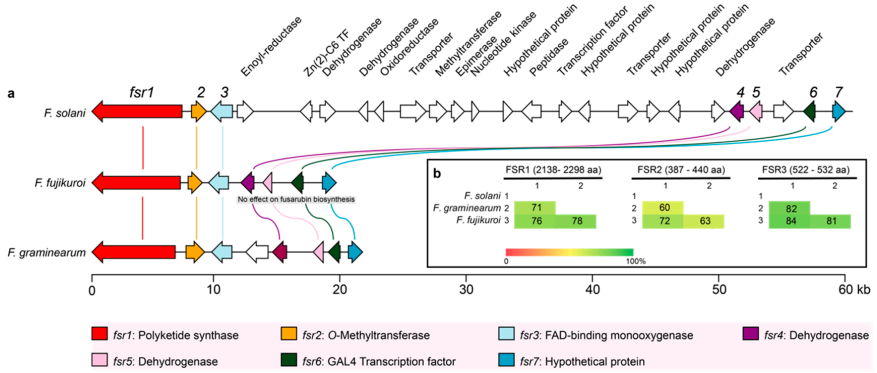

Figure 2. (**a**) Overview of the fusarubin gene clusters in *F. solani*, *F. fujikuroi*, and *F. graminearum*, where the seven conserved genes have been highlighted. The additional genes were tentatively identified using protein prediction software InterPro and NCBI's Conserved Domain Database (CDD) [22,23]. (**b**) Similarity matrices (% identity) of the amino acid sequences of the three core enzymes based on clustalW alignments.

The aim of study was to determine whether the three core genes contribute to the metabolic diversification through heterologous expression in *S. cerevisiae*.

2. Results and Discussion

2.1. Comparison of the PKS3 Gene Clusters

In *F. fujikuroi*, the end product in the pathway is predicted to be 8-*O*-methylfusarubin, which has an additional methyl group compared with fusarubin produced by *F. solani* as one of the main products As this difference is most likely mediated by FSR2, we performed an alignment analysis of the three core enzymes (Figure 2b). The alignment showed that the FSR3 is the most conserved among the three analyzed enzymes in *F. solani*, *F. fujikuroi*, and *F. graminearum*, with sequence identity ranging from 81 to 84% on amino acid level. FSR2 on the other hand displayed the largest variation, where *F. graminearum* displayed only 60 and 63% sequence identity to the orthologues in *F. solani* and *F. fujikuroi*, respectively

2.2. Heterologous Expression of the Three Fusarubin Core Genes

In order to determine the contributions of the three core genes to the biosynthetic pathway, we generated the four combinations (*S. cerevisiae* BY4743::*FvPPT+fsr1*), (*S. cerevisiae* BY4743::*FvPPT+fsr1+2*), (*S. cerevisiae* BY4743::*FvPPT+fsr1+3*), and (*S. cerevisiae* BY4743::*FvPPT+fsr1+2+3*), from here on referred to as Sc::*fsr1*, Sc::*fsr1+2*, Sc::*fsr1+3*, and Sc::*fsr1+2+3*, respectively. For each combination, a representative transformant was grown in conditions inducing the *Gal1/10* promotor system for two days, alongside a wild type *S. cerevisiae*. Changes in color were visible after one day (left) and evident already after two (right) (Figure 3a).

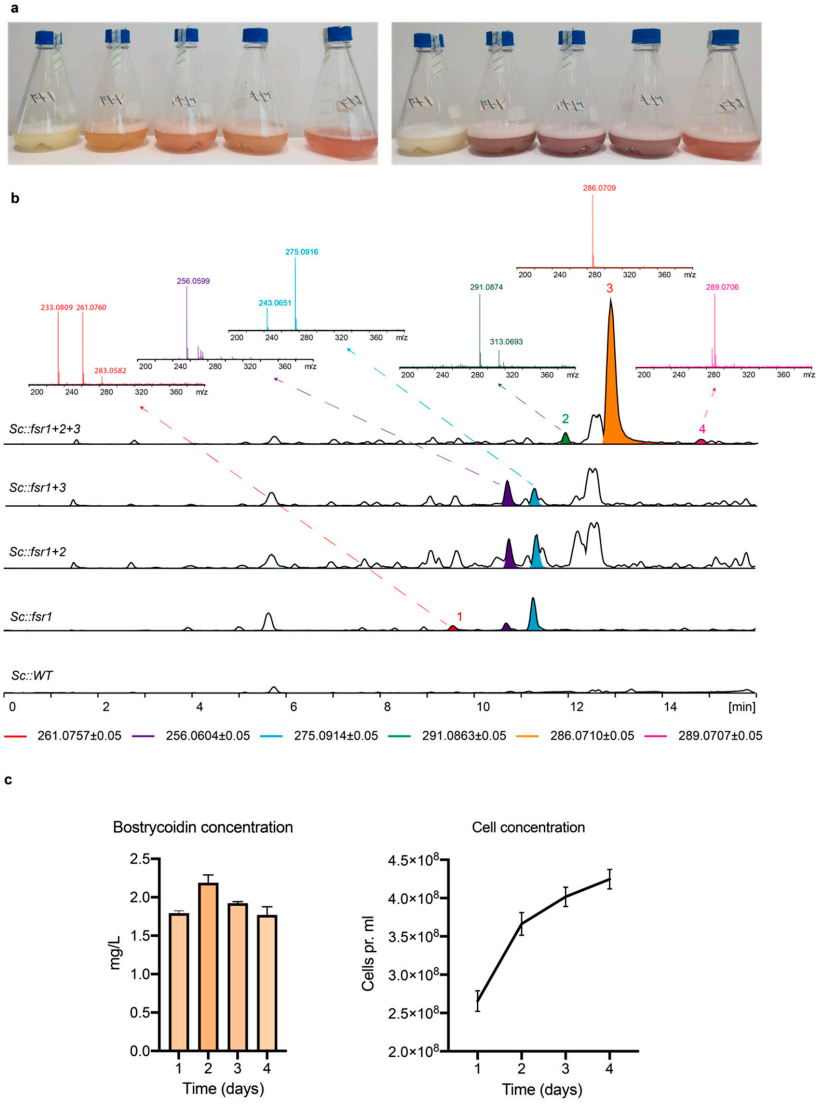

Figure 3. (**a**) Growth cultures after 24 h and 48 h, containing, from left to right, Sc::WT, Sc::*fsr1*, Sc::*fsr1+2*, Sc::*fsr1+3*, and Sc::*fsr1+2+3*. (**b**) Total ion chromatograms (TIC, black) and extracted ion chromatogram (EIC; colored, intervals listed below) of the yeast cultures. The selected mass spectra of compounds mentioned in the text have been included and the following compounds are indicated: (1) 6-O-demethylfusarubinaldehyde, (2) javanicin, (3) bostrycoidin, and (4) anhydrofusarubin. (**c**) Results from triplicate growth cultures grown for 1–4 days, showing the production of bostrycoidin alongside the cell concentration.

The subsequent metabolite analyses showed that three new peaks emerged with *fsr1* as the sole member of the gene cluster, when compared with the spectrum of Sc::WT. One of these peaks matched the expected spectrum for 6-*O*-demethylfusarubinaldehyde ($C_{14}H_{12}O_5$, $[M+H]^+_{exp}$: 261.0757; $[M+H]^+_{obs}$: 261.0760), which is the expected release product of FSR1. Another compound identified in Sc::*fsr1* was tentatively assigned to $C_{15}H_{14}O_5$ ($[M+H]^+_{exp}$: 275.0914; $[M+H]^+_{obs}$: 275.0916). So far, attempts to isolate and identify this compound have not been successful in the present or previous studies [24]. The hypothetical next step towards bostrycoidin is a spontaneous ammonium incorporation, resulting in 6-*O*-demethyl-5-deoxybostrycoidin anthrone ($C_{14}H_{11}N_1O_3$; $[M+H]^+_{exp}$: 256.0604) [15,25]. However, this compound was not detected in the extracts of any of the strains. Instead, another peak was observed in Sc::*fsr1* with a suggested chemical formula of $C_{14}H_9N_1O_4$ ($[M+H]^+_{exp}$: 256.0604; $[M+H]^+_{obs}$: 256.0599), which could be an oxidized form of 6-*O*-demethyl-5-deoxybostrycoidin anthrone. The latter two tentatively assigned compounds were also observed when *fsr1* was expressed with either *fsr2* or *fsr3*. However, we were not able to determine other pathway intermediates.

Co-expression of *fsr1–3* resulted in the production of javanicin, anhydrofusarubin, and bostrycoidin, with the latter as the dominating peak. The highest titer of bostrycoidin was achieved after 2 days of induction, reaching 2.2 mg/L (Figure 3c), very similar in titer level when compared with other complex polyketide expression studies in *S. cerevisiae* [11,12]. An explanation for the slight decrease in bostrycoidin concentration after 3 and 4 days could be the accumulation of bostrycoidin within the cell pellet due to limited solubility of bostrycoidin in the media. It was evident that the cell pellet of the cultures from day 3 and 4 was significantly larger and more dark red than that of cultures from day 1 and 2, indicating an intercellular accumulation (Figure S1). The observation of 6-*O*-demethylfusarubinaldehyde in Sc::*fsr1* confirms its identity as the PKS release product [14,15]. The following biosynthetic pathway can then branch out in two main directions, ending in bostrycoidin on one side and javanicin and anhydrofusarubin on the other side. The ability of Sc::*fsr1+2+3* to produce bostrycoidin suggests that ammonia is incorporated by a conserved fungal enzyme or, more likely, non-enzymatically as proposed previously [15,25]. Given the structural similarities of tolypocladin [19], scorpinone [20], and bostrycoidin, it seems very likely that the compounds share similar pathways including the amination step. A similar situation has also been observed in *Monascus* spp., where spontaneous amination with NH_3 is observed in the pathways, leading to the red pigment rubropunctamine and monascorubramine [18].

Anhydrofusarubin is structurally very similar to bostrycoidin, differing in the presence of an oxygen or nitrogen molecule in the C ring. It thus seems likely that anhydrofusarubin biosynthesis follows the path of bostrycoidin, where formation of the third ring occurs in one of the early steps (Figure 4). Whether javanicin is produced directly by FSR2 and FSR3 en route to anhydrofusarubin remains unknown. Alternatively, it could result from reopening of ring C in anhydrofusarubin. The ability to catalyze oxygenation and methylation reactions towards anhydrofusarubin and bostrycoidin suggests that the two enzymes have a promiscuous nature. It is striking that FSR2 from *F. solani* only adds one methyl group, while the orthologue from *F. fujikuroi* performs two. The alignments showed that the two enzymes are relatively similar (Figure 2b), but more complex comparison studies of their tertiary structures may shed light on the nature of the catalytic differences.

In our study, we only observed a minor portion of the fusarubins that have been reported in literature. This leaves the possibility that the remaining compounds are produced spontaneously or through actions of the enzymes encoded by the additional tailoring genes in the cluster from *F. solani*. Furthermore, the promiscuous nature of a 4´-phosphopantetheinyl transferase (PPTase) from *Fusarium verticillioides* exhibited adequate function for regenerating the acyl carrier protein (ACP) domain of the polyketide synthase (*fsr1*) from the closely related *Fusarium solani*.

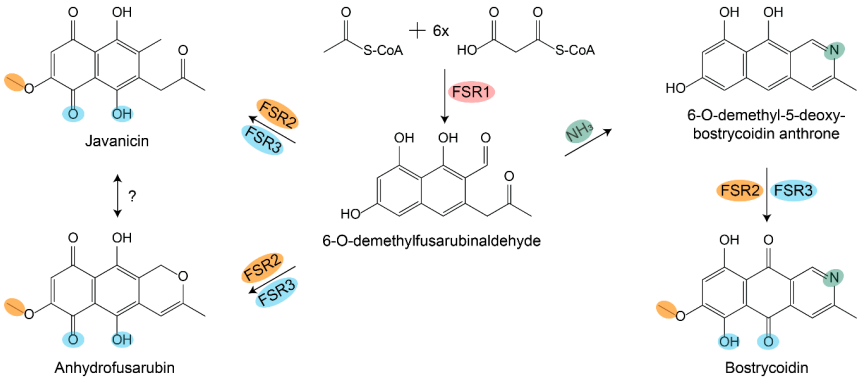

Figure 4. Suggested biosynthetic pathways leading to bostrycoidin, javanicin, and anhydrofusarubin. The polyketide synthase FSR1 is responsible for the first step, which results in 6-*O*-demethylfusarubinaldehyde. Non-enzymatic incorporation of ammonia followed by oxygenation and o-methylation by FSR3 and FSR2 result in bostrycoidin. The two enzymes can also act independently on ammonia incorporation, which results in anhydrofusarubin and javanicin.

3. Materials and Methods

3.1. Strains

Yeast cloning and heterologous expression were performed utilizing *S. cerevisiae* BY4743 (*genotype:* MATα, his3Δ1, leu2Δ0, lys2Δ0, met15Δ0, ura3Δ0) ATCC 201390 and electroporation was performed on bacterial strain *Escherichia coli* DH5α. The genome sequenced *F. solani* FGSC9596 [26] was used as a donor of DNA for amplification of *fsr2*.

3.2. Pairwise Alignment

Pairwise comparison of the protein encoded by the cluster genes was performed in CLC Main Workbench 8.1 using the clustalW algorithm (CLC Bio-Qiagen, Aarhus, Denmark) as previously described [27]. The sequences of FSR1-3 from *F. fujikuroi* (FFUJ_03984-86), *F. graminearum* (FGSG_09182-84), and *F. solani* (NECHADRAFT_101778-80) were retrieved from GenBank.

3.3. Enzymes, Oligonucleotides, and Plasmids

All enzymes were purchased from Thermo Fisher Scientific (Waltham, MA, USA) and oligonucleotides were designed using Primer3Plus software [28] and purchased from Eurofins Genomics (Ebersberg, Germany). The primer table including sequences can be found in Table S1. An overview of purchased and constructed plasmids can be found in Table S2 along with restriction enzymes used for digestion.

3.4. Gene Isolation and Synthesis

Coding sequences for *fsr1* and *fsr3* were codon optimized towards expression in yeast and synthesized (GenScript), while *fsr2* was amplified from genomic DNA prepared through DNeasy Plant Mini Kit (Qiagen, Hilden, Germany) from *F. solani* and the two exons were fused together to obtain intron-free CDS of *fsr2* using transformation associated recombination (TAR)-cloning. To facilitate polyketide formation in *S. cerevisiae*, we co-expressed *fsr1* with the *Sfp*-type phosphopantetheinyl transferase from *F. verticillioides* (FVEG_01894).

The four target genes were amplified by PCR using the primers, which contained 25–30 bp identical sequences to the target insert site of the vector expression system of pESC-URA or pESC-LEU,

used for auxotrophic selection on uracil (URA) and leucin (LEU) deficient media. The PCR reactions were performed in a 150 µL volume containing (30 µL High Fidelity buffer, 0.2 mM dNTP-mix, 0.2 mM forward/reverse Primer, 0.5 units Phusion HSII polymerase (New England Biolabs, Ipswich, MA, USA), 97.5 µL MQ H_2O, and 1 ng template DNA), split into 3 × 50 µL PCR-tubes.

3.5. Cloning

Prior to assembly of the expression plasmid, the receiving pESC-URA or pESC-LEU were linearized by double restriction enzyme digest (2 µL Fast Digest Buffer (Thermo Fisher Scientific, Waltham, MA, USA), 2 µL plasmid miniprep (QIAquick Miniprep kit), 1 µL FD Enzyme 1 (Thermo Fisher Scientific, Waltham, Massachusetts, USA), 1 µL FD Enzyme 2 (Thermo Fisher Scientific, Waltham, Massachusetts, USA), and 14 µL MQ H_2O at 37 °C for 15 min). The digested plasmids were separated on 1% w/v agarose gel and subsequently purified with the QIAquick Gel Extraction Kit (Qiagen, Hilden, Germany). TAR-cloning was performed according to the LiAc/PEG3350 protocol [29]. Selection of *S. cerevisiae* transformants was conducted using synthetic complete (SC) agar plates, lacking either uracil, leucine, or both [24].

The plasmid from the obtained transformants were recovered through adaptation of the QIAprep Spin Miniprep Kit (Qiagen, Hilden, Germany) protocol, adding 5 µL Zymolyase-mix (2 mg/mL Zymolyase in 0.5 M sorbitol) (MP Biomedicals Germany) to the P1 Buffer step and incubating at 37 °C for 1 h. The purified plasmids were electroporated into *E. coli* for proliferation and subsequently initially validated using Sanger-sequencing (Eurofins, Ebersberg) using the primers listed in Table S1 before full plasmid sequencing was performed using a MinION Flow Cell for nanopore sequencing (See 3.8 Plasmid verification). The verified plasmids were transformed into *S. cerevisiae* to obtain combinations where *fsr1* was expressed alone (Sc::*fsr1*), together with either *fsr2* (Sc::*fsr1*+*2*) or *fsr3* (Sc::*fsr1*+*3*), and all together (Sc::*fsr1*+*2*+*3*), as seen in Figure 5.

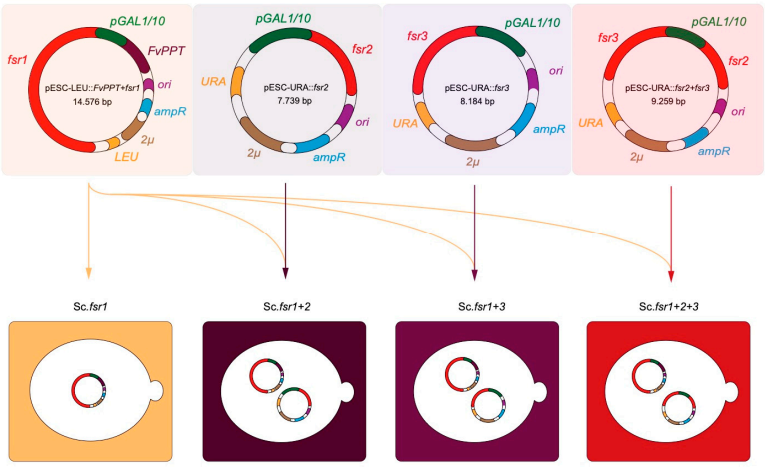

Figure 5. Final constructs of expression vectors utilizing the URA or LEU auxotrophic selection in *S. cerevisiae* BY4743, GAL1/10 inducible promotor, bacterial (*ori*), yeast (2μ) origin of replication along with the bacterial selection marker (amp^R). Sc::*fsr1* contains only the *fsr1*-gene, the main biosynthetic gene; a type I non-reducing PKS (NR-PKS) and *FvPPT*, a 4´-phosphopantetheinyltransferase (PPTase) from *Fusarium verticillioides* for successful phosphopantetheinylation of the acyl carrier protein (ACP)-domain of *fsr1*. The following strains contain a dual vector system. Sc::*fsr1*+*2* contains both *FvPPT*, *fsr1*, and the *fsr2*-gene, a O-methyltransferase. Sc::*fsr1*+*3* contains *FvPPT*, *fsr1*, and the *fsr3*-gene encoding a monooxygenase. Finally, Sc::*fsr1*+*2*+*3* contains all core biosynthetic genes involved in the synthesis and tailoring, *FvPPT*, *fsr1*, *fsr2*, and *fsr3*.

3.6. Production of Fusarubins Using Galactose Induction

Single colonies of transformants carrying biosynthetic genes were inoculated in 10 mL appropriate selective drop-out medium containing 2% glucose overnight at 30 °C, 200 rpm. Overnight cultures were vortexed and cell titers were estimated using a NanoDrop 2000 c (Thermo Fisher Scientific, Waltham, MA, USA). The cells were transferred into 1000 mL baffled shake flasks containing 250 mL selective media with 2% raffinose (D(+)-raffinose pentahydrate, Acros organics, China) to an OD600 = 0.2. The cells were grown for approximately 9–10 h at 30 °C, 200 rpm until an OD600 at 1 was achieved. The cultures were spiked with 25 mL 40% galactose (D(+)-galactose, VWR chemicals, Belgium) and maintained at 30 °C and 200 rpm for 1–4 days to induce expression of the fungal biosynthetic genes.

3.7. Chemical Analysis

After cultivation, the cells were pelleted by centrifugation at 5.000 G for five minutes. Approximately 300 mL of media was decanted into a 1000 mL bluecap flask and extracted as previously described for aurofusarin in *F. graminearum* [30]. The dried extracts were dissolved in 2 mL methanol and analyzed on a Hitachi Elite LaChrom HPLC in accordance with the chemical analysis performed in [24]. The identities of javanicin, anhydrofusarubin, and bostrycoidin were determined using data from previous experiments where they were isolated and structurally verified in *F. solani* [24].

3.8. Plasmid Verification

Library preparation was performed using the Rapid Barcoding Kit SQK-RBK004 (Oxford Nanopore Technologies, Oxford, UK) according to the manufacturer's guidelines and subsequently sequenced using a R.9.4.1 (FLO-MIN106D) MinION Flow Cell (Oxford Nanopore Technologies, Oxford, UK; Figure S2). The flow cell had previously been used, but was washed according to the manufacturer's instructions with the Flow Cell Wash Kit EXP-WSH003 (Oxford Nanopore Technologies, Oxford, UK). Fast5 files were basecalled and demultiplexed using GPU driven Guppy v3.6.1 (Oxford Nanopore Technologies, Oxford, UK) with the following model: dna_r9.4.1_450bps_hac.cfg. Filtlong v0.2.0 (https://github.com/rrwick/Filtlong) was used to filtrate the reads to a minimum length of 100 and minimum quality of 80. Minimap2 v2.17 [31] was used to create overlaps between the reads and the assemblies were generated by Miniasm v0.3 [32]. The assemblies were first polished with Racon v1.3.3 [33] and then with two rounds of Medaka v1.0.1 (https://github.com/nanoporetech/medaka); both with default settings.

Supplementary Materials: Supplementary materials can be found at http://www.mdpi.com/1422-0067/21/20/7601/s1.

Author Contributions: Conceptualization: T.B.P. and J.L.S.; Experimental work: T.B.P., S.B.K., E.M.L.S., W.Y., R.M., T.S., C.P., R.W. and M.R.N.; Data analysis: T.B.P., J.L.S., R.W., E.M.L.S., W.Y., R.M., and M.R.N.; Supervision: J.M., K.L.N., T.E.S., and J.L.S.; Manuscript: T.B.P., M.R.N., T.S., C.P., S.E.K.K., K.L.N., T.E.S., R.W. and J.L.S. All authors have read and agreed to the published version of the manuscript.

Funding: This study was supported by grants from The Danish Research Council, Technology, and Production (Grant No. 7017-00167) and the Novo Nordisk Foundation (NNF18OC0034952).

Conflicts of Interest: The authors declare no conflict of interest.

References

1. Tobert, J.A. Lovastatin and beyond: The history of the HMG-CoA reductase inhibitors. *Nat. Rev. Drug Discov.* **2003**, *2*, 517–526. [CrossRef] [PubMed]
2. Jahromi, M.F.; Liang, J.B.; Ho, Y.W.; Mohamad, R.; Goh, Y.M.; Shokryazdan, P. Lovastatin Production by Aspergillus terreus Using Agro-Biomass as Substrate in Solid State Fermentation. *J. Biomed. Biotechnol.* **2012**. [CrossRef]

3. Katz, L.; Baltz, R.H. Natural product discovery: Past, present, and future. *J. Ind. Microbiol. Biotechnol.* **2016**, *43*, 155–176. [CrossRef]
4. Kristensen, S.B.; Mourik, T.V.; Pedersen, T.B.; Sørensen, J.L.; Muff, J. Simulation of electrochemical properties of naturally occurring quinones. *Sci. Rep.* **2020**, *10*, 1–10. [CrossRef] [PubMed]
5. Alberti, F.; Foster, G.D.; Bailey, A.M. Natural products from filamentous fungi and production by heterologous expression. *Appl. Microbiol. Biotechnol.* **2017**, *101*, 493–500. [CrossRef] [PubMed]
6. Harvey, C.J.B.; Tang, M.; Schlecht, U.; Horecka, J.; Fischer, C.R.; Lin, H.-C.; Li, J.; Naughton, B.; Cherry, J.; Miranda, M.; et al. HEx: A heterologous expression platform for the discovery of fungal natural products. *Sci. Adv.* **2018**, *4*, eaar5459. [CrossRef] [PubMed]
7. Bond, C.; Tang, Y.; Li, L. *Saccharomyces cerevisiae* as a tool for mining, studying and engineering fungal polyketide synthases. *Fungal Genet. Biol.* **2016**, *89*, 52–61. [CrossRef]
8. Pfeifer, B.A.; Khosla, C. Biosynthesis of Polyketides in Heterologous Hosts. *Appl. Environ. Microbiol.* **2012**, *65*, 106–118. [CrossRef]
9. Cardenas, J.; Da Silva, N.A. Engineering cofactor and transport mechanisms in *Saccharomyces cerevisiae* for enhanced acetyl-CoA and polyketide biosynthesis. *Metab. Eng.* **2016**, *36*, 80–89. [CrossRef]
10. Kealey, J.; Liu, L.; Santi, D.V.; Betlach, M.C.; Barr, P.J. Production of a polyketide natural product in nonpolyketide- producing prokaryotic and eukaryotic hosts. *Proc. Natl. Acad. Sci. USA* **1998**, *95*, 505–509. [CrossRef]
11. Zhao, M.; Zhao, Y.; Hu, Q.; Iqbal, H.; Yao, M.; Liu, H. Pathway engineering in yeast for synthesizing the complex polyketide bikaverin. *BioRxiv* **2019**, 1–23. [CrossRef]
12. Rugbjerg, P.; Naesby, M.; Mortensen, U.H.; Frandsen, R.J.N. Reconstruction of the biosynthetic pathway for the core fungal polyketide scaffold rubrofusarin in *Saccharomyces cerevisiae*. *Microb. Cell Fact.* **2013**, *12*, 1–9. [CrossRef] [PubMed]
13. Brown, D.W.; Proctor, R.H. Insights into natural products biosynthesis from analysis of 490 polyketide synthases from Fusarium. *Fungal Genet. Biol.* **2016**, *89*, 37–51. [CrossRef] [PubMed]
14. Studt, L.; Wiemann, P.; Kleigrewe, K.; Humpf, H.; Tudzynski, B. Biosynthesis of Fusarubins Accounts for Pigmentation of *Fusarium fujikuroi* Perithecia. *Appl. Environ. Microbiol.* **2012**, *78*, 4468–4480. [CrossRef] [PubMed]
15. Frandsen, R.J.N.; Rasmussen, S.A.; Knudsen, P.B.; Uhlig, S.; Petersen, D.; Lysøe, E.; Gotfredsen, C.H.; Giese, H.; Larsen, T.O. Black perithecial pigmentation in *Fusarium* species is due to the accumulation of melanin. *Nat. Publ. Gr.* **2016**, *6*, 1–13.
16. Awakawa, T.; Kaji, T.; Wakimoto, T.; Abe, I. A heptaketide naphthaldehyde produced by a polyketide synthase from Nectria haematococca. *Bioorg. Med. Chem. Lett.* **2012**, *22*, 4338–4340. [CrossRef]
17. Medentsev, A.G.; Akimenko, V.K. Naphthoquinone metabolite s of the fungi. *Phytochemistry* **1998**, *47*, 935–959. [CrossRef]
18. Chen, W.; Chen, R.; Liu, Q.; He, Y.; He, K.; Ding, X. Orange, red, yellow: Biosynthesis of azaphilone pigments in Monascus fungi. *Chem. Sci.* **2017**, *8*, 4917–4925. [CrossRef]
19. Grafe, U.; Ihn, W.; Tresselt, D.; Miosga, N.; Kaden, U.; Schlegel, B.; Bormann, E.-J.; Sedmera, P.; Novák, J. Tolypocladin–a new metal-chelating 2-aza-anthraquinone from Tolypocladium inflatum. *Biol. Met.* **1990**, *3*, 39–44. [CrossRef]
20. Mantle, P.G.; Hawksworth, D.L.; Pazoutova, S.; Collinson, L.M.; Rassing, B.R. Amorosia littoralis gen. sp. nov. a new genus and species name for the scorpinone and caffeine-producing hyphomycete from the littoral zone in The Bahamas. *Mycol. Res.* **2006**, *110*, 1371–1378. [CrossRef]
21. Hansen, F.T.; Gardiner, D.M.; Lysøe, E.; Fuertes, P.R.; Tudzynski, B.; Wiemann, P.; Sondergaard, T.E.; Giese, H.; Brodersen, D.E.; Sørensen, J.L. An update to polyketide synthase and non-ribosomal synthetase genes and nomenclature in *Fusarium*. *Fungal Genet. Biol.* **2015**, *75*, 20–29. [CrossRef] [PubMed]
22. Hunter, S.; Apweiler, R.; Attwood, T.K.; Bairoch, A.; Bateman, A.; Binns, D.; Bork, P.; Das, U.; Daugherty, L.; Duquenne, L.; et al. InterPro: The integrative protein signature database. *Nucleic Acids Res.* **2009**, *37*, 211–215. [CrossRef] [PubMed]
23. Marchler-bauer, A.; Derbyshire, M.K.; Gonzales, N.R.; Lu, S.; Chitsaz, F.; Geer, L.Y.; Geer, R.C.; He, J.; Gwadz, M.; Hurwitz, D.I.; et al. CDD: NCBI's conserved domain database. *Nucleic Acids Res.* **2015**, *43*, 222–226. [CrossRef]

24. Nielsen, M.R.; Holzwarth, A.K.R.; Brew, E.; Chrapkova, N.; Kaniki, S.E.K.; Kastaniegaard, K.; Sørensen, T.; Westpgal, K.R.; Wimmer, R.; Sondergaard, T.E.; et al. A new vector system for targeted integration and overexpression of genes in the crop pathogen *Fusarium solani*. *Fungal Biol. Biotechnol.* **2019**, *6*, 25. [CrossRef] [PubMed]
25. Parisot, D.; Devys, M.; Barbier, M. Conversion of Anhydrofusarubin lactol into the antibiotic bostrycoidin. *J. Antibiot. (Tokyo)* **1898**, *42*, 1189–1190. [CrossRef] [PubMed]
26. Coleman, J.J.; Rounsley, S.D.; Rodriguez-Carres, M.; Kuo, A.; Wasmann, C.C.; Grimwood, J.; Schmutz, J.; Taga, M.; White, G.J.; Zhou, S.; et al. The Genome of nectria haematococca: Contribution of supernumerary chromosomes to gene expansion. *PLoS Genet.* **2009**, *5*, e1000618.
27. Wollenberg, R.D.; Saei, W.; Westphal, K.R.; Klitgaard, C.S.; Nielsen, K.L.; Lysøe, E.; Gardiner, D.M.; Wimmer, R.; Sondergaard, T.E.; Sørensen, J.L.; et al. Chrysogine biosynthesis is mediated by a two-module nonribosomal peptide synthetase. *J. Nat. Prod.* **2017**, *80*, 2131–2135. [CrossRef] [PubMed]
28. Untergasser, A.; Cutcutache, I.; Koressaar, T.; Ye, J.; Faircloth, B.C.; Remm, M.; Rozen, S.G. Primer3-new capabilities and interfaces. *Nucleic Acids Res.* **2012**, *40*, 1–12. [CrossRef]
29. Gietz, R.D. Yeast transformation by the LiAc/SS carrier DNA/PEG method. *Methods Mol. Biol.* **2006**, *313*, 107–120. [CrossRef]
30. Westphal, K.R.; Wollenberg, R.D.; Herbst, F.; Sondergaard, T.E.; Wimmer, R. Enhancing the production of the fungal pigment aurofusarin in *Fusarium graminearum*. *Toxins* **2018**, *10*, 485. [CrossRef]
31. Li, H. Minimap2: Pairwise alignment for nucleotide sequences. *Bioinformatics* **2018**, *34*, 3094–3100. [CrossRef]
32. Li, H. Minimap and miniasm: Fast mapping and de novo assembly for noisy long sequences. *Bioinformatics* **2016**, *32*, 2103–2110. [CrossRef] [PubMed]
33. Vaser, R.; Sović, I.; Nagarajan, N.; Šikić, M. Fast and accurate de novo genome assembly from long uncorrected reads. *Genome Res.* **2017**, *27*, 737–746. [CrossRef] [PubMed]

Paper 6

Pedersen, T.B.; Nielsen, M.R.; **Kristensen, S.B**.; Spedtsberg, E.M.L.; Sørensen, T.; Petersen, C.; Muff, J.; Søndergaard, T.S.; Nielsen, K.L.; Wimmer, R.; Gardiner, D.M.; Sørensen, J.L. (2021) *Speed dating for enzymes! Finding the perfect Phosphopantetheinyl Transferase partner for Your Polyketide Synthase.*

Due to rights and permissions is this paper not present for publishing.

ISSN (online): 2446-1636
ISBN (online): 978-87-7210-987-9

AALBORG UNIVERSITY PRESS